FRICTION AND HEAT TRANSFER COEFFICIENTS IN SMOOTH AND ROUGH PIPES WITH DILUTE POLYMER SOLUTIONS

Thesis by

Paul M. Debrule

In Partial Fulfillment of the Requirements
for the Degree of
Doctor of Philosophy

California Institute of Technology
Pasadena, California

1972

(Submitted May 5, 1972)

ACKNOWLEDGMENTS

I wish to express my deepest appreciation for the thoughtful advice and encouragement extended during the course of this research by my adviser, Professor R. H. Sabersky. Thanks are due to other members of the Institute faculty, Drs. Acosta, Brennen, Raichlen and Rannie, with whom I had occasion to discuss my work. I am also very thankful to Dr. D. Dipprey for his constant interest in this subject.

Financial support was given to the project by the Department of the Navy (Contract N66001-72-C-0009), by the DuPont de Nemours Co., and by the Humble Oil Co. through a Fellowship. This support is gratefully acknowledged.

Special thanks are due to Mr. D. Laird, Mr. F. MacDonald, and to many others at the Mechanical Engineering Shop for the high quality of workmanship which they have contributed to all phases of the experimental program. I am also grateful to Mrs. P. Henderson, Mrs. L. Lacy, Mrs. J. Powell, Miss C. Lin and Mr. F. Linton for their assistance in preparing the manuscript.

Finally, my deep appreciation is offered to my parents, for their understanding and moral support.

ABSTRACT

Measurements of friction and heat transfer coefficients were obtained with dilute polymer solutions flowing through electrically heated smooth and rough tubes. The polymer used was "Polyox WSR-301", and tests were performed at concentrations of 10 and 50 parts per million. The rough tubes contained a close-packed, granular type of surface with roughness-height-to-diameter ratios of 0.0138 and 0.0488 respectively. A Prandtl number range of 4.38 to 10.3 was investigated which was obtained by adjusting the bulk temperature of the solution. The Reynolds numbers in the experiments were varied from $\simeq 10,000$ ($Pr = 10.3$) to 250,000 ($Pr = 4.38$).

Friction reductions as high as 73% in smooth tubes and 83% in rough tubes were observed, accompanied by an even more drastic heat transfer reduction (as high as 84% in smooth tubes and 93% in rough tubes). The heat transfer coefficients with Polyox can be lower for a rough tube than for a smooth one.

The similarity rules previously developed for heat transfer with a Newtonian fluid were extended to dilute polymer solution pipe flows. A velocity profile similar to the one proposed by Deissler was taken as a model to interpret the friction and heat transfer data in smooth tubes. It was found that the observed results could be explained by assuming that the turbulent diffusivities are reduced in smooth tubes in the vicinity of the wall, which brings about a thickening of the viscous layer. A possible mechanism describing the effect of the polymer additive on rough pipe flow is also discussed.

SYMBOLS AND ABBREVIATIONS

a_1	constant appearing in definition of fundamental relaxation time of the polymer molecule, taken equal to 0.5 (Chapter II).
a_i	numerical constant in polynomial least square fits.
A	slope of logarithmic velocity profile, defined in Eqns. (21) and (22).
B	constant defined in Eqn. (29).
C	polymer concentration
C_F	friction coefficient for tubes, defined by Eqn. (1).
C_H	heat transfer coefficient (Stanton number) for tubes, defined by Eqn. (2).
C_{H_c}	cavity Stanton number, defined by Eqn. (59).
C_ℓ	onset criterion constant, in the length hypothesis (Chapter II).
C_p	specific heat at constant pressure.
C_t	onset criterion constant in the time hypothesis (Chapter II).
d	function, defined by Eqn. (112).
D	tube inside diameter.
f	general function.
F	function, defined by Eqn. (67).
g	function, defined by Eqn. (118).
G	function, defined by Eqn. (35).
h	heat transfer film conductance, $h = \dot{q}_0/(T_w - T_L)$.
h_{av}	root mean square average distance between the ends of the polymer molecule for all possible configurations.
h_{ex}	fully extended length of the polymer molecule.

j	Colburn factor, $j \equiv C_H \, Pr^{2/3}$
J	function defined in Eqn. (104).
k	thermal conductivity.
k_d	a dissipative wave number, used in onset criterion based on length hypothesis.
K	constant, appearing in Eqn. (90)
ℓ_1	macromolecular length, characteristic of the polymer in solution.
L	length of the heated test section.
M	polymer molecular weight.
n	constant appearing in Deissler's Eqn. (92).
Nu	Nusselt number, defined by Eqn. (102).
p, p', p''	parameters characterizing the polymer in solution.
P, P', P''	dimensionless groups characterizing the polymer in solution.
Pr	Prandtl number, defined as $Pr \equiv C_p \mu / k$.
Pr^*	a dimensionless group, $Pr^* \equiv (\epsilon_H / \epsilon_M) Pr = \lambda Pr$.
$\dot{q}$	local heat flux normal to a surface parallel to the tube wall.
$\dot{q}_0$	mean heat flux normal to the tube wall.
r	radius coordinate.
$\langle r^2 \rangle$	mean square, end-to-end length of polymer chain.
R	tube radius, $R \equiv \frac{D}{2}$, unless otherwise defined (gas constant in Chapter II).
R^*	dimensionless tube radius, defined as $R^* = R u_\tau / \nu$.
Re	Reynolds number for tubes, defined as $Re = \bar{u} D / \nu$.

Re_c	cavity Reynolds number, defined by Eqn. (58).
Re_L	sublayer Reynolds number, defined as $Re_L = (y_L u_\tau)/\nu$.
R_F	fractional drag reduction.
R_G	rms radius of gyration of the polymer molecule.
t_1	fundamental relaxation time of polymer.
T	temperature.
T'	temperature fluctuation in radial direction.
T^*	dimensionless temperature, defined by Eqn. (78).
T_L	mixed-mean fluid temperature, defined by Eqn. (4).
T_L^*	dimensionless mixed-mean fluid temperature, defined by Eqn. (80).
T_w	tube wall temperature.
u	mean axial velocity.
$\overline{u}$	tube discharge velocity, defined in Eqn. (3).
u^*	dimensionless mean axial velocity, defined as $u^* = u/u_\tau$.
u'	velocity fluctuation in axial direction.
u_L	mean axial velocity at edge of viscous sublayer in two layer model.
u_t	translation velocity, used in Eqn. (15).
u_τ	shear (friction) velocity, defined as $u_\tau \equiv \sqrt{\tau_0/\rho}$.
v'	velocity fluctuation in radial direction.
$\dot{w}$	mass flow rate.
x	axial distance coordinate, originates at the start of the heating.
y	distance from the wall coordinate.
y^*	dimensionless distance from the wall, defined as $y^* = yu_\tau/\nu$.

y_L	thickness of viscous sublayer in two layer model.
z_i	functions defined by Eqn. (82).
α	a function of polymer concentration defined in Meyer's correlation (Eqn. 86).
β	constant, defined by Eqn. (32).
δ	thickness of "laminar sublayer" in three layer model.
δu^*	an increment of u^*
ΔB	dimensionless shift in logarithmic velocity profile, due to the combined effect of polymer and roughness, defined in Eqn. (25′).
$\Delta B \cdot R$	dimensionless shift in logarithmic velocity profile, due to roughness only.
ΔT_f	temperature difference between the wall and the local mixed-mean fluid, $\Delta T_f \equiv T_w - T_L$.
Δu^*	dimensionless shift in logarithmic velocity profile, in smooth tube, due to the presence of polymer additive.
ΔV	incremental volume of a section of the tube.
Δx	tube length increment.
ε	average roughness height.
ε^*	dimensionless roughness height, defined as $\varepsilon^* = \varepsilon u_\tau/\nu$.
ε_H	turbulent heat diffusivity, defined as $\varepsilon_H = -\overline{T'v'}/(dT/dy)$.
ε_M	turbulent momentum diffusivity, defined as $\varepsilon_M = -\overline{u'v'}/(du/dy)$.
η	normalized radius coordinate, defined as $\eta \equiv r/R$.
η_L	value taken by η at the edge of viscous sublayer in two layer model.
$[\eta]$	zero shear intrinsic viscosity of 100 cc/g polymer solution.

θ_m	bulk to wall temperature difference, normalized with respect to the centerline to wall temperature difference, $\theta_m \equiv (T_L - T_w)/(T_{CL} - T_w)$.
κ	Von Karman's constant = $\frac{1}{A}$.
λ	ratio of turbulent heat and momentum diffusivities, $\lambda \equiv \varepsilon_H / \varepsilon_M$.
μ	absolute viscosity.
ν	kinematic viscosity.
ρ	density
ρ_p	density of dispersion of polymer molecules in solvent.
τ	mean shear stress.
τ_0	mean shear stress at the tube wall.
Φ_m	tube discharge velocity, normalized with respect to centerline velocity, $\Phi_m = \overline{u}/u_{CL}$.

Subscripts

as	asymptotic.
av	longitudinal average.
CL	tube centerline.
cr	critical.
exp	experimental.
F.R	fully rough.
g	average value on that surface described by the tip of the roughness elements.
in	inlet.
outl	outlet.
p	polymer.

s	solvent.
x	refers to any of the thermocouple locations.

Abbreviations

amp	amperes.
AC	alternating current.
cc	cubic centimeter.
DC	direct current.
Deiss	Deissler.
emf	electromotive force.
g	gramme.
LHS	left-hand side.
log	logarithm(ic).
ppm	parts per million.
psig	pounds per square inch gage.
RC	resistance-capacitance.
rms	root mean square.
vs	versus.
μV	microvolt.
Ω	ohm.

LIST OF FIGURES

TABLE OF CONTENTS

Chapter I

INTRODUCTION

By far the largest part of experimental work in heat transfer has been performed with rather simple, single-component fluids and most often the fluid has been air or water. This, of course, is entirely logical because heat transfer to water and air is of most immediate interest in every day life as well as in industrial processes. However, as our technology becomes more and more sophisticated, design information on less common and more complex fluids is needed. An example of this type of development is the fact that a considerable effort has already been devoted to the heat transfer to liquid metal. Water solutions of polymers have received widespread study in recent years, after it was discovered (Toms, [59], 1948) that tremendous reductions of turbulent pipe friction could be achieved by using dilute solutions of various polymeric additives. The practical possibilities of using this phenomenon — the Toms phenomenon — in several applications certainly justify the numerous efforts to achieve a better understanding of the mechanisms involved in drag reduction. Much of the early work was carried out at naval establishments with a view toward application in this field. Perhaps the most immediate one is the drag reduction of ships, which could be brought about by injecting small amounts of the solute into the boundary layer around the surfaces of the vessel. Other applications include the use of polymer solutions instead of pure water for fire fighting. In addition thought is being given to the use of polymer additives in order to reduce the friction in pumping oils, slurries, and irrigation water.

Most of the experiments conducted so far have been concerned with the determination of friction in smooth pipes and a few have been performed with rough pipes. Heat transfer data are still rather scarce. Most probably, such information will, however, be needed in the future. In some applications, for instance, water to which a polymer has been added for the purpose of friction reduction, may also be involved in a heat exchange process; in other instances the polymer (or a similar drag reducer) may be dissolved in the water unintentionally as a contaminant; and as a third example a liquid with drag reducing characteristics may constitute one of the components in a chemical process.

The study of the effect of roughened surfaces on heat and momentum transfer is of importance, as very often roughness occurs naturally either from the original manufacture of a surface or from subsequent chemical attack. Roughened surfaces have been used intensively in recent years to improve the heat transfer coefficients in heat exchangers. If an analogy between heat and momentum transfer exists for polymer solutions as it does for water, a friction reduction would also cause a reduction in the heat transfer. Hopefully then the use of rough surfaces might counterbalance that loss in heat transfer effectiveness caused by the polymer while still maintaining the friction loss low.

The types of problems mentioned above have been the stimulus for the present research program. The program was designed so that it would yield information on friction and heat transfer coefficients which might be directly useful in certain engineering applications. In addition it was hoped that the interpretation of the data would also allow an insight into the mechanism by which the polymer affects the friction and heat transfer. The experiments were limited to hydrodynamically and thermally fully established pipe flow with negligible radial fluid property variations and to roughness elements of a fixed type. In this way, it should be possible to express the results in terms of relationships between the friction coefficient C_F and the heat transfer coefficient C_H on the one hand, and the Reynolds number, Re, Prandtl number, Pr, roughness ratio, ϵ/D, the concentration, C, and a parameter characterizing the shape of the polymer on the other. The experiments were designed to allow a systematic variation over a fairly wide range of Re, Pr, and ϵ/D.

The type of roughness of the tubes in the current experiments is a three-dimensional, close-packed, granular form not greatly different from the close-packed sand-grain surface used by Nikuradse [37] for rough pipe friction measurements. The roughness ratio of the rough tubes is 0.0138 and 0.0488 respectively. The present heat transfer experiments were conducted with water solutions of Polyox WSR-301 (polyethylene oxide of high molecular weight) flowing upward through a nominally 0.4 inch diameter tube which was heated by the passage of alternating current electricity through the tube walls. Friction coefficients were determined from fluid flow rate and pressure drop measurements, and the heat transfer coefficients were determined from measurements of heating power, outside tube wall temperatures and fluid temperature. Although the present results are restricted to one type of roughness and to other simplifying conditions, it is expected that in many cases of practical interest the conditions of these experiments will be met closely enough to permit direct use of the data obtained, or at least of the clear trends exhibited by the latter.

Chapter II

SURVEY OF PREVIOUS WORKS

A. General Comments

In many previous reports it has been shown that under certain conditions of turbulent flow, very small amounts of certain solutes can produce a very significant reduction in friction drag: with these dilute solutions, a lower pressure gradient is needed to maintain the same flow rate, or a higher flow rate can be attained for the same pressure gradient as the pure solvent. This effect, called Toms phenomenon, after Toms who first discovered it in a solution of polymethylmethacrylate in monochlorobenzene [59] has received considerable attention in recent years and extensive tests on the reduction of friction in pipes as well as with rotating disks with a variety of solutes were carried out. The purpose of this chapter is to describe the main features of the Toms effect and to provide the background for some of the assumptions which have been made in developing an analytical model (Chapter III).

An important class of solutes that produces drag reduction is constituted by a large number of polymers diluted in a suitable solvent The term polymer (coming from the Greek "polys" meaning many and "meros" meaning part) designates a large assembly of identical subunits linked by covalent bonds to make a single large molecule. A "linear polymer" is an unbranched chain represented schematically as

$$P'-P-P-P-P-\cdots-P''$$

where the monomer units P are all identical, and the terminal units P′ and P″ have essentially the same composition as P, but are monovalent.

Polyox (polyethylene oxide), the polymer that was used in the present experiments, is an example of a linear polymer. It can be represented as

$$C_2H_5O-C_2H_4O-C_2H_4O-C_2H_4O-\cdots\cdots-C_2H_5O.$$

The monomer unit, C_2H_4O has the following linear assemblage

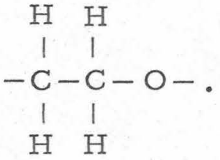

$$\begin{array}{ccccc} & H & & H & \\ & | & & | & \\ - & C & - & C & - O - . \\ & | & & | & \\ & H & & H & \end{array}$$

Branched polymers will be schematically represented as

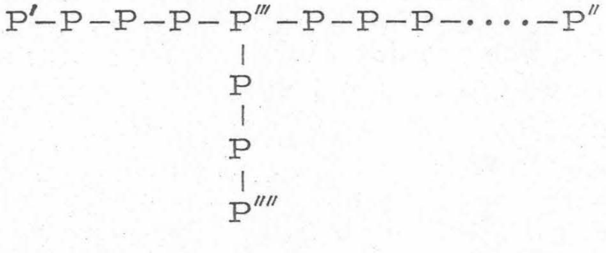

$$\begin{array}{l} P'-P-P-P-P'''-P-P-P-\cdots\cdots-P'' \\ \qquad\qquad\qquad\quad | \\ \qquad\qquad\qquad\quad P \\ \qquad\qquad\qquad\quad | \\ \qquad\qquad\qquad\quad P \\ \qquad\qquad\qquad\quad | \\ \qquad\qquad\qquad\quad P'''' \end{array}$$

We will see later that the polymer structure seems to be closely related to its efficiency as a friction reducer. The size of a polymer molecule in solution can be characterized by an average end-to-end distance h_{av} defined as the root mean square average distance between the ends of the polymer chain for all possible configurations, taking into consideration the interaction between components of the chain elements and the relative attraction between polymer components and solvent molecules, or by a fully extended length h_{ex}, defined as the length of a chain stretched out on a plane to give the maximum possible extension, taking into account the angular relationships involved in each type of bond present in the molecule. These two quantities have been evaluated for Polyox of $\cong 4 \times 10^6$ molecular weight in water [53, 58],

$$h_{av} \simeq 3600\,\mathring{A} = 0.00036 \text{ mm.}$$

$$h_{ex} \simeq 357000\,\mathring{A} = 0.035700 \text{ mm.}$$

Thus the length of a polyox molecule in water seems to be of the order of a hundredth of mm.

Other substances than polymer solutions also exhibit drag reduction. Among these are soap-like chemicals, [45, 51, 69], fibers and mucous or slime secreted by living materials (algae). [29].

B. Main Features of Toms Phenomenon and Review of Friction Data

When one increases the flow rate of a dilute polymer solution and simultaneously records the pressure drop over a certain length of a smooth pipe, one recognizes the following distinct regimes [66].

a) First the flow is laminar and the polymer solution behaves like the pure solvent, except for a very slight increase in the viscosity.

b) Then the transition between laminar and turbulent regimes occurs. There is little doubt that the polymer additives affect the transition. Although Virk [65] (working with Polyox) did not observe a delay of transition, Castro [5] (working with a family of Polyox), Chung [6] (Polyox and Separan) and W. D. White [71] (Polyox and

Separan) among others agree to conclude that the presence of polymer in solution shifts the transition to turbulent flow to a higher flow rate than for pure solvent. This shift depends on the molecular weight and concentration of the polymer, as well as on the degree of degradation (or age) of solution. (The problem of age and degradation of a solution will be discussed later in this chapter).

c) As one increases the flow rate, the friction loss of the solution at first follows the trends of the pure fluid in fully developed turbulent flow.

d) Finally drag reduction begins and the polymer solution exhibits the Toms' effect.

It should be emphasized that the drag reduction only occurs in turbulent flow regime — never under laminar flow conditions — and that moreover there is a critical wall shear stress below which drag reduction does not take place. Qualitatively the extent of drag reduction increases with increasing flow rate, until a maximum drag reduction asymptote is reached. Sometimes the onset shear stress below which there is no drag reduction lies in the transition region from laminar to turbulent flow and drag reduction occurs immediately as turbulent flow is attained [26, 51].

The onset of drag reduction has received much attention and several hypotheses have been proposed to explain what mechanisms could trigger this major modification in the turbulent flow structure.

It is well accepted now that the onset of drag reduction is associated with a critical shear stress [66]. The Toms' phenomenon will start at a well defined wall shear stress $\tau_{0_{cr}}$, depending on:

a) The nature of the polymer: $\tau_{0_{cr}}$ seems to be approximately inversely proportional to molecular weight [65]. Nevertheless, polymers of equal molecular weight but of different monomeric structures begin to reduce friction at a different onset shear stress. The onset of drag reduction seems to be strongly related to the number of links in the macromolecular backbone.

b) The nature of the solvent: The molecules in "good" solvents tend to expand while those in "poor" solvents tend to contract. The onset of drag reduction in the poorest solvent occurs at a significantly higher wall shear stress. This suggests that it is more significant to characterize polymers for drag reduction by a conformational parameter (such as the rms radius of gyration of polymers in solution) rather than by a configurational one (such as the molecular weight).

On the other hand, the critical shear stress seems fairly independent of the concentration [65] and pipe diameter [66]. Note that ageing the solutions increases somehow the threshold stress [69].

The absence of anomalous effects in the laminar regime and the abruptness of the onset of drag reduction in turbulent pipe flow suggests an explicit connection between the turbulent flow field and the macromolecule in solution. Although the basic nature of the polymer - turbulence interaction is unclear, two hypotheses deserve attention: the time hypothesis (Elata [14], Fabula [16]) and the length hypothesis (Virk [64]). We shall briefly compare these two hypotheses.

a) Time Hypothesis

The time hypothesis is essentially based on the viscoelastic properties of the polymer solutions. It is suggested that under high shear rates, the flexible polymer molecules become greatly extended and stiffer than in a low shear rate field, and may damp down local velocity fluctuations. Such high shear rates do exist in the laminar sublayer. Elata argues that when the shear rate du/dy becomes greater than the inverse of the fundamental relaxation time of the molecule $1/t_1$, the macromolecules start to affect the flow in the sublayer by damping the high frequency disturbances. The onset criterion is then

$$\frac{\tau_{0_{cr}}}{\mu} t_1 = 1 = c_t \; .$$

Following Fabula, and according to the theories of Rouse and Sittel [49] and Tschoegl [62], t_1, fundamental relaxation time of the macromolecular coil is given by

$$t_1 = a_1 \mu_s \, \frac{100\,[\eta]\,M}{RT}$$

where

a_1 is taken equal to 1/2

μ_s = solvent viscosity

$[\eta]$ = zeroshear intrinsic viscosity in 100 cc/g

M = molecular weight of the polymer

R = gas constant

T = temperature.

This onset criterion predicts that $\tau_{0_{cr}}$ will depend on the concentration (through the viscosity), the temperature (through the viscosity and T) and will vary as the inverse of the molecular weight. One can also show that

$$\tau_{0_{cr}} \propto \left(R_G^2\right)^{-3/2}$$

where R_G = rms radius of gyration of the molecule.

b) Length Hypothesis

Virk [64] suggests that the onset of friction reduction corresponds to a turbulent scale (characteristic of the smallest eddies near the pipe wall) becoming small enough with respect to a macromolecule scale, which is chosen as twice the rms radius of gyration R_G of the random coiling macromolecule in dilute solution (i. e., in which the conformation of an individual macromolecule is unaffected by its neighbours).

A dissipation wavenumber k_d with dimension of inverse length is used to scale the turbulence: $k_d = ku_\tau/\nu$ where k is a dimensionless quantity depending on y^* and u_τ is the shear velocity, defined as $\sqrt{\tau_{w/\rho}}$. "k" is evaluated at $y^* = 10$, where the dissipation of turbulent energy is near the maximum, and is found, from Laufer's data [32] to be equal to approximately 0.2 (a Newtonian spectrum is used since the polymer solution behaves like a Newtonian fluid before the onset of drag reduction occurs).

The onset criterion is then

$$2R_G \frac{k}{\nu}\sqrt{\frac{\tau_w}{\rho}} = C_\ell$$

where C_ℓ, ratio of the dimensions of the macromolecule and the fine scale of the turbulent shear flow is expected to be a universal dimensionless constant.

It follows from this hypothesis that $\tau_{0_{cr}}$ will depend only slightly on concentration (through ν), will vary with temperature (through ν) and inversely as R_G^2. It will also be independent of the pipe diameter.

If we compare now these two hypotheses, we see that both theories predict the onset of drag reduction when a dimensionless ratio of two times or lengths characteristic of the macromolecule and the flow reaches a constant value (C_t or C_ℓ). In the time hypothesis, one expects $\tau_{0_{cr}} \propto (R_G^2)^{-3/2}$ while in the length hypothesis, $\tau_{0_{cr}} \propto (R_G^2)^{-1}$. Furthermore, both theories predict a concentration dependence (not present in experimental data) and a temperature effect. From the existing data, Virk [66] has calculated C_t, using linear viscoelastic theories to compute t_1. He found that this dimensionless ratio varies from 0.036 to 3.33 suggesting that the criterion $(u_\tau^2/\nu)t_1 = 1$ is questionable. Nevertheless the value of the ratio C_t indicates that the macromolecular relaxation time t_1 is of the same order of magnitude as the turbulence time scale. C_ℓ, calculated from available data, turns out to be remarkably constant for a large variety of polymer-solvent systems but is found close to $C_\ell = 0.0025$. This low value of the ratio of macromolecule to dissipative eddy size at onset suggests that the individual macromolecules are too small to interfere with the turbulent structure in a particulate manner. Yet, Virk found that the best correlation between $\tau_{0_{cr}}$ and R_G^2 follows a law in $(R_G^2)^{-1}$, which is what the length hypothesis predicts. It should be pointed out that the estimates of the macromolecular and turbulence scales are uncertain, so that the successful fitting of Virk's hypothesis to the experimental data remains worthy of interest. It is also possible that the macromolecules are in fact not individually dispersed, but that, as suggested by Barenblatt [3], some of the surrounding solvent molecules are entrapped by the polymer molecules, or that several molecules become mechanically interlinked to form clusters or networks. These macromolecular entanglements would be big enough to interfere with the turbulent structure.

From the numerous tests performed with a wide variety of natural and synthetic polymers, it appears that for a given concentration, the most effective polymers as drag reducing agents are very soluble long-chain materials having an essentially unbranched structure, of high molecular weight [29]. Polyox in water known as a very efficient drag reducer satisfies these three criteria. For a given polymer-solvent system, the fractional drag reduction, defined by

$$R_F = \left(1 - \frac{\tau_{0_p}}{\tau_{0_s}}\right)_{\dot{w}}$$

(where τ_{0_p} and τ_{0_s} are the wall shear stresses in polymer solution and solvent respectively at flow rate $\dot{w}$), increases initially with increasing concentration but tends to a maximum value $R_{F_{max}}$ at high concentration [65]. Thus there exists a high concentration asymptote limiting the maximum obtainable drag reduction.

So far in this chapter, the principle features of the Toms' phenomenon have been described qualitatively. The polymer molecules dissolved in an appropriate solvent somehow modify the structure of the turbulent flow with, as a result, a reduction of the shear stress at the wall. A first step toward the understanding of the physics of the phenomenon is to consider velocity profiles of polymer solutions in pipe flow and compare them with those of the pure solvent.

As a basis for discussing some experimental results with dilute polymer solutions, Prandtl's two layers model [42] will be taken. For a Newtonian fluid, in the viscous sublayer

$$\frac{u}{u_\tau} = \frac{yu_\tau}{\nu}$$

in the turbulent core

$$\frac{u}{u_\tau} = \frac{1}{\varkappa} \ln \frac{yu_\tau}{\nu} + \text{const.}$$

at the edge of the sublayer

$$\frac{u_L}{u_\tau} = \frac{y_L u_\tau}{\nu} = \frac{1}{\varkappa} \ln \frac{y_L u_\tau}{\nu} + \text{const.}$$

Determining the constant from the condition at the edge, integrating the velocity profile valid in the turbulent core over the whole pipe cross section, (neglecting the flow through the sublayer as small) and using the definition of the Fanning friction factor yields

$$\frac{1}{\sqrt{C_F}} = \frac{1}{\varkappa\sqrt{2}}\left[\ell n\,\frac{Re}{2}\sqrt{\frac{C_F}{2}} + \varkappa\, Re_L - \ell n\, Re_L - \frac{3}{2}\right]$$

where

$Re_L = \frac{y_L u_\tau}{\nu}$ = sublayer Reynolds number, which is found to be $\simeq 11.6$ for Newtonian fluids.

If we assume now that such a model still holds for polymer solutions, we immediately see from the latter equation that a reduction of the friction factor must be due to an increase of Re_L (i. e., a thickening of viscous layer) or a reduction of $\varkappa$ (mixing length constant) or both.

Numerous velocity profiles for a large variety of polymers are available in the literature and if they all seem to exhibit a thickening of the viscous region, yet they don't allow a definite conclusion on whether the mixing length constant (or the slope of the logarithmic profile) is modified by the addition of polymers. One reason is that these measurements are extremely delicate to perform. The use of Pitot-static tubes, together with Bernoulli's equation appears questionable for these solutions because of possible effects due to normal stresses and shear-dependent viscosities [18]. The film anemometer probes used to measure the fluctuating velocity components of a turbulent field exhibits anomalous behavior as well [18], which means that these probes cannot generally be used to measure velocity, and interpretation of turbulence measurements would seem to be open to question. A more recent technique, the laser Doppler velocimeter [17, 21] seems more appropriate for velocity profile measurements, but the accuracy of the data leaves somewhat to be desired, at least in small diameter tubes.

Elata [14], using a Pitot tube, performed measurements of velocity profiles with guar gum for concentrations from 0 up to 10,000 wppm in water. The data show clearly a thickening of the viscous layer, but no change in the slope of the logarithmic profile in the central region of the pipe. On the other hand, Wells [67], using guar gum (500 to 4000 ppm) in water concluded that in addition to a thickening of the viscous layer, the Prandtl mixing length constant was decreased. The slope of the logarithmic profile was believed to be a function of the Re and pipe diameter, as well as polymer concentration. However, a reevaluation of his results has been made by W. Meyer [36] to show that actually the same data could be interpreted to show the value of the mixing length constant to be unchanged. Fabula [16] discusses Wells' results as well.

Ernst [15], working with a dilute concentration (500 ppm) of CMC 7 HSP in water found a thickening of the laminar and buffer layers near the wall, but an unchanged turbulent core. This contradicts the data due to Shaver and Merrill [52], working with higher concentrations of CMC (above 0.18%), which clearly show a modification in the slope of the logarithmic profile. Virk [65], working with Polyox N 3000, claims that the mixing length constant is essentially unchanged, while Goren [22] working with Polyox WSR 301 believes in a decrease of the mixing length constant near the wall for $0 < \frac{y}{R} < 0.25$, but concludes that the velocity defect law is similar for water as for Polyox in the region between $y/R = 0.25$ and centerline.

Recent data of velocity profiles obtained with a laser Doppler velocimeter seem to conclude in favor of an unchanged defect law.

This brief review of some of the papers published on measurements of velocity profiles illustrates that there remains some uncertainty as to the effect of polymers on the defect law. All these measurements were made in smooth tubes. Only a few data are available in rough tubes.

A. White [68] tested Polyox WSR 301 in a threaded pipe, the ratio of the depth of the thread to the pipe diameter being of the order of 0.1 over a range of Re from 2000 to about 40,000 and a range of concentration of 0 to 66 ppm. He found that the Polyox additive results in a drag reduction (when compared to the similar drag for water) for all except the very lowest concentrations. These results are confirmed by McNally [35]. The roughness used in these experiments was so extreme that fully rough flow is apparently established at a relatively low Re. On the other hand, the same experiments performed with guar gum solutions (concentrations of 240 and 480 ppm) didn't show any sign of drag reduction. Spangler [56], using Polyhall (an anionic copolymer of polyacrylamide and polyacrylic acid with a molecular weight of 5 - 6 million) at a concentration of 31 ppm found the onset of the roughness effect delayed from that for water. At flow below that corresponding to the onset, the friction factor was equal to that of a smooth wall. Moreover, the percentage friction reduction in rough pipes initially increases with Re, reaching a maximum in the transition roughness regime and then decreases with further increase in Re until little or no net friction reduction is realized in the fully rough regime. For small roughnesses, the net drag will be even less in part of the transition regime than for Newtonian fluids at the same Re in smooth pipes. All these trends are dependent on the height of the protrusions, the concentration and the polymer. Data for CMC (sodium carboxymethyl-cellulose) are available in [4].

A next step toward a better understanding of the mechanism(s) involved in drag reduction consists in measuring the rms intensity and the spectral distribution of turbulent energy for the axial as well as radial velocity components. The conclusion to be drawn from these spectra observations [6, 30, 56, 65] is that the principal effects of the polymer additives seem to be confined to the high wave number region of the turbulent spectrum, the turbulent energies being lower at high wave number range than those found for water, when measured close to the wall. Very little difference in the water and polymer spectra is seen at the centerline. This would lead us to the conclusion that the small scale turbulence (characterized by a high wave number) is somewhat damped out near the wall by the polymer additives.

Before we review the current data on heat transfer with polymer solutions, a word must be said about the mechanical and thermal degradation of polymer solutions, as well as their degradation with age.

Mechanical degradation has been observed by many investigators using a wide variety of polymers. Drag reduction and degradation properties were systematically studied by Poreh et al [40]. The standard test was a 120 minute run in a closed circulating system and the head loss was measured every few minutes. The results of the tests clearly indicate that one can divide the polymers tested into two general groups according to their degradation properties. One group of polymer additives gives stable solutions which only show very little degradation (constant drag reduction with time). Guar gum is the most efficient polymer of this group, in terms of drag reduction. The second group of polymers degrades continuously. However, very large drag reductions are still obtained even after the solutions show the first signs of degradation. The most effective polymers of this group are Polyhall 654, Polyox WSR 301 and Separan AP 30. (See Table 1, p. 100 of [40] for the complete list of polymers tested, as well as the companies manufacturing them). Note that the shear degradation suffered by many solutions makes more ambiguous the analysis of the data obtained at a high shear level. This problem will be discussed later in Chapter VI.

Numerous data for Polyox solution degradation at different concentrations are available in the literature [19, 20] (for instance). Several days aged Polyox solutions tested in pipe flow are still very effective in reducing turbulent skin friction but, as noted by Brennen and Gadd [20], they loose the elastic effects exhibited by the fresh solutions (measureable second normal stresses differences). Since "ageing" can be greatly speeded up even by a fairly gentle mixing [20] it seems that the performance of some dilute polymer solutions depends much on the mixing procedure. Differences in preparing the solutions may account for many of the anomalous results which are numerous in the literature.

Only few data exist in the literature about the effect of temperature on the drag reducing effectiveness. Tests conducted by Pruitt [44] with Polyox, polyacrylamide and guar gum at four concentrations and at temperatures of 35°F, 70°F, 105°F and 140°F show that the maximum drag reduction was obtained at temperatures less than 105°F and at 140°F, solutions of all three polymers suffered a decrease in drag reduction (thermal degradation). According to W. D. White [71], the drag reduction effectiveness of high-molecular weight polymers is not a direct function of temperature.

C. Review of Heat Transfer Data

Some experimental work on heat transfer with drag reducing fluids has been performed but the literature on this subject is not extensive and the range of variables (Reynolds number, Prandtl number, concentration, different drag reducing agents, range of roughness) is quite limited. One of the first heat transfer studies in this field was that by Gupta, Metzner and Hartnett [24] and their work clearly shows the reduction in heat transfer coefficient which accompanies the reduction in friction. They were using a water soluble partially hydrolyzed polyacrylamide of high molecular weight (ET 597, Dow Chemical Co.)

at concentrations from 0.01 to 0.8% in a 0.745 in I. D. smooth tube. Their experimental results show that at a given flow rate, the reduction in heat transfer rates is greater than the reduction in the turbulent drag or pressure drop. Note that they compared at the same velocity the data of their solutions with that of the solvent, but failed to consider the difference in viscosity (quite important in this case) which might lead to a misinterpretation of the reduction of both momentum and heat transfer. Using data gathered at 17 different axial stations, they systematically studied the thermal entry length characteristics for their solutions and concluded that at higher concentrations of ET 597 (0.05% and up), thermal entry lengths values exceeded the Newtonian values (10 to 25 diameters) and went up to 45 diameters for a 0.45% concentrated solution. Also presented in the paper is a method of analysis of the data (following Reichardt's approach) which allows some insight into the transfer mechanism, particularly close to the wall where the most important changes in velocity and temperature occur. The same polymer at concentrations of 600 and 1000 ppm was used by Marrucci and Astarita [34] and their data can be reduced to

$$j = C_H \times Pr^{2/3} = 0.6\, C_F/2$$

where j is the Colburn factor.

McNally [35] working with Polyox WSR 301 at concentrations of 2, 10, 20 and 40 ppm in a 0.78 in. I. D. smooth pipe over a 25,000 to 167,000 Reynolds number range concluded that the heat transfer coefficients were reduced as drastically as the friction factor, the

Colburn analogy $j = C_H \times Pr^{2/3} = C_F/2$ satisfactorily relating the heat and momentum transport in these solutions, provided a normalization with respect to the onset Reynolds number is made. Smith, G. H. Keuroghlian, Virk and Merrill [55], using Polyox WSR 301 as well (10 ppm) found that only the heat transfer coefficient corresponding to the maximum heat transfer obtained with the polymer solutions obeyed a Colburn type analogy

$$C_H \times Pr^{0.6} = C_F/2.$$

Experimental data of C_F and C_H with Polyox WSR 301 for concentrations of 5, 12.5, 50 and 100 ppm at temperatures of 65° and 40°F are also available in [27, 28]. This set of data, however, contains considerable scatter. In addition, the range of Reynolds number is limited to about 30,000.

The only set of heat transfer data in rough pipe which was found in the literature is that due to A. White [70]. Using a threaded pipe of extreme roughness, he found that whereas the Polyox reduced the friction factor considerably, the Stanton number was reduced by an even greater amount. He concluded that ϵ_H reduces more than ϵ_M. This point will be discussed in a future chapter.

A certain number of analyses have been conducted predicting friction coefficients as well as heat transfer coefficients. Some of these approaches will be analyzed in Chapter V.

Chapter III

FUNDAMENTALS

The analysis developed in this section is limited to the following conditions:

1) fully turbulent steady pipe flow
2) hydrodynamically fully established flow in which the mean fluid motions are invariant with axial station
3) thermally fully established conditions whereby the radial temperature profile referenced to the local wall temperature is independent of axial location
4) constant fluid properties, density (ρ), viscosity (μ), thermal conductivity (k), specific heat (C_p)
5) surface roughness patterns which are statistically independent of circumferential or axial position and geometrically similar from tube to tube with only a geometrical scale factor being different.

These conditions were well approximated in similar experiments conducted by D. Dipprey [10], who investigated the heat and momentum transfer in the same smooth and rough tubes, but with a Newtonian fluid (pure water). A few authors (Castro [5]; Chung [6]; W. D. White [71] among others) observed a delay of the transition from laminar to turbulent regime, when a small amount of polymer is added to water, and they also found that, for a given ratio of entrance length to diameter, hydrodynamically fully established flow is reached at a higher Reynolds number with Polyox than with Newtonian fluids [6]. In the present experiments, however, Conditions (1) and (2) are satisfied as the minimum Re used was larger than 10,000. The thermal entrance-length required to obtain fully developed heat transfer with diluted polymer solution, although slightly exceeding the Newtonian values, is found to be of the same order of magnitude as the latter [24]. In the present experiments, the temperature measurements are taken at a station about 40 diameters away from the entrance of the heated tube, so that Condition (3) is also satisfied [9, 25]. Condition (4) was approached by keeping the wall to bulk temperature difference in the neighbourhood of 10° F, and by extrapolating the data to a zero heat flux. Photomicrographs of samples of each tube taken by Dipprey revealed that Condition (5) was reasonably approximated (see Figures 6, 7, 8).

A dimensional analysis has been developed for heat and momentum transfer of Newtonian fluids in smooth and rough pipes [10, 61]. The purpose here is to extend these existing theoretical notions to the flow of Polyox solutions and develop a relationship between the friction coefficient C_F and the heat transfer coefficient C_H.

These coefficients are defined as

$$C_F = \frac{2\tau_0}{\rho \overline{u}^2} \tag{1}$$

$$C_H = \frac{\dot{q}_0}{\rho \overline{u} C_p (T_w - T_L)} \tag{2}$$

where

$\overline{u}$ = tube discharge velocity, defined as

$$\overline{u} = \frac{2}{R^2} \int_0^R u(r) r \, dr \tag{3}$$

R = pipe radius

τ_0 = shear stress at wall

ρ = density

$\dot{q}_0$ = local heat flux

T_w = tube wall temperature

T_L = mixed-mean fluid, defined by

$$T_L = \frac{2}{R^2 \overline{u}} \int_0^R T(r) u(r) r \, dr \tag{4}$$

C_p = specific heat of fluid.

The friction coefficient C_F is the ratio of the shear stress τ_0 to the dynamic pressure $\frac{\rho \overline{u}^2}{2}$. It can also be considered as the ratio of the momentum transferred across the stream to one half of the momentum carried by the fluid in the direction of the stream. C_H appears as the ratio of the heat flux across the stream and the heat carried per unit cross-sectional area by a fluid of temperature T and velocity $\overline{u}$.

In order to calculate C_F, as well as C_H, one must calculate $\overline{u}$, which, in turn, requires the knowledge of the velocity profile. The first concern will be to examine u(r).

A. Velocity Profile

For a fully turbulent steady pipe flow in which all average velocities have the same direction parallel to the x-axis, a time averaging of the momentum equation for pipe flow gives

$$\frac{\tau}{\rho} = -\overline{u'v'} + \nu \frac{du}{dy} . \tag{5}$$

From an overall force balance on the flow, it is easy to show that the shear distribution over the cross section of the tube is linear, so that

$$\tau = \tau_0 \left(1 - \frac{y}{R}\right) \tag{6}$$

where

τ_0 = shear stress at wall
y = distance from wall
R = tube radius.

Combining (5) and (6)

$$\frac{\tau_0}{\rho}\left(1 - \frac{y}{R}\right) = -\overline{u'v'} + \nu \left(\frac{du}{dy}\right) \tag{7}$$

which relates the turbulent shear stress $\rho\overline{u'v'}$ and the mean velocity profile u(y) with the shear stress at the wall as a parameter.

Similarity arguments presented by Townsend [61] and valid for smooth as well as rough pipes enable us to describe the velocity profile and hence the $\overline{u'v'}(y)$ dependence over part of the flow.

First the Reynolds number similarity principle states that there exists, in a turbulent flow at high Re, a region in which the direct effect of viscosity on the mean flow is negligible. In other words, in this region

$$-\frac{\overline{u'v'}}{\frac{du}{dy}} >> \nu \qquad (8)$$

For the case of turbulent pipe flow, this similarity principle holds in regions outside of the vicinity of the wall. In the very vicinity, the turbulent term $\overline{u'v'}$ is damped by the wall so that the molecular term $\nu \frac{du}{dy}$ is predominant.

Thus we can divide the flow into three regions:

(1) A region adjacent to the wall, where the flow is predominantly governed by viscous forces. We will assume that this region does not extend too far from the wall, so that $y/R << 1$ remains a fair approximation and $\tau = \tau_0$. This region will be referred to as "constant shear stress region".

(2) A central flow region wherein shearing stresses are negligible compared with the turbulent stresses (Reynolds number similarity principle). Following the previous assumption, the bounding shear stress of that region is τ_0.

(3) A region of overlap within which viscous forces are negligible and constant shear stress assumed.

Let us follow Townsend to describe the velocity profile in these three regions.

(1) Constant Shear Stress Region

Considering the equation for the turbulent energy, Townsend shows that the production of turbulent energy by the mean flow takes place mainly within the region of nearly constant shear stress, very near the wall. He is then led to the conclusion that the velocity in the neighbourhood of the wall must be determined by the conditions at the wall, the fluid properties and the distance from the wall. The quantities which might be expected to be relevant to describe u(y) in this system are thus

y = distance from the wall
τ_0 = wall shear stress
ε = average height of roughness elements of differing scale
ρ_s = solvent density
ρ_p = density of dispersion of polymer molecules in solvent
ν = solution viscosity
p = a parameter characterizing the polymer in solution.

As mentioned in Chapter II, the most common concepts used in explaining drag reduction are the length hypothesis and time hypothesis. The general idea of these attempts to describe the Toms effect is that drag reduction occurs when the turbulent flow field starts to interact with the macromolecules in solution. In the length hypothesis, it is assumed that the macromolecules, individually or aggregated, interfere with the turbulence structure. The macromolecular length ℓ_1, chosen as the double of the radius of gyration of the coil, is the suitable parameter to select for p. In the time hypothesis it is argued that the polymer molecules will interact with the flow field when the shear rate $\frac{du}{dy}$ is greater than the reverse of the fundamental relaxation time of the macromolecular coil. This relaxation time t_1 is then an appropriate parameter to characterize the polymer in solution.

A more general way of thinking in terms of the time hypothesis is to say that the Toms phenomenon occurs first when the shear rate very close to the wall becomes greater than a threshold value

$$\left.\frac{du}{dy}\right|_{cr} .$$

Following this thought, it is no longer necessary to postulate that this value is equal to the inverse of a fundamental relaxation time of the polymer molecules, but one only needs to think of $(du/dy)_{cr}$ as a characteristic of the polymer in solution. Since very close to the wall $\overline{u'v'}$ appearing in Eqn. (5) is negligible compared to $\nu \frac{du}{dy}$,

$$\nu \left.\frac{du}{dy}\right|_{cr} = \left.\frac{\tau_0}{\rho}\right|_{cr} = u_{\tau_{cr}}^2$$

where u_τ is the shear velocity, defined as

$$u_\tau = \sqrt{\frac{\tau_0}{\rho}} . \tag{9}$$

Thus this reasoning leads us to choose $u_{\tau_{cr}}$ as a characteristic parameter to describe the polymer in solution. We mentioned previously that the onset of drag reduction is indeed found experimentally to occur at a value of τ_0, well defined for each polymer at a given temperature.

We shall summarize this discussion by saying that p is described either by a characteristic length ℓ_1 (length hypothesis), or a characteristic time t_1 or a characteristic velocity $u_{\tau_{cr}}$ (time hypothesis). It should be kept in mind that the action of the polymer in the flow is probably very complex and can hardly be described by only one relevant parameter. Nevertheless this approach constitutes a good starting point in describing the polymer. Thus, the relevant characteristics to consider in the constant stress region are

$$\begin{aligned} & u\left[LT^{-1}\right],\ y\left[L\right],\ \epsilon\left[L\right],\ \tau_0\left[ML^{-1}T^{-2}\right],\ \rho_s\left[ML^{-3}\right] \\ & \nu\left[L^2T^{-1}\right],\ \rho_p\left[ML^{-3}\right],\ \ell_1\left[L\right] \text{ or } t_1\left[T\right] \text{ or } u_{\tau_{cr}}\left[LT^{-1}\right]. \end{aligned} \qquad (10)$$

These quantities represent eight variables measured in terms of three fundamental dimensions. According to the Π theorem, which states that "a relationship between m different variables can be reduced to a relationship between m-n groups of variables which are dimensionless in terms of the n fundamental dimensions in which the variables are measured", we can describe the velocity profile in that region in terms of 8-3 = 5 dimensionless groups. These groups are chosen as

$$\begin{aligned} & \frac{u}{\sqrt{\frac{\tau_0}{\rho}}},\ \frac{\sqrt{\frac{\tau_0}{\rho}}\,y}{\nu},\ \frac{\sqrt{\frac{\tau_0}{\rho}}\,\epsilon}{\nu},\ C=\frac{\frac{\rho_p}{\rho_0}}{1+\frac{\rho_p}{\rho_0}}, \\ & \frac{\frac{\tau_0}{\rho}\,t_1}{\nu} \text{ or } \frac{\sqrt{\frac{\tau_0}{\rho}}\,\ell_1}{\nu} \text{ or } \frac{\sqrt{\frac{\tau_0}{\rho}}}{\sqrt{\frac{\tau_0}{\rho}}_{cr}} \end{aligned} \qquad (11)$$

and we can write

$$\frac{u}{u_\tau}=f_1\left[y^*,\ \epsilon^*,\ C,\ P\right] \qquad (12)$$

where

$$u_\tau = \sqrt{\frac{\tau_0}{\rho}}$$

$$y^* = \frac{yu_\tau}{\nu}$$

$$\epsilon^* = \frac{\epsilon u_\tau}{\nu}$$

$$P = \frac{u_\tau^2 t_1}{\nu} \text{ or } \frac{u_\tau \ell_1}{\nu} \text{ or } \frac{u_\tau}{u_{\tau_{cr}}}$$

P is a function of u_τ times a constant, regardless of the parameter (ℓ_1, t_1 or $u_{\tau_{cr}}$) selected to describe the polymer in solution. Its precise description is not necessary for the derivation of the equations contained in this chapter.

(2) Core Region

The statement of the Reynolds number similarity for the core region states that the viscous forces are negligible. This leaves only the shear stress τ_0 — assuming that the central flow regime extends to a region close enough to the wall that y/R remains $<< 1$ and $\tau = \tau_0$ is the bounding shear stress —, the roughness height ϵ, the tube diameter D and the fluid properties excluding viscosity, ρ_0, ρ_p defined previously and a parameter describing the effect of the polymer on the turbulent core. The nature of turbulence is very different in the turbulent core than it is close to the wall and one might expect the polymer to interact with the flow in a different fashion in these two regions. Therefore, the parameter characterizing the polymer near the wall might no longer be relevant in the turbulent core. That polymer characteristic will be called p' in the turbulent core. It will turn out that its specific nature is not of primary importance in the derivation of the law governing the motion in that region.

Thus the following parameters will be considered in the region outside of the vicinity of the wall

$$u\left[LT^{-1}\right],\ y\left[L\right],\ D\left[L\right],\ \varepsilon\left[L\right],\ \tau_0\left[ML^{-1}T^{-2}\right],\ \rho_s\left[ML^{-3}\right],\ \rho_p\left[ML^{-3}\right],\ p'. \tag{13}$$

These are now seven variables expressed in three fundamental variables. Following the Π theorem a relationship between these seven variables can be reduced to a relationship between five dimensionless groups. These groups are

$$\frac{u-u_t}{\sqrt{\frac{\tau_0}{\rho}}}\ ,\ \frac{y}{D}\ ,\ \frac{\varepsilon}{D}\ ,\ C\ ,\ P' \tag{14}$$

and, therefore,

$$\frac{u}{u_\tau}=\frac{u_t}{u_\tau}+f_2\left[\frac{y}{D},\frac{\varepsilon}{D},C,P'\right] \tag{15}$$

where P' is a dimensionless group containing the parameter p' of the polymer in solution. The translation velocity u_t must be included in Eqn.(15) since the zero velocity at the wall cannot be used as a reference, the wall being outside of the region in which the equation is valid. This translation velocity will be defined later.

(3) Overlap Region

The region of overlap is defined as that region within which viscous forces are negligible (fully turbulent region) and constant shear stress can be assumed, and thus in which both Reynolds number similarity and wall similarity should hold.

In that region, the velocities given by Eqns. (12) and (15) should coincide

$$\frac{u}{u_\tau} = f_1\left[\frac{yu_\tau}{\nu}\ ,\ \frac{\varepsilon u_\tau}{\nu}\ ,\ C\ ,\ P\right] \tag{16a}$$

$$\frac{u}{u_\tau} - \frac{u_t}{u_\tau} = f_2\left[\frac{y}{R}\ ,\ \frac{\varepsilon}{R}\ ,\ C\ ,\ P'\right]. \tag{16b}$$

Let now u_t/u_τ be the value taken by the function f_1 at the centerline (which is not necessarily the actual velocity at $y=R$). Taking the difference between Eqns. (16a) and (16b)

$$\frac{u_t}{u_\tau} = f_1\left[\left(\frac{y}{R}\right)\left(\frac{Ru_\tau}{\nu}\right),\ \frac{\varepsilon u_\tau}{\nu},\ C,\ P\right] - f_2\left[\frac{y}{R},\ \frac{\varepsilon}{R},\ C,\ P'\right]$$

$$= f_1\left[\frac{Ru_\tau}{\nu}\ ,\ \frac{\varepsilon u_\tau}{\nu}\ ,\ C,\ P\right]$$

from the definition of u_t/u_τ. Thus the difference between f_1 and f_2 is independent of y/R. In order to satisfy this condition the functions f_1 and f_2 must be of the form

$$f_1 = A(\varepsilon^*, C, P)\,\ell n\, y^* + f_3(\varepsilon^*, C, P) \tag{17}$$

$$f_2 = A(\frac{\varepsilon}{R}, C, P')\,\ell n \frac{y}{R} + f_4(\frac{\varepsilon}{R}, C, P') \tag{18}$$

provided that

$$A(\varepsilon^*, C, P) = A(\frac{\varepsilon}{R}, C, P'). \qquad (19)$$

Now

$$\varepsilon^* = \frac{\varepsilon u_\tau}{\nu}\frac{R}{R} = \frac{\varepsilon R^*}{R}$$

and P' can be expressed as a function of P

$$P' = P'(P).$$

(For instance if a length is chosen to characterize the polymer, $P = P(\ell_1)$ and $P' = P'(\ell_1)$ hence $P' = P'(P)$.) Therefore the condition (19) becomes

$$A\left(R^*\frac{\varepsilon}{R}, C, P\right) = A\left(\frac{\varepsilon}{R}, C, P'(P)\right) \qquad R^* \neq 1$$

This condition will be satisfied only if

$$A = A(C, P). \qquad (20)$$

Finally

$$\frac{u}{u_\tau} = f_1 = A(C, P)\,\ell n\, y^* + f_3(\varepsilon^*, C, P) \qquad (21)$$

$$\frac{u}{u_\tau} - \frac{u_t}{u_\tau} = f_2 = A(C, P)\,\ell n\,\frac{y}{R} + f_4(\frac{\varepsilon}{R}, C, P'). \qquad (22)$$

Taking the difference between the velocities given by (22) at two points y and y_1 which fall within the region of overlap

$$\frac{u - u_1}{u_\tau} = A(C, P)\,\ell n\,\frac{y}{y_1} \qquad (23)$$

which shows that the velocity profile is independent of Re and roughness.

It should be expected that the latter equation can be applied rigorously only to the region of overlap where the flow is fully turbulent but where the shear stress is still substantially constant. Nevertheless, it seems reasonable to assume that the velocity profile given by Eqn. (23), which is independent of f_4 in the overlap region, remains independent of the same function further from the wall. We will assume that the defect law given by Eqn. (23) is still valid outside of the constant stress layer and on out to the center of the pipe. Thus one can write

$$\frac{u_{CL} - u}{u_\tau} = f_5\left(\frac{y}{D}\right) = - A(C, P)\, \ell n\, \frac{2y}{D}. \tag{24}$$

Experimental measurements of velocity profiles with water in smooth and rough tubes as well as with polymer solutions in smooth tubes support this assumption [6, 37, 50, 65] although, apparently no velocity profile has ever been measured in a rough tube with a polymer solution. Furthermore, there is no conclusive experimental proof that the slope of the logarithmic profile is changed by the presence of the polymer in solution, nor that the concentration has any effect on that slope. For that reason it is logical to adopt the same value of A for Polyox as for a Newtonian fluid. This means that the concept of momentum transfer contained in the Prandtl hypothesis [43] remains equally valid.

Equations (21) and (24) are finally written

$$\frac{u}{u_\tau} = A\, \ell n\, y^* + f_3(\epsilon^*, C, P) \tag{25}$$

$$= A\, \ell n\, y^* + B + \Delta B \tag{25'}$$

$$\text{with}\quad \Delta B(\epsilon^*, C, P) = f_3(\epsilon^*, C, P) - B \tag{26}$$

$$\frac{u_{CL} - u}{u_\tau} = - A \ln \frac{2y}{D}. \tag{27}$$

In the smooth case

$$\frac{u}{u_\tau} = A \ln y^* + f_6(C, P). \tag{28}$$

Comparing this equation with the corresponding one for pure water in smooth tubes

$$\frac{u}{u_\tau} = A \ln y^* + B \tag{29}$$

we see that the shift in the velocity profile (smooth tube) due to the presence of the polymer additive is

$$\Delta u^* = f_6(C, P) - B \tag{30}$$

and that Eqn. (28) can be written (smooth case)

$$\frac{u}{u_\tau} = A \ln y^* + B + \Delta u^*(C, P). \tag{31}$$

A relationship for the friction factor may now be deduced.

B. Friction Factor

The Fanning friction factor is defined by

$$C_F = \frac{\tau_0}{\frac{\rho \bar{u}^2}{2}}$$

with

$$\overline{u} = \frac{2}{R^2} \int_0^R u(r) r \, dr$$

where r is the radial location. Following the Nikuradse treatment, [37], it is customary to neglect the very thin region near the wall wherein the velocity deficiency law (Eqn. 27) is invalid. Integrating Eqn. (27) as prescribed by the definition in Eqn. (3), noting that $y/D = \frac{1}{2}\left(1 - \frac{r}{R}\right)$ and converting the variable of integration to $r/R \equiv \eta$ yields the definite integral

$$\frac{u_{CL} - \overline{u}}{u_\tau} = 2 \int_0^1 f_7 \left[\frac{1}{2}(1-\eta)\right] \eta \, d\eta \tag{32}$$
$$= \beta$$

β is independent of the roughness as well as the polymer group.

Nevertheless, all the experimental data (see review of literature) seem to lead to the conclusion that the presence of the polymer in solution actually thickens somehow the part of the flow mainly governed by viscous forces, so that the region where the velocity deficiency law is invalid may not always be negligible in the calculation of the integral in (3). In these cases a piece by piece integration seems necessary at least at low Re in the case of a smooth wall. A one-piece integration is expected to be sufficiently accurate, however, in the smooth case when the Reynolds number is sufficiently high and the same integration procedure will be used for all rough tubes. In performing the piece by piece integration, the simplest two layer model will be adopted (smooth case).

$$\left.\begin{array}{l}\text{In the constant stress region:}\quad 0 \le \eta \le \eta_L \\[1ex] \qquad\qquad u^* = y^* \quad \text{or} \quad u = \dfrac{Ru_\tau^2}{\nu}\,\eta \\[2ex] \text{In turbulent core:}\quad \eta_L \le \eta \le 1 \\[1ex] \qquad\qquad \dfrac{u_{CL}-u}{u_\tau} = -A\,\ell n\,\eta \quad \text{or} \quad u = u_{CL} + Au_\tau\,\ell n\,\eta \end{array}\right\} \qquad (33)$$

these quantities defined as before.

Equation (3) is now written as

$$\bar{u} = 2\int_0^1 u(1-\eta)d\eta = 2\left[\int_0^{\eta_L} u(1-\eta)d\eta + \int_{\eta_L}^1 u(1-\eta)d\eta\right]. \qquad (34)$$

Performing the integrations of Eqn. (34) and using Eqns. (33) yields

$$\begin{aligned} \frac{u_{CL}(1-\eta_L)^2 - \bar{u}}{u_\tau} &= \frac{3}{2}A - f(\eta_L) - \eta_L^2\,\frac{u_\tau R}{\nu} \\ &= G(\eta_L, R^*) \end{aligned} \qquad (35)$$

where $\eta_L = y/R$ is defined by

$$y_L^* = A\,\ell n\, y_L^* + f_6(C, P) \qquad (36)$$

so

$$\eta_L = \eta_L(C, P) \quad \text{and} \quad G = G(C, P, R^*)$$

and

$$f(\eta_L) = 2A\left[\eta_L + \frac{\eta_L^2}{2}\ell n\,\eta_L - \frac{\eta_L^2}{4} - \eta_L\,\ell n\,\eta\right]. \qquad (37)$$

Using Eqn. (32) (rough tubes and smooth tubes at high Re) and the definition of C_F, (Eqn. (1))

$$\begin{aligned}\frac{\bar{u}}{u_\tau} &= \frac{u_{CL}}{u_\tau} - \beta \\ &= \sqrt{\frac{2}{C_F}}\ .\end{aligned} \tag{38}$$

From Eqn. (27)

$$\frac{u_{CL}}{u_\tau} = -A\,\ell n\,\eta + \frac{u}{u_\tau}.$$

But from Eqn. (25)

$$\frac{u}{u_\tau} = A\,\ell n\,\frac{yu_\tau}{\nu} + f_3(\epsilon^*, C, P)$$

hence

$$\frac{u_{CL}}{u_\tau} = A\,\ell n\,\frac{u_\tau D}{2\nu} + f_3(\epsilon^*, C, P)$$

or, with the definition of C_F

$$\frac{u_{CL}}{u_\tau} = A\,\ell n\,\mathrm{Re}\sqrt{C_F} - A\,\ell n\,2\sqrt{2} + f_3(\epsilon^*, C, P).$$

With the aid of Eqn. (38), one may then write

$$\left.\begin{aligned}\sqrt{\frac{2}{C_F}} &= A\,\ell n\,\mathrm{Re}\sqrt{C_F} + f_3(\epsilon^*, C, P) - A\,\ell n\,2\sqrt{2} - \beta \\ \sqrt{\frac{2}{C_F}} &= A\,\ell n\,\mathrm{Re}\sqrt{C_F} + f_6(C, P) - A\,\ell n\,2\sqrt{2} - \beta\end{aligned}\right\}\begin{aligned}&\text{(rough)}\\ &\text{(smooth).}\end{aligned} \tag{39a}$$

Similarly, using Eqn. (35) instead of Eqn. (32) (smooth tube at low Reynolds numbers) yields

$$\sqrt{\frac{2}{C_F}} = (1-\eta_L)^2 \ell n \, Re\sqrt{C_F} + (1-\eta_L)^2\left[f_6(C,P) - A\,\ell n\, 2\sqrt{2}\right] - G. \quad (39b)$$

Note that since

$$y^* = \frac{yu_\tau}{\nu} = \frac{yu_\tau \epsilon}{\nu\epsilon} = \epsilon^* \frac{y}{\epsilon}$$

Eqn. (25) can be written

$$\frac{u}{u_\tau} = A\,\ell n\, \epsilon^* + A\,\ell n \frac{y}{\epsilon} + f_3(\epsilon^*, C, P)$$

and Eqn. (27) ≡

$$\frac{u_{CL}}{u_\tau} = A\,\ell n\, \frac{D}{2\epsilon} + A\,\ell n\, \epsilon^* + f_3(\epsilon^*, C, P)$$

so that

$$\sqrt{\frac{2}{C_F}} = A\,\ell n\, \frac{D}{2\epsilon} + A\,\ell n\, \epsilon^* + f_3(\epsilon^*, C, P) - \beta. \quad (40a)$$

Similarly, using Eqn. (35)

$$\sqrt{\frac{2}{C_F}} = (1-\eta_L)^2\left[A\,\ell n\, \frac{D}{2\epsilon} + A\,\ell n\, \epsilon^* + f_6(C,P)\right] - G. \quad (40b)$$

Equations (39a) and (39b)—or (40a) and (40b)—enable us to calculate directly from pressure drop data the actual shift in the velocity profile due to the presence of Polyox in solution (function f_6 in smooth case) or the combined effect of the roughness and polymer (function f_3 in rough cases), as well as the coordinate of the edge of the purely viscous region in the two layers model (valid only in the smooth case). Indeed in that model, the dimensionless distance from the wall (y^*_L) at which the logarithmic profile given by Eqn. (28) meets the purely viscous profile, described by $u^* = y^*$ is defined by

$$y^*_L = A \ln y^*_L + f_6(C, P). \tag{36}$$

We know that for water

$$y^*_L = A \ln y^*_L + B \tag{41}$$

where B is a constant and the solution of this equation is $y^*_L = 11.6$. Using this result, Eqn. (36) can more suitably be written as

$$y^*_L = 11.6 + \Delta u^* \tag{42}$$

where Δu^* is defined by Eqn. (30).

Equation (39a) gives directly the function $f_3(\varepsilon^*, C, P)$ (rough case) or $f_6(C, P)$ from the knowledge of C_F at a given Re. Then for the smooth tube, y^*_L is calculated with the help of Eqn. (42). Equation (39b) relates three unknown quantities (f_6, η_L, G) with Re and C_F known from pressure drop data. But

$$\eta_L = \frac{y^*_L}{R^*} = \frac{11.6 + \Delta u^*}{R^*} = \frac{11.6 + \Delta u^*}{\frac{Re}{2}\sqrt{\frac{C_F}{2}}} = \eta_L\left[f_6, \frac{Re}{2}\sqrt{\frac{C_F}{2}}\right]$$

$$G = \frac{3}{2}A - \eta_L^2 R^* - 2A\left[-\frac{\eta_L^2}{4} - \eta_L \ln \eta_L + \eta_L + \frac{\eta_L^2}{2}\ln \eta_L\right]$$

$$= G\left[\eta_L, R^*\right]$$

$$= G\left[\eta_L, \frac{Re}{2}\sqrt{\frac{C_F}{2}}\right]$$

$$= G\left[f_6, \frac{Re}{2}\sqrt{\frac{C_F}{2}}\right].$$

Thus Eqn. (39b) actually enables us to compute f_6 from the pressure drop data, as did Eqn. (39a). The process used in a computer program to perform that calculation can be described as follows. First an initial value of η_L is chosen

$$\eta_L = \frac{11.6}{\frac{Re}{2}\sqrt{\frac{C_F}{2}}} .$$

G is then calculated, introduced into Eqn. (39b) and this equation is solved for f_6. The value of f_6 is then used to calculate the second value of η_L in the converging process:

$$\Delta u^* = f_6 - B$$

and

$$\eta_L = \frac{11.6 + \Delta u^*}{\frac{Re}{2}\sqrt{\frac{C_F}{2}}} .$$

The previous operations are repeated until two successive values of Δu^* differ by less than 0.0001. This was usually achieved after only four steps. y^*_L and $\eta_L = y^*_L / R^*$ were then calculated with the help of Eqn. (42).

It should be emphasized that pressure drop data are sufficient to completely evaluate the constants in this very simple two-layer model for the velocity profile which is based essentially on two hypotheses: a parallel shift of the logarithmic velocity (Δu^*) and a thickening of the viscous sublayer (up to y^*_L). It is important to point out that this model, universal for water (the two regions meeting at $y^* = 11.6$ regardless of the Re), is no longer so when we are dealing with a polymer solution. Indeed Δu^* is a function of the concentration and $P(u_\tau)$. We can see furthermore from the definition of C_F that $u_\tau = \sqrt{\frac{C_F}{2}}\,\mathrm{Re}\,\frac{\nu}{D}$; hence P, and consequently Δu^*, will depend on the flow rate.

It is evident that the model used for the derivation of the Fanning friction factor is exaggeratedly simple. It was felt, however, that there was no point in using a more refined velocity profile at this stage of the investigation. If desired, the piece by piece integration of the expression $\int_0^{\eta_L} u(1-\eta)d\eta = Ru_\tau^2 \eta/\nu$, could, of course, be repeated with an improved expression for the velocity near the wall.

C. Heat Transfer Problem

a) Dimensional Considerations

In what follows we will assume that

(1) The energy involved in the pressure work and viscous dissipation terms is negligible in comparison to the heat energy transferred.

(2) The axial temperature gradients are negligible compared to the radial temperature gradients.

(3) The flow is thermally fully established such that $\partial T/\partial x$ is independent of radial position.

(4) The heat flux $\dot{q}(r)$ varies linearly with radial location

$$\frac{\dot{q}(r)}{\dot{q}_0} = \frac{r}{R}. \tag{43}$$

In fact, the variation of $\dot{q}$ is determined by the balance between the heat carried by the fluid in the flow direction and the heat flow across the stream, and therefore depends on the velocity distribution. Nevertheless, the deviation from a linear distribution is not very significant and the error introduced by using Eqn. (43) estimated by Reichardt [47] is small except for extremely low values of the Pr.

Under these assumptions, the general energy equation for pipe flow written in terms of time-averaged quantities is

$$-\frac{\dot{q}_0}{\rho C_p}(1-y/R) = \left(\epsilon_H + \frac{\nu}{Pr}\right)\frac{dT}{dy} \tag{44}$$

where $\epsilon_H = -\overline{T'v'}/(dT/dy)$ = turbulent heat diffusivity. $\overline{T'v'}$ is a time-average of the product of the turbulent fluctuations in the velocity radially away from the wall and in the temperature. This equation will be used simultaneously with the momentum equation

$$\frac{\tau_0}{\rho}\left(1-\frac{y}{R}\right) = (\epsilon_M + \nu)\frac{du}{dy} \tag{45}$$

where $\epsilon_M = -\overline{u'v'}/(du/dy)$ = turbulent momentum diffusivity. $\overline{u'v'}$ is a time average of the product of the turbulent fluctuation in the axial and radial directions.

We will assume that the large changes in temperature and velocity occur very close to the wall. With this assumption, $y/R << 1$ and the Eqns. (44) and (45) become

$$-\frac{\dot{q}_0}{\rho C_p} = \left(\epsilon_H + \frac{\nu}{Pr}\right)\frac{dT}{dy} \qquad (44')$$

$$\frac{\tau_0}{\rho} = \left(\epsilon_M + \nu\right)\frac{du}{dy} \,. \qquad (45')$$

We will also retain the assumption usually made for smooth tubes that the respective distances from the wall at which the velocity equals $\overline{u}$ and at which the temperature equals T_L are the same ($\overline{u}$ and T_L defined as previously). Dipprey showed that this assumption can possibly be poorer in rough tubes than for the smooth case but that nonetheless it does not introduce a significant error in the final heat transfer formulation. This aspect can actually be checked, as a treatment of the heat transfer problem has been formulated without making the latter two assumptions. This treatment consists essentially of extending to rough tubes Reichardt's derivation for smooth tubes [47]. The complete approach is given in Appendix IV. The results will be presented later in this section and compared with those involving the two assumptions mentioned above in the smooth case.

In both approaches, use will be made of the Reynolds analogy which states that $\epsilon_H = \epsilon_M$ for the fully turbulent region of the flow is assumed to hold throughout the pipe. The physical idea of the Reynolds analogy is that when a lump of fluid travels in the transverse direction

($v' \neq 0$) due to the fluctuating motion of the turbulent flow, it retains its original momentum and thus exchanges momentum between two layers of different velocities, and also by the same process exchanges heat energy when temperature gradients in the y-direction are present. The x-momentum and heat transfer through a surface parallel to the pipe axis and due to the fluctuating motion in the turbulent flow are given by $\rho \overline{u'v'}$ and $C_p \rho \overline{v'T'}$ respectively. Since both heat and momentum are exchanged by the same process, there must exist an intimate connection between heat and momentum transfer. This connection is expressed by the equality of ε_M and ε_H.

The experimental confirmation of the Reynolds analogy is still lacking for Newtonian fluids. In fact the data of several investigators for air in pipe flow yield an average value of $\varepsilon_H/\varepsilon_M = 1.4$ [54]. Measurements of temperature and velocity profiles in free turbulence indicate a value of $\varepsilon_H/\varepsilon_M = 2.0$. Yet, the fairly good agreement between theory and heat transfer data in pipes are obtained when $\varepsilon_H/\varepsilon_M$ is taken as unity. Reichardt [47] offers a possible explanation of these observations by noting that the experimental evidence that $\varepsilon_H/\varepsilon_M$ is smaller in friction layers than in free turbulence permits the tentative conclusion that the reduction of the ratio $\varepsilon_H/\varepsilon_M$ is due to the influence of the wall. He suggests that $\varepsilon_H/\varepsilon_M$ is unity in the immediate vicinity of the wall (the most important region since the large changes in temperature and velocity occur there) and tends to approach the free turbulence value of 2 at larger distances from the wall. The question arises as to whether the Reynolds analogy still holds with polymer solutions. As we mentioned previously, there is no conclusive experimental evidence that the Von Karman's constant is different than in the Newtonian case, since the defect law still holds for polymer solutions. This supports the idea that the simplified mechanism of momentum exchange suggested by Prandtl would not be altered by the presence of the polymer in solution: a part of a turbulent eddy initially in velocity and temperature equilibrium with the surrounding fluid and moving in the transverse direction would still exchange momentum with the surrounding fluid by simple viscous shear and in the mean time exchange heat by simple conduction. A priori, one could imagine a mechanism in which momentum is transferred otherwise than by viscous interaction, the polymer molecules acting like a spring after being elongated by the shear flow. But if it were so, the slope of the defect law would probably be noticeably different than the Newtonian one since a totally different mechanism of transfer would be involved. This has not been observed and we are led to the conclusion that it is not unreasonable to think that the preceding discussion about the ratio $\varepsilon_H/\varepsilon_M$ for Newtonian fluids can still be supported for polymer solutions and that the choice of $\varepsilon_H/\varepsilon_M = 1$ still makes some sense.

With the above assumptions, a relationship between C_F and C_H can be developed in the following way. From the definition of C_H

$$C_H = \frac{\dot{q}_0}{\rho \bar{u} C_p (T_w - T_L)} \tag{2}$$

where

$$\bar{u} = \frac{2}{R^2}\int_0^R u(r) r \, dr \tag{3}$$

$$T_L = \frac{2}{R^2 \bar{u}}\int_0^R T(r) u(r) r \, dr \tag{4}$$

$$\frac{1}{C_H} = \frac{\rho C_p \bar{u}}{\dot{q}_0}(T_w - T_2) + \frac{\rho C_p \bar{u}}{\dot{q}_0}(T_2 - T_L) \tag{46}$$

where T_2 is the temperature at a distance y_2 from the wall, far enough that viscous shear stresses are negligible. Writing down Eqns. (44′) and (45′) between y_2^* and y_m^* (y_m^* is the dimensionless distance at which both T_L and $\bar{u}$ are assumed to occur), where viscous forces are negligible ($\nu << \varepsilon_M$)

$$u_\tau^2 = \varepsilon_M \frac{du}{dy}$$

or

$$\frac{dy^*}{\varepsilon_M/\nu} = \frac{du}{u_\tau}.$$

Integrating between y_2^* and y_m^* yields

$$\frac{\bar{u} - u_2}{u_\tau} = \int_{y_2^*}^{y_m^*} \frac{dy^*}{\varepsilon_M/\nu}. \tag{47}$$

Likewise, using the Reynolds analogy

$$\frac{\rho C_p u_\tau}{\dot{q}_0}(T_2 - T_L) = \int_{y_2^*}^{y_m^*} \frac{dy^*}{\varepsilon_M/\nu}. \tag{48}$$

From (47) and (48)

$$\frac{\overline{u}-u_2}{u_\tau} = \frac{\rho C_p u_\tau}{\dot{q}_0}(T_2 - T_L)$$

or, multiplying by $\overline{u}/u_\tau$ and using $\overline{u}/u_\tau = \sqrt{2/C_F}$

$$\frac{\rho C_p \overline{u}}{\dot{q}_0}(T_2 - T_L) = \frac{2}{C_F} - \frac{u_2/u_\tau}{\sqrt{\frac{C_F}{2}}}. \tag{49}$$

But in the region of negligible viscous forces and constant shear stress (since it has been assumed that $y/R << 1$ or $\tau = \tau_0$), from Eqn. (12)

$$\frac{u}{u_\tau} = f_1(y^*, \varepsilon^*, C, P) \tag{12}$$

hence

$$\frac{u_2}{u_\tau} = f_8(y_2^*, \varepsilon^*, C, P). \tag{50}$$

Next, a dimensional analysis using the parameters of the law of the wall, together with the parameters $\dot{q}_0$, C_p, k which must be added for the heat transfer problem gives

$$\frac{\rho C_p u_\tau}{\dot{q}_0}(T_w - T_2) = f_9(Pr, y_2^*, \varepsilon^*, C, P) \tag{51}$$

or, multiplying Eqn. (51) by $\overline{u}/u_\tau$

$$\begin{aligned}\frac{\rho C_p \overline{u}}{\dot{q}_0}(T_w - T_2) &= \frac{\overline{u}}{u_\tau} f_9\left[Pr, y_2^*, \varepsilon^*, C, P\right] \\ &= \frac{1}{\sqrt{\frac{C_F}{2}}} f_9\left[Pr, y_2^*, \varepsilon^*, C, P\right].\end{aligned} \tag{52}$$

Introducing (49) and (52) into (45) and using (50) yields

$$\frac{1}{C_H} = \frac{1}{\sqrt{\frac{C_F}{2}}} f_9 + \frac{1}{\frac{C_F}{2}} - \frac{f_8}{\sqrt{\frac{C_F}{2}}}$$

or

$$\frac{\sqrt{\frac{C_F}{2}}}{C_H} = f_9 + \frac{1}{\sqrt{\frac{C_F}{2}}} - f_8$$

or

$$\frac{\frac{C_F}{2C_H} - 1}{\sqrt{\frac{C_F}{2}}} = f_9(Pr, y_2^*, \varepsilon^*, C, P) - f_8(y_2^*, \varepsilon^*, C, P). \tag{53}$$

Since y_2^* is a constant number independent of the parameters of the problem, it may be dropped from the functions and Eqn. (53) becomes

$$\frac{\frac{C_F}{2C_H} - 1}{\sqrt{\frac{C_F}{2}}} = f_{10}(Pr, \varepsilon^*, C, P). \tag{54}$$

(b) Attempts to Describe the f_{10} Function

Following Dipprey's approach [10], the flow is divided into two regions by an imaginary cylinder passing through the tips of the roughness elements at $y = \varepsilon$. At the interface, the axial velocity is u_g, the temperature T_g, the heat flux $\dot{q}_0$ and the shear stress τ_0. These are statistical spatial mean values over an interval including many roughness elements. They are then independent of axial and circumferential location in the pipe, so that the one-dimensional aspect of the problem is preserved.

By continuity, the net flow through the interface, i. e., into and out of the roughness cavities, is zero, and this motion is thought of as a part of the turbulent motion. Also the net axial fluid motion on the wall side of this interface is assumed negligible. From the definition of C_H

$$C_H = \frac{\dot{q}_0}{\rho \overline{u} C_p (T_w - T_L)} \tag{2}$$

$$\frac{1}{C_H} = \frac{\rho C_p \overline{u}}{\dot{q}_0}(T_w - T_g) + \frac{\rho C_p \overline{u}}{\dot{q}_0}(T_g - T_L). \tag{55}$$

The term $\frac{\rho C_p \overline{u}}{\dot{q}_0}(T_w - T_g)$ appearing in the RHS of Eqn. (55) will be considered first.

The cavity flow can be considered as a separate flow system with the cavity walls as one boundary and velocity u_g and shear stress τ_0 representing the conditions at the open boundary. In order to see what parameters are necessary to describe the turbulent motion at the interface, let us write the equation of motion in a dimensionless form for the constant stress region

$$1 = -\frac{\overline{u'v'}}{u_\tau^2} + \frac{\partial(u/u_\tau)}{\partial y^*}. \tag{56}$$

But in that region of constant stress,

$$\frac{u}{u_\tau} = A \ln y^* + f_3(\epsilon^*, C, P) \tag{25}$$

hence

$$\frac{\partial(u/u_\tau)}{\partial y^*} = f(y^*) \quad \text{only}$$

and from (56)

$$\left.\frac{\overline{u'v'}}{u_\tau^2}\right|_{y^* = \epsilon^*} = f(\epsilon^*) \quad \text{only.} \tag{57}$$

So the complete motion at the cavity opening is described by u_g, u_τ (mean motion) and ϵ^* (turbulent motion).

These three parameters can be combined in a Re_{cavity}

$$Re_c = \frac{\epsilon u_g}{\nu} = \epsilon^* \frac{u_g}{u_\tau}(\epsilon^*, C, P). \tag{58}$$

Note that Re_c is no longer a function of ϵ^* only, as it was for water but also depends on the characteristics of the polymer (C and P). Let us define a Stanton number for the mean time cavity heat exchange as

$$C_{H_c} = \frac{\dot{q}_0}{\rho u_g C_p (T_w - T_g)}. \tag{59}$$

By dimensional considerations of the cavity flow

$$C_{H_c} = C_{H_c}(Re_c, Pr). \tag{60}$$

Using $\frac{\overline{u}}{u_\tau} = \frac{1}{\sqrt{\frac{C_F}{2}}}$,

$$\frac{\rho C_p \overline{u}(T_w - T_g)}{\dot{q}_0} = \frac{1}{\sqrt{\frac{C_F}{2}}\, \frac{u_g}{u_\tau}\, C_{H_c}} \tag{61}$$

with, from Eqn. (25)

$$\frac{u_g}{u_\tau} = A\, \ell n\, \epsilon^* + f_3(\epsilon^*, C, P)$$

C_{H_c} defined by (38) and (39).

Next the central flow region will be treated following the same procedure presented by Dipprey. In the region where $y/R << 1$

a) $$\frac{\tau_0}{\rho} = \left(\frac{\epsilon_M}{\nu} + 1\right)\nu\, \frac{du}{dy} = u_\tau^2$$

or

$$\frac{du^*}{dy^*} = \frac{1}{\frac{\epsilon_M}{\nu} + 1} \tag{62}$$

b) $$-\frac{\dot{q}_0}{\rho C_p} = \left(\frac{\epsilon_H}{\nu} + \frac{1}{Pr}\right)\nu\, \frac{dT}{dy}$$

or

$$-\frac{dT}{dy^*}\, \frac{u_\tau \rho C_p}{\dot{q}_0} = \frac{1}{\frac{\epsilon_H}{\nu} + \frac{1}{Pr}} . \tag{63}$$

Far enough from the wall, the turbulent stresses are predominant, so that $\epsilon_M/\nu >> 1$ or $\epsilon_M/\nu >> 1/Pr$ in Eqn. (62) and (63).

Integrating (62) and (63) from ϵ^* to y_m^*, where $\bar{u}$ and T_L are attained (still close enough to the wall to assume that $y/R << 1$) and making use of the Re analogy ($\epsilon_M = \epsilon_H$)

$$\frac{\bar{u} - u_g}{u_\tau} = \int_{\epsilon^*}^{y_2^*} \frac{dy^*}{\frac{\epsilon_M}{\nu} + 1} + \int_{y_2^*}^{y_m^*} \frac{dy^*}{\frac{\epsilon_M}{\nu}} \tag{64}$$

$$\frac{\rho C_p u_\tau}{\dot{q}_0} (T_g - T_L) = \int_{\epsilon^*}^{y_2^*} \frac{dy^*}{\frac{\epsilon_M}{\nu} + \frac{1}{Pr}} + \int_{y_2^*}^{y_m^*} \frac{dy^*}{\frac{\epsilon_M}{\nu}}. \tag{65}$$

Subtracting (65) from (64) and multiplying by $\frac{\bar{u}}{u_\tau} = \sqrt{\frac{2}{C_F}}$

$$\frac{\rho C_p \bar{u}}{\dot{q}_0} (T_g - T_L) = \frac{2}{C_F} - \frac{u_g/u_\tau}{\sqrt{\frac{C_F}{2}}} + \frac{1}{\sqrt{\frac{C_F}{2}}} F \tag{65'}$$

with

$$F = \int_{\epsilon^*}^{y_2^*} \left[\frac{1}{\frac{\epsilon_M}{\nu} + \frac{1}{Pr}} - \frac{1}{\frac{\epsilon_M}{\nu} + 1} \right] dy^*. \tag{66}$$

Replacing the left hand sides of Eqns. (61), (65) and (66) by their respective values in Eqn. (55) yields

$$\frac{1}{C_H} = \frac{2}{C_F} - \frac{u_g/u_\tau}{\sqrt{C_F/2}} + \frac{F}{\sqrt{\frac{C_F}{2}}} + \frac{1}{\sqrt{\frac{C_F}{2}}\,\frac{u_g}{u_\tau}\,C_{H_c}}$$

or, rearranging the latter equation

$$\frac{\frac{C_F}{2C_H} - 1}{\sqrt{\frac{C_F}{2}}} = F + \frac{1}{\frac{u_g}{u_\tau}\,C_{H_c}} - \frac{u_g}{u_\tau} \tag{67}$$

$$= f_{10}(Pr, \varepsilon^*, C, P) \tag{54}$$

with

$$F = \int_{\varepsilon^*}^{y_2^*} \left[\frac{1}{\frac{\varepsilon_M}{\nu} + \frac{1}{Pr}} - \frac{1}{\frac{\varepsilon_M}{\nu} + 1} \right] dy^*$$

$$\frac{u_g}{u_\tau} = \frac{u_g}{u_\tau}(\varepsilon^*, C, P)$$

$$C_{H_c} = C_{H_c}(\varepsilon^* \frac{u_g}{u_\tau}, Pr).$$

We shall now examine the two extreme cases: the case of a smooth wall and the fully rough regime.

Smooth Tube

In Eqn. (67),

ε, height of the roughness elements → 0

T_g, temperature at the interface $= T_w$ and $\dfrac{\rho C_p \overline{u}(T_w - T_g)}{\dot{q}_0} = 0$

$u_g \rightarrow 0$ (no slip condition at the wall)

so that

$$\frac{\dfrac{C_F}{2C_H} - 1}{\sqrt{\dfrac{C_F}{2}}} = \int_0^{y_2^*} \left[\frac{1}{\dfrac{\epsilon_M}{\nu} + \dfrac{1}{Pr}} - \frac{1}{\dfrac{\epsilon_M}{\nu} + 1} \right] dy^* . \tag{68}$$

The right hand side of Eqn. (68) can be written under a different form as follows. We know, from Eqn. (62) that if $y/R << 1$,

$$dy^* = \left(\frac{\epsilon_M}{\nu} + 1 \right) du^* . \tag{62'}$$

Using the latter equation, the right hand side of Eqn. (68) becomes:

$$\int_0^{y_2^*} \left[\frac{1}{\dfrac{\epsilon_M}{\nu} + \dfrac{1}{Pr}} - \frac{1}{\dfrac{\epsilon_M}{\nu} + 1} \right] dy^* = \int_0^{y_2^*} \frac{(Pr - 1)}{\left(\dfrac{\epsilon_M Pr}{\nu} + 1 \right) \left(\dfrac{\epsilon_M}{\nu} + 1 \right)} dy^*$$

$$= \int_0^{\frac{u_2}{u_\tau}} \frac{(Pr - 1)}{\dfrac{\epsilon_M Pr}{\nu} + 1} du^* \tag{69}$$

$$= \int_0^{u^*_{CL}} \frac{(Pr - 1)}{\dfrac{\epsilon_M Pr}{\nu} + 1} du^* - \int_{u_2^*}^{u^*_{CL}} \frac{(Pr - 1)}{\dfrac{\epsilon_M Pr}{\nu} + 1} du^*$$

or

$$\frac{\frac{C_F}{2C_H}-1}{\sqrt{\frac{C_F}{2}}} = \int_0^{u^*_{CL}} \frac{(Pr-1)}{\frac{\epsilon_M Pr}{\nu}+1}\, du^* \qquad (70)$$

since, when $y/R << 1$ is no longer valid, ϵ_M/ν becomes so large that the second integral in (69) is negligible.

It may be noted that the ratio of heat transferred by pure molecular conduction and the total heat transferred can be written as

$$\frac{\dot{q}_{mo}}{\dot{q}_0} = \frac{\dot{q}_{mo}}{\dot{q}_{mo}+q_t}$$

where q_t = heat flux transferred by the turbulent fluctuations

$$= \frac{k}{k+\rho C_p \epsilon_H} = \frac{1}{1+\frac{\rho C_p \epsilon_H}{k}} = \frac{1}{1+Pr\frac{\epsilon_M}{\nu}} \qquad (71)$$

Therefore the right hand side of Eqn. (68) divided by (Pr-1) represents the integral over the velocity profile of the ratio of the heat transferred by molecular process to the total heat transferred.

Again it should be pointed out that the foregoing was based on the assumptions that the large changes in temperature and velocity occur very close to the wall and that the respective distances from the wall at which the velocity equals $\overline{u}$ and at which the temperature equals T_L are the same. As mentioned earlier, an approach can be formulated without these two assumptions, by generalizing to rough tubes the derivation which Reichardt has developed for smooth tubes. The derivation is presented in Appendix IV. In the smooth case, the whole expression for C_H reduces to

$$C_H = \frac{\frac{C_F}{2} \frac{\Phi_m}{\theta_m} \frac{\epsilon_H}{\epsilon_M}}{1 + (Pr^* - 1)\Phi_m \sqrt{\frac{C_F}{2}} \int_0^{u^*_{CL}} \frac{du^*}{1 + Pr^* \frac{\epsilon_M}{\nu}}} \tag{72}$$

where

$\theta_m = \frac{T_L - T_w}{T_{CL} - T_w}$ (T_{CL} being the centerline temperature)

$\Phi_m = \frac{\bar{u}}{u_{CL}}$ (u_{CL} being the centerline velocity)

$\frac{\epsilon_H}{\epsilon_M} = 1$ following the Reynolds analogy

$Pr^* = \frac{\epsilon_H}{\epsilon_M} Pr = Pr.$

Rearranging Eqn. (72)

$$\frac{\frac{C_F}{2C_H} \frac{1}{\theta_m} - \frac{1}{\Phi_m}}{\sqrt{\frac{C_F}{2}}} = (Pr - 1) \int_0^{u^*_{CL}} \frac{du^*}{1 + Pr \frac{\epsilon_M}{\nu}}. \tag{73}$$

Comparing this equation with Eqn. (70)

$$\frac{\frac{C_F}{2C_H} - 1}{\sqrt{\frac{C_F}{2}}} = (Pr - 1) \int_0^{u^*_{CL}} \frac{du^*}{1 + Pr \frac{\epsilon_M}{\nu}} \tag{70}$$

it is seen that the difference between the approach using the hypothesis that $\bar{u}$ and T_L are reached at the same distance from the wall and the more general derivation without that assumption turns out to be two connective factors: $\frac{1}{\theta_m}$ and $\frac{1}{\Phi_m}$. These quantities can be evaluated as follows:

- The Factor Φ_m

By definition,

$$\Phi_m = \frac{\bar{u}}{u_{CL}} = \frac{\bar{u}^*}{u^*_{CL}}$$

$\bar{u}$ and u_{CL} are related by

$$\frac{u_{CL}(1-\eta_L)^2 - \bar{u}}{u_\tau} = G$$

with G defined by

$$G = \frac{3}{2}A - \eta_L^2 R^* - 2A\left[-\frac{\eta_L^2}{4} - \eta_L \ln \eta_L + \eta_L + \frac{\eta_L^2}{2}\ln \eta_L\right]. \qquad (35),(37)$$

From (35),

$$\Phi_m = \frac{(1-\eta_L)^2}{G\sqrt{\frac{C_F}{2}} + 1}.$$

- The Factor θ_m

It has been shown that for a two layers temperature profile in viscous region ($0 < y < y_L$) (cf. Deissler [8] for instance)

$$T^* = y^* Pr \qquad (74)$$

in turbulent core ($y_L < y < R$)

$$T^* = C_1 + \frac{1}{\varkappa} \ell n\, y^* \tag{75}$$

at the centerline

$$T^*_{CL} = C_1 + \frac{1}{\varkappa} \ell n\, R^* \tag{76}$$

and a defect law for the temperature in the turbulent core can be written

$$T^* = T^*_{CL} + A\, \ell n\, \eta \tag{77}$$

with

$$T^* = \frac{(T_w - T)\, \tau_0 C_p}{\dot{q}_0\, u_\tau} \tag{78}$$

$$\eta = \frac{y}{R}.$$

Next a dimensionless quantity T^*_L is defined such that

$$T^*_L = \frac{(T_w - T_L)\, \tau_0 C_p}{\dot{q}_0\, u_\tau}$$

$$= \frac{u_\tau}{\overline{u}} \; \frac{(T_w - T_L)\, \rho \overline{u} C_p}{\dot{q}_0}$$

or

$$T^*_L = \frac{\sqrt{\frac{C_F}{2}}}{C_H}. \tag{79}$$

But T^*_L is also defined as

$$T^*_L = \frac{\int_0^R T^*\, u\, r\, dr}{\int_0^R u\, r\, dr} \tag{80}$$

$$= \frac{\int_0^1 T^*[\eta]u[\eta](1-\eta)d\eta}{\int_0^1 u[\eta](1-\eta)\,d\eta}. \qquad (80)\ \text{cont.}$$

From the definition of θ_m (Eqn. 72), then

$$\theta_m = \frac{T_L - T_w}{T_{CL} - T_w} = \frac{T_L^*}{T_{CL}^*}. \qquad (81)$$

The calculation of the integrals in (80) will give a relation between T_L^* (which is known from friction and heat transfer data, and given by (79)) and T_{CL}^*, which in turn will make it possible to calculate θ_m given by (81).

The numerator of Eqn. (80) is written as

$$N = \int_0^{\eta_L} T^*[\eta]u[\eta](1-\eta)d\eta + \int_{\eta_L}^1 T^*[\eta]u[\eta](1-\eta)d\eta.$$

In the first integral, $T^* = y^* P_2$ or $T^* = R^* Pr\, \eta$ with

$$R^* = \frac{Ru_\tau}{\nu} = \frac{Re}{2}\sqrt{\frac{C_F}{2}}$$

and

$$u^* = y^* \quad \text{or} \quad u = R^* u_\tau \eta.$$

In the second integral,

$$T^* = T_{CL}^* + A\,\ell n\,\eta$$

$$u = u_{CL} + Au_\tau\,\ell n\,\eta.$$

Performing the integrations yields

$$N = R^{*2} \Pr u_\tau z_1 + \frac{u_{CL} T^*_{CL}}{2} z_2 + A\left(u_{CL} + T^*_{CL} u_\tau\right) z_3 + A^2 u_\tau z_4$$

where

$$A = \frac{1}{\kappa}$$

$$z_1 = \frac{\eta_L^3}{3} - \frac{\eta_L^4}{4}$$

$$z_2 = (1 - \eta_L)^2$$

$$z_3 = -\frac{3}{4} + \eta_L \ln \eta_L \left(\frac{\eta_L}{2} - 1\right) + \eta_L \left(1 - \frac{\eta_L}{4}\right)$$

$$z_4 = \frac{7}{4} + \frac{\eta_L^2}{2}\left[\left(\ln \eta_L - \frac{1}{2}\right)^2 + \frac{1}{4}\right] - \eta_L \left[\left(\ln \eta_L - 1\right)^2 + 1\right]$$

η_L can be calculated using Eqn. (42). Now by definition of $\overline{u}$,

$$\frac{\overline{u}}{2} = \int_0^1 u[\eta](1 - \eta)\, d\eta.$$

Hence

$$T_b^* = \frac{\sqrt{\frac{C_F}{2}}}{C_H} \tag{79}$$

$$= (2R^{*2} \Pr z_1 + 2A^2 z_4)\frac{u_\tau}{\overline{u}} + z_2 T^*_{CL} \frac{u_{CL}}{\overline{u}} + 2Az_3 \frac{u_{CL}}{\overline{u}} + 2Az_3 T^*_{CL} \frac{u_\tau}{\overline{u}}.$$

But

$$\frac{u_\tau}{\overline{u}} = \sqrt{\frac{C_F}{2}}$$

$$\frac{u_{CL}}{\overline{u}} = \frac{1}{\Phi_m} .$$

Defining z_5 and z_6 as

$$z_5 = (2R^{*2} \Pr z_1 + 2A^2 z_4)\sqrt{\frac{C_F}{2}} + \frac{2A z_3}{\Phi_m}$$

and

$$z_6 = \frac{z_2}{\Phi_m} + 2A z_3 \sqrt{\frac{C_F}{2}} ,$$

one may write

$$T^*_{CL} = \frac{T^*_b - z_5}{z_6}$$

$$= \frac{\dfrac{\sqrt{\frac{C_F}{2}}}{C_H} - z_5}{z_6} \tag{82}$$

and

$$\theta_m = \frac{T^*_b}{T^*_{CL}} .$$

Fully Rough Regime

In the case of a fully rough regime, the Reynolds number similarity extends to the tips of the roughness elements and beyond, so that F appearing in Eqn. (67) becomes negligible and

$$\frac{\frac{C_F}{2C_H}-1}{\sqrt{\frac{C_F}{2}}}=\frac{1}{\frac{u_g}{u_\tau}C_{H_c}}-\frac{u_g}{u_\tau}. \tag{83}$$

But since the tips of the protrusions fall within the region of constant shear stress, $\frac{u_g}{u_\tau}=f(\epsilon^*, C, P)$ can be calculated for a given polymer and concentration from the pressure drop data. Therefore the simultaneous knowledge of C_F and C_H provides information about C_{H_c}, the only unknown quantity in Eqn. (83).

Information on the cavity Stanton number can also be obtained from the more general expression of C_H presented in Appendix IV in the fully rough case.

Chapter IV

EXPERIMENTAL APPARATUS AND METHOD

A. Test Facility

A general view of the test facility as well as a simplified schematic of the installation are shown in Figures 1 and 2. The flow through the test section is supplied from a hydraulic cylinder operated by a variable speed motor through a linear actuator (1 to 10 of Figure 2). This simple displacement method of supplying the flow was preferred to a pump in order to reduce the mechanical degradation of the solutions before they enter the test section. After passing through the test section, the fluid is discharged into a reservoir tank (12). This tank is equipped with an immersion thermometer (15), two heating rods (13) and a heat exchanger coil, which allows temperature control during a series of tests. The apparatus is designed so that it can operate at pressures exceeding one atmosphere. For this purpose the reservoir (12) tank can be connected to a nitrogen bottle through a pressure regulator (22), and the pressure difference between the two sides of the piston (1) is kept small by means of a pressure equalizing line going from the reservoir to the cylinder (14). Excursions of pressure are prevented by a safety valve (16). The solutions were prepared either in the reservoir tank (12) or generally in auxiliary drums directly connected to the cylinder by a flexible hose. These drums are insulated and provided with heat exchange coils to allow temperature conditioning. By moving the piston from right to left (see

Figure 2), and properly positioning three globe valves (19) in addition to a filler valve (20) and a drain valve (21) it was possible to draw the solutions into the cylinder from either the reservoir (12) or the mixing drums.

The test section, described in detail in the next paragraph and sketched in Figure 4, is heated by passing alternating current through the wall of the tube. As the electrical resistance of the wall is only about 0.002Ω, a relatively large current (of the order of 1000 amps) is required, which is supplied through a special set of transformers. The primary of these transformers is equipped with a variable ratio switch which makes it possible to vary the intensity of the current in the secondary circuit from 200 to 1200 Amp. Heavy copper conductors connect the transformer secondary to the electrodes of the test section. The test section itself is enclosed in a safety housing. Three safety devices are included in the electric circuit: the power can be turned on only if the door of the housing is closed (safety switch 17) and if the motor driving the piston is running. An additional circuit breaker opens the main power circuit when the wall temperature of the test section exceeds a critical value. Finally two limit switches (11) stop automatically the drive of the piston (and shut the power off because of the interlock described above) at the end of its run.

B. Experimental Tubes

The tubes used in the experiments are the ones already utilized by Dipprey in similar experiments performed with distilled water.

They are described in detail in [10]. In the present chapter, a brief description of the main features only will be given. All tubes are made of nickel, a material of thermal conductivity sufficiently well established to permit accurate calculation of inner wall temperature from measurements on the outer wall; their inside diameter is about 3/8 in. The rough tubes were constructed by electroplating nickel onto a sand-covered mandrel and by subsequently dissolving the mandrel with chemicals leaving a pure nickel shell which served as the test tube. More details on the basic tube construction are presented in [10]. At the time, the tubes were checked in several ways. Samples taken from each tube revealed a very uniform nickel grain structure and showed no evidence of inclusions or voids. Figure 5 presents the significant dimensions of each of the three experimental tubes. The values used for the inside diameter were based on 12 outside diameter measurements of the original mandrel with corrections for the mean sand protrusions. As a check the diameter was also determined volumetrically, using the relation

$$D = \left[\frac{4\Delta V}{\pi \Delta x}\right]^{1/2}$$

where ΔV is the volume contained in the length Δx. The effective tube-wall thickness used in determining the temperature drop in the wall was calculated from electrical resistivity measurements of the wall material, and compared with the thickness measured on photomicrographs taken from end samples of each tube. A slight longitudinal taper in the tube wall was observed on all tubes and is taken into account in the data reduction.

The roughness ratio ϵ/D of each of the two rough tubes is defined to obey the friction similarity law (for water) presented in Chapter III. A one-inch long smooth section was formed near the start of the heated section of the two rough tubes at two circumferential locations. Three equally spaced, 0.032-inch diameter holes connecting the center of this smooth region to a small ring manifold constitute the pressure tap at the entrance of the heated test section. The downstream pressure tap having the same geometry is located in a smooth section 1/2-inch from the exit end of the rough tube. Copper blocks, silver-brazed to the nickel tube, serve as electrode attachment points and distributors of the electric current. The exit end of the test section is electrically isolated by a special flange which also incorporates a thermal mixing chamber. The mixing chamber consists of a brass thermal equalizer which is isolated from the other metal parts by a teflon sleeve. The equalizer has drilled holes directing the flow first into an outer chamber and then back into the central passage.

Three wall-thermocouple stations are located in the heated test section, but in the present experiments, the downstream one only was used as the purpose was to study the heat and momentum transfer in fully established conditions. At each station, three thermocouples are mounted 120 degrees apart. The thermocouple junctions were formed by discharge welding 0.005-inch diameter chromel and alumel wires to the nickel tube leaving a 0.020-inch gap between the ends of the wires such that a chromel-nickel junction and a nickel-alumel junction are formed in series. The insulated leads were wrapped several turns around the tube and secured to the tube with high temperature cement.

C. Measurements Necessary to Determine C_F and C_H and Instrumentation

The principal measurements to be made consist of the flow rate, outside wall temperatures at two circumferential locations, inlet and outlet temperatures, pressure drop in the test section and the electric power. The friction and heat transfer coefficients are calculated from these measurements following a procedure described in Appendix II. The flow rate is derived from the speed of the gear driving the piston actuator, and the speed of the gear in turn is determined from the rate at which the gear teeth pass a magnetic sensor. The signals emitted by the magnetic pick-up are counted over a period of 10 seconds and read on a digital counter. The pressure drop is obtained by means of a Statham diaphragm type differential transducer, connected to the test section pressure taps following the sketch shown in Figure 4. The transducer output is amplified and recorded continuously on a chart recorder. All temperatures are measured by means of chromel-alumel thermocouples. The outputs from the couples are amplified and recorded continuously on a two-channel plotter.

A schematic diagram of the circuits for the measurement of the temperatures is shown in Figure 9. All wires of inlet, outlet and wall thermocouples are connected to copper wires in the ice bath, thus allowing all switch interconnections to be made with copper wire. Each cold junction is inserted in a small glass tube filled with oil, and all tubes are placed in the ice bath contained in a Dewar. Furthermore, the mixture of ice and water can be stirred periodically by a small propeller. The outlet immersion thermocouple is directly connected to an amplifier, and to the channel 1 of the plotter through an RC circuit. The two wall thermocouples and the inlet immersion thermocouple are connected to a rotary switch and the output of the latter to the channel 2 of the plotter via an amplifier and an RC circuit. The purpose of the RC circuit is to eliminate the 60 cycles noise present in the couples signals. The power required to heat the tube walls is derived from the voltage drop across the test section and the electric resistance of each tube as a function of temperature. A specific list of the instrumentation used in these experiments is given hereafter.

a. Measurement of flow scale
    1 Counter timer Model 101A (Monsanto)
b. Measurement of pressure drop
    1 Differential pressure transducer, 0 → 50 psid, Model 3509, PL280 TC-50-250 (Statham)
    1 DC-Vacuum tube voltmeter, Model 412A (Hewlett Packard)
    1 Visicorder, Model 1508 (Honeywell)
c. Measurement of temperatures
    2 DC micro volt-ammeters, Model 425A (Hewlett Packard)
    1 x-y plotter, two channels, Model 850 PR (Moseley)
d. Measurement of voltage drop across test section
    1 RMS voltmeter, Model 3400 A (Hewlett Packard).

D. Procedures

1. Preparation of Solutions

Fifty gallons of fresh 10 (50) parts per million Polyox solutions were prepared as follows (the quantities corresponding to a 50 ppm solution are given in parenthesis)

(I) First 1.893 gr (9.465 gr) of Polyox were carefully weighed in a small beaker.

(II) About 25 cc (125 cc) of alcohol was added to the chemical. This was stirred vigorously to produce a temporary suspension.

(III) The suspension was then poured into about 5 liters of water while this was also being stirred.

(IV) The resulting concentrate was left to dissolve for about a day, being disturbed gently at intervals.

(V) One of the mixing drums was filled with tap water up to a horizontal mark corresponding to 188 (184) liters (50 gallons - 1 (5) liters), and the concentrate was added to the solvent after the latter was brought to the appropriate temperature.

(VI) The final mixture was stirred very gently with a rod at intervals for a period of one hour.

(VII) The solution was then ready to be sucked in the cylinder and forced through the test section.

Samples of the solutions thus obtained were tested in the flowmeter described in Appendix V in order to identify a possible biological or mechanical degradation due to the mixing process. The results of these tests were surprisingly consistent, indicating that the solutions did not differ very much from batch to batch. A 50 gallon drum was sufficient for four to six tests, depending on the selected flow rate.

2. Test Operation

A series of 25 to 40 heat transfer tests were performed at different Reynolds numbers, for each of the three tubes, for each Polyox concentration (0, 10 and 50 ppm) and for each of three Prandtl numbers (nominally 4.38, 6.16 and 10.3). Thus the determination of one experimental curve corresponding to a given concentration and bulk temperature required 4 to 8 batches of fresh solution. The concentrate was prepared the day before a series of tests, following the procedure described in the previous paragraph. The mixing drum was filled with tap water at room temperature (before runs at $Pr = 6.16$ and 10.3) or at about 105°F (before runs at $Pr = 4.38$). Blocks of ice were used to cool the water from room temperature to about 40°F (prior to tests at $Pr = 10.3$) and the temperature suitable for the tests was finally attained with help of the heating rods or heat exchange coil equipping the mixing drum; the drum's insulation prevented the temperature from fluctuating too much during a series of runs (less than 2°F in 3 hours). Once the solution was ready, the following operations were performed:

1) The solution was tested in the flowmeter described in Appendix V.

2) The piston was moved to the end of its run (minimum cylinder volume). The valve establishing the communication

between the mixing drum and the cylinder (drum's valve) was opened. All the other valves were closed, with the exception of the drain valve. This valve was always open so that the solution could be continuously discharged into a sink after it flowed through the test section.

3) The piston was moved backwards at a speed low enough to avoid degradation of the fresh solutions and stopped automatically when the cylinder was filled, as the end of the actuator rod (4) on Figure 2) hit the limit switch (11). Note that the valve located downstream of the test section (test section valve) was kept closed during the process of filling up the cylinder, thus preventing air to be trapped in the cylinder.

4) The valve at the drum was closed and the test section valve opened, thus allowing the solution to be forced through the test section.

5) The pressure lines, connecting the pressure taps to the differential transducer were opened by setting two three-way valves adjacent to the transducer to the desired position ((6) on Figure 4).

6) The piston was moved forward very slowly, allowing the solution to flow through the test section and the pressure lines and purge the latter.

7) The pressure lines were reconnected to the transducer and the motor stopped.

8) The balance of the pressure transducer and the purge of the pressure lines were checked on the visicorder (recording the pressure drop between the two taps of the test section). A zero reading on the visicorder under no-flow condition means that the transducer is well balanced and the lines properly purged.

9) The gains of the amplifiers and the scales of the recorders were chosen to give the most accurate readings.

10) The variable ratio switch of the transformer's primary was positioned to provide the output voltage that, in turn, supplies the appropriate test section heat flux.

11) The displacement rate of the piston was selected by setting a selector switch. Each switch position corresponds to a different Reynolds number of the test.

12) The visicorder and the plotter (recording on two channels the amplified outputs of the thermocouples) were turned on, the latter recording the outlet temperature (channel 1) and inlet temperature (channel 2).

13) The motor was switched on and the solution was forced through the test section at the selected flow rate.

14) The power was turned on and the test section electrically heated. Note that this operation takes five seconds, due to a delay-relay inserted in the electric circuit; the purpose of this relay is to enable the experimenter to interrupt the test before the five seconds have elapsed in

case of emergency.

15) The number of teeth of the gear driving the piston that passes the magnetic sensor in 10 seconds was read on the counter.

16) The inlet temperature and wall temperatures at two stations were successively recorded on channel 2 of the plotter. This was done by positioning a rotary switch so as to select the desired thermocouple.

17) The voltage drop between the two electrodes of the test section was read on a RMS voltmeter.

18) The motor was stopped either manually or automatically (limit switch), and the recorders turned off.

19) The valves were set for another refill of the cylinder. In the mean time, the recordings were read and the readings tabulated.

3. Calibrations

Numerous calibrations were performed during the experimental program. They are described in Appendix I.

4. Data Reduction

Once a series of tests relative to one curve was completed, the data were reduced by computer. A general program was written in AID on PDP-10 time sharing system, taking into account the results of all calibrations and the small corrections inherent to the problem.

The input consisted of the readings of all graphs and instruments (in graduations), and the program calculated Re, Pr, C_F, C_H and other interesting parameters for each test. The program is presented and explained in Appendix II, along with the procedure used to calculate C_F and C_H from the basic measurements described in paragraph C of this present chapter.

Chapter V

DATA ANALYSIS

As stated in the previous chapter, the measurements of the pressure drop along the tube, of the temperatures at the wall and at the outlet, of the flow rate and heat flux were sufficient to calculate the friction and heat transfer coefficients, as well as the Reynolds and Prandtl numbers of each test. These calculations were made on a computer, following a procedure described in detail in Appendix II. Each experimental C_F or C_H thus obtained was plotted versus Re using the Calcomp plotter (IBM-370), and a least square fit of all the data relative to a tube, a bulk temperature and a concentration was computed and plotted. At this stage of the data reduction, the information was contained in a set of 54 polynomials of the form C_F (or C_H) $= a_0 + a_1 \times Re^2 + \cdots + a_i \times Re^i$ for the three tubes of different roughness, three bulk temperatures and three concentrations. The further analysis of the data were performed on the basis of these expressions.

A. Data Analysis for Smooth Tube (E-3)

The first step of the data analysis consisted in evaluating the constants A and B appearing in the velocity profile of pure water in smooth tube

$$u^* = A \ln y^* + B. \tag{84}$$

A and B are the two constants that define the universal velocity profile $u^* = f(y^*)$ for Newtonian fluids and are thus independent of the Reynolds number. This was done by using the relation for the friction coefficient which also contains these constants (Eqn. 39a (smooth) applied to water)

$$\sqrt{\frac{2}{C_F}} = A \ln Re \sqrt{C_F} - A \ln 2\sqrt{2} - \beta + B \tag{39'}$$

with β defined by Eqn. (32). The two sides of this equation were evaluated for different values of A from the experimental expression of $C_F = f(Re)$. It was found the value of A that keeps B the most nearly constant over a range of Re from 10,000 to 250,000 is $A = 2.46$. Over that range of Re and for $A = 2.46$, B varied from 5.999 to 6.021 and an average value of B was chosen as 6.01.

Thus the logarithmic velocity profile that fits best our friction data is

$$u^* = 2.46 \ln y^* + 6.01. \tag{84'}$$

These values compare very well with those of the literature. According to Clauser [7], $A = 2.44$ and $B = 4.9$. Townsend [61] remarks that many of the observed data seem to indicate a value of B nearer to 7 than to the above value of 4.9. Nikuradse [37] proposes $A = 2.5$ and $B = 5.5$. Deissler [8] selects from his own data $A = 2.78$, $B = 3.8$. The present values of $A = 2.46$ and $B = 6.01$ were adopted in all subsequent calculations.

The data for Polyox at concentration of 10 and 50 ppm were analyzed next. First from the knowledge of C_F versus Reynolds number, we are able to calculate the shift $\Delta u^*(C, P)$ in the logarithmic velocity profile (Eqn. (31))

$$\sqrt{\frac{2}{C_F}} = 2.46\,\ell n\,Re\,\sqrt{C_F} - 2.46\,\ell n\,2\sqrt{2} - \beta + 6.01 + \Delta u^*(C,P) \qquad (39a)$$

(one piece integration)

or

$$\sqrt{\frac{2}{C_F}} = 2.46\,(1-\eta_L)^2\,\ell n\,Re\,\sqrt{C_F} + (1-\eta_L)^2\left[6.01 + \Delta u^* - 2.46\,\ell n\,2\sqrt{2}\right] - G \qquad (39b)$$

where η_L and G are given by Eqn. (35). (piece-by-piece integration).

The way to calculate simultaneously Δu^*, η_L and G from Eqn.(39b) was described in Chapter III. Δu^* was directly calculated from Eqn.(39a), C_F and Re being known. Δu^* was calculated from both Eqns. (39a) and (39b) for a Re varying by increments of 5000 from its lowest to highest value available at each temperature so that a direct comparison could be made of the values obtained by using the logarithmic velocity profile over the entire cross-section of the pipe (one piece integration) or by dividing the velocity profile into a viscous part ($u^* = y^*$) and a turbulent one (defect law).

The shear velocity was calculated from

$$u_\tau = \sqrt{\frac{\tau_0}{\rho}} = Re\sqrt{\frac{C_F}{2}}\,\frac{\nu}{D} \qquad (85)$$

and the correlation

$$\Delta u^* = \alpha\,(C)\,\log_{10}\frac{u_\tau}{u_{\tau_{cr}}} \qquad (86)$$

due to Meyer [36], to which reference is made in many papers, was checked by plotting Δu^* versus $\log_{10} u_\tau$. In this equation $u_{\tau_{cr}}$ is the threshold shear velocity at which the solution begins to exhibit the Toms phenomenon, and α is a function of the concentration as well as the temperature. Next, the ratios

$$\frac{\frac{C_F}{2C_H}-1}{\sqrt{\frac{C_F}{2}}(Pr-1)} \quad \text{and} \quad \frac{\frac{C_F}{2C_H}\frac{1}{\theta_m}\frac{1}{\Phi_m}}{\sqrt{\frac{C_F}{2}}(Pr-1)}$$

appearing in Eqns. (70) and (73) respectively were obtained from the analytical expressions of C_F and $C_H = f(Re)$. This was done again for a series of Reynolds numbers ranging in increments of 5000 from the lowest to highest values that could be reached experimentally at a given temperature. The correction factors θ_m and Φ_m were computed according to the procedure given in Chapter III. These two ratios represent the integral over the velocity profile of the ratio of the heat transferred by molecular process and the total heat transferred, respectively with and without the assumption that the average velocity and the bulk temperature are reached at the same distance from the wall. A comparison of their values is a good test of validity of that assumption. Considering now Eqns. (70) and (73), it is seen that these ratios provide overall information about ϵ_M/ν, the ratio of the turbulent diffusivity of momentum and kinematic viscosity: a higher value of the left-hand side of Eqns. (70) and (73) with respect to the Newtonian value will indicate a significant reduction of ϵ_M/ν, and vice versa. Rewriting Eqn. (45) one can show that ϵ_M/ν is related to the velocity profile by

$$\frac{\epsilon_M}{\nu} = \frac{1 - \frac{y^*}{R^*}}{\frac{du^*}{dy^*}} - 1. \tag{45''}$$

Thus a model for the velocity profile $u^* = f(y^*)$ would permit the calculation of $\epsilon_M/\nu\ (u^*)$, which, in turn, would make it possible to compute the integral appearing in the right-hand side of Eqns. (70) or (73). The value of the integral would then be compared with that of the ratios written above as a check of the validity of the assumed velocity profile. Another approach consists of assuming that ϵ_M/ν varies with y^* (or with u^*) according to a certain law that contains a free parameter and to choose that parameter in such a way that the two sides of Eqns. (70) or (73) are equal. A velocity profile $u^* = f(y^*)$ can then be generated from the knowledge of ϵ_M/ν. The latter approach was adopted in the subsequent analysis.

From the equation of continuity and the basic one dimensional character of the flow, it is known that $\overline{u'^*v'^*} = \frac{\epsilon_M}{\nu}\frac{du^*}{dy^*}$ varies with the fourth power of y^*, as y^* goes to zero. Since, as $y^* \to 0$, $u^* = y^*$, $\frac{\epsilon_M}{\nu}$ must be proportional to y^{*4} as well. Van Driest [63] and Deissler [8] have proposed equations for $\frac{\epsilon_M}{\nu}$ that satisfies this condition.

Deissler's equation, which is based on dimensional considerations (and on intuition) has been used very successfully in predicting heat transfer coefficients for Newtonian fluids. Deissler wrote that near the wall

$$\varepsilon_M = \varepsilon_M\left(u, y, \frac{\mu}{\rho}, \frac{du}{dy}, \frac{d^2u}{dy^2}, \frac{d^3u}{dy^3}, \text{etc.}\right).$$

Close to the wall

$$\frac{du}{dy} \rightarrow \frac{u}{y}$$

$$\frac{d^2u}{dy^2} \rightarrow 0$$

and therefore $\varepsilon_M = \varepsilon_M(u, y, \frac{\mu}{\rho})$.

From dimensional analysis

$$\varepsilon_M = n^2 uy\, F\left(\frac{n^2 uy}{\nu}\right). \qquad (87)$$

Expressed in dimensionless form, this equation becomes

$$\frac{\varepsilon_M}{\nu} = n^2 u^* y^* F(n^2 u^* y^*). \qquad (88)$$

Some assumptions on the form of the F function led Deissler to conclude that

$$\frac{\varepsilon_M}{\nu} = n^2 u^* y^* \left(1 - e^{-n^2 u^* y^*}\right). \qquad (89)$$

In an analogous way one may write for polymer solutions that

$$\varepsilon_M = \varepsilon_M\,(u, y, \mu, \text{ polymer characteristic, } \rho_p, \rho_0)$$

and, again from dimensional considerations

$$\varepsilon_M = K\, uy\, F\left(\frac{Kuy}{\nu}, C, P\right) \qquad (90)$$

where P is a dimensionless group characterizing the polymer and K is a constant. Introducing the dimensionless quantities u^* and y^*,

$$\frac{\epsilon_M}{\nu} = Ku^*y^*F(Ku^*y^*, C, P). \tag{91}$$

A comparison with Deissler's equation (88) suggests that, for polymer solutions,

$$\frac{\epsilon_M}{\nu} = n^2(C, P)u^*y^*F[n^2(C, P)u^*y^*]. \tag{92}$$

Since the semi-empirical Deissler's formula

$$\frac{\epsilon_M}{\nu} = n^2u^*y^*\left(1 - e^{-n^2u^*y^*}\right) \tag{89}$$

is so successful in predicting the heat transfer coefficient for water, it is plausible to assume that, for polymer solutions, F can still be written

$$F(n^2u^*y^*) = 1 - e^{-n^2(C, P)u^*y^*}$$

and

$$\frac{\epsilon_M}{\nu}\,(\text{Deissler}) = n^2[C, P]u^*y^*\left(1 - e^{-n^2(C, P)u^*y^*}\right). \tag{93}$$

A development in series of the exponential in the latter equation shows that, as $y^* \to 0$, $\frac{\epsilon_M}{\nu} \propto y^{*4}$, as before.

This relation must, of course, be considered an empirical one, as no rigorous reasoning could entirely justify its specific form. This model predicts that the variation of $\frac{\epsilon_M}{\nu}$ with the distance from the wall will depend on the nature as well as the concentration of the polymer through the function n(C, P). A temperature effect should also be present, as P is very likely to depend on temperature as well. In order to compute the integral

$$\int_0^{u^*_{CL}} \frac{du^*}{1 + Pr\,\frac{\epsilon_M}{\nu}}$$

appearing in Eqns. (70) and (73), we must express ϵ_M/ν as a function of u^* only

$$\frac{\epsilon_M}{\nu}\,(\text{Deissler}) = n^2 u^* y^*[u^*] \left\{1 - \exp\left(-n^2 u^* y^*[u^*]\right)\right\}. \qquad (93')$$

Near the wall, $\tau = \tau_0$ and

$$\frac{\tau_0}{\rho} = u_\tau^2 = \nu\left(\frac{\epsilon_M}{\nu} + 1\right)\frac{du}{dy}$$

or

$$1 = \left(\frac{\epsilon_M}{\nu} + 1\right)\frac{du^*}{dy^*}$$

or

$$\frac{dy^*}{du^*} - \frac{\epsilon_M}{\nu} = 1. \qquad (94)$$

Therefore $y^*[u^*]$ is the solution of the differential equation

$$\frac{dy^*}{du^*} + \left[n^2 u^* \left(e^{-n^2 u^* y^*} - 1\right)\right] y^* = 1 \qquad (95)$$

coupled with the boundary conditions:

$$u^* = 0 \quad \text{at} \quad y^* = 0.$$

A numerical integration of this differential equation (using the subroutine DIFEQ in Fortran on IBM 370) by u^* increments of 0.05 gives the velocity profile corresponding to the assumed $\frac{\epsilon_M}{\nu}$ distribution. This was done for different values of n, ranging from n=0.020 to n=0.124 (Newtonian values). Equations (93′) and (95) are valid only close to the wall. Further away, the logarithmic velocity profile prevails, that is

$$u^* = A \ell n\, y^* + B + \Delta u^* . \tag{31}$$

Since $\frac{\epsilon_M}{\nu}$ is related to the velocity profile by

$$\frac{\epsilon_M}{\nu} = \frac{1 - y^*/R^*}{\frac{du^*}{dy^*}} - 1, \tag{45''}$$

one obtains for this region,

$$\frac{\epsilon_M}{\nu} = \frac{(1 - y^*/R^*)y^*}{A} - 1.$$

In computing the integral $\int_0^{u^*_{CL}} \frac{du^*}{1 + \Pr \epsilon_M/\nu}$ the main contribution comes from a region which is still close to the wall. Further away ϵ_M/ν will be sufficiently large to make the integrand negligible. The expression for ϵ_M/ν will therefore be evaluated at distances for which $y^*/R^* << 1$ and ϵ_M/ν may therefore be approximated by

$$\frac{\epsilon_M}{\nu} = \frac{y^*}{A} - 1. \tag{96}$$

Clearly this expression states that at a given radial location y in the vicinity of the wall $\frac{\epsilon_M}{\nu}$ will practically vary proportionally to

u_τ or $\sqrt{\tau_0}$. This suggests that a reduction of the shear stress, due to the action of the polymer additives, is also accompanied by a reduction of $\frac{\epsilon_M}{\nu}$ in the region where the above equation is valid.

In order to calculate

$$\int_0^{u^*_{CL}} \frac{du^*}{1 + Pr \frac{\epsilon_M}{\nu}}$$

where $\frac{\epsilon_M}{\nu}$ is given by Eqn. (96), this expression must be expressed as a function of u^*. This is done by writing that

$$\ell n\, y^* = \frac{u^* - B - \Delta u^*}{A}$$

or

$$y^* = \exp\left[\frac{u^* - B - \Delta u^*}{A}\right]. \qquad (97)$$

Therefore Eqn. (96) becomes

$$\frac{\epsilon_M}{\nu} = \frac{\exp\left[\frac{u^* - B - \Delta u^*}{A}\right]}{A} - 1. \qquad (98)$$

Note that this expression is a function of Δu^*, hence depends on the flow conditions. Now the right-hand side of Eqns. (70) and (73) may be calculated:

$$I = \int_0^{u^*_{CL}} \frac{du^*}{1+Pr \frac{\epsilon_M}{\nu}} = \int_0^{u^*_L} \frac{du^*}{1+Pr \frac{\epsilon_M}{\nu}(\text{Deiss})} + \int_{u^*_L}^{u^*_{CL}} \frac{du^*}{1+Pr \frac{\epsilon_M}{\nu}(\log)}. \qquad (99)$$

The dimensionless velocity u^*_L is defined as the intersection of the velocity profile solution of the differential equation (95) with the logarithmic velocity profile. The value of the parameter n(C, P) in Eqn. (93) that leads to the equality of the two sides of Eqns. (70) or (73) was determined as follows.

First the differential equation (93) was integrated numerically point by point for different values of n. The results were presented in a multicolumn table giving u_i^*, the corresponding y_i^*, $\frac{du_i^*}{dy_i^*}$, $\frac{\epsilon_M}{\nu}i$ and $\frac{1}{1+\Pr\frac{\epsilon_M}{\nu}i}$.

Another computation provided a second table giving u_j^* (two successive u_j^* differing by 0.05), y_j^* calculated from Eqn. (97), as well as $\frac{\epsilon_M}{\nu}j$ computed from Eqn. (96) and the corresponding

$$\frac{1}{1+\Pr\frac{\epsilon_M}{\nu}i}.$$

The intersection (u_L^*, y_L^*) of the two profiles (Deissler's and the logarithmic one) was determined by examination of the two tables, a pair (u_L^*, y_L^*) being associated with each n.

Next the integral

$$\int_0^{u_L^*} \frac{du^*}{1+\Pr\frac{\epsilon_M}{\nu}}\Bigg|_{\text{Deiss}} = \sum_{i=1}^{N} \frac{1}{1+\Pr\frac{\epsilon_M}{\nu}i}\,\delta u^*$$

was computed using the method of trapezes. The number N is given by the ratio of u_L^* and the u^* increment, in this case

$$\frac{u_L^*}{0.05}$$

$\frac{\epsilon_M}{\nu}$, as well as the upper limit of integration u_L^* are functions of n, and so is the integral. The same method was used to compute

$$\int_{u_L^*}^{u_{CL}^*} \frac{du^*}{1+Pr\,\frac{\epsilon_M}{\nu}}\bigg|_{log}$$

depending on n through the lower limit of integration.

The two integrals were then added and the left-hand side of Eqn. (99) was thus known by points as a function of n. An appropriate least square fit through these points made it possible to analytically express n = f (integral (99)) and hence to determine the value of n such that I equals the left-hand side of Eqns. (70) or (73). That value of n was introduced into the differential equation (95) and the corresponding velocity profile computed and plotted. This procedure was used for six to eight different Reynolds numbers at each temperature and concentration. The results are presented and discussed in the next chapter.

Other velocity profiles such as two layer or three layer models could have been used to calculate $\frac{\epsilon_M}{\nu}$ and the right-hand side of Eqns. (70) or (73), but it was felt that the present model did contain the features of key importance. It does not violate any physical law (such as continuity) and allows $\frac{\epsilon_M}{\nu}$ to depart from zero and vary continuously in regions close to the wall, where the major changes in velocity and temperature occur. For this reason the above model was thought to be the most appropriate for the calculation of

$$\int_0^{u^*_{CL}} \frac{du^*}{1+\Pr\frac{\epsilon_M}{\nu}},$$

the integral which appears in Eqns. (70) or (73).

Before describing the procedure used to analyze the rough tube data, a brief review of some of the models proposed by other investigators will be presented.

1. Two Layer Model (Howard and McCrory) [28]

The flow is divided into two regions

a. A viscous part ($0 \leq y \leq y_L$) where $\epsilon_H = \epsilon_M = 0$ and where τ and q vary according to the same law. Using Eqns. (44) and (45) and integrating between T_w and T yields

$$T_w - T = \frac{\dot{q}_0}{k} y = \frac{\dot{q}_0 \nu}{u_\tau k} y^* \tag{100}$$

b. A turbulent core ($y_L \leq y \leq y_{CL}$) where $\epsilon_H = \lambda \epsilon_M$, q and τ vary according to the same law and $\nu/\Pr$ and ν are negligible compared to ϵ_H or ϵ_M. Performing the integration of Eqns. (44) and (45) between T_L (temperature at the edge of the viscous layer) and T, one gets

$$\frac{(T_L - T) k u_\tau}{\dot{q}_0 \nu} = \frac{A}{\Pr \lambda} \ln \frac{y^*}{y^*_L}. \tag{101}$$

The elimination of T_L between (100) and (101) gives the temperature profile in that region. Now

$$\mathrm{Nu} = \frac{D\dot{q}_0}{(T_w - T_b)k} \tag{102}$$

where

$$T_b = \frac{\int_0^R T\,uy\,dy}{\int_0^R uy\,dy} = \frac{\int_0^{y_L} T\,uy\,dy + \int_{y_L}^R T\,uy\,dy}{\int_0^{y_L} uy\,dy + \int_{y_L}^R uy\,dy}\,.$$

2. Three Layer Model (Howard) [27]

In this approach, the flow is divided into three regions.

a. A viscous region ($0 \le y^* \le \delta^*$) where $\epsilon_H = \epsilon_M = 0$ and τ and q vary according to the same law. As previously,

$$T_w - T = \frac{\dot{q}_0 \nu}{u_\tau k} y^*. \tag{100}$$

b. A buffer zone ($\delta^* \le y^* \le y_T^*$) in which ν/Pr and ν are kept in equations, as well as ϵ_M and ϵ_H. Moreover $\epsilon_H = \lambda\epsilon_M$ with λ chosen as 1.6. Again τ and q vary according to the same linear law with the distance from the wall. Following the usual steps, one obtains

$$T_\delta - T = \int_{\delta^*}^{y^*} \frac{\dot{q}_0 (Ru_\tau - y^*\nu)\,\nu^2}{ku_\tau R\,\mathrm{Pr}\left[\alpha + \lambda\nu\left(\dfrac{Ru_\tau - y^*\nu}{Ru_\tau \dfrac{du^*}{dy^*}} - 1\right)\right]}\,dy^*. \tag{103}$$

In order to determine du^*/dy^* in the buffer zone, the author uses an expression proposed by Granville [23]:

$$u^* = A \ln (y^* - J) + B \tag{104}$$

with J such that the temperature profile as well as its derivative with respect to y^* coincide at the edge of the viscous region.

c. A turbulent core, where the effects of viscosity are neglected, a linear variation of q with distance from the wall assumed. The temperature profile in that region is given by the same expression as in the previous approach. Two unknowns remain to be determined in order to calculate the Nusselt number: the edge of the viscous region, δ^*, and the edge of the buffer region y_T^*. The author proposes that $\delta^* = 5 + \Delta u^*$, Δu^* being determined from pressure drop data (shift in logarithmic velocity profile). The dimensionless distance y_T^* is determined by expressing that the temperature profile and its slope are the same at $y^* = y_T^*$.

3. Three Layer Model (Poreh) [39]

Poreh uses the same hypotheses as those of the previous three layer model derivation, but a different expression of the velocity profile in the buffer zone. This velocity profile is an extension for polymer solutions of the Von Karman's profile derived for Newtonian fluids [31]. In Von Karman's model

$$\begin{aligned} &\text{in the viscous region:} && 0 \le y^* \le 5 && u^* = y^* \\ &\text{in the buffer zone:} && 5 \le y^* \le 30 && u^* = 5 \ln \frac{y^*}{5} + 5 \end{aligned} \tag{105}$$

in the turbulent core: $30 \leq y^* \leq R^*$ $u^* = 2.5 \ln y^* + 5.5.$

In Poreh's model,

in the viscous region: $0 \leq y^* \leq \delta^*$ $u^* = y^*$ (105) cont.

in the buffer zone: $\delta^* \leq y^* \leq y_T^*$ $u^* = \delta^* \ln \frac{y^*}{\delta^*} + \delta^*$

in the turbulent core: $y_T^* \leq y^* \leq R^*$ $u^* = 2.5 \ln y^* + 5.5 + \Delta u^*.$

According to Von Karman, the velocity prevailing in the viscous region intersects the logarithmic profile at $y_j^* = 11.6$ and

$$\frac{\delta^*}{y_j^*} = \frac{5}{11.6} = 0.43.$$

Poreh assumes that for polymer solutions, δ^* is still equal to $0.43\, y_j^*$ and determines y_j^* by expressing that

$$y_j^* = 2.5 \ln y_j^* + 5.5 + \Delta u^*.$$

He is then able to calculate the Nusselt number by making use of the Reynolds analogy. Note that this model is limited to moderate values of Pr (say $Pr < 6$), as is Von Karman's model.

4. Gupta, Metzner and Hartnett Approach [24]

The authors followed the Reichardt approach and computed from their experimental data the left-hand side of Eqn. (73), which yields the overall value of the integral

$$\int_0^{u^*_{CL}} \frac{du^*}{1+\Pr \frac{\epsilon_M}{\nu}} .$$

However, they did not calculate Φ_m and θ_m appearing in Eqn. (73) but rather took $\theta_m = 1$ and tried different values of $1/\Phi_m$, ranging from 1.18 to 2.0. The values of the integral different for each value of $1/\Phi_m$ were compared with the value for purely viscous fluids

$$\int_0^{u^*_{CL}} \frac{du^*}{1+\Pr \frac{\epsilon_M}{\nu}} = 11.8\,(\Pr_w)^{-1/3} .$$

These selected values of $1/\Phi_m$ are not very realistic, however, since it is apparent from experimental data and theoretical considerations that the velocity profile $u = f(y)$ is flatter than the corresponding one for Newtonian fluids over most of the cross section of the tube, which implies a value of $1/\Phi_m$ smaller than 1.18 (Newtonian value).

B. Data Analysis for Rough Tubes (C-9, A-4)

For the analysis of the measurements with the rough tubes the relations between C_F and Re will be considered first. From these data one may calculate $\Delta B(\epsilon^*, C, P)$, the shift in velocity profile due to the combined effect of roughness and polymer additive, and

$$u_\tau = \mathrm{Re} \sqrt{\frac{C_F}{2}}\, \frac{\nu}{D} \qquad (85)$$

the shear velocity, or $\epsilon^* = \frac{\epsilon u_\tau}{\nu}$ (ϵ is the height of the roughness elements).

Indeed, making use of Eqn. (25′), Eqn. (39a) may be written in the form

$$\sqrt{\frac{2}{C_F}} = A \ln Re\sqrt{C_F} - A \ln 2\sqrt{2} - \beta + B + \Delta B(\epsilon^*, C, P) \qquad (39'a)$$

or

$$\Delta B(\epsilon^*, C, P) = \sqrt{\frac{2}{C_F}} - 2.46 \ln (Re\sqrt{C_F}) + 2.46 \ln 2\sqrt{2} + \beta - 6.01 \qquad (106)$$

where β is defined by Eqn. (32).

The velocity shift $\Delta B(\epsilon^*, C, P)$ was calculated for each concentration and at each temperature from the analytic expression for $C_F = f(Re)$, which is the best polynomial least square fit of the experimental data. The Reynolds number was allowed to increase from its minimum to its maximum available value at a given Prandtl number by steps of 5000 and ΔB was then plotted versus $\log_{10}\epsilon^*$ using the Calcomp plotter.

These values of ΔB_{exp} were compared with the corresponding values predicted by a model due to Poreh [41]. Poreh writes the velocity profile in rough tubes with or without polymer additives as

$$u^* = A \log_{10} y^* + B + \Delta B \qquad \text{with } A = 5.75 \text{ and } B = 5.5 \qquad (107)$$

where ΔB describes the roughness effect in case of a Newtonian fluid and the combined effect of polymer and roughness with polymer additives. For a Newtonian fluid, a fit of Nikuradse's data [37] gives

$$\Delta B = - f(\epsilon^*) \qquad (108)$$

with

$$f(\varepsilon^*) = 0 \qquad \varepsilon^* < 3.35$$

$$f(\varepsilon^*) = 0.26(\varepsilon^* - 3.35) - 0.0026(\varepsilon^* - 3.35)^2 \qquad 3.35 \le \varepsilon^* < 20 \qquad (109)$$

$$f(\varepsilon^*) = 5.75 \log_{10}\left[\varepsilon^* - 2.0 - 17.4/(\varepsilon^*)^{1/2}\right] - 3.0 \qquad 20 \le \varepsilon^*$$

or, introducing the concept of relative roughness size

$$\Delta B = - f_{as}(\varepsilon^*)\, d\left(\frac{\varepsilon}{y_L}\right) \qquad (110)$$

where f_{as} is the asymptotic value of f as defined by Eqn. (109) for very large values of ε^*:

$$f_{as} = 5.75 \log_{10}\varepsilon^* - 3.0 \qquad (111)$$

$$d\left(\frac{\varepsilon}{y_L}\right) = 0$$

$$d\left(\frac{\varepsilon}{y_L}\right) = \left\{0.26\left[11.6\left(\frac{\varepsilon}{y_L}\right) - 3.35\right] - 0.0026\left[11.6\left(\frac{\varepsilon}{y_L}\right) - 3.35\right]^2\right\} / f_{as} \qquad (112)$$

$$d\left(\frac{\varepsilon}{y_L}\right) = \left\{5.75 \log_{10}\left[11.6\left(\frac{\varepsilon}{y_L}\right) - 2.0 - 17.4/\left(11.6\frac{\varepsilon}{y_L}\right)^{1/2}\right] - 3.0\right\} / f_{as}$$

for $\frac{\varepsilon}{y_L} < 0.29$, $0.29 \le \frac{\varepsilon}{y_L} < 1.72$ and $1.72 \le \frac{\varepsilon}{y_L}$ respectively.

y_L is the height of the intersection of the viscous sublayer and the log law (such that $y_L u_\tau / \nu = 11.6$).

For a polymer solution,

$$\Delta B = \Delta u^*(C, P) - \Delta B . R(\varepsilon^*, C, P) \qquad (113)$$

where Δu^* is the shift in velocity profile due to the polymer, ignoring any effect of roughness, i.e., the shift that would exist in a smooth tube at the same u_τ. The quantity $\Delta B.R$ is the shift in velocity profile due to the presence of roughness elements.

Poreh describes $\Delta u^*(C, P)$ according to Meyer's model [36]

$$\begin{aligned} \Delta u^* &= \alpha(C) \log_{10} \frac{u_\tau}{u_{\tau_{cr}}} & u_\tau > u_{\tau_{cr}} \\ &= 0 & u_\tau < u_{\tau_{cr}} \end{aligned} \tag{86}$$

Next he assumes that there is no drag reduction in very rough pipes (assumption based on Spangler's conclusions [56]) so that

$$\begin{aligned} \left.\frac{u}{u_\tau}\right._{as} &= A \log y^* + B + \Delta u^* - \Delta B.R_{as} \\ &= A \log y^* + B - f_{as} & \text{(using Eqn. (107) and (108))} \\ &= A \log \frac{y}{\epsilon} + B + 3.0 & \text{(using Eqn. (111).} \end{aligned}$$

Therefore

$$\begin{aligned} \Delta B.R_{as} &= A \log \epsilon^* + \Delta u^* - 3.0 \\ &= \Delta u^* + f_{as}\,. \end{aligned} \tag{114}$$

Poreh finally assumes that $\Delta B.R = \Delta B.R_{as} \times d\left(\frac{\epsilon}{y_L}\right)$ and, using Eqn. (113)

$$\Delta B = \Delta u^* - \Delta B.R_{as} \times d\left(\frac{\epsilon}{y_L}\right). \tag{115}$$

y_L is defined by the intersection of the viscous sublayer and the log-law, while ignoring any effect of roughness

$$y_L^* = A \log_{10} y_L^* + B + \Delta u^*. \qquad (116)$$

It may be noted, incidentally, that the equations written for polymer solution reduce to the Newtonian case if $\Delta u^* = 0$, as they should.

The shift following Poreh's approach, ΔB_{Poreh}, was calculated except that Δu^* was not derived from Meyer's model (Eqn. 86); instead the values of $\Delta u^* = f(u_\tau)$ based on the measurements of the present experiments were taken. The results of the comparison between ΔB_{exp} and ΔB_{Poreh} will be presented and discussed in the next chapter.

Finally the ratio

$$\frac{\frac{C_F}{2C_H} - 1}{\sqrt{\frac{C_F}{2}}} = f(Pr, \epsilon^*, C, P) \qquad (54)$$

was calculated from the analytic expressions of C_F and $C_H = f(Re)$. Attention was focused on this ratio rather than on the corresponding one containing Reichardt's correction factors. The fact that the values of the left-hand sides of Eqns. (70) and (73) were very close for smooth tubes indicates that the simplifications involved in the derivation of Eqn. (70) were not significantly altering the final results.

$$C_H = C\,Pr^{-0.58}\,Re^{-0.16}. \qquad (117)$$

Dipprey's data for the C-9 and A-4 tubes satisfy the equation

$$\frac{\frac{C_F}{2C_H} - 1}{\sqrt{\frac{C_F}{2}}} + 8.48 = g(\epsilon^*, Pr) = g(\epsilon^*)Pr^{0.44}. \qquad (118)$$

At high values of ϵ^* the experimental points taken at $Pr = 1.20$, 2.79, 4.38 and 5.94 fall on a common curve when $g(\epsilon^*, Pr)\,Pr^{-0.44}$ is plotted vs. ϵ^*. Therefore, in that region

$$C_{H_{Pr=6.16}} = C_{H_{Pr=5.94}} \times \frac{1 + \sqrt{\frac{C_F}{2}}\left[g(\epsilon^*) \times 5.94^{0.44} - 8.48\right]}{1 + \sqrt{\frac{C_F}{2}}\left[g(\epsilon^*) \times 6.16^{0.44} - 8.48\right]} \qquad (119)$$

with

$$g(\epsilon^*) = g\left(Re\sqrt{\frac{C_F}{2}}\,\frac{\epsilon_s}{D}\right). \qquad (120)$$

In order to compare the present data to those of Dipprey, $\epsilon^* = Re\sqrt{\frac{C_F}{2}}\left(\frac{\epsilon_s}{D}\right)$ was calculated from the C_F vs. Re data. Next $g(\epsilon^*)$ was determined from the Figure 36 of Dipprey's thesis and C_H extrapolated from $Pr = 5.94$ to $Pr = 6.16$ with the help of Eqn. (119).

The same procedure was used to extrapolate Dipprey's data from $Pr = 5.94$ to $Pr = 10.3$ for the two rough tubes (C-9 and A-4). The present heat transfer coefficients obtained for the smooth tube at $Pr = 10.3$ were also compared with the values predicted by Dittus-Boelter and Eagle-Ferguson's, and to Sparrow's formula, Eqn. (117).

According to Dittus-Boelter, [11]

$$C_H = 0.023 \times Re^{-0.2} \times Pr^{-0.6}. \tag{121}$$

The Eagle-Ferguson formula can be written [12],

$$C_H = \frac{C_F}{2} \times \frac{1}{a + b(Pr-1) - c(Pr-1)^2} \tag{122}$$

where a, b and c are functions of the Re. The calculation of C_H at $Pr = 10.3$ was performed from an analytic expression for C_F due to Allen [2]

$$\frac{C_F}{2} = 0.000695 + 0.054 \times Re^{-0.308}. \tag{123}$$

All these predicted values of C_H are presented vs. Re on Figure 13 along with the data obtained from the present experiments. The latter fall a little below Allen's data, as extrapolated according to Eagle-Ferguson.

The excellent agreement between the friction and heat transfer coefficients for water obtained in the present investigation and the extrapolated values of other authors seemed to indicate that the instrumentation was working properly and that the calibrations were satisfactorily performed. This agreement established the necessary reference base to carry on the numerous tests with Polyox solutions with confidence.

Before describing the experimental results with Polyox WSR 301 at 10 and 50 ppm, it should be mentioned that all the data presented in this thesis are extrapolated values for a zero "wall-to-fluid" temperature difference, ΔT_f. Tests conducted with water at three different

ΔT_f and different Re verified Allen's data [2] (smooth tube) within the limits of accuracy of our data: the smooth tube showed a decrease in C_F and an increase of C_H with increasing wall-to-mixed-fluid temperature difference, depending on the Re. Therefore, Allen's results were applied systematically in the extrapolation. The rough tubes showed little, if any, C_F or C_H dependence on ΔT_f and no extrapolation seemed justified.

B. Presentation of C_F and C_H Data for Polyox Solutions at Concentrations of 10 and 50 ppm

Tests with Polyox similar to those conducted with water in smooth tubes for purposes of zero ΔT_f extrapolation revealed that the slopes of C_F and C_H vs. ΔT_f are slightly steeper with Polyox than Allen's slopes for water, the slopes increasing with the concentration. Nevertheless the accuracy of the measurements was not quite sufficient to describe quantitatively the C_F or C_H dependence on ΔT_f and Re. Since ΔT_f was maintained between 5 and 10° F, it was felt that a systematic use of Allen's slopes would still give a satisfactory approximation of the isothermal values for C_F or C_H. Isothermal measurements of C_F (no heat flux) compared very well with the values obtained by Allen's extrapolation from an actual ΔT_f to zero and supports the above argument. The C_F or C_H dependence on ΔT_f for the rough tubes, which was negligible with pure water, was now noticeable over a wide range of Re. Several runs were performed at three different ΔT_f at three different Re ($\simeq$ 20000, 60000 and 120000), and the average values of C_F and C_H

over the tests corresponding to a given ΔT_f were plotted vs. ΔT_f. Qualitatively, the C_F and C_H dependence on ΔT_f was felt most at an Re in the vicinity of 60000 and was barely noticeable at high Re. Here again the scatter in the data did not allow an analytical expression for the dependence of C_H and C_F on ΔT_f and Re. As a consequence it was decided to determine C_F from strictly isothermal tests (zero heat flux) and C_H from tests where ΔT_f is kept small, say between 5 and 10°F so that $C_H(\Delta T_f) \simeq C_H(0)$.

1. Description of Smooth Tube Data (E-3)

The friction coefficients for 10 ppm and 50 ppm Polyox solutions in smooth tube (E-3) are displayed in Figures 10 and 11 respectively as functions of Re. The corresponding curve for water is shown as a comparison. It should be mentioned that the Re used in these figures is the Re of the solution which, however, differs from that of pure water by less than 2%. The difference is due to the change in viscosity when polymers are added to the solvent. Data could, of course, be replotted vs. $Re_{solution}$ using the change of variables

$$Re_{solution} = Re_{water} \times \frac{\nu_{water}}{\nu_{solution}}. \qquad (124)$$

Figures 10 and 11 clearly exhibit the Toms effect: the minimum Re obtainable experimentally with the present installation is far greater than the threshold Re at which the onset occurs. The fractional drag reduction, defined as

$$R_F = 1 - \frac{\tau_{0_p}}{\tau_{0_s}} = 1 - \frac{C_{F_p}}{C_{F_s}}\bigg|_{Re} \tag{125}$$

(where τ_{0_p} and τ_{0_s} are the shear stress at the wall with and without polymer respectively), is considerable (maximum around 73%) and appears to be only slightly dependent on concentration (a 50 ppm solution yields about one percent more fractional drag reduction than a 10 ppm solution). The fractional drag reduction vs. Re is plotted on Figure 17 for the three different Pr (4.38, 6.16 and 10.3) and the two concentrations (10 ppm and 50 ppm). For the 50 ppm solution the fractional drag reduction increases continuously over the range of Re tested at all Pr. The 10 ppm solution shows a similar behavior at $Pr = 6.16$ and 10.3. At $Pr = 4.38$, however, the 10 ppm solution reaches a maximum of 72.25% at $Re = 120,000$ and then decreases monotonically. This suggests a possible degradation of the polymer molecules at the corresponding temperature of 103°F, leading to a loss in efficiency of the solution.

A slight temperature effect is also present, the solutions being most efficient at the lowest temperature ($T = 48°F$). This effect tends to disappear at high Re, the curves merging around $Re = 100,000$, before degradation begins at the high temperature. An extrapolation of the three curves to their intersection with the friction curve of the solvent would probably lead to different values of the Re at the onset of drag reduction. However, the minimum Re attainable in the present experiments was still too high to allow a satisfactory extrapolation. An examination of Figures 14 and 15 (C_H vs. Re for 10 and 50 ppm solutions) reveals that a Pr effect is present with the polymer solutions as it was with pure water. The similarity between the C_F and C_H curves is striking: for the 50 ppm solution and for all three Pr, the fractional heat transfer reduction, defined as $1 - (C_{H_P}/C_{H_S})$, increas s over the whole range of Re. The 10 ppm solutions show a similar trend at Pr = 10.3. At Pr = 6.16 and 4.38, however, the 10 ppm solution curve reaches a maximum drag reduction around Re = 90,000 and then decreases. The fractional heat transfer reduction is plotted on Figure 17 in the same fashion as the fractional drag reduction. It appears that heat transfer is reduced even more than the friction (about 6% more reduction of C_H than C_F for the 10 ppm solutions, and about 10% for the 50 ppm solutions). The effect of concentration is more marked here than it was for C_F: a 50 ppm solution brings about 5% more heat transfer reduction than the 10 ppm solution. Thus an increase of concentration, while having little influence on the friction coefficient, does affect the heat transfer coefficient somewhat. A comparison of the heat transfer reductions attained at Re = 100,000 for different Pr indicates that the solution at room temperature is slightly more efficient in reducing the heat transfer than at at higher or lower temperatures (79.8% at Pr = 6.16 compared to 79.5% at Pr = 10.3 and 4.38 respectively for 10 ppm solutions, 84.5% at Pr = 6.16 against 83.5% and 81.6% at Pr = 10.3 and 4.38 respectively for 50 ppm solutions).

It seems, from Figures 10, 11, 14 and 15, that the 50 ppm solution is more stable than the 10 ppm one, the C_F and C_H-50 ppm curves showing no signs of degradation even at high flow rate. The problem of possible mechanical degradation of the solutions under high shear conditions will be discussed later in this section.

Figures 12 and 16 show C_F and C_H curves vs. Re obtained with a one-month old undisturbed solution. Corresponding curves for a fresh solution are presented for comparison. Ageing decreases the efficiency of the solution as a friction and heat transfer reducer, but yet a considerable reduction is still obtained (as high as 61.8% for drag reduction and 69.4% for heat transfer reduction at Re = 100,000). Again the similarity of the C_F and C_H curves is striking.

2. Description of Rough Tubes Data (C-9 and A-4)

The two rough tubes (C-9 and A-4) used are characterized by a ratio ε/D of 0.0054 and 0.0195 respectively. With pure water, the "fully rough" regime is reached at a Re of about 75,000 for C-9 tube and 18,000 for A-4 tube; the friction coefficient is then independent of Re. Such a behavior is not apparent with Polyox, as shown by Figures 18 and 19 (C-9 tube) and 23 and 24 (A-4 tube). The curves exhibited on these figures display the same trends, (although the features are more accentuated with the A-4 tube), and will be described simultaneously. For both tubes the friction coefficient first decreases with increasing Re, reaches a minimum, then again increases. The curve for the 10 ppm solution converges toward that of pure water at high Re, while the curve for the 50 ppm solution remains considerably below the curve for water. A large reduction in frictional drag is obtained (as high as 83.5% for the C-9 tube and 83% for the A-4 tube). Over part of the Re range the friction factor is actually smaller than the one for pure water in a smooth tube. The fractional drag reduction is presented vs. Re in Figures 22(C-9 tube) and 28 (A-4 tube). It is evident from these figures that the 50 ppm solutions remain more effective as drag reducers than the 10 ppm solutions. A temperature effect is also present as can be seen from Figures 9, 18, 19, 23 and 24: the "cold" solution (48°F) appears the most efficient in reducing drag at low Re. The curves corresponding to the three different Pr merge at a Re between 60,000 and 100,000, then depart again from each other but with a reverse trend: "hot" solutions become then the most effective.

The curves for the heat transfer coefficients will be described next. Figures 20, 21 (C-9 tube) and 25, 26 (A-4 tube) clearly show a similarity between the C_F and C_H curves. Just like the friction coefficient, C_H decreases first with increasing Re, reaches a minimum, then converges toward the solvent curve. The curve for the 10 ppm solution almost meets the latter at high Re. The reduction of C_H at low Re is most remarkable; it reaches a maximum of 93.25% for the C-9 tube and 93.6% for the A-4 tube.

The fractional heat transfer reduction is plotted vs. Re on Figures 22 (C-9 tube) and 28 (A-4 tube) along with the fractional drag reduction, which allows a direct comparison of magnitude of both heat and momentum transfer reductions. It is apparent from these curves that the heat transfer is decreased even more drastically than the friction, and that at high Re the more concentrated solution (50 ppm) remains much more effective than the 10 ppm solutions.

The heat transfer coefficients are dependent on the Pr for Polyox solutions as they were for pure water. The curves for Polyox solutions, however, differ from those for water, in that they have the tendency to merge at high Re. The heat transfer coefficients obtained with 10 ppm solutions at $Pr = 10.3$ even exceed the ones obtained for $Pr = 4.38$ or 6.16, if Re is sufficiently large.

The values of C_H predicted by Poreh's model [41] are also displayed on Figures 18, 19, 23 and 24. Clearly they are all higher than the ones obtained in the present experiments. The reason why his model seems to fail with Polyox, while being quite successful with other polymers [41, 56] will be discussed later in this section.

It might be mentioned that all of the coefficients C_H which were presented are actually averages of two values calculated from measurements of the wall temperature at two different circumferential locations (and the same axial location). Some discrepancy between these two computed C_H was apparent for the rough tubes (C-9 and A-4). A typical example of the local variation of the heat transfer coefficient for the A-4 tube is shown in Figure 27. The upper and lower curves were obtained from wall temperature measurements at two locations 120° apart at the same axial distance from the edge of the heated portion of the tube. The average experimental points, as well as their best fit are also displayed on this figure along with the curve for water. The circumferential dispersion at the same station (at most 10% of the C_H polymer), is probably related to the exact location of the thermocouples in respect to a roughness element. It seems to be more pronounced with Polyox than with pure water.

3. Comparison of Data Obtained at a Given Pr in the Three Tubes with Water, 10 ppm and 50 ppm Polyox Solutions

Figures 29, 30 and 31 show a comparison of the friction coefficients obtained in the smooth and rough tubes (E-3, C-9, A-4) with water, 10 ppm and 50 ppm Polyox solutions at Pr of 4.38, 6.16 and 10.3 respectively. These three figures, as well as Figures 32, 33 and 34, all display the same trends, and will be described simultaneously. A first important feature, apparent on Figures 29, 30 and 31, is that the friction factors obtained in the two rough tubes always exceed the ones with a smooth wall, as it was the case for water. Moreover, the curves for Polyox in the two rough tubes all tend to converge toward the curves for the E-3 tube at low Re. It should be noticed also that, in the two rough tubes, the curves for the 10 ppm solutions depart from the corresponding 50 ppm ones at low Re. For the A-4 tube, this departure begins at about Re = 20,000, and for the C-9 tube, at Re = 40,000 to 50,000. For a smooth E-3 tube this deviation is noticeable at Pr = 4.38 only. The friction factor obtained with 10 ppm solutions always exceeds the corresponding value with a 50 ppm solution and eventually the data for 10 ppm solutions in rough tubes approach the value for the pure solvent at high Re. As was said previously, it is believed that the 10 ppm solutions degrade more easily than the 50 ppm solutions. Finally, it may be seen that the C_F curves with Polyox at both concentrations fall below the C_F curve for water in smooth tube over a wide range of Re, particularly with

50 ppm solutions.

In Figures 32, 33 and 34 the results are shown for the heat transfer coefficients which have been obtained in the three tubes with 0, 10 and 50 ppm Polyox solutions at the Pr of 4.38, 6.16 and 10.3. An examination of these figures reveals that the heat transfer coefficient in a rough tube can be smaller than that in a smooth tube; this never happens with water, where the roughness elements always improve the heat transfer. The curves obtained with the C-9 and A-4 tubes for a 10 ppm solution fall under the corresponding curves for the E-3 tube for a range of Re up to about 60,000 and 30,000 respectively, while the heat transfer coefficients for a 50 ppm solution remain smaller than the corresponding values for the E-3 tube up to Re of about 125,000 (C-9 tube) and 50,000 (A-4 tube). A possible explanation of these surprising results will be given later in this chapter. Like the friction coefficients, the C_H data with 10 ppm solutions always exceed the ones with 50 ppm solutions for every tube, the two curves departing from one another at very low Re (around 10,000 it seems). The data for the 10 ppm solutions rapidly converge toward the corresponding ones for water, while this trend is not so pronounced with the 50 ppm solutions. It should be pointed out that most of the heat transfer data relative to Polyox remain lower than the data obtained with pure water in smooth tubes under similar flow conditions.

The experimental results described so far in this section will form the subject of a general discussion presented in a subsequent paragraph. The C_F and C_H data were analyzed following the procedure described in Chapter V. The results of that analysis will be considered next.

C. Presentation of Results of Data Analysis for the Smooth Tube (E-3)

A correlation between the shear stress at the wall τ_0, or the shear velocity u_τ and the shift Δu^* in the velocity profile, due to the action of the polymer molecules, has been proposed by Meyer [36] and is used frequently in the literature

$$\Delta u^* = \alpha(C) \log_{10} \frac{u_\tau}{u_{\tau_{cr}}} \cdot \qquad (u_\tau \geq u_{\tau_{cr}}) \qquad (86)$$

where $\alpha = \alpha(C)$ is a function of concentration, C.

The quantity $u_{\tau_{cr}}$ is the shear velocity at which onset of drag reduction occurs.

In order to test the validity of this correlation with Polyox (10 and 50 ppm) at three different temperatures (48°, 76° and 103°F), Δu^* was plotted vs. $\log_{10} u_\tau$. Meyer's formula predicts a straight line, the slope of which is $\alpha(C)$ and whose intercept at $\Delta u^* = 0$ defines $u_{\tau_{cr}}$. The curves Δu^* vs. $\log_{10} u_\tau$ are displayed in Figure 35 (10 ppm) and Figure 36 (50 ppm).

Meyer's correlation 10 ppm solutions (Figure 35) is well verified at Pr = 6.16 and 10.3, while at Pr = 4.38, a possible thermal degradation of the solutions limits the validity of the formula to $u_\tau \simeq 0.5$ ft/sec. The slopes of the curves differ for each Pr, indicating that the parameter α in Eqn. (86) is not only dependent on concentration, but also on the temperature of the solution. It appears that α decreases with temperature. The results for the 50 ppm solutions (Figure 36) are slightly different from those for the 10 ppm ones. The data are well correlated by Meyer's equation at Pr = 10.3 but Δu^* no longer varies quite linearly with $\log_{10} u_\tau$ at Pr = 4.38 and 6.16. Nevertheless the departure from a straight line remains reasonably small, so that Meyer's correlation constitutes a fairly good approximation. Here again a temperature effect is present, similar to that noticed with 10 ppm solutions. From reports in the literature one would expect an increase of α with increasing concentration [36], and this is in agreement with the present results satisfying Meyer's correlation best (Pr = 10.3). As mentioned previously, the critical shear velocity appearing in Eqn. (86), cannot be determined from the measurements reported here as no data were taken near the onset of drag reduction. In addition, the possibility of mechanical degradation would not justify any major extrapolation.

The smooth tube data were analyzed following the procedure described in Chapter V. In order to evaluate the right-hand side of Eqns. (70) and (73) close to the wall, a relationship for $\frac{\epsilon_M}{\nu}$ was used which is similar to that proposed by Deissler:

$$\frac{\epsilon_M}{\nu} = n^2(C, P) u^* y^* \left(1 - e^{-n^2 u^* y^*}\right). \tag{93}$$

The integration

$$\int_0^{u^*} \frac{du^*}{1 + Pr \left.\frac{\epsilon_M}{\nu}\right|_{Deis.}} = f(u^*)$$

was then performed for different values of n, ranging from 0.02 to 0.124 (Newtonian value) and plotted vs. u^*. Figure 37 shows one of these plots at $Pr = 6.16$. The values of the parameter n(C, P) that best fit the C_F and C_H data were determined as indicated in Chapter V. These values are plotted on Figure 38 vs. $\log_{10} u_\tau$ for 10 and 50 ppm and at three temperatures of 48°, 77° and 103°F. The factor, n(C, P) is shown as a function of u_τ because it is likely that, close to the wall, the dimensionless group characterizing the polymer (P) depends itself on the shear stress: in the derivation of the law of the wall, (cf. p. 31) P was chosen as $\ell u_\tau/\nu$ or an equivalent dimensionless group based on the time hypothesis. The value of n for water ($n = 0.124$) exceeds by far the ones for Polyox. Thus the proposed model (Eqn. 93) predicts that the addition of polymer in water reduces drastically ε_M/ν near the wall. Moreover, the points relative to the 50 ppm solutions fall below the ones for the 10 ppm solutions, indicating a more important reduction of ε_M/ν near the wall when Polyox is present in solution at higher concentration (50 ppm).

A temperature effect is apparent at both concentrations, which is not surprising since P is probably dependent on temperature as well. This will be discussed in more detail later in this chapter. The values of n predicted by the model are difficult to analyze for Polyox 10 ppm. The curves seem to indicate that a possible degradation exists at $Pr = 4.38$ and 6.16 for values of u_τ as low as 0.5.

In general one would expect the factor n to approach the value $n = 0.124$ both when u_τ becomes very large or when u_τ becomes smaller than the critical value.

The velocity near the wall corresponding to each n(C, P) was computed by integrating point by point the differential equation

$$\frac{dy^*}{du^*} + \left[n^2 u^* \left(e^{-n^2 u^* y^*} - 1\right)\right] y^* = 1$$
$$u^* = 0 \quad \text{at} \quad y^* = 0. \tag{95}$$

Away from the wall, the logarithmic defect law was assumed to hold, the slope being the same for Polyox as for water. The shift Δu^* in the profile was calculated following the procedure given in Chapter V. The results are shown in Figures 39 and 40 for 10 and 50 ppm solutions respectively at $Pr = 6.16$ (room temperature), along with the profile $u^* = y^*$ obtained by totally neglecting $\frac{\epsilon_M}{\nu}$ near the wall (Prandtl's model [42]). The velocity profile $u^* = f(y^*)$ is universal with water. This is no longer true with Polyox as the shift Δu^* in the profile depends on the flow conditions, as well as the nature and concentration of the polymer. It is clear from these figures that the slight change of n with u_τ or with the flow rate does not affect the resulting velocity profiles very much. The curves corresponding to different Re remain relatively close together, particularly with the 50 ppm solution. The profile calculated from Deissler's formula departs from the law $u^* = y^*$ at $y^* \simeq 5$ for water, while with Polyox it begins to differ noticeably from $u^* = y^*$ around $y^* = 10$ (10 ppm) and 15 (50 ppm) only. Thus the proposed model predicts a thickening of the "laminar sublayer" with addition of polymer. The profiles with Polyox are steeper than that with water in the region usually called "buffer zone", i.e., the region within which the motion is governed by viscous and turbulent forces, indicating that with Polyox the viscous forces remain significant further away from the wall than with water. These results will also be discussed in a further paragraph of this chapter.

D. Presentation of Results of Data Analysis for Rough Tubes (C-9, A-4)

The shifts in the velocity profile due to the simultaneous effect of Polyox and roughness were first calculated from the friction data (Eqn. 106). $\Delta B(\epsilon^*, C, P)$, obtained for the C-9 and A-4 tubes with 10 and 50 ppm solutions are plotted vs. $\log_{10}\epsilon^*$ on Figures 41, 42 and 43 at Pr of 4.38, 6.16 and 10.3, along with $\Delta B(\epsilon^*)$ for water. The function $\Delta B(\epsilon^*, C, P)$ can also be written

$$\Delta B = \Delta B\left[\epsilon^*, C, P(\epsilon^* P'')\right] \tag{126}$$

where

$$\begin{aligned} P(\epsilon^* P'') &= \epsilon^* \frac{\ell_1}{\epsilon} &\quad \text{if} \quad P &= \frac{\ell_1 u_\tau}{\nu} \\ &= (\epsilon^*)^2 \frac{t_1 \nu}{\epsilon^2} &\quad \text{if} \quad P &= \frac{u_\tau^2 t_1}{\nu} \\ &= \epsilon^* \frac{\nu}{\epsilon u_{\tau_{cr}}} &\quad \text{if} \quad P &= \frac{u_\tau}{u_{\tau_{cr}}} . \end{aligned}$$

In this representation P'' would then be equal to the factor multiplying ϵ^* (or ϵ^{*2}). Hence a plot of ΔB vs. ϵ^* for two tubes of different roughness and two polymer concentrations ought to display four different curves corresponding to all combinations of C and P''. Note that P''

contains in its group a polymer characteristic, which is likely to depend on temperature, and so will ΔB.

The figures 41, 42 and 43 will be considered next. The curves for C-9 and A-4 tubes all fall considerably above that for water, and form two different families. The concentration effect, first small at low u_τ, becomes rapidly very significant, the ΔB corresponding to the 50 ppm solutions always exceeding that for the 10 ppm solutions. Note that a positive (negative) ΔB means that the Polyox logarithmic profile is shifted toward higher (lower) values of u^* with respect to that of water in smooth tubes, due to the combined effect of polymer and roughness. Thus the 50 ppm solutions, leading to a higher ΔB than the 10 ppm solutions, seem to be less affected by the roughness elements than the latter. The shift ΔB remains positive over the whole domain of variations of ϵ^* for the C-9 tube with a 50 ppm solution. For the C-9 tube and a 10 ppm solution ΔB becomes negative when ϵ^* exceeds 85. For the roughest tube (A-4) ΔB becomes negative for ϵ^* larger than 150 (10 ppm) or 200 (50 ppm). A slight temperature effect is also present, probably due to a change in the configuration of the polymer molecules in solution, expressed by a change in P″.

The friction and heat transfer coefficients were combined in a dimensionless group

$$\frac{\frac{C_F}{2C_H} - 1}{\sqrt{\frac{C_F}{2}}} = g(Pr, \epsilon^*, C, P) \qquad (54)$$

and the g function was calculated from data for the two rough tubes (C-9 and A-4) and for concentrations of 10 and 50 ppm. The g function is plotted vs. $\log_{10}\epsilon^*$ on Figures 44, 45 and 46 for Pr of 4.38, 6.16 and 10.3 respectively. Similar curves for water are shown for comparison. As was done previously, $g(Pr, \epsilon^*, C, P)$ may be written as

$$g = g\left[Pr, \epsilon^*, C, P(\epsilon^* P'')\right]. \tag{127}$$

One obtains, at a given Pr, four experimental curves corresponding to the various combinations of the two concentrations and of the two dimensionless groups P'', which are directly related to the average height of the roughness elements.

The concentration effect is important, the values corresponding to 50 ppm solutions exceeding sometimes that for 10 ppm solutions by as much as a factor two. For water, as ϵ^* increases, the dimensionless group g first decreases, then reaches a minimum before increasing as the fully rough regime is attained. Exactly the opposite trend is observed with Polyox: $g(Pr, \epsilon^*, C, P)$ first increases with increasing ϵ^*, reaches a maximum then decreases drastically, eventually adopting an asymptotic behavior at high values of ϵ^*. The shape of the curves might be caused by a combined effect of shear degradation and modification of the nature of the regime toward a fully rough one. These considerations will be developed in the general discussion of the results.

The influence of Pr clearly appears in Figures 47, 48, 49 and 50, which contain data for the C-9 tube at 10 ppm and 50 ppm and for the A-4 tube at the same two concentrations. Each combination was tested at three Pr (4.38, 6.16 and 10.3). The function g increases with increasing Pr with Polyox as well as with water, but while the curves with water remain parallel, varying according to a law in $Pr^{0.44}$ at ε^* high enough to be in the fully rough region [10], the ones with Polyox tend to merge into a single curve independent of Pr at high ε^*.

The g function is also presented vs. $\log_{10} u_\tau$ on Figures 51, 52 and 53. The reason is that $g(Pr, C, \frac{\varepsilon u_\tau}{\nu}, P)$ can also be written as

$$g = g\,[Pr, C, \varepsilon p'', P(u_\tau)] \qquad (128)$$

where

$$p'' = \frac{1}{\ell_1} \qquad \text{if} \qquad P = \frac{\ell_1 u_\tau}{\nu}$$

$$= \frac{1}{\sqrt{\nu t_1}} \qquad \text{if} \qquad P = \frac{u_\tau^2 t_1}{\nu}$$

$$= \frac{u_{\tau_{cr}}}{\nu} \qquad \text{if} \qquad P = \frac{u_\tau}{u_{\tau_{cr}}} \; .$$

Each curve will now correspond to a combination of the parameters C and $\varepsilon p''$.

E. Discussion of Results for Smooth Tube (E-3)

One of the purposes of this present experiment was to obtain information on the ratio of the turbulent momentum diffusivity and kinematic viscosity, ε_M/ν. This can be achieved by calculating C_F and C_H from simultaneous pressure drop and heat transfer data. The friction and heat transfer coefficients are indeed related to ε_M/ν by the equation (see Chapter III and Appendix IV)

$$\frac{\dfrac{C_F}{2C_H}\,\dfrac{1}{\theta_m}\,\overline{\dfrac{\varepsilon_H}{\varepsilon_M}} - \dfrac{1}{\Phi_m}}{\sqrt{\dfrac{C_F}{2}}\left(\dfrac{\varepsilon_H}{\varepsilon_M}\,Pr - 1\right)} = \int_0^{u^*_{CL}} \frac{du^*}{1 + Pr\,\dfrac{\varepsilon_H}{\varepsilon_M}\,\dfrac{\varepsilon_M}{\nu}} \qquad (73')$$

where

$$\Phi_m = \frac{\bar{u}}{u_{CL}}$$

$$\theta_m = \frac{T_L - T_w}{T_{CL} - T_w}$$

T_{CL} and u_{CL} are respectively the temperature and velocity at centerline.

$\dfrac{\varepsilon_H}{\varepsilon_M}$ is the ratio of the heat and momentum turbulent diffusivities.

The calculation of the left-hand side of the latter equation, performed at Pr of 4.38, 6.16 and 10.3 with the ratio $\varepsilon_H/\varepsilon_M$ varying from 0.5 to 1.5 reveals that the integral in the right-hand side of the same equation must take a much higher value with Polyox than with water. This in turn implies that either ε_M/ν must be considerably reduced when Polyox is present in solution, or that $\varepsilon_H/\varepsilon_M$ takes a much lower value for polymeric flows than it does for water. A lower value of the ratio of the diffusivities means that, unlike water, momentum can be transferred without being accompanied by a similar transfer of heat. In other words, the idea behind the Reynolds analogy would not hold with polymer solutions. It may be pointed out that, as u^* increases, i.e., as the distance from the wall increases, ϵ_M/ν becomes very large, and the integrand of Eqn. (73′) goes rapidly to zero and therefore does not bring any contribution to the integral. Hence the use of Eqn. (73′) gives information on ϵ_M/ν (or ϵ_H/ϵ_M) only near the wall. But this region is of particular interest since most of the changes in velocity take place there.

A careful examination of the values taken by the left-hand side of Eqn. (73′) shows that a reduction of ϵ_H/ϵ_M from 1 (assumed value for water near the wall) to as low as 0.5 could not provide a value of the integral that can match the left-hand side of this equation, unless ϵ_M/ν is also drastically reduced (with respect to corresponding values for water). The comparison of the values obtained from data with 50 ppm Polyox and water at Pr = 6.16 and Re = 100,000 illustrates this point.

$\frac{\epsilon_H}{\epsilon_M}$	Values of LHS of Eqn. (73′) for Polyox 50 ppm	Values of LHS of Eqn. (73′) for water
0.5	23.788	
1.0	28.061	7.875
1.5	29.140	8.736

From the measured values of the friction and heat transfer coefficients alone and without using any restrictive assumption, it may, therefore, be concluded that ϵ_M/ν must be reduced near the wall when Polyox is added to water, even in minute quantities. Clearly this means that compared to pure water, ϵ_M/ν becomes $>>1$ much further away from the wall with Polyox solutions, or, in other words, that the region governed by viscous forces extends much further from the wall. This in turn implies that the normalized velocity profile for Polyox (u^* vs. y^*) in the region close to the wall (and before the start of the logarithmic profile) is much steeper than the one for water at a given y^*. This is a direct consequence of the integration of the differential equation $\frac{dy^*}{du^*} - \frac{\epsilon_M}{\nu} = 1$, valid near the wall. This change in the velocity profile may also be described by saying that the laminar sublayer and buffer zone extend further from the wall with Polyox than with water. This is in agreement with the "thickening of laminar sublayer" proposed in many papers explaining the Toms phenomenon. It is felt, however, that it may be more appropriate to think of the "thickening of the viscous sublayer" as the result, rather than as the cause, of the reduction of momentum transfer. The model used in the present work – based on the following assumptions: $\epsilon_H/\epsilon_M = 1$, same slope of logarithmic profile with Polyox as with water, $\epsilon_M = n^2 u^* y^* (1 - e^{-n^2 u^* y^*})$ – leads to the same previous conclusions. As mentioned in Chapter V, near the wall, but sufficiently far so that the velocity profile is logarithmic,

$$\frac{\epsilon_M}{\nu} = \frac{y^*}{A} - 1. \qquad (96)$$

This expression states that at a given radial location in y in the vicinity of the wall, ϵ_M/ν will practically vary proportionally to u_τ/A or $\sqrt{\tau_0}/A$ (A is the slope of the logarithmic profile). Thus, unless A is changed tremendously by the addition of Polyox in water, which is very unlikely (see Chapter II), ϵ_M/ν is reduced in the turbulent core as well.

In the proposed model, n depends explicitly on the concentration as well as on a group characteristic of the polymer in solution: $n = n(C, P)$. Moreover, a temperature effect was noticed, which can be explained by the fact that P is certainly temperature dependent itself. For the sake of argument, assume that a characteristic length ℓ is selected to describe the polymer in solution, and $P = \ell u_{\tau}/\nu$. The length ℓ is usually chosen as the rms radius of gyration of the molecule. It could also be the mean square, end-to-end length $\langle r^2 \rangle$ of the polymer chain. J. E. Mark and P. J. Flory [33] studied the variation of $\langle r^2 \rangle$ with temperature and concluded that, for Polyox, $d\ell n \langle r^2 \rangle_0 / dT = (0.23 \pm 0.02) \times 10^{-3} \text{deg}^{-1}$. Thus the molecule expands with an increase in temperature, and the dimensionless group P is temperature dependent through ℓ and the kinematic viscosity ν. ℓ depends also on the degree of degradation of the molecules (polymer chain cleavage), hence depends implicitly on the local shear stress level. A similar reasoning could be held for P based on the time-hypothesis (cf. Chapter II).

The examination of C_F (Figures 10 and 11), C_H (Figures 14 and 15), of the friction and heat reduction curves (Figure 17) as well as the check of Meyer's correlation (Figures 35 and 36) and the plots of n(C, P) vs. $\log_{10} u_{\tau}$ (Figure 38) all seem to reveal that a degradation of the Polyox solutions takes place under certain shear conditions. The degree of degradation seems to depend on the temperature of the tests as well as the concentration of the polymer. It is believed that degradation begins at values of the shear velocity as low as 0.5 ft/sec for the tests run at $Pr = 4.38$. It is predictable that the degradation occurs sooner in "hot" solutions than in "cold" ones, because of the increase of energy of vibration and rotation of the molecules with an increase of temperature, leading to a looseness of the chemical bonds.

The results of a previous experiment consisting in forcing a solution of two polymers of the same family (say Polyox) but of different molecular weights into a straight pipe and measuring the pressure drop along the tube could be used to explain why the 50 ppm solution seems to be less subject of degradation than the 10 ppm ones. It was found that the polymer of higher molecular weight governs the behavior of the mixture. It is then easy to conceive intuitively that even if a relatively large proportion of the molecules are broken under high shear conditions, the intact molecules will still be numerous enough in a high concentrated solution to govern the phenomenon almost as if no degradation took place.

To close the subject of degradation, it should be mentioned that Polyox solutions lose some of their efficiency as drag reducers when stored for more than one week [69]. In the present series of experiments a significant reduction in effectiveness was noted after one month. It has been suggested [44] that physical absorption on the solid surfaces of the container, as well as possible reactions of impurities contained in water with the polymer could be responsible for that effect.

F. Discussion of Results for RoughTubes (C-9, A-4)

Mechanical degradation occurs in most of the tests run in the rough tubes as the level of shear velocity exceeds by far 1 ft/sec (usually considered as the upper limit beyond which degradation takes place). The following experiment proves it. Two tests were performed with the A-4 tube, in which u_τ was equal to 2.18 ft/sec and 0.82 ft/sec respectively. A fresh solution was used for each test. The solutions from each test were then rerun separately in the smooth tube at low Re (to avoid new shear degradation) and the friction coefficients obtained were compared with those of a fresh solution. The friction coefficients obtained in the smooth tube with the solutions previously tested under the shear conditions indicated above were respectively 86.5% and 28% higher than those of a fresh solution, indicating that indeed mechanical degradation took place during the tests in the rough tube. The mechanical degradation thus noticed reduces the effectiveness of the solution as friction (and heat transfer) reducer, and is certainly partly responsible for the drastic increase of C_F at high Re.

This drastic increase of C_F and C_H with Re which, at high Re, makes the values of these coefficients approach those for pure water might, however, also be due to a change in hydraulic regime. For pure water, it may be recalled, C_F increases in the transition regime with increasing Re, until it reaches a horizontal plateau as the "fully rough" regime is attained. Moreover a number of recent analyses and experimental studies of turbulence with polymer solutions suggest that the presence of polymer in solution affects mainly the high wave number region of the turbulent spectrum. In smooth tubes the production of small eddies of great intensity takes place very close to the wall, in a region governed by viscous forces. Such a region is suppressed in a fully rough regime and some authors argue that the absence of that viscous layer affects the ability of Polyox to damp out some of the turbulence as it does in smooth pipe; this in turn would lead to a loss of efficiency of the polymer as a drag reducer.

The criterion for the onset of a fully rough regime is, however, much more ambiguous in the case of Polyox than it is with water. For Newtonian fluids, it is usually well accepted that the fully rough regime is attained when

$$\frac{\epsilon u_\tau}{\nu} \geq 70 \tag{129}$$

where ϵ is the height of the protrusions, or, if this criterion is expressed in terms of ϵ/y_L (where y_L is a characteristic length defined as the intersection of the viscous sublayer and the fully turbulent region in the two layer model), the fully rough regime is attained when

$$\frac{\epsilon}{y_L} = \frac{70}{11.6} = 6.0345.$$

In dimensionless quantities,

$$\epsilon^*_{F.R} = 6.0345 \times y^*_L. \tag{130}$$

Since the velocity profile u^* vs. y^* is universal for water, y^*_L (water) is is constant and takes the value of 11.6. This is no longer true for Polyox solutions, as y^*_L now depends on the shift in the logarithmic profile $\Delta u^*(C, P)$. Since P is a function of u_τ, we can write that

$$y^*_L = f[\Delta u^*]$$

$$= f[C, p\, f(u_\tau)]$$

where p contains a length or time characterizing the polymer in solution, and $f(u_\tau)$ designates a function of u_τ. Thus y_L^*, hence $\epsilon_{F.R}^*$ takes a different value for each wall shear stress.

In order to find out whether we actually attain the fully rough conditions in our experiments, y_L^* was first computed on the basis of the shear velocity u_τ in a smooth tube at the same temperature and flow rate. Next $\epsilon_{F.R}^*$ was determined from Eqn. (128) and compared with the actual ϵ^* of the test. The fully rough conditions are considered satisfied if

$$\epsilon^* > \epsilon_{F.R}^* . \tag{131}$$

This calculation reveals that ϵ^* becomes larger than $\epsilon_{F.R}^*$ for $u_\tau > 1.4$ in the roughest tube (A-4). Clearly, $u_\tau = 1.4$ is the intersection of the straight line $\epsilon^* = \epsilon u_\tau/\nu$ with the curve $\epsilon_{F.R}^* = f[\Delta u^*]$. At $Pr = 6.16$, $u_\tau = 1.4$ corresponds to Re of about 80,000 and 110,000 for 10 ppm and 50 ppm solutions respectively.

One may conclude from this discussion that the fully rough regime is attained with the roughest tube over a range of Re greater than 80,000 for 10 ppm solutions and 110,000 for the 50 ppm solutions, and yet a substantial drag reduction is still obtained (58% of friction reduction with 10 ppm solutions at Re = 80,000, and 77% of friction reduction with 50 ppm solutions at Re = 110,000). Therefore, even in the fully rough regime, the polymer is still very effective in reducing the ratio of the turbulent eddy diffusivity and kinematic viscosity ϵ_M/ν, Eqn. (96) being valid in rough pipes as well. It will not be attempted here to propose any specific mechanism of interaction between the macromolecules in solution and the turbulent flow field that would explain the friction data obtained in rough tubes. It may be suggested, however, that Polyox is still able to damp out turbulence of some scale in rough pipe flows. The heat transfer data support this suggestion.

In discussing the results for the rough tubes further, it may be useful to imagine the flow near the roughness in terms of flow over cavities [60]. For water the general pattern of cavity flow seems to be the following. For values of ϵ^* between ≈ 10 to 100, the cavity flow picture is described by four modes: "divide" – very little or no fluid entering or leaving the cavity; "inflow" – denoting flow into the cavity from the outside; "weak exchange" – denoting some removal of cavity flow; and "strong exchange" – characterizing a removal of a large part of the cavity fluid. As the ϵ^* value increases, a vortex motion becomes more pronounced, becoming dominant around $\epsilon^* = 200$. Good heat transfer requires both transfer from the wall to the cavity fluid and from the cavity fluid into the main flow. For water, the flow modes generally promote good fluid exchange between the cavity and the external flow; therefore the cavity wall boundary layer remains as the major resistance to heat transfer from a rough wall. The mode appearing to cause the largest disturbance in the cavity flow is the so-called "strong exchange" one, as a large removal of cavity fluid takes place, which destroys the wall boundary layer as well. Such action may lead to an important reduction of the thermal resistance of this layer, and hence to a better heat transfer. On the other hand the rather strong and stable vortex motion observed at large ϵ^* values would tend to have a more stable cavity wall boundary layer, and thus may not be as favorable to heat transfer. The conclusion of this reasoning is that an unsteady flow in the cavity probably improves the heat transfer of the cavity walls by periodically destroying the wall boundary layer. The incredibly low heat transfer coefficients obtained with Polyox in the two rough tubes – in fact, the heat transfer coefficients in the rough tubes can be even lower than the corresponding ones in smooth tubes – suggests that Polyox stabilizes the cavity flow at relatively low ϵ^* (say less than 100) leaving the cavity wall boundary layer practically undisturbed. The cavity wall boundary layer offers then a substantial resistance to heat transfer. It is also possible that the postulated stabilization of the cavity flow produces, as a consequence, a reduction of exchange of fluid between the cavity and the external flow; as a result a non-negligible resistance to heat transfer might take place at the interface itself. Eventually, at very high values of Re, the level of turbulence is likely to become sufficiently high to leave the cavity wall boundary layer as the only resistance to heat transfer, leading to an increase of the heat transfer coefficients.

Considering now again the results of the present experiments, the friction data in rough pipe reveal a dependence of C_F on Re, even in the fully rough regime. With pure water, C_F is a function of ϵ^* only. Moreover, in the fully rough regime, C_F becomes constant, i.e., independent of ϵ^*. Since

$$\epsilon^* = \mathrm{Re}\sqrt{\frac{C_F}{2}}\,\frac{\epsilon}{D}, \tag{120}$$

C_F is then independent of Re. For polymer solutions the friction coefficient is not only a function of ϵ^*, but also of C and P. P, in turn, is probably shear stress dependent; even if C_F becomes explicitly independent of ϵ^* in the fully rough regime, it might still depend on P, i. e., on the wall shear stress, i. e., implicitly on $\epsilon^* = \epsilon u_\tau / \nu$ and finally on the Re. It is believed that it is for this reason that C_F continues to be Re dependent even in the so-called "fully rough" regime. Mechanical degradation, becoming more and more important as the wall shear stress increases, is certainly partly responsible for this behavior.

Finally it should also be mentioned that different polymers which all lead to drag reduction in smooth tubes, seem to differ in their effect in rough tubes. There are reports, for example, that guar gum and Polyhall do not reduce friction in the fully rough regime, [56], [68], as does Polyox. In the present experiments only Polyox WSR301 was used, and no further evidence was collected as to this question. It could well be, however, that certain specific molecular characteristics lead to such different results for rough tubes.

One of Poreh's model assumptions is that no drag reduction is obtained in the fully rough regime. This might explain why his model does not hold with Polyox solutions.

Chapter VII

CONCLUSIONS

The principal parts of the discussion presented in the previous chapters may be summarized as follows:

1. Considerable friction reduction is attained with Polyox, in smooth as well as in rough tubes. The percentage friction reduction with respect to the solvent can be as high as 73% in smooth tubes and 83% in rough tubes. The friction coefficient is only slightly dependent on temperature and concentration under low shear stress conditions, ($u_\tau < 1$ ft/sec). Under higher shear stress, degradation takes place and the solutions of low concentration (10 ppm) is affected more than the 50 ppm solutions. The solution of higher concentration then becomes the more effective one in reducing the friction and heat transfer.
2. The friction reduction is accompanied with an even more drastic reduction of heat transfer. The similarity of the shape of the curves of friction and heat transfer coefficients, when plotted versus Reynolds number, suggests a Reynolds type analogy between heat and momentum transfer. The heat transfer coefficient in rough tubes is reduced so drastically that in some ranges the heat transfer coefficients with Polyox can be lower in rough tubes than in smooth tube.
3. Simultaneous measurements of the friction and heat transfer coefficients reveal that the turbulent diffusivities

are reduced near the wall by the addition of Polyox. As a consequence, the region governed by viscous forces extends further from the wall with "Polyox" than with water (thickening of viscous layer). This is in agreement with many of the models that have been proposed to explain the effect of polymers.

4. It is suggested that the low value of the heat transfer coefficients observed in rough tubes may be explained in terms of the cavity model. In terms of this model, the low heat transfer coefficient is due to an increase of the resistance to heat transfer in the cavity wall boundary layer, as well as a reduction of the exchange of fluid between the cavity and the external flow.

5. The tremendous reduction of heat transfer accompanying the reduction of friction with Polyox might limit its practical use to applications in which a low friction <u>and</u> heat transfer is desired — such as in the transport of oil by pipelines through a very cold area — or in which the poor heat transfer characteristics of the polymer solution are of minor importance compared to the advantages of dealing with a fluid lowering the friction.

REFERENCES

1. Acosta, A. J. and James, D. F., "Laminar flow of dilute polymer solutions around circular cylinders," Jour. of Fluid Mech., vol. 42, p. 269 (June 1970).

2. Allen, R. W., "Measurements of friction and local heat transfer for turbulent flow of a variable property fluid (water) in a uniformly heated tube," Ph. D. Thesis, Univ. of Minnesota (Sept. 1959).

   Also --

   Allen, R. W. and Eckert, E. R. G., "Friction and heat transfer measurements to turbulent pipe flow of water ($Pr = 7$ and 8) at uniform wall heat flux," Transactions of ASME, Journal of Heat Transfer, vol. 86, p. 301 (Aug. 1964).

3. Barenblatt, G. I., Gorodtsov, V. A., and Kalashnikov, V. N., "Turbulence of anomalous fluids," Heat Transfer, Soviet Research, vol. 1, p. 1 (January 1969).

4. Brandt, H., McDonald, A. T. and Boyle, F. W., "Skin friction of polymer solutions in rough pipes," in Viscous drag reduction, Plenum Press, New York (1969), p. 159.

5. Castro, W. and Squire, W., "The effect of polymer additives on transition in pipe flow," Appl. Sci. Res., 18, p. 81 (1967).

6. Chung, J. S. and Graebel, W. P., "Laser anemometer measurements of turbulence in non-newtonian pipe flows," Department of the Navy, ONR Contract No. Nonr-1224(49), NR NO No. 062-342, ORA Project 06505, Washington, D. C. (1969).

7. Clauser, F. H., "The turbulent boundary layer," Advances in Appl. Mechanics, 4, p. 1 (1956).

8. Deissler, R. G., "Analysis of turbulent heat transfer, mass transfer, and friction in smooth tubes at high Prandtl and Schmidt numbers," NACA Techn. note 3145 (1954).

9. Deissler, R. G., "Turbulent heat transfer and friction in the entrance regions of smooth passages," Trans. of the ASME, p. 1221 (Nov. 1965).

10. Dipprey, D. F., "An experimental investigation of heat and momentum transfer in smooth and rough tubes at various Prandtl numbers," Ph. D. Thesis, California Institute of Technology (1961).

11. Dittus, F. W. and Boelter, L. M. K., "Heat transfer in automobile radiators of the tubular type," University of Calif. Publications in Engineering, vol. 2, no. 13, 1930.

12. Eagle, A. and Ferguson, R. M., "On the coefficient of heat transfer from the internal surface of tube walls," Proc. Roy. Soc., vol. 127, pp. 540-566 (June 1930).

13. Eckert, E. R. G. and Drake, R. M., Jr., Heat and mass transfer, Second Edition, McGraw-Hill, New York (1959).

14. Elata, C., Lehrer, J. and Kahanovitz, A., "Turbulent shear flow of polymer solutions," Isr. J. of Tech., vol. 4, no. 1, pp. 87-95 (1966).

15. Ernst, W. D., "Investigation of the turbulent shear flow of dilute aqueous CMC solutions," AIChE J., vol. 12, no. 3, p. 581 (May 1966).

16. Fabula, A. G., Lumley, J. L. and Taylor, W. D., "Some interpretations of the Toms effect" in Modern developments in the mechanics of continua, Academic Press, New York (1966)

17. Foreman, J. W. et al, "8C2-Fluid flow measurements with a laser-doppler velocimeter," IEEE Journal of Quantum Electronics, vol. QE-2, no. 8 (Aug. 1966).

18. Friehe, C. A. and Schwarz, W. H., "The use of pitot-static tubes and hot-film anemometers in dilute polymer solutions," in Viscous drag reduction, Plenum Press, New York (1969), p. 281-296.

19. Gadd, G. E., "Turbulence damping and drag reduction produced by certain additives in water," Nature, vol. 206, no. 4983, pp. 463-467 (May 1965).

20. Gadd, G. E. and Brennen, C., "Ageing and degradation in dilute polymer solutions," Nature, vol. 215, p. 1368 (Sept. 1967).

21. Goldstein, R. J. and Kreid, D. K., "Measurement of laminar flow development in a square duct using laser-Doppler flowmeter," Journal of Applied Mechanics, Paper No. 67-APM-37 (Jan. 1967).

22. Goren, Y. and Norbury, J. F., "Turbulent flow of dilute aqueous polymer solutions," ASME J., Basic Eng., 89, p. 814 (1967).

23. Granville, Paul S., "The frictional resistance and velocity similarity of drag-reducing dilute polymer solutions," Naval Ship Res. & Dev. Center, Washington, D.C., Report 2502 (1966).

24. Gupta, M. K., Metzner, A. B. and Hartnett, J. P., "Turbulent heat transfer characteristics of viscoelastic fluids," Int. Jour. of Heat & Mass Transfer, vol. 10, pp. 1211-1224 (1967).

25. Hartnett, J. P., "Experimental determination of the thermal entrance length for the flow of water and of oil in circular pipes," Ph. D. Thesis, U. of Calif. (1954); also, Trans. ASME, vol. 77, pp. 1211-1220 (1955).

26. Hershey, H. C. and Zakin, J. L., "Existence of two types of drag reduction in pipe flow of dilute polymer solutions," Ind. Eng. Chem. Fund., 6, p. 381 (1967).

27. Howard, R. G., "Heat and momentum transfer in drag-reducing solutions," Naval Ship Res. & Dev. Lab., Annapolis, Report 3226 (Oct. 1970).

28. Howard, R. G. and McCrory, D. M., "The correlation between heat and momentum transfer for solutions of drag-reducing agents," Naval Ship Res. & Dev. Lab., Annapolis, Report 3232 (Jan. 1971).

29. Hoyt, J. W. and Fabula, A. G., "The effect of additives on fluid friction," U. S. Naval Ord. Test Sta., NAVWEPS Report 8636 (1964).

30. Johnson, B. and Barchi, R., "The effect of drag-reducing additives on boundary layer turbulence," AIAA Paper No. 67-459 (1967).

31. Karman, T. von, "The analogy between fluid friction and heat transfer," Trans. ASME, vol. 61, pp. 705-710 (1939).

32. Laufer, J., "The structure of turbulence in fully developed pipe flow," NACA Tech. Rept. 1174 (1954).

33. Mark, J. E. and Flory, P. J., "The configuration of the polyoxyethylene chain," J. Am. Chem. Soc., 87, p. 1415 (1965).

34. Marrucci, G. and Astarita, G., "Turbulent heat transfer in viscoelastic liquids," IEC Fundamentals, vol. 6, no. 3, pp. 470-471 (Aug. 1967).

35. McNally, W. A., "Heat and momentum transport in dilute polyethylene oxide solutions," Naval Underwater Weapons Res. & Engineering Station, Newport, Rhode Island, TR No. 44 (Dec. 1968).

36. Meyer, W. A., "A correlation of the frictional characteristics for turbulent flow of dilute viscoelastic non-newtonian fluids in pipes," AIChE J, vol. 12, no. 3, p. 522 (May, 1966).

37. Nikuradse, J., "Laws for flow in rough pipes," VDI-Forschungsheft 361, Series B, vol. 4 (1933); Translation, Brielmaier, A. A., NACA TM 1292 (1950).

38. Pisolkar, V. G., "Effect of drag reducing additive on pressure loss across transitions," *Nature*, *vol. 225*, p. 936 (March 1970).

39. Poreh, M. and Paz, U., "Turbulent heat transfer to dilute polymer solutions," *Int. J. of Heat & Mass Transfer*, *vol. 11*, no. 5, pp. 805-812 (1968).

40. Poreh, M., Rubin, H. and Elata, C., "Studies in rheology and hydrodynamics of dilute polymer solutions," Israel Inst. of Tech., Publ. 126 (March 1969).

41. Poreh, H., "Flow of dilute polymer solutions in rough pipes," Iowa Institute of Hydraulic Research, Report No. 126 (April 1970).

42. Prandtl, L., "Eine Beziehung zwischen Wärmeaustausch und Strömungswiderstand der Flüssigkeiten," *Phys. Z.*, *11*, pp. 1072-1078 (1910).

43. Prandtl, L., "Über die ausgebildete Turbulenz," *ZAMM*, *5*, pp. 136-139 (1925) and *Proc. 2nd Int. Congr. Appl. Mech.*, Zurich, pp. 62-75 (1926).

44. Pruitt, G. T., Rosen, B. and Crawford, H. R., "Effect of polymer coiling on drag reduction," Western Co. Research Div., Dallas, Texas, Rep. No. DTMB-2 (Aug. 1966).

45. Radin, I., Zakin, J. L. and Patterson, G. K., "Exploratory drag reduction studies in non-polar soap systems," in *Viscous drag reduction*, Plenum Press, New York (1969), pp. 213-231.

46. Rannie, W. D., "Heat transfer in turbulent shear flow," Ph. D. Thesis, California Institute of Technology (1951); also *Journ. Aero. Sci.*, *vol. 23*, pp. 485-489 (May 1956).

47. Reichardt, H., "Fundamentals of turbulent heat transfer," translated from *Arch. ges. Warmtech.*, No. 6/7 (1951), NACA TM 1408 (1957) and N-41947 (1956).

48. Roshko, A., "Some measurements of flow in a rectangular cutout," NACA TN 3488 (Aug. 1955).

49. Rouse, P. E., Jr. and Sittel, K., "Viscoelastic properties of dilute polymer solutions," *J. Appl. Phys.*, *24*, pp. 690-696 (1953).

50. Rudd, M. J., "Measurements made on a drag reducing solution with a laser velocimeter," *Nature*, *vol. 224*, No. 5219, p. 587 (Nov. 8, 1969).

51. Savins, J. G., "Contrasts in the solution drag reduction characteristics of polymeric solutions and micellar systems," in *Viscous drag reduction*, Plenum Press, New York (1969), pp. 183-212.

52. Shaver, R. G. and Merrill, E. W., "Turbulent flow of pseudoplastic polymer solutions in straight cylindrical tubes," *AIChE J*, *5*, pp. 181-188 (1959).

53. Shin, H., "Reduction of drag in turbulence by dilute polymer solutions," Sc. D. Thesis, Massachusetts Institute of Technology, 1965.

54. Sleicher, C. A., Jr., "Experimental velocity and temperature profiles for air in turbulent pipe flow," *Trans. ASME*, *80*, p. 693 (1958).

55. Smith, K. A., Keuroghlian, G. H., Virk, P. S. and Merrill, E. W., "Heat transfer to drag-reducing polymer solutions," *AIChE J*, *vol. 15*, No. 2, pp. 294-297 (March 1969).

56. Spangler, J. G., "Studies of viscous drag reduction with polymers including turbulence measurements and roughness effects," in *Viscous drag reduction*, Plenum Press, New York (1969), p. 131.

57. Sparrow, E. M., Hallman, T. M. and Siegel, R., "Turbulent heat transfer in the thermal entrance region of a pipe with uniform heat flux," *Appl. Sci. Res.*, *Section A*, *vol. 7*, 1955.

58. Tanford, C., *Physical chemistry of macromolecules*, John Wiley and Sons, Inc., New York, 1963.

59. Toms, B. A., "Some observations on the flow of linear polymer solutions through straight tubes at large Reynolds numbers," North Holland Publishing Company, *Proc. 1st Int. Congr. on Rheology*, *Vol. II*, pp. 135-141 (1949).

60. Townes, H. W., "Flow over a rough surface," Ph. D. Thesis, California Institute of Technology (1965).

61. Townsend, A. A., *The structure of turbulent shear flow*, University Press, Cambridge (1956).

62. Tschoegl, N. W., "Influence of hydrodynamic interaction on the viscoelastic behavior of dilute polymer solutions in good solvents," *J. Chem. Phys.*, *40*, pp. 473-479 (1964).

63. Van Driest, E. R., "On turbulent flow near a wall," Heat Transfer Fluid Mech. Inst., Paper XII (1955).

64. Virk, P. S., Merrill, E. W., Mickley, H. S. and Smith, K. A., "The critical wall shear stress for reduction of turbulent drag in pipe flow," in The mechanics of continua, S. Eskinazi, Ed., Academic Press, New York (1966), p. 37.

65. Virk, P. S., Merrill, E. W., Mickley, H. S., Smith, K. A. and Mollo-Christensen, E. L., "The Toms phenomenon: Turbulent pipe flow of dilute polymer solutions," J. Fluid Mech., vol. 30, part 2, pp. 305-328 (1967).

66. Virk, P. S. and Merrill, E. W., "The onset of dilute polymer solution phenomena," in Viscous drag reduction, Plenum Press, New York (1969), pp. 107-130.

67. Wells, C. S., "Anomalous turbulent flow on non-newtonian fluids," Am. Ins. Aero. Asto. Journ., 3, pp. 1800-1805 (Oct. 1965).

68. White, A., "Turbulence and drag reduction with polymer additives," Research Bulletin No. 4, p. 75, Hendon College of Techn. (Jan. 1967).

69. White, A., "Studies of the flow characteristics of dilute high polymer solutions," Research Bulletin No. 5, Hendon College of Technology (March 1968).

70. White, A., "Heat transfer characteristics of dilute polymer solutions in fully rough pipe flow," Nature, vol. 227, p. 486-487 (Aug. 1970).

71. White, W. D., "Drag reduction measurements for three polymers at 4°C," in Viscous drag reduction, Plenum Press, New York (1969), p. 173-182.

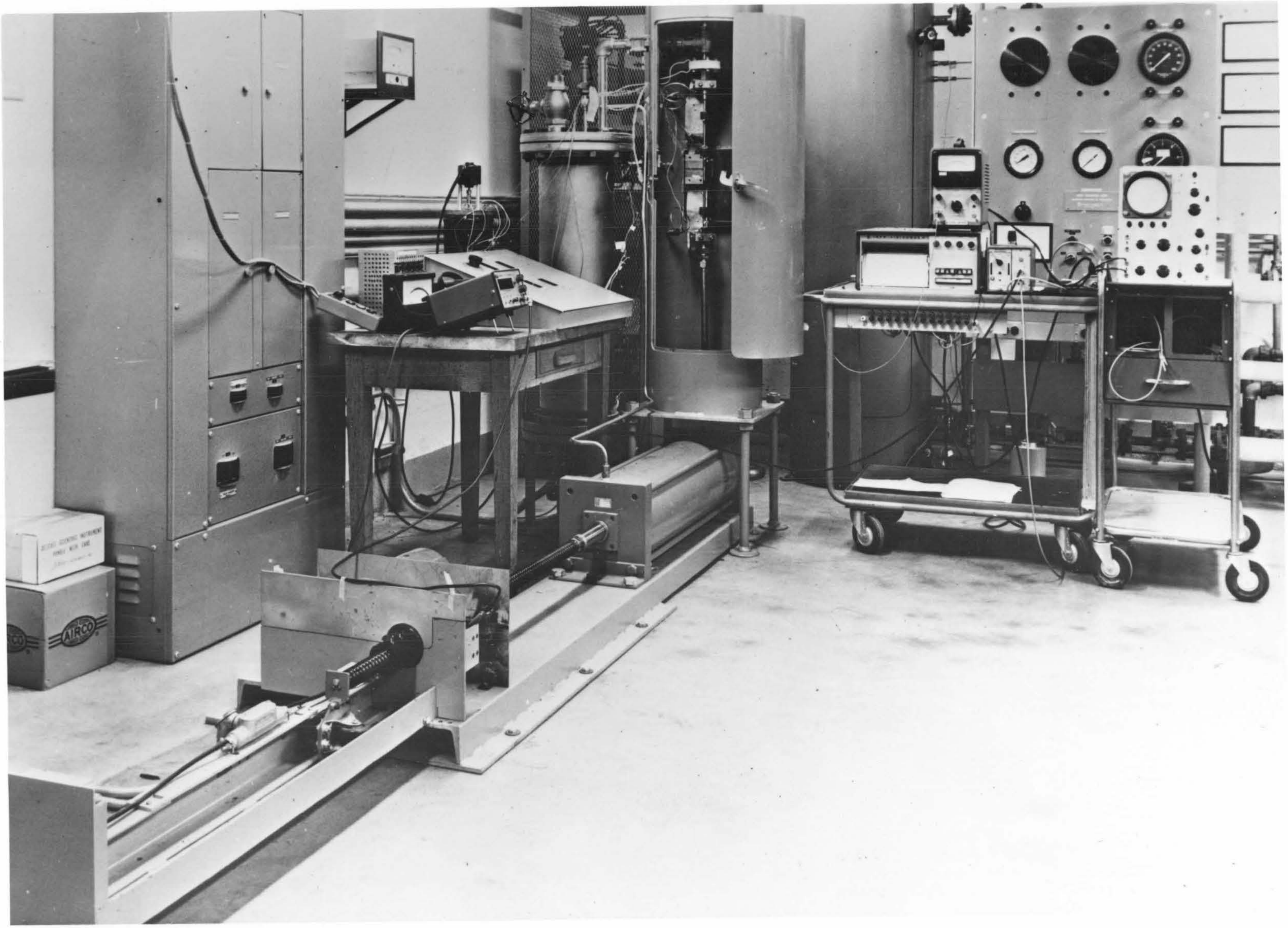

Fig. 1. View of Test Facility

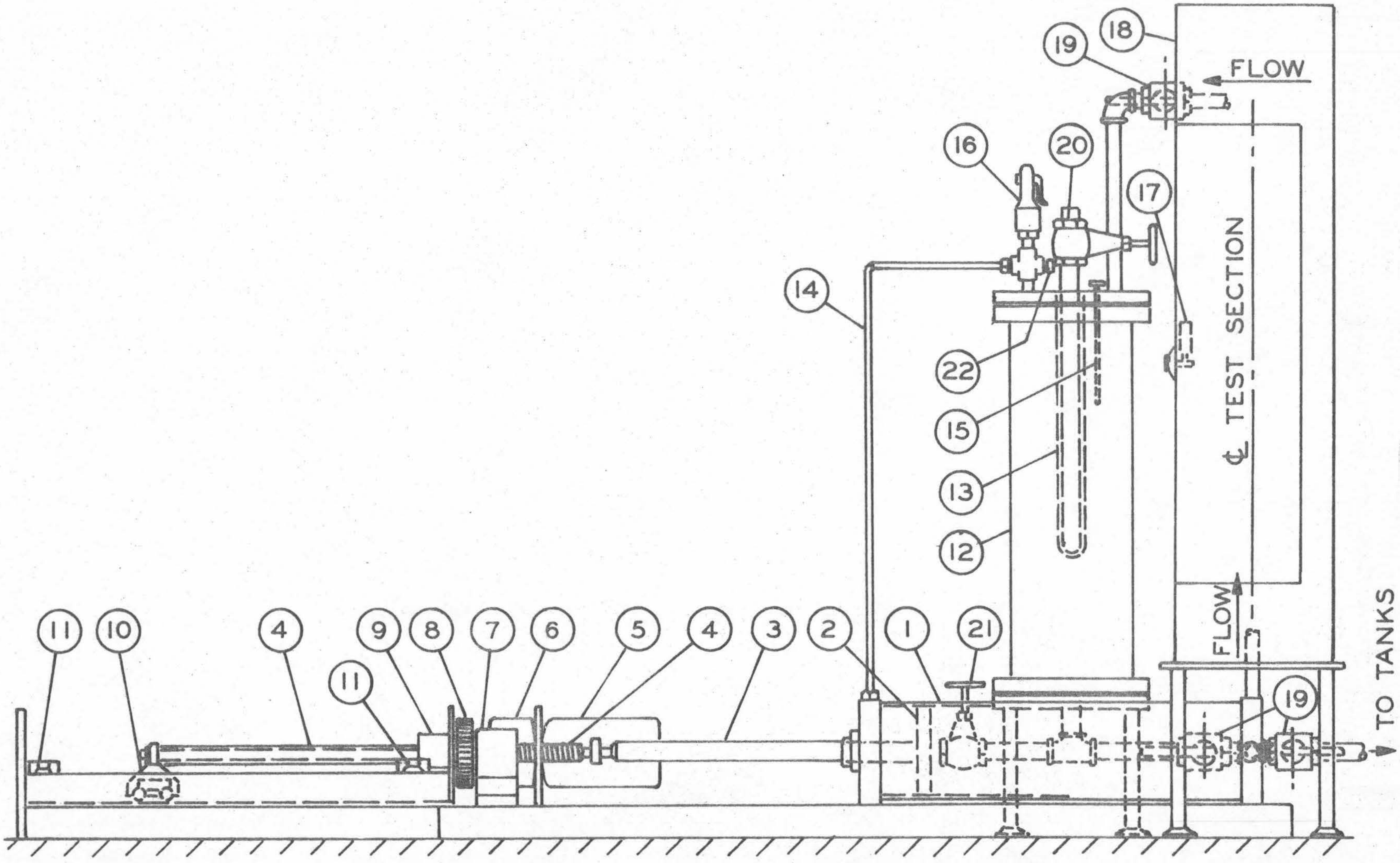

Fig. 2. Simplified test facility schematic.

Legend for Figure 2

(1) Cylinder, 10 in. diameter

(2) Piston

(3) Piston rod

(4) Ballscrew

(5) D-C motor, variable speed

(6) Speed reducer

(7) Pillow block with two bearings

(8) Gears

(9) Drive nut

(10) Anti-rotation device

(11) Limit switches

(12) Reservoir

(13) Heating rods

(14) Pressure equalizing line

(15) Immersion thermometer

(16) Safety valve

(17) Safety switch

(18) Test section housing

(19) Globe valves

(20) Filler valve

(21) Drain

(22) Connection to pressure regulator and N_2 bottle

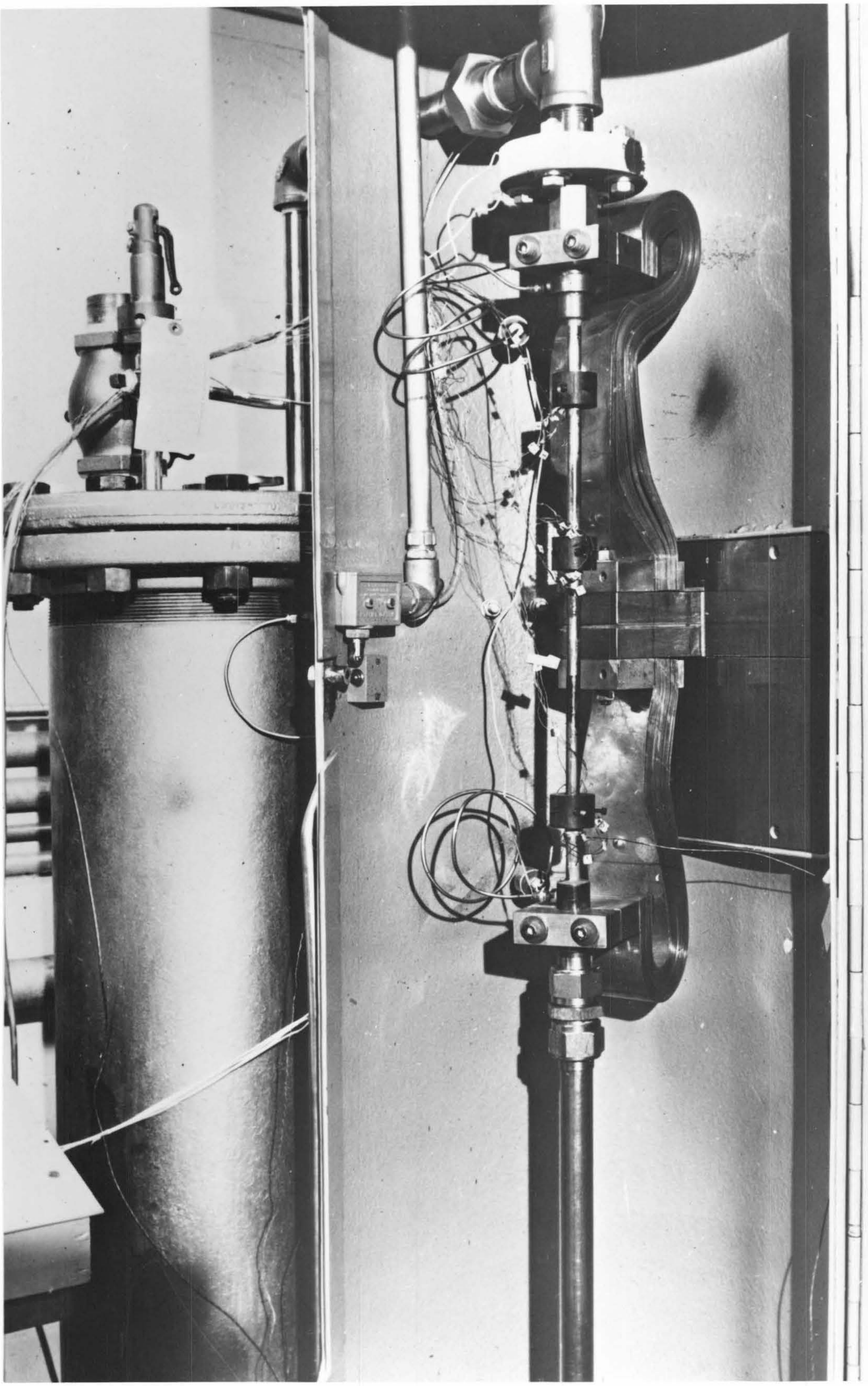

Fig. 3. View of Tube Installed.

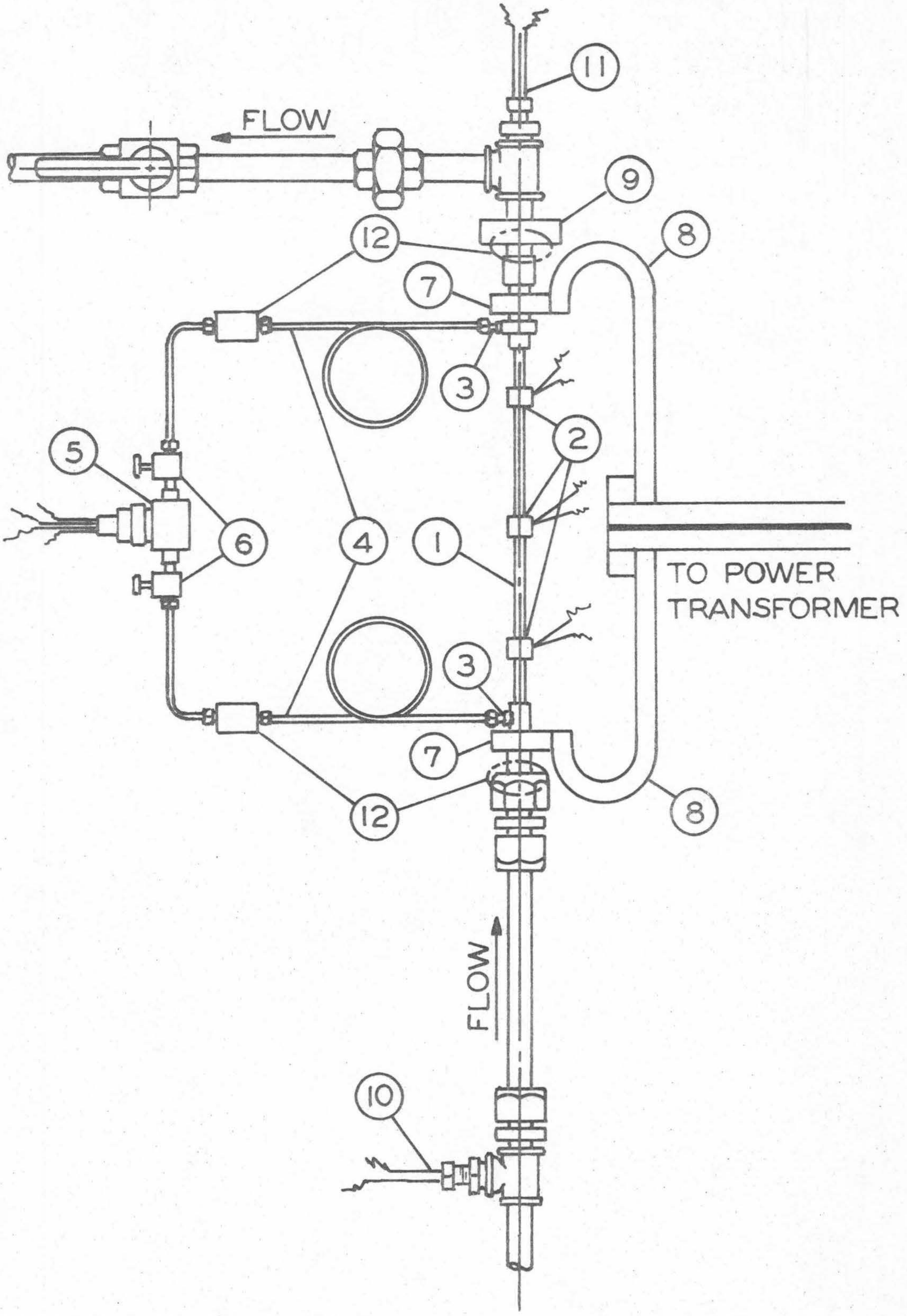

Fig. 4. Test section schematic

Legend for Figure 4

(1) Nickel T.S.
(2) Thermocouples stations (3)
(3) Pressure tap
(4) Pressure lines
(5) Differential pressure transducer
(6) Three-way valves
(7) Copper electrodes
(8) Copper buses
(9) Mixing chamber
(10) Inlet immersion thermocouple
(11) Outlet immersion thermocouple
(12) Teflon electric insulation

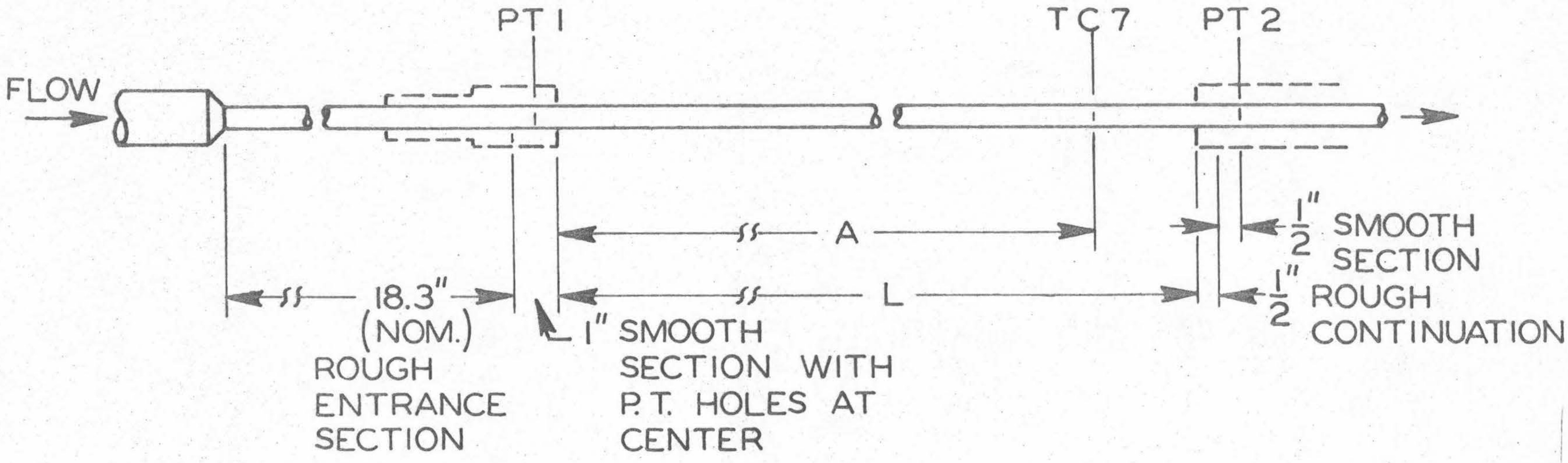

TUBE	D	L	A	t	ϵ	ϵ_S/D
E-3	0.377	17.40	15.14	0.0201	—	—
C-9	0.393	17.39	15.14	0.0176	0.0054	0.0138
A-4	0.399	17.41	15.12	0.0187	0.0195	0.0488

ALL DIMENSIONS IN INCHES
PT = PRESSURE TAP
t = WALL THICKNESS AT T.C. STATION
TC = THERMOCOUPLE

Fig. 5. Tube dimensions.

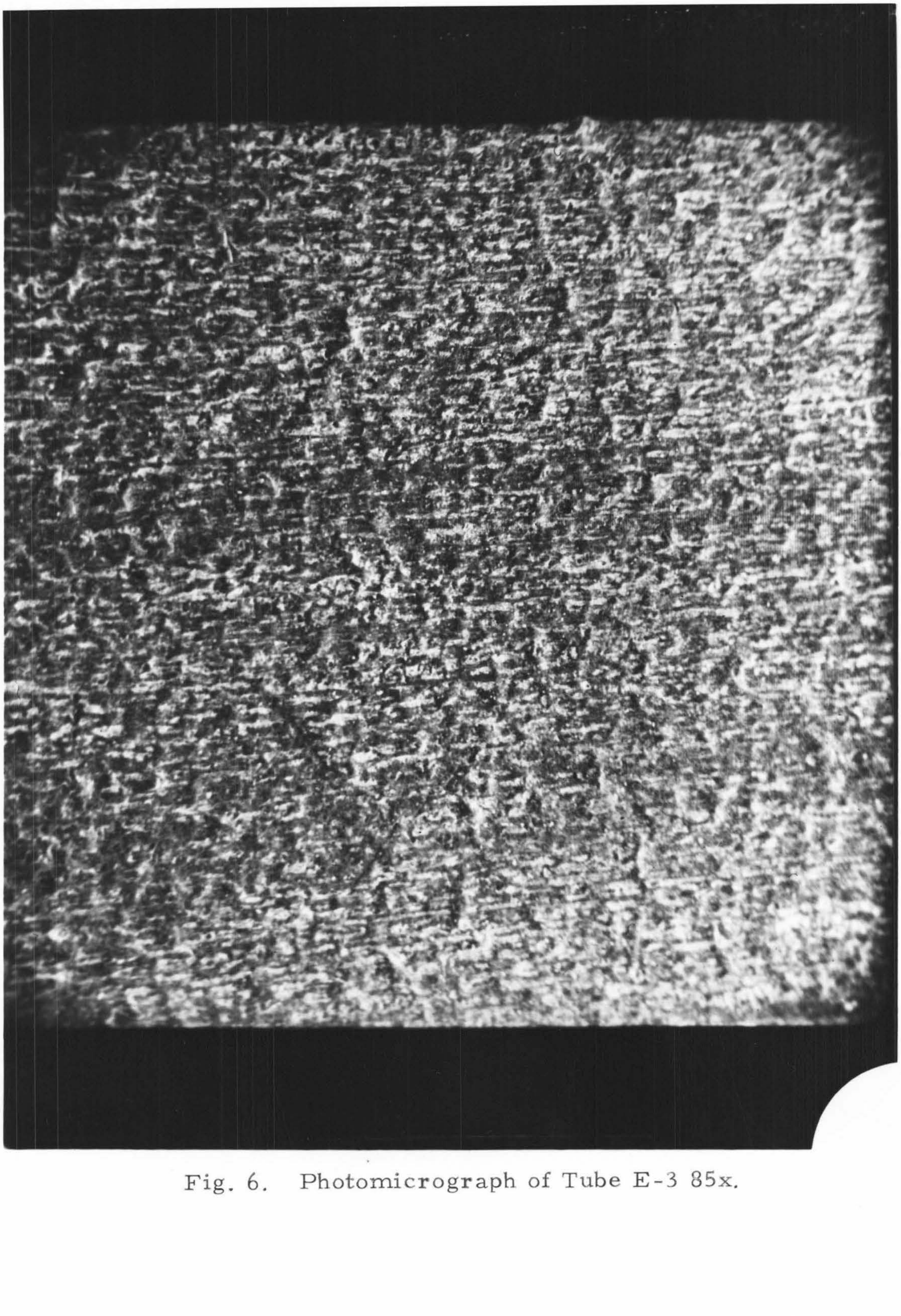

Fig. 6. Photomicrograph of Tube E-3 85x.

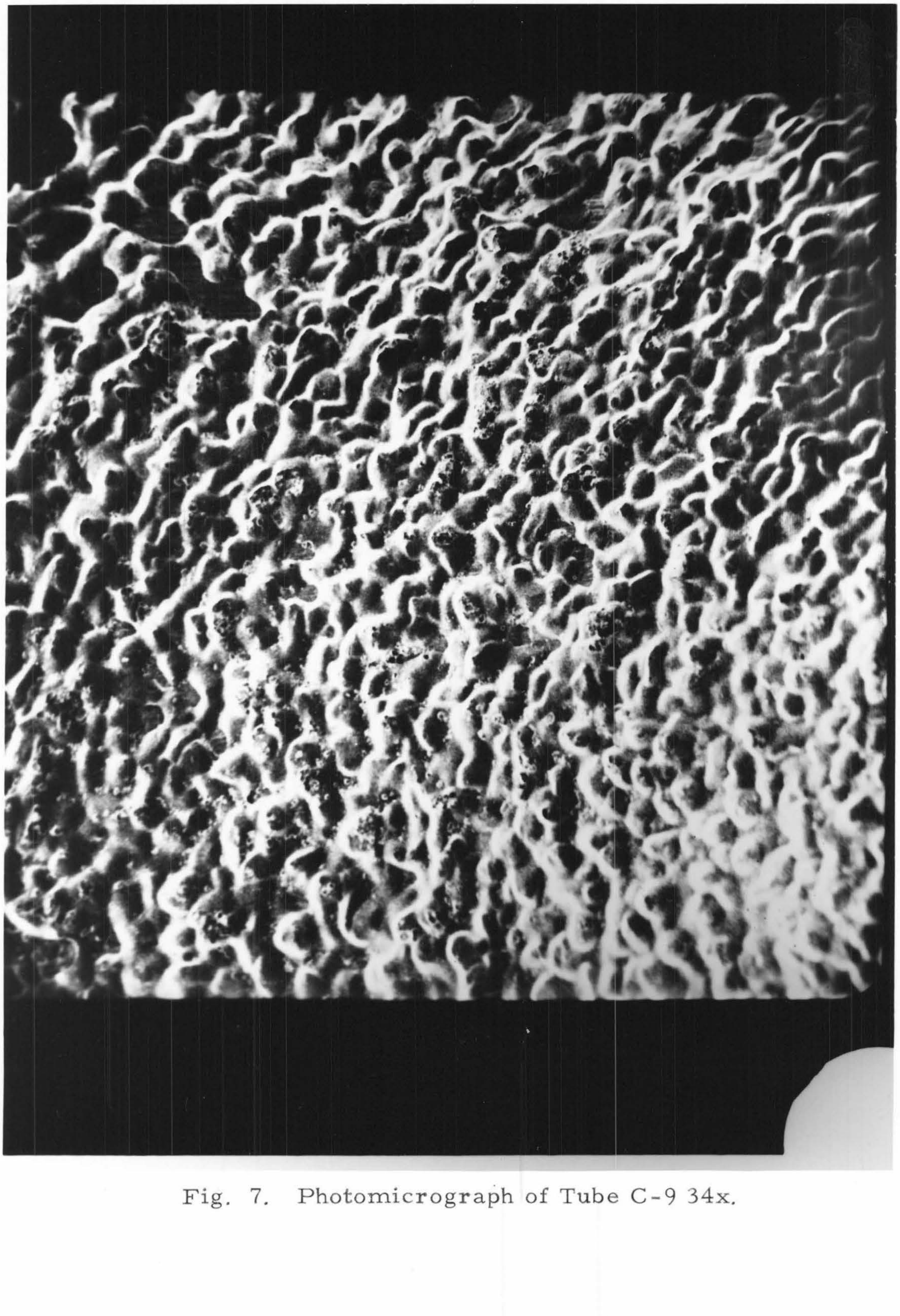

Fig. 7. Photomicrograph of Tube C-9 34x.

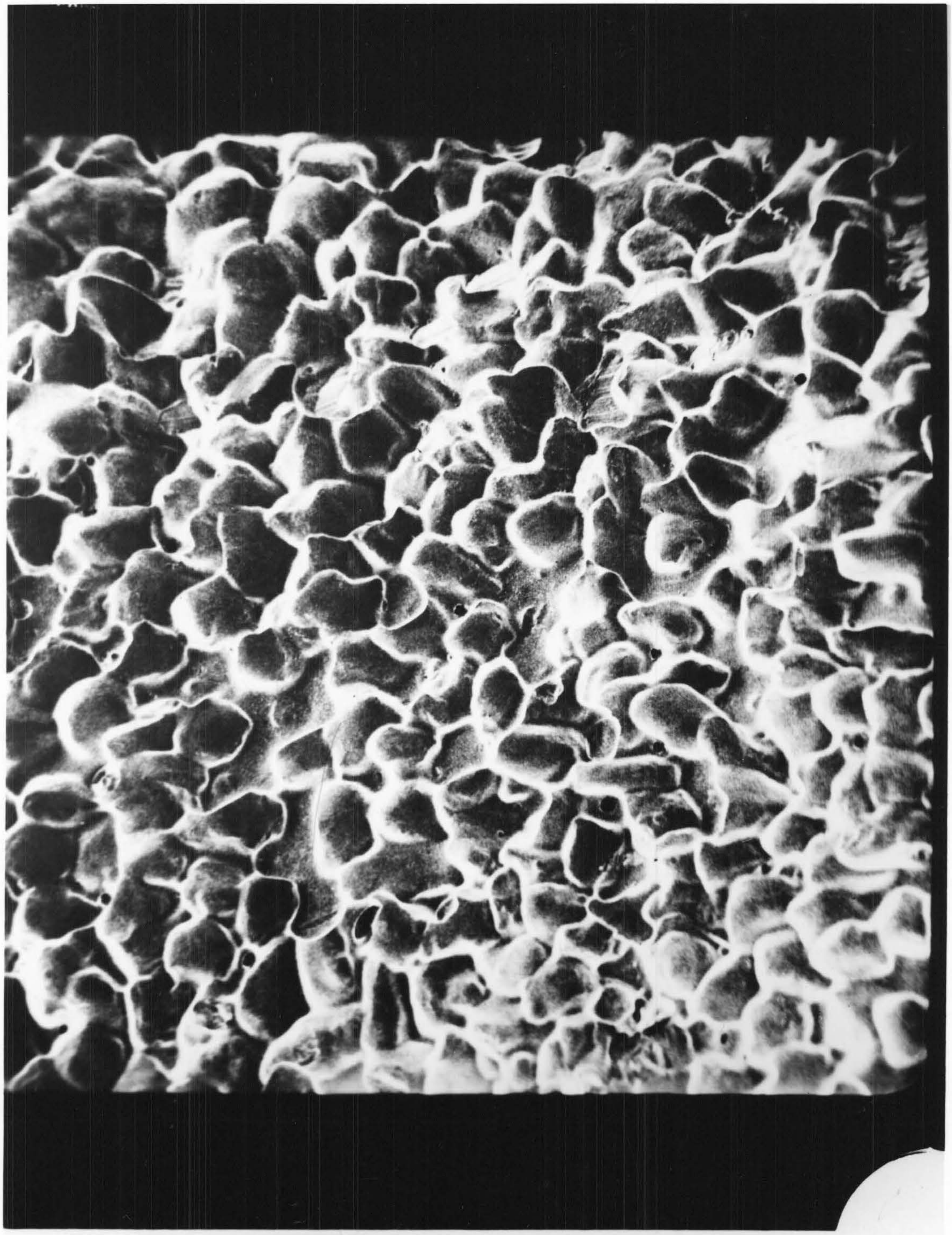

Fig. 8. Photomicrograph of Tube A-4 34x.

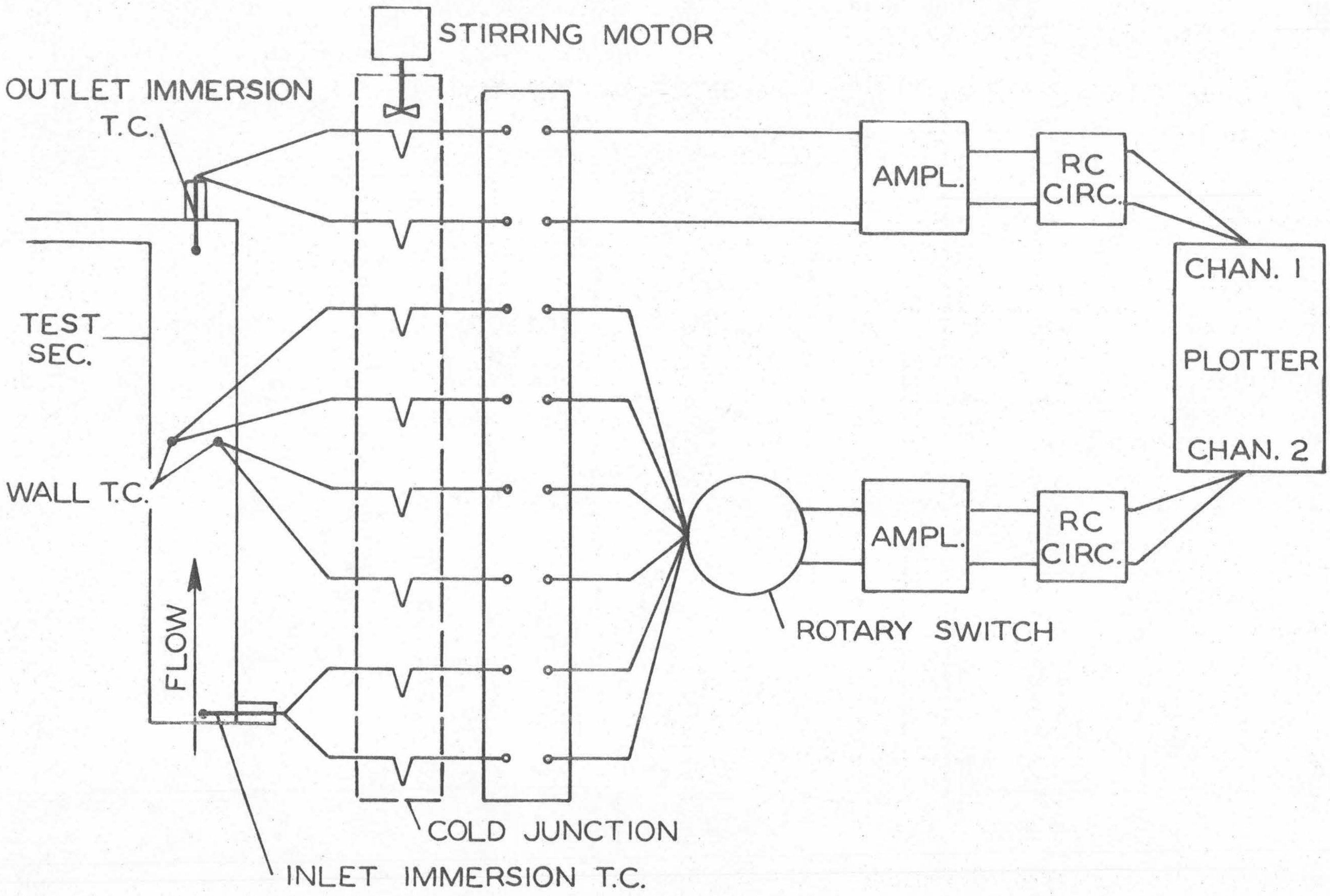

Fig. 9. Schematic of circuit for measurement of temperatures.

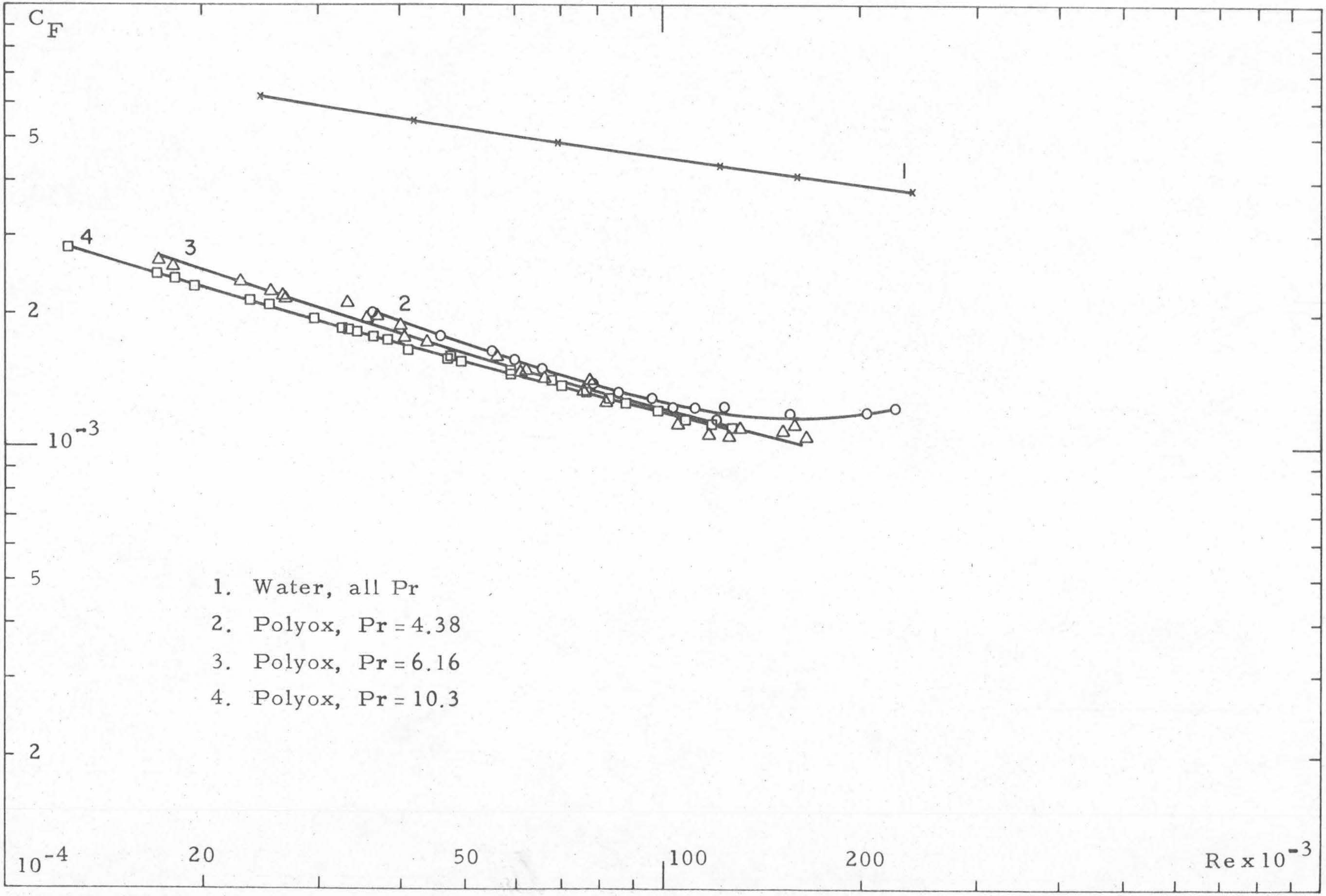

Fig. 10. Polyox 10 ppm, friction coefficient vs. Reynolds number for tube E-3.

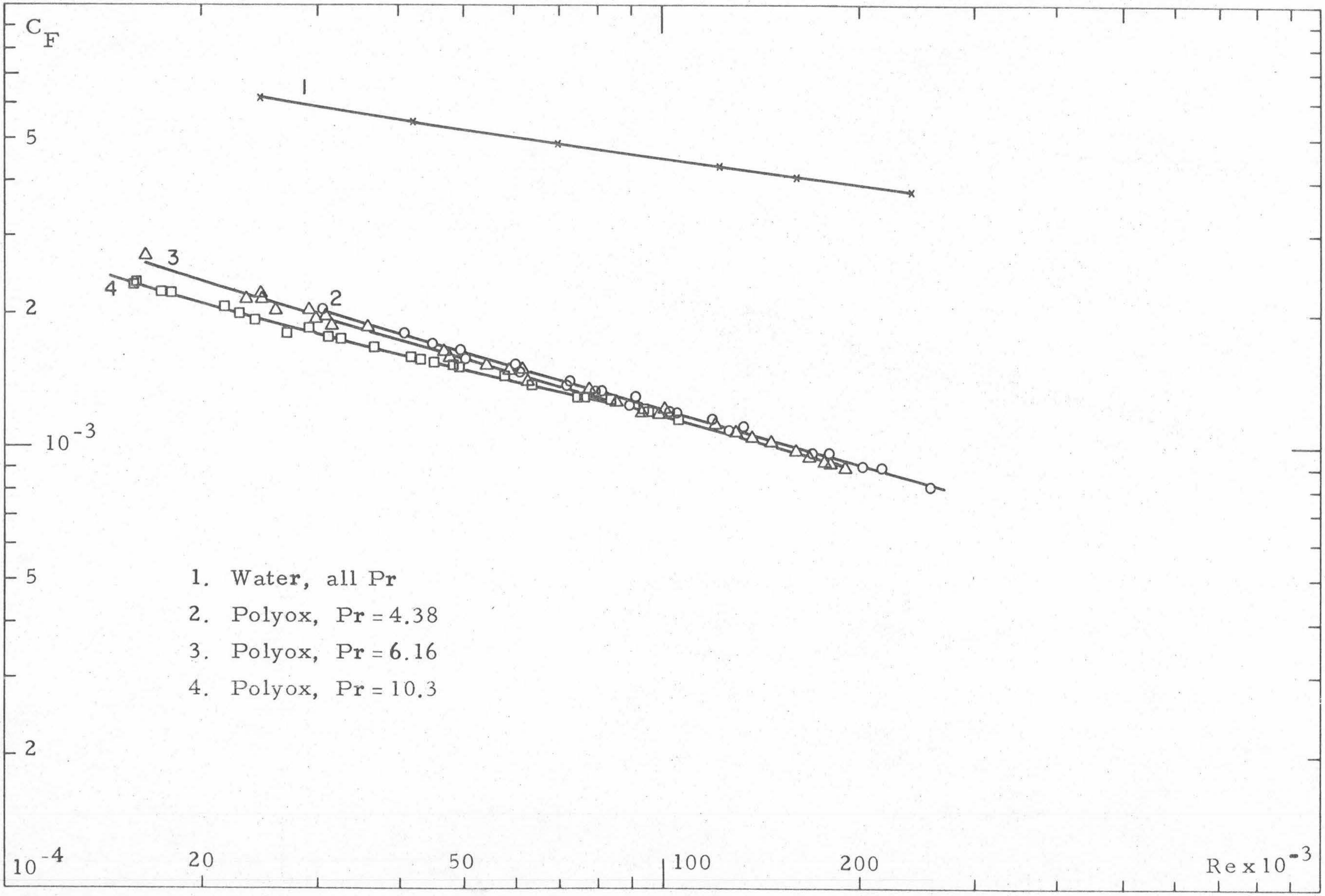

Fig. 11. Polyox 50 ppm, friction coefficient vs. Reynolds number for tube E-3

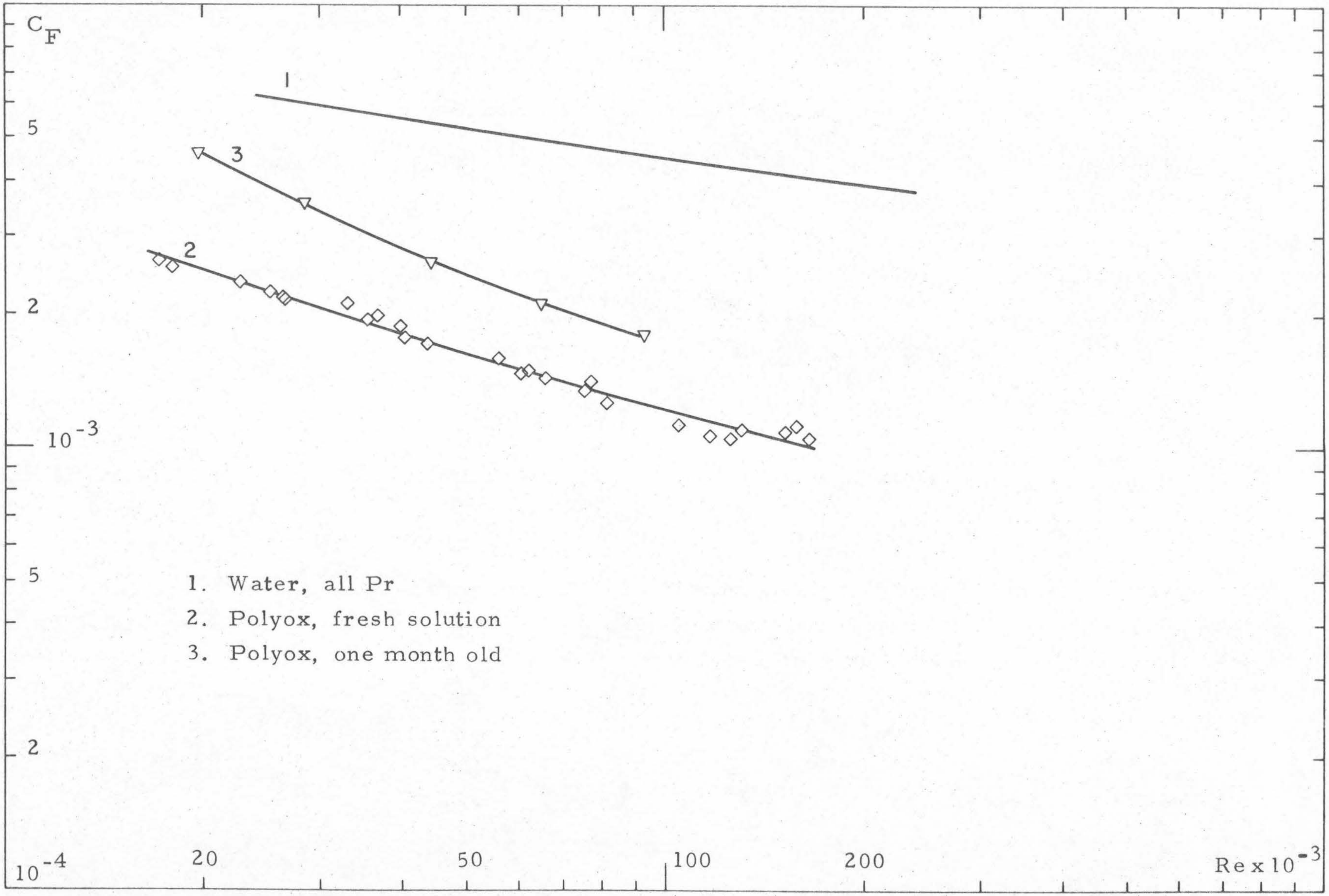

Fig. 12. Polyox 10 ppm, fresh and one month old solution, C_F vs. Re for tube E-3 ($Pr = 6.16$).

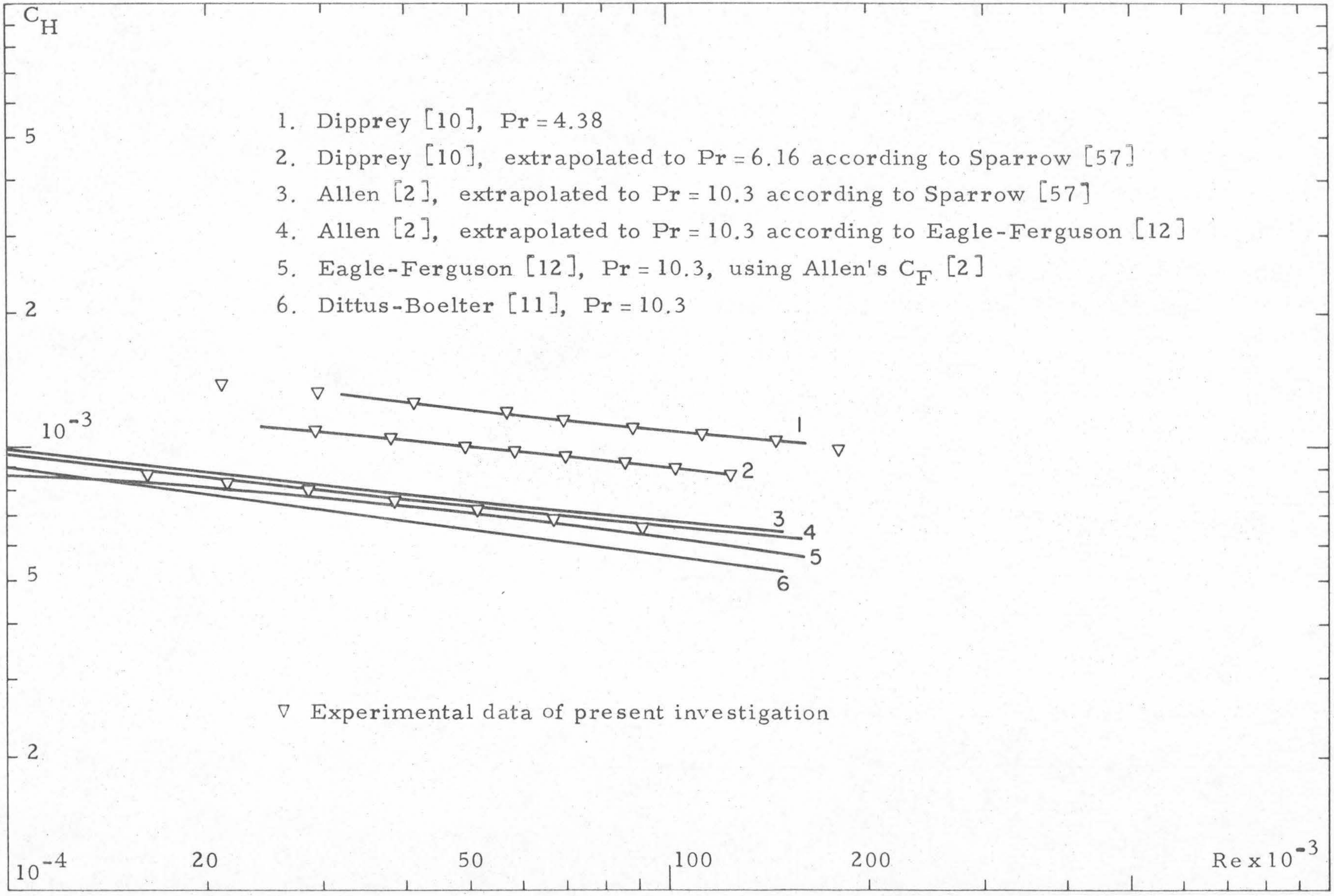

Fig. 13. Water, heat transfer coefficient vs. Reynolds number for tube E-3.

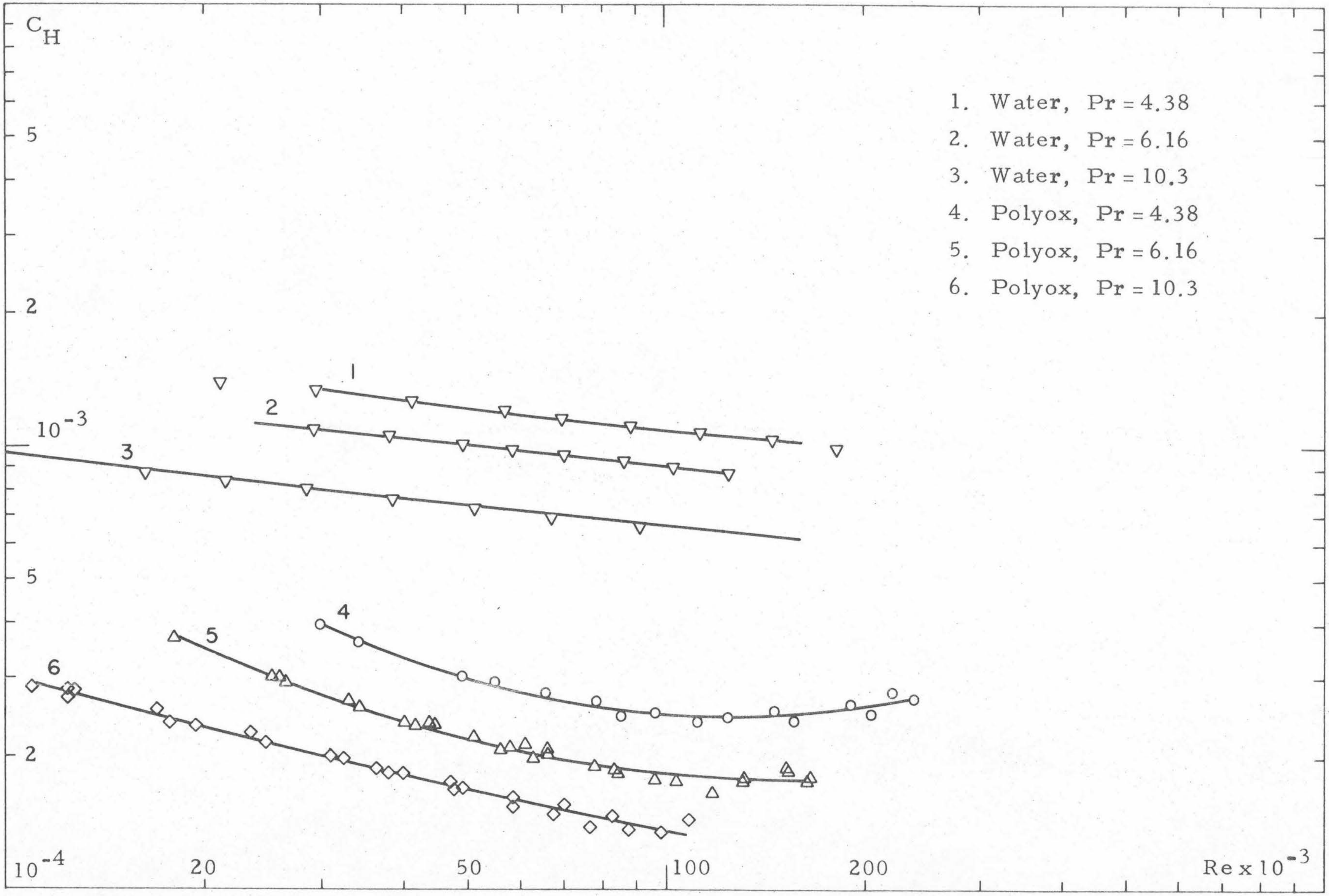

Fig. 14. Polyox 10 ppm, heat transfer coefficient vs. Reynolds number for tube E-3.

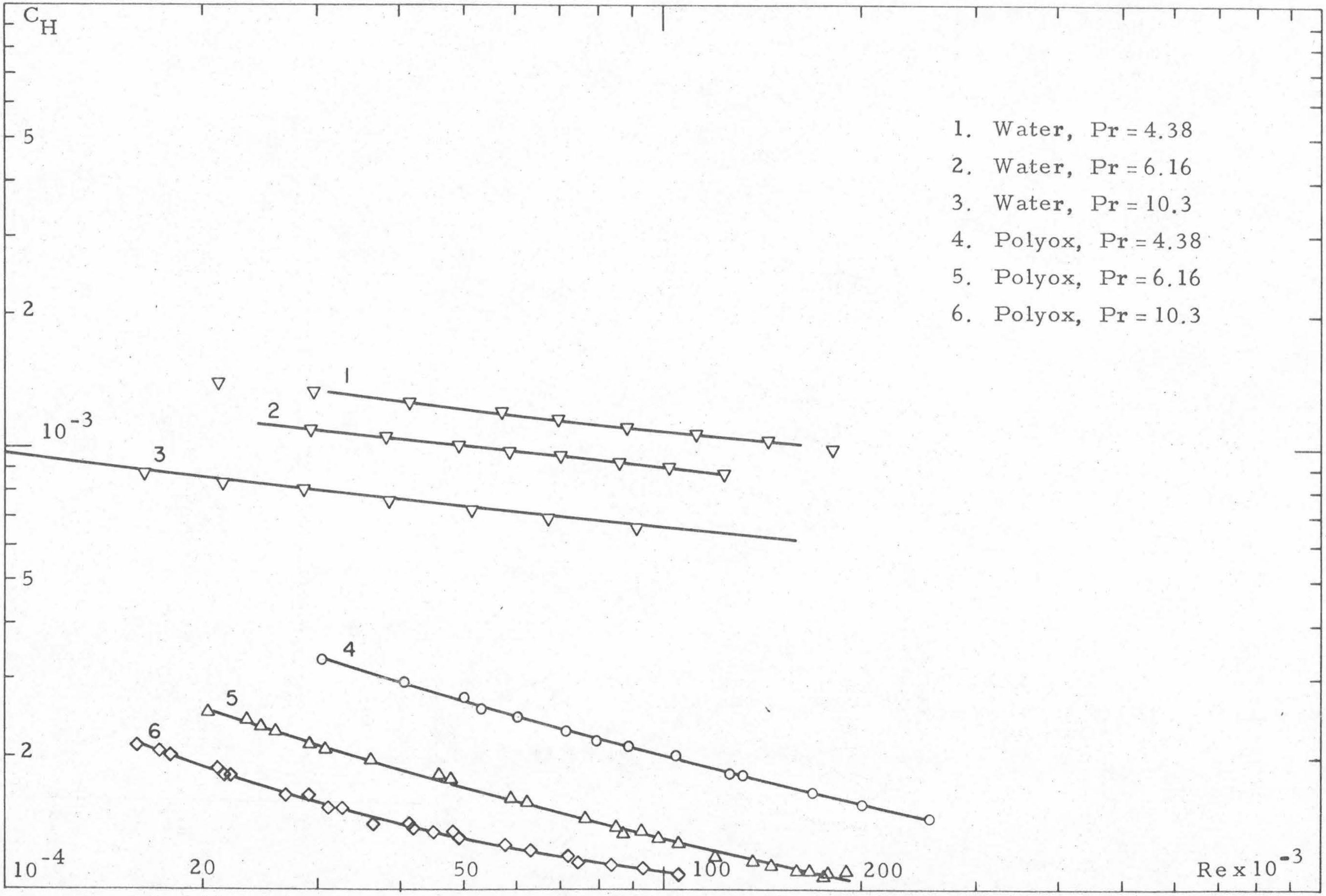

Fig. 15. Polyox 50 ppm, heat transfer coefficient vs. Reynolds number for tube E-3.

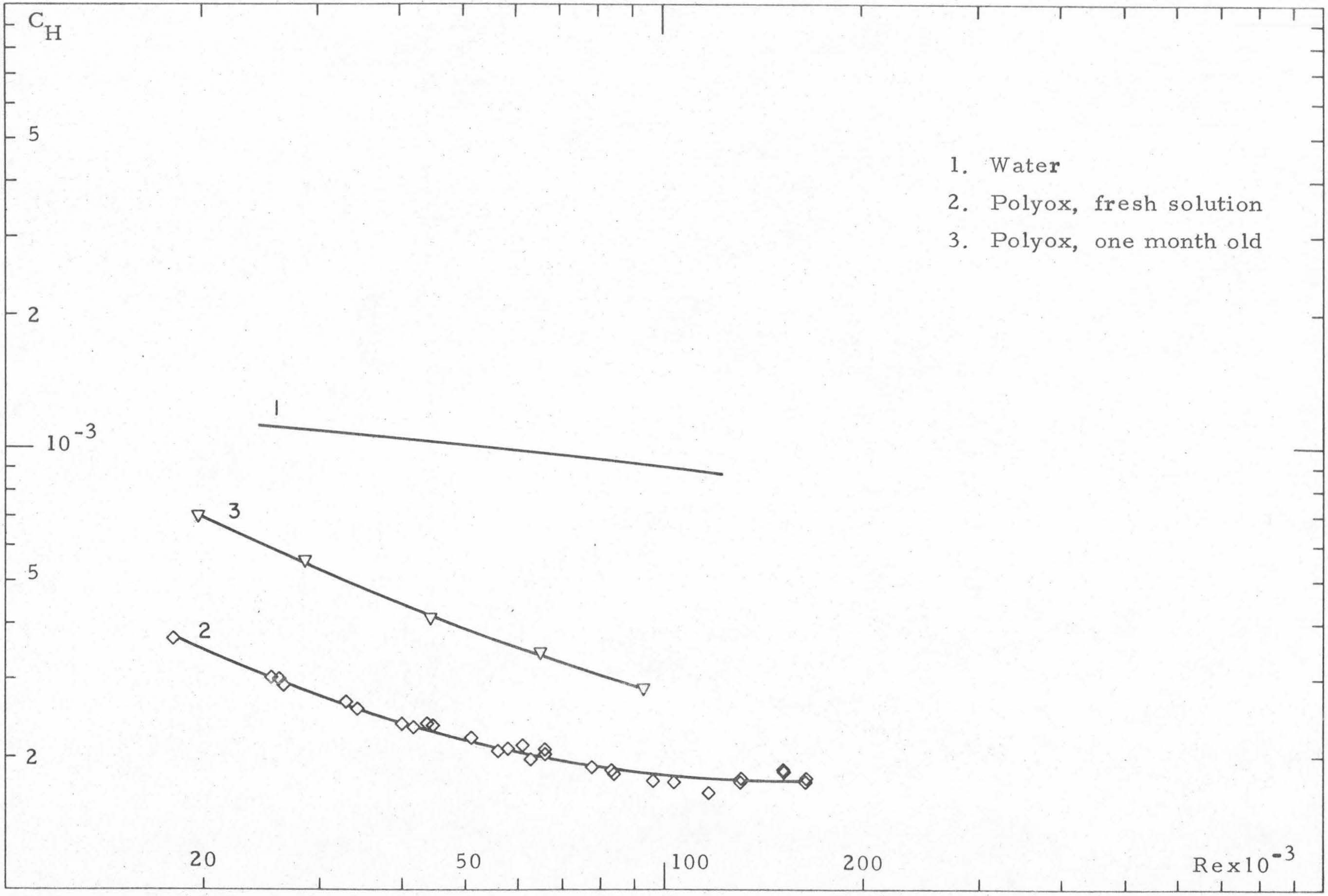

Fig. 16. Polyox 10 ppm, fresh and one month old solutions, C_H vs. Re for tube E-3.

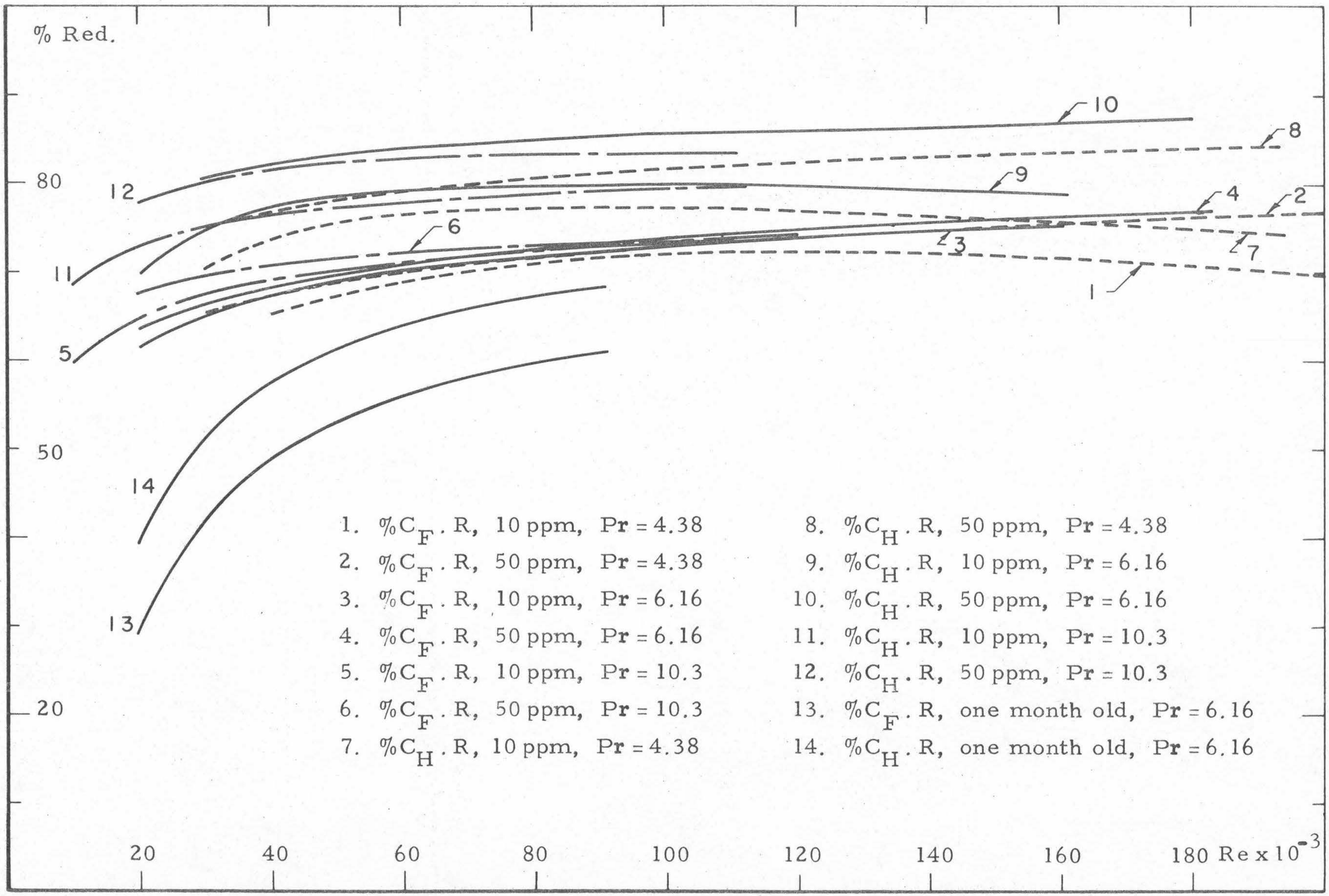

Fig. 17. Polyox 10 and 50 ppm - % friction and heat transfer reduction vs. Re for tube E-3.

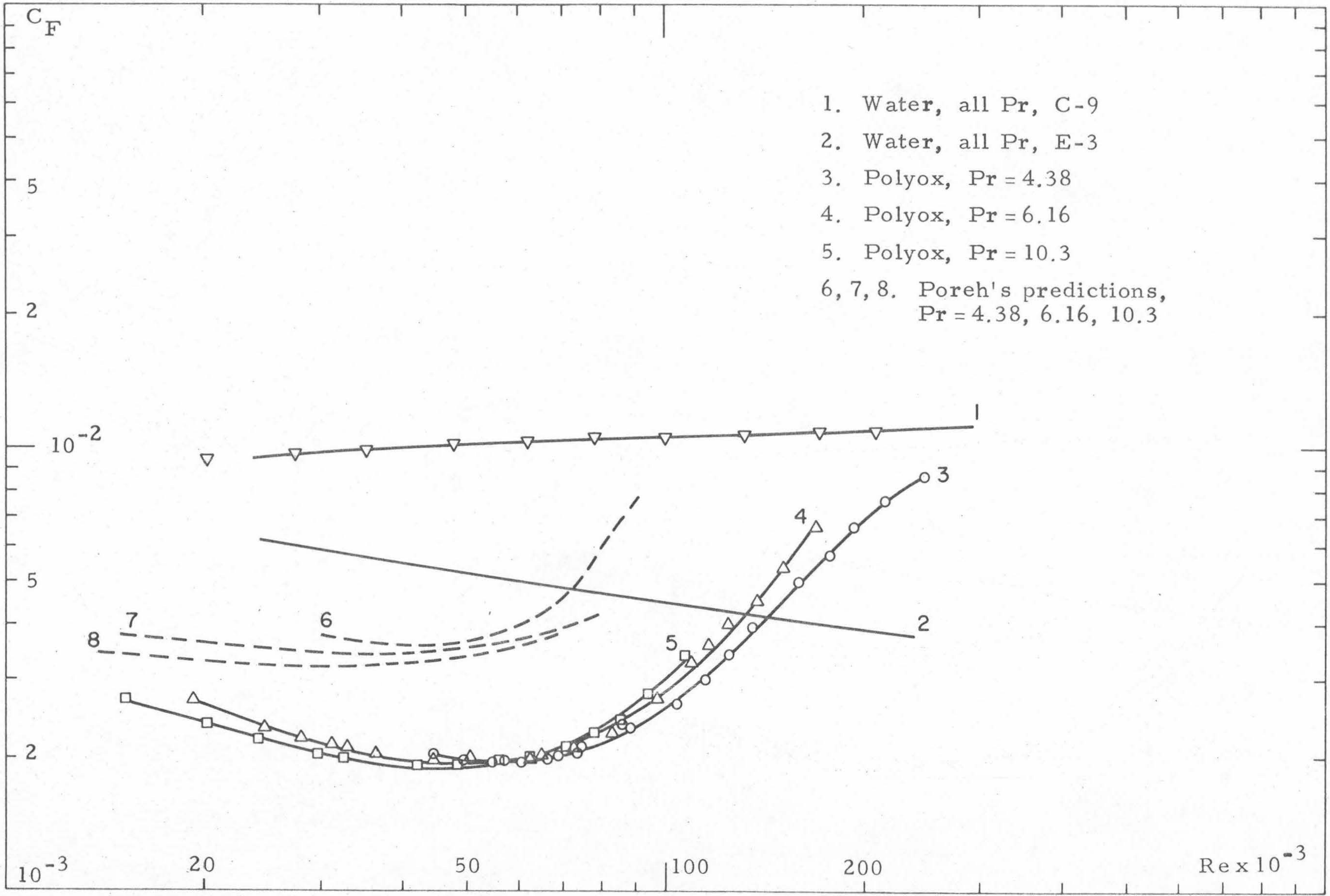

Fig. 18. Polyox 10 ppm, friction coefficient vs Reynolds number for tube C-9.

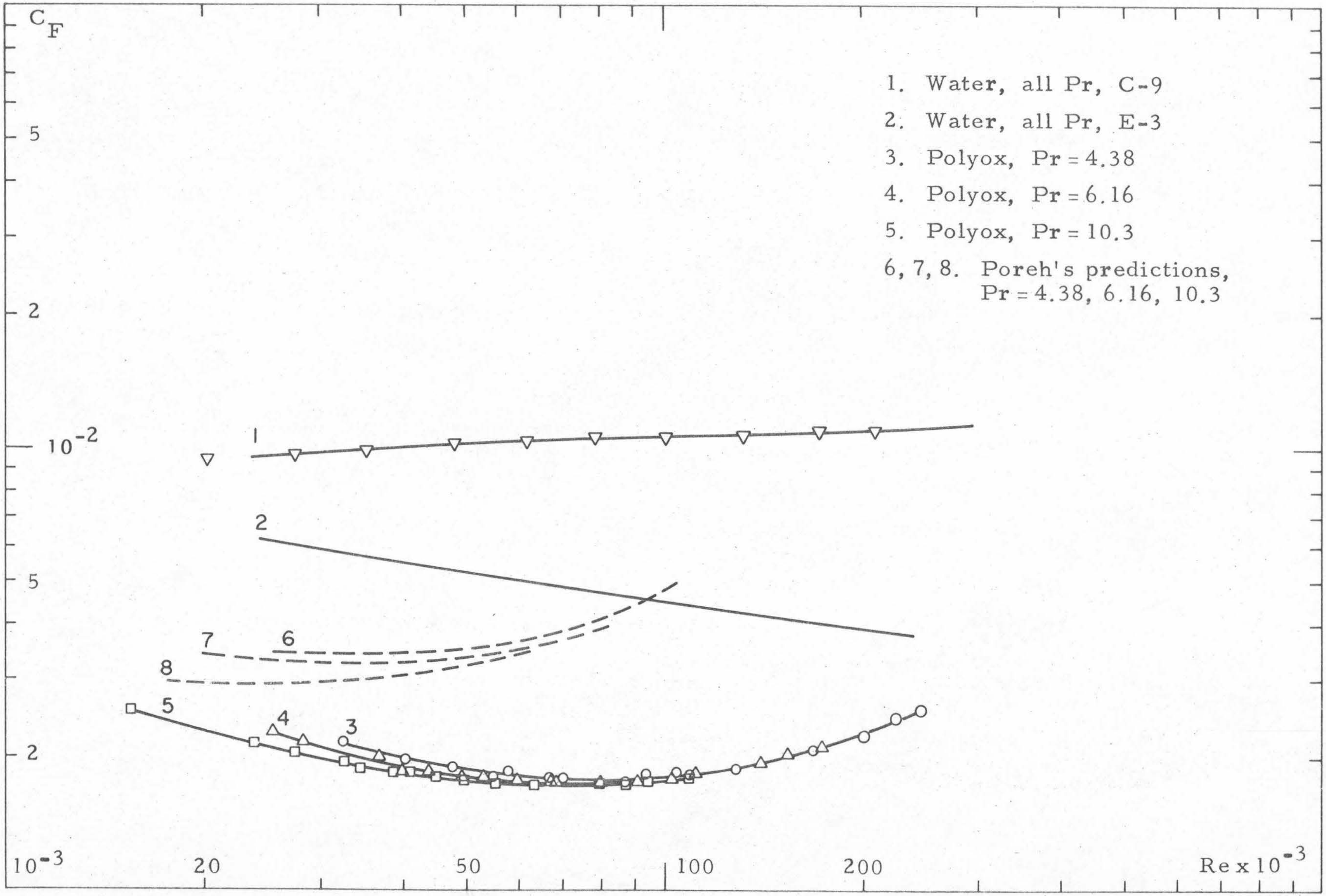

Fig. 19. Polyox 50 ppm, friction coefficient vs. Reynolds number for tube C-9.

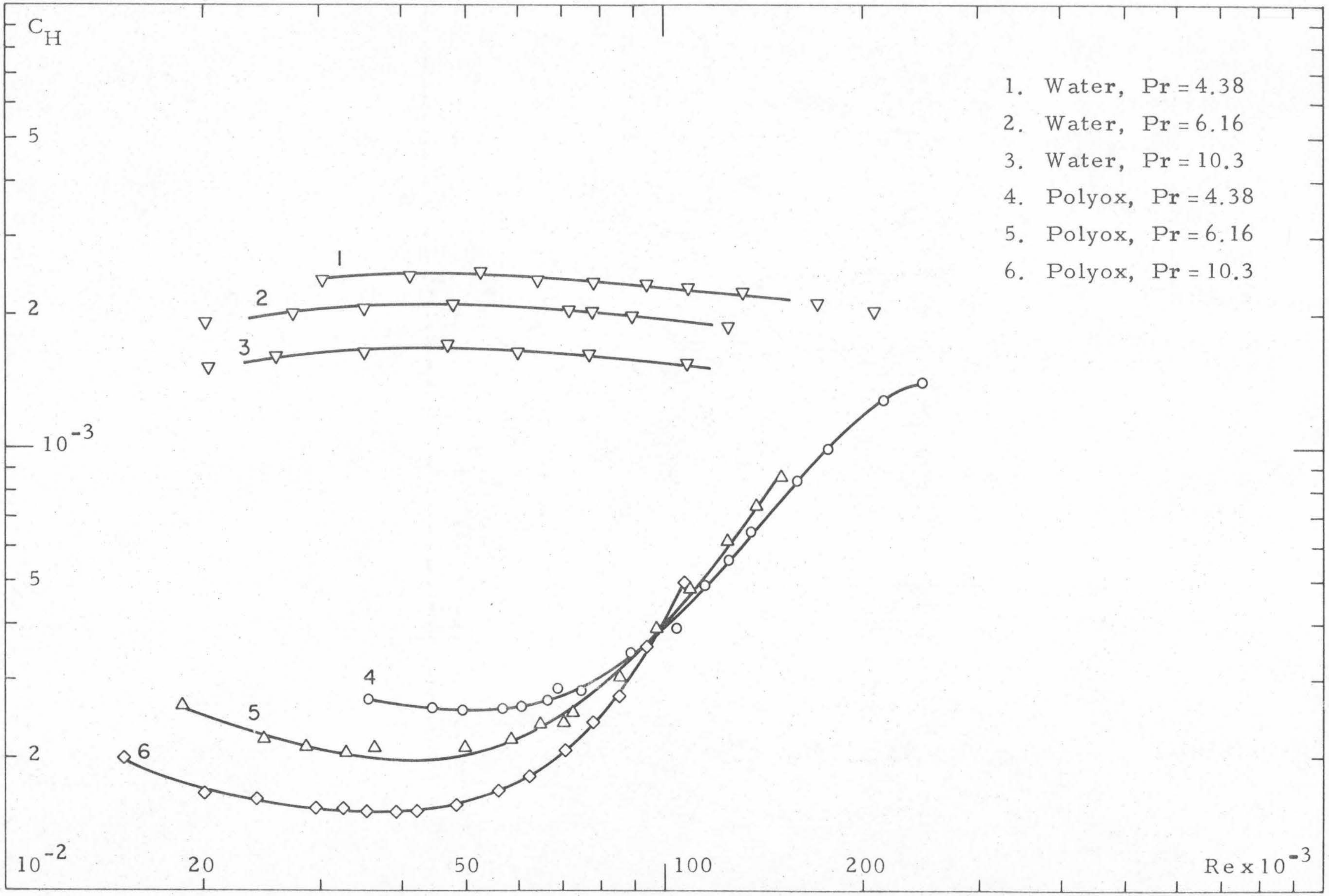

Fig. 20. Polyox 10 ppm, heat transfer coefficient vs. Reynolds number for tube C-9.

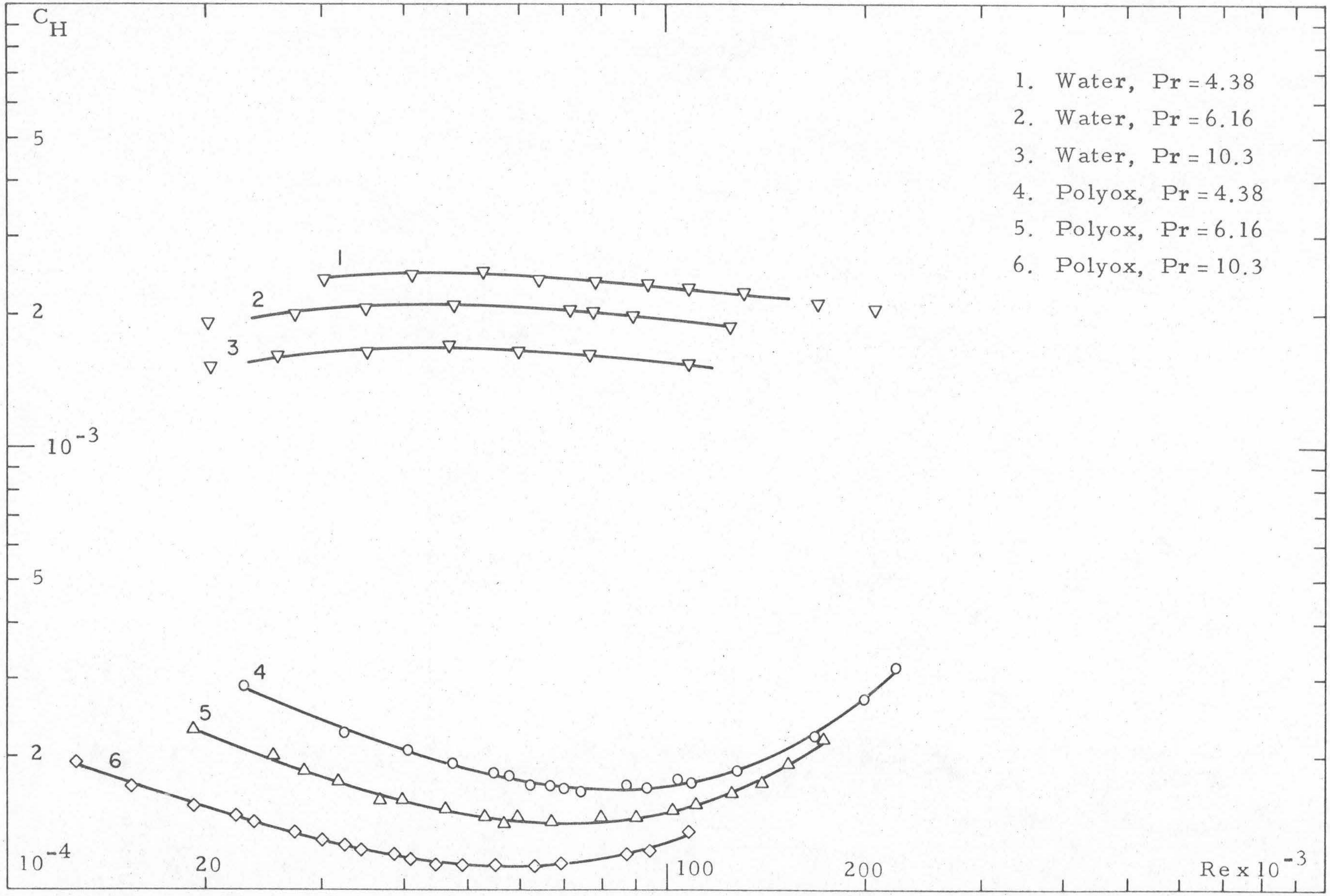

Fig. 21. Polyox 50 ppm, heat transfer coefficient vs. Reyonlds number for tube C-9.

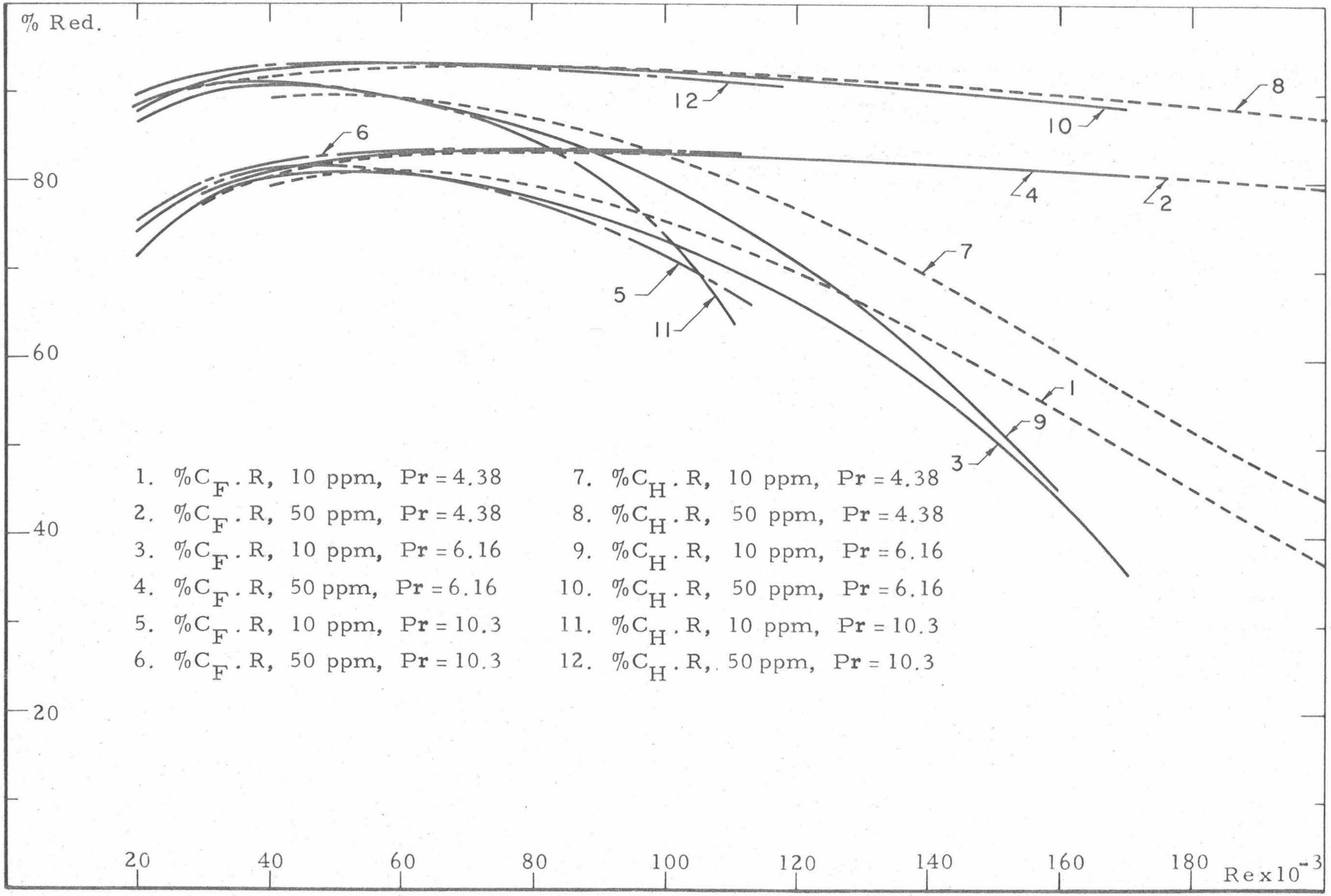

Fig. 22. Polyox 10 and 50 ppm, % friction and heat transfer reduction vs. Re for tube C-9.

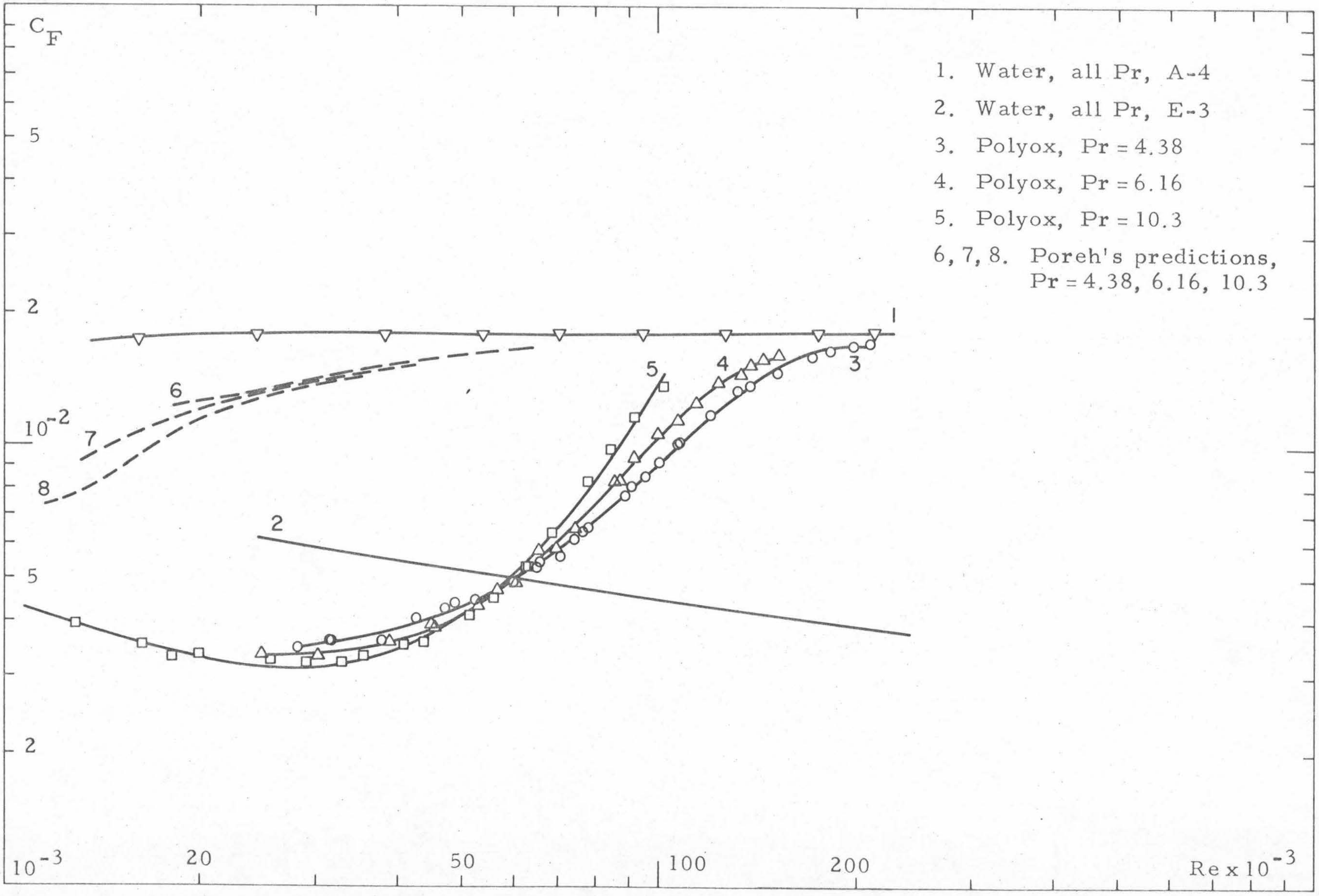

Fig. 23. Polyox 10 ppm, friction coefficient vs. Reynolds number for tube A-4.

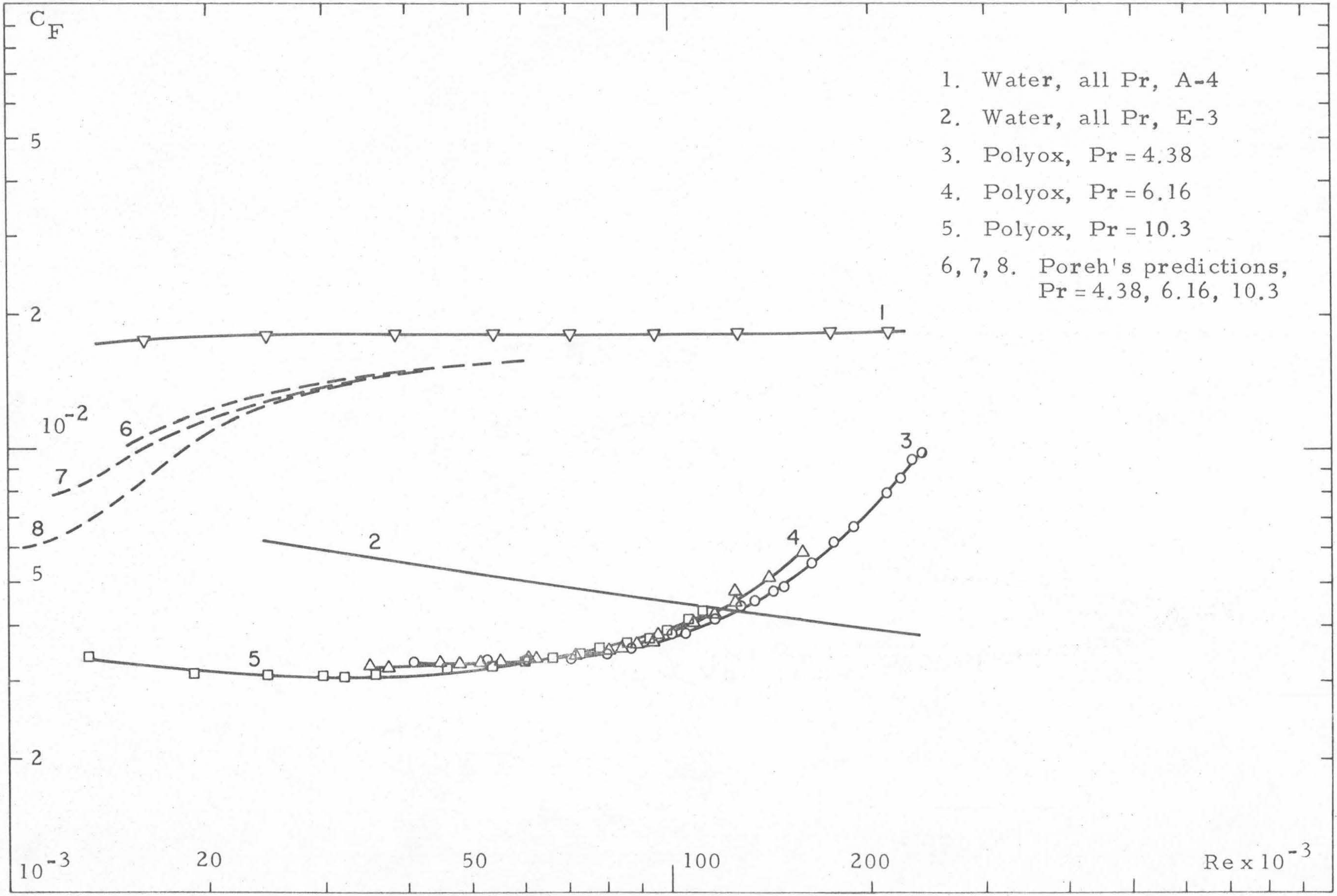

Fig. 24. Polyox 50 ppm, friction coefficient vs. Reynolds number for tube A-4.

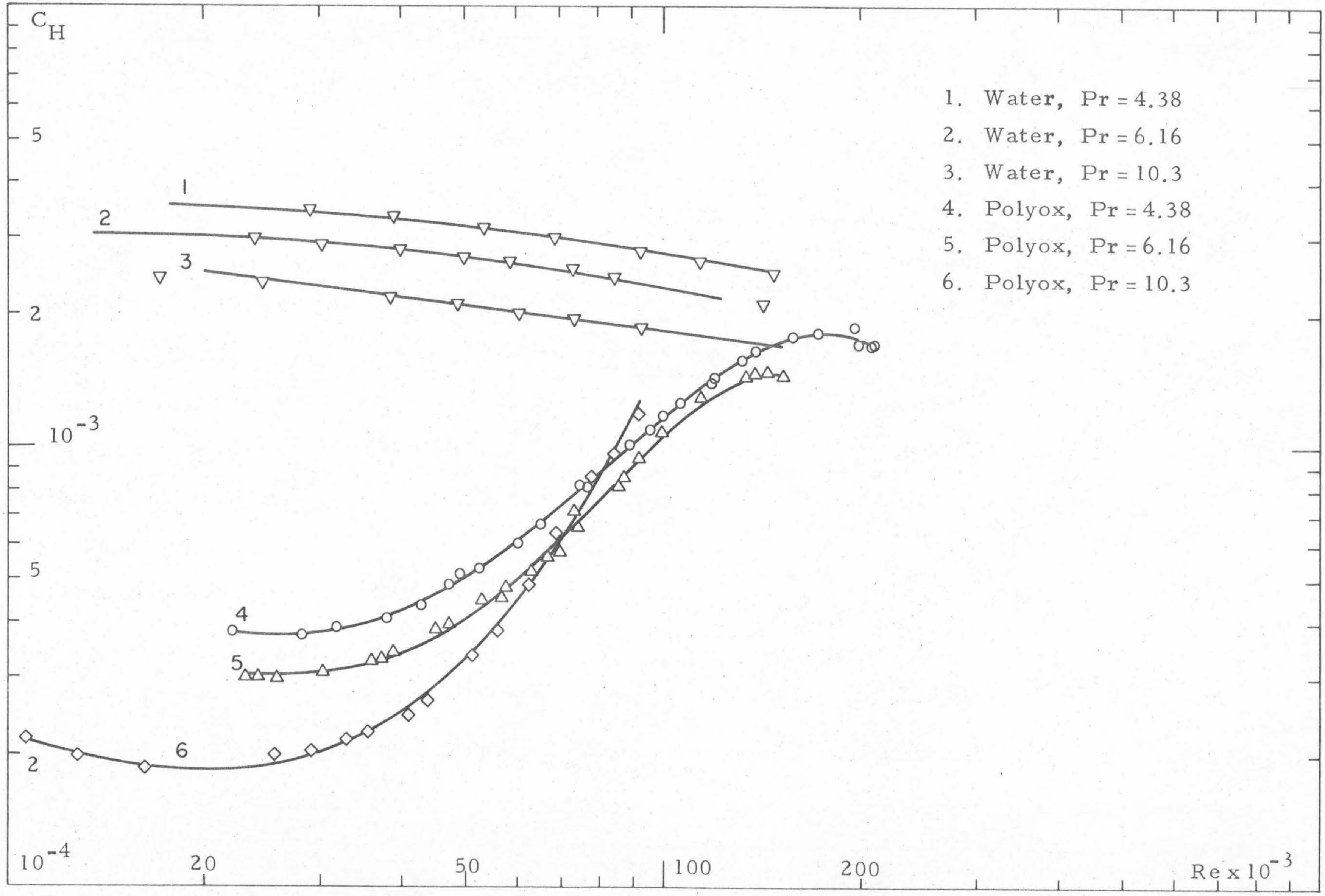

Fig. 25. Polyox 10 ppm, heat transfer coefficient vs. Reynolds number for tube A-4.

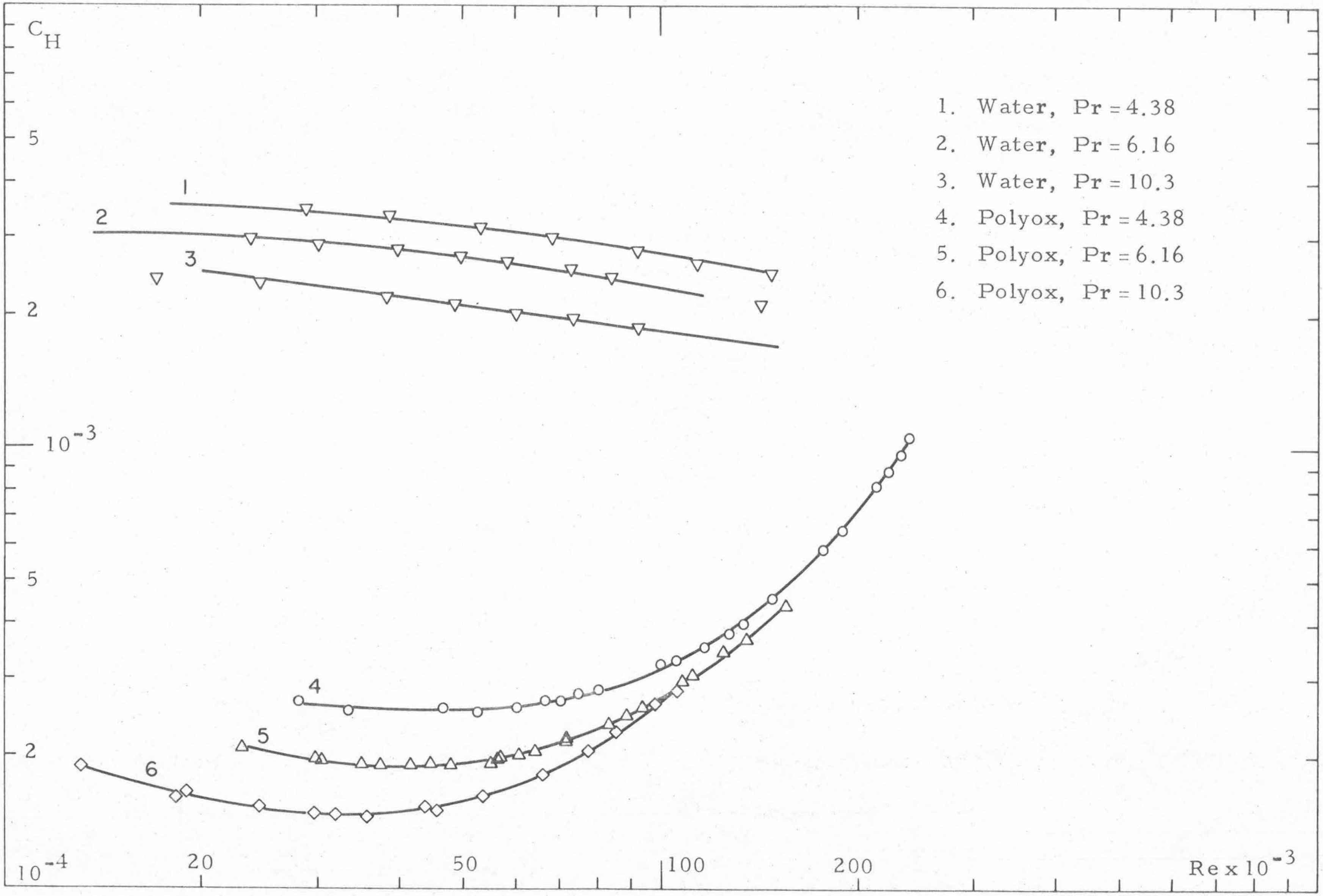

Fig. 26. Polyox 50 ppm, heat transfer coefficient vs. Reynolds number for tube A-4.

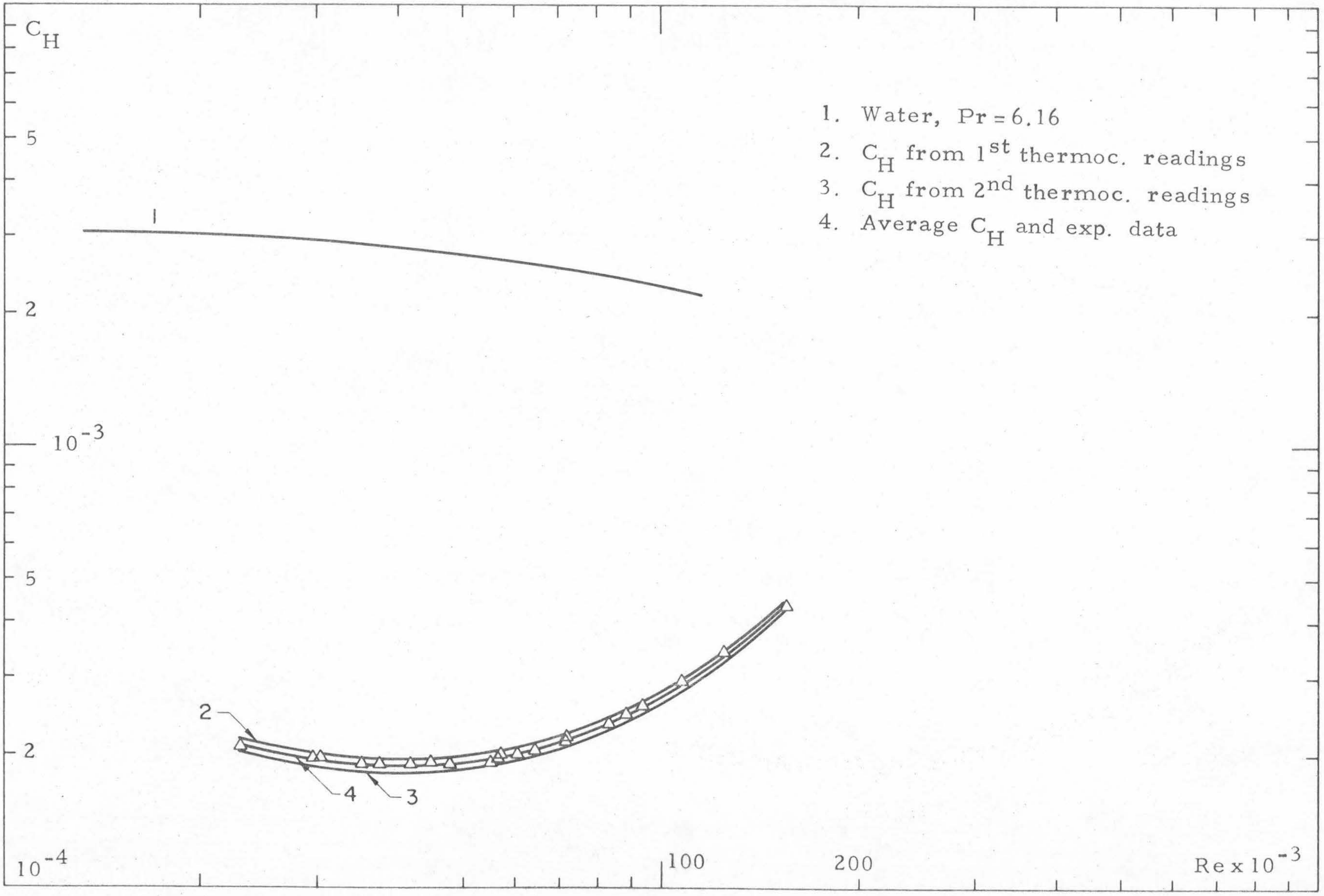

Fig. 27. Polyox 50 ppm, C_H vs. Re for tube A-4 at two circumferential locations.

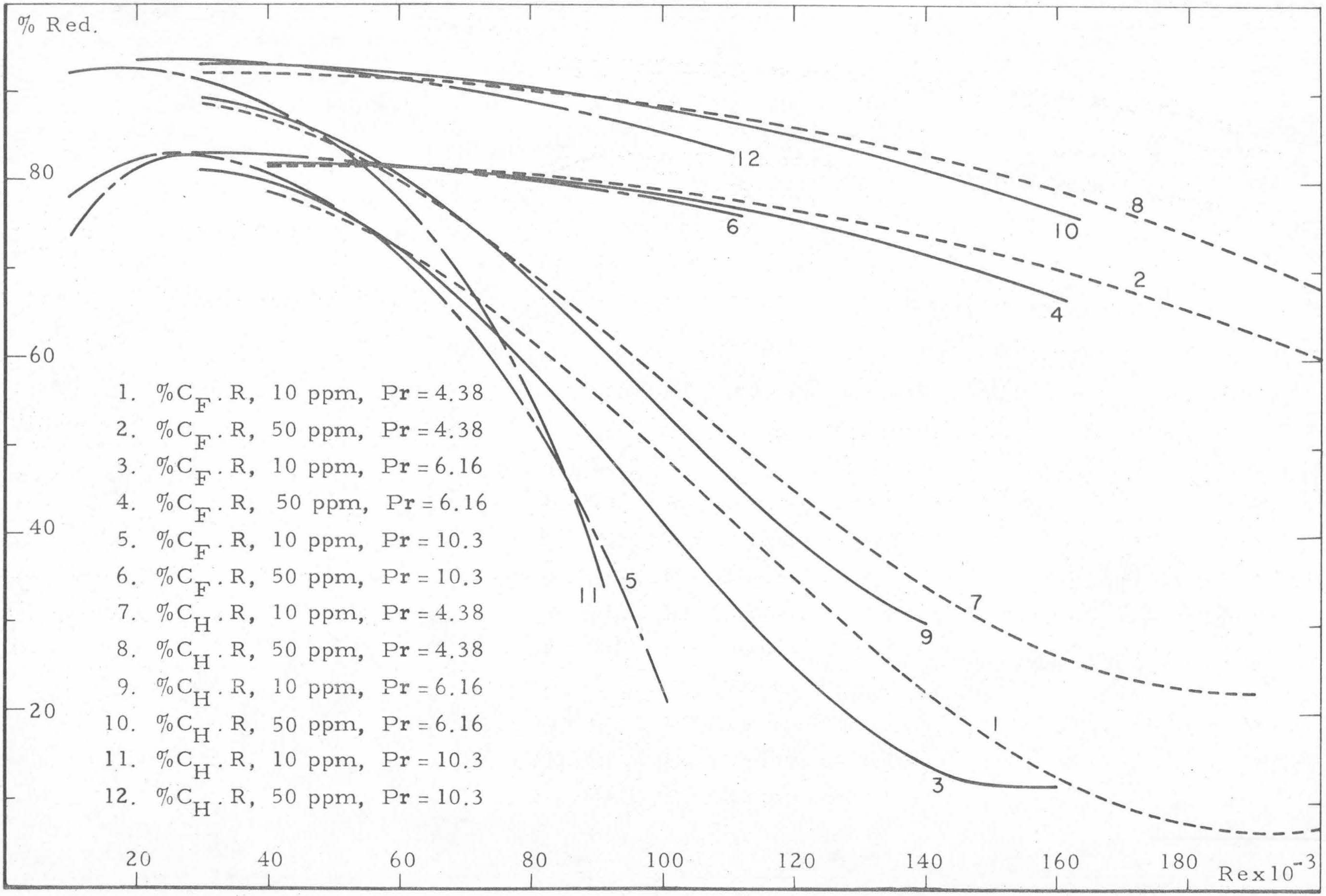

Fig. 28. Polyox 10 and 50 ppm, % friction and heat transfer reduction vs. Re for tube A-4.

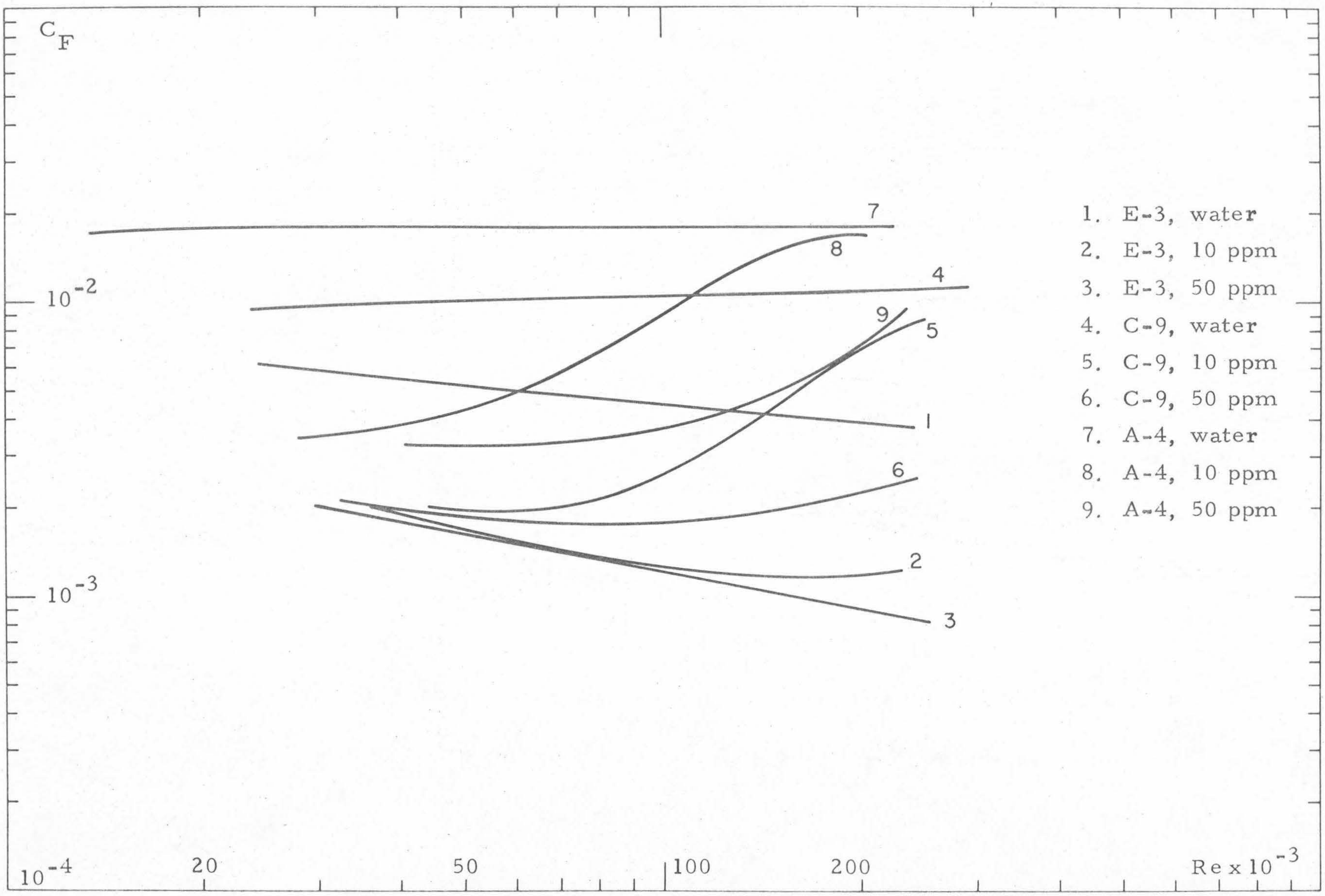

Fig. 29. Water, Polyox 10 and 50 ppm, C_F vs. Re for 3 tubes at Pr = 4.38.

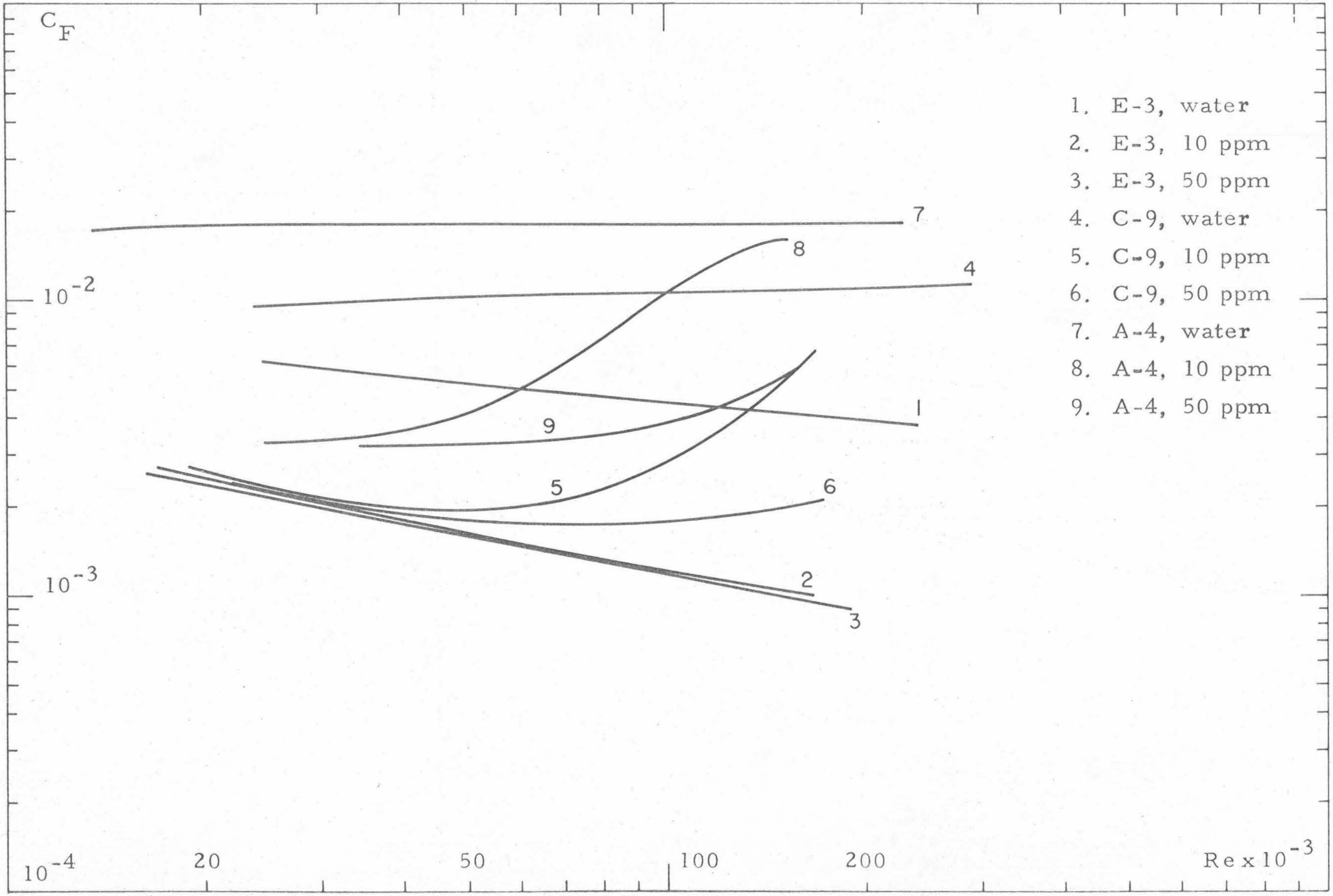

Fig. 30. Water, Polyox 10 and 50 ppm, C_F vs. Re for 3 tubes at Pr = 6.16.

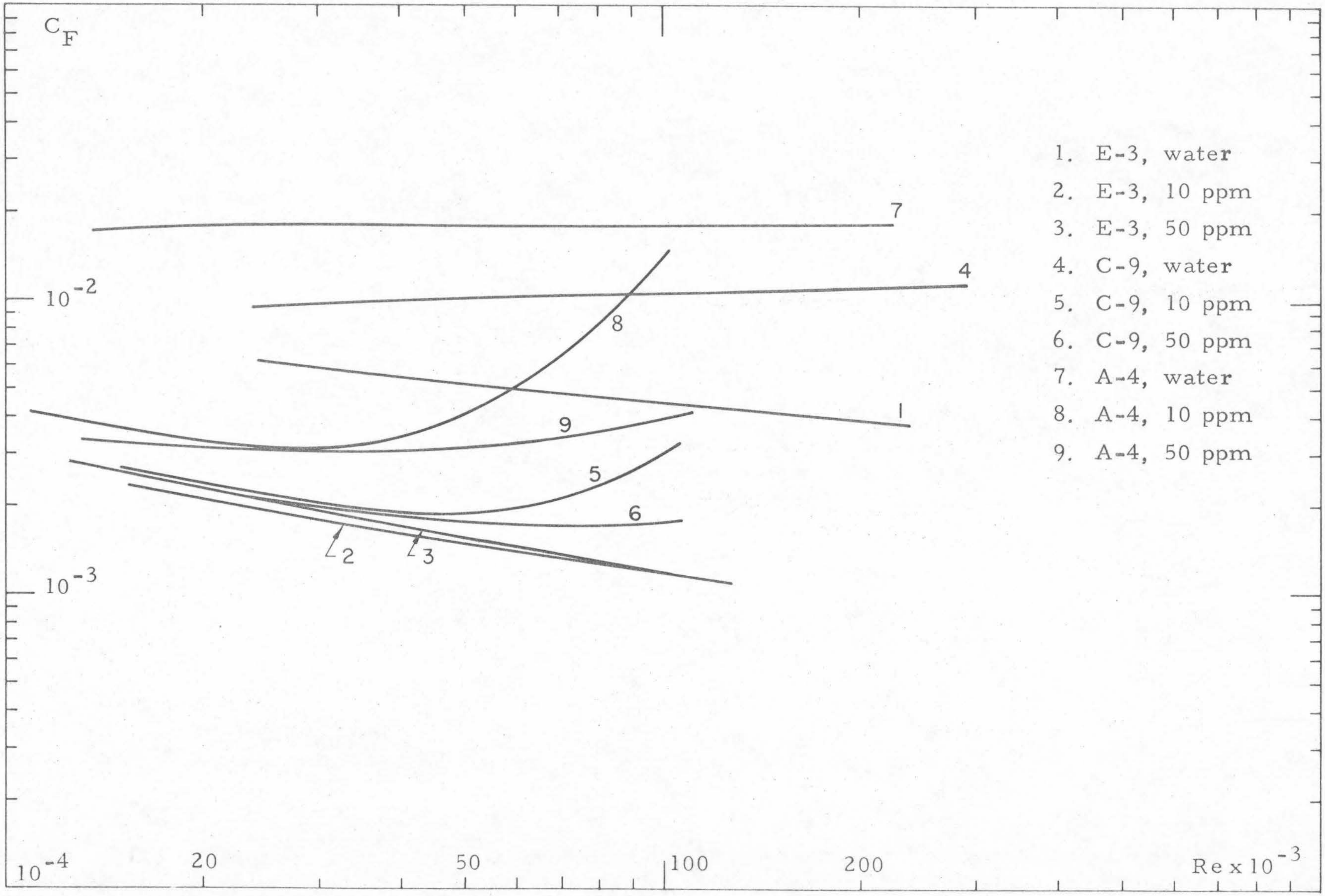

Fig. 31. Water, Polyox 10 and 50 ppm, C_F vs. Re for 3 tubes at Pr = 10.3.

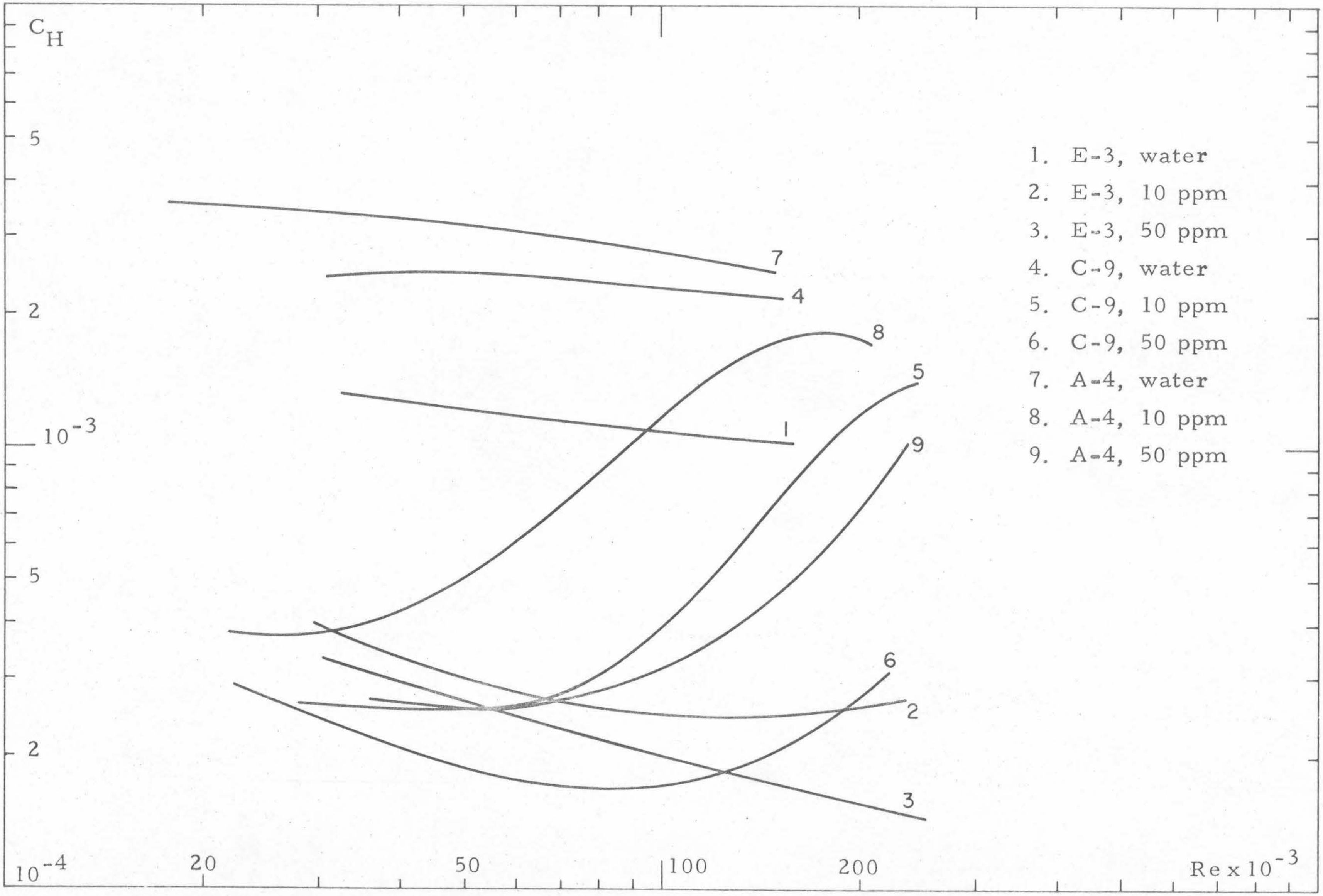

Fig. 32. Water, Polyox 10 and 50 ppm, C_H vs. Re for 3 tubes at Pr = 4.38.

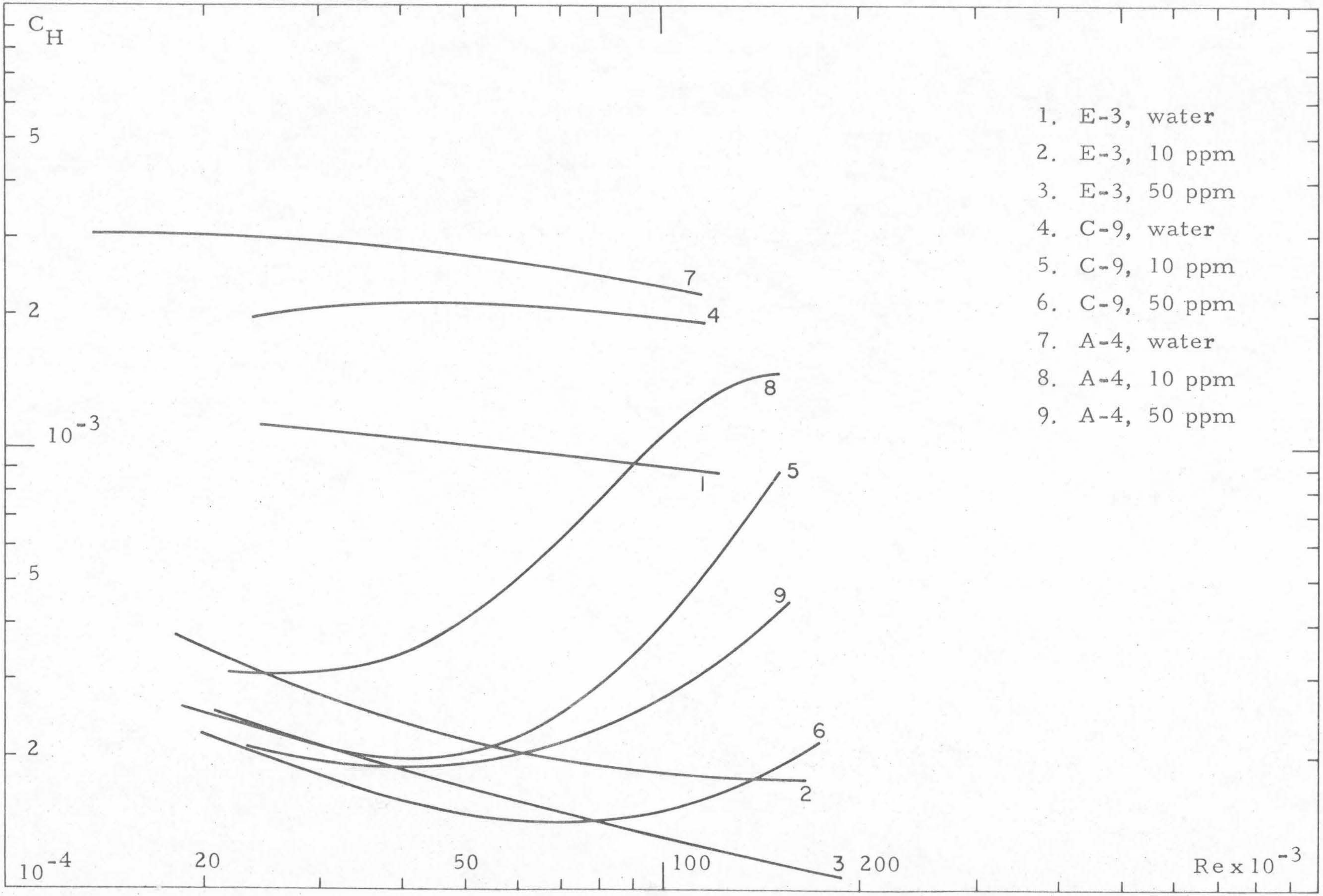

Fig. 33. Water, Polyox 10 and 50 ppm, C_H vs. Re for 3 tubes at Pr = 6.16.

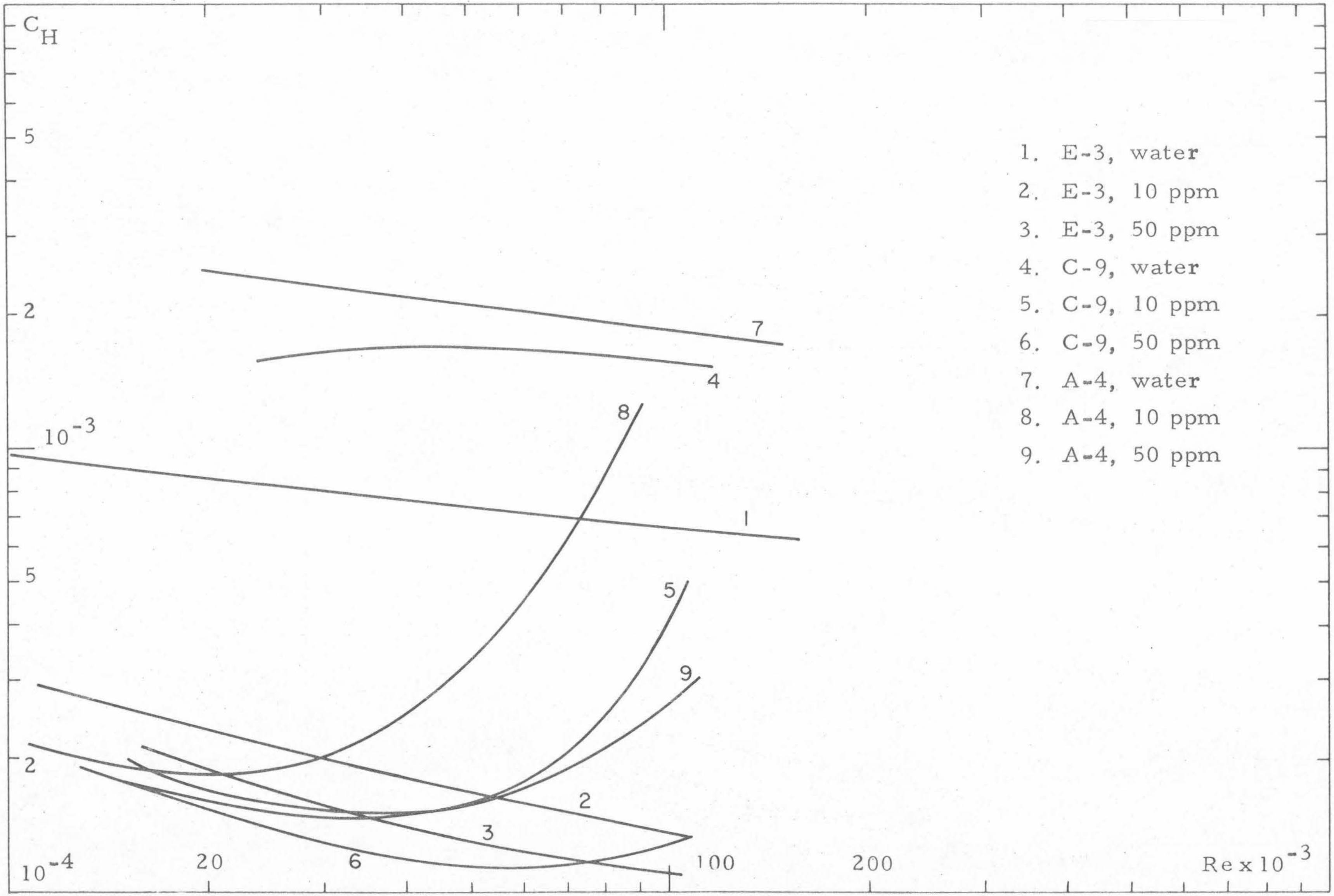

Fig. 34. Water, Polyox 10 and 50 ppm, C_H vs. Re for 3 tubes at Pr = 10.3.

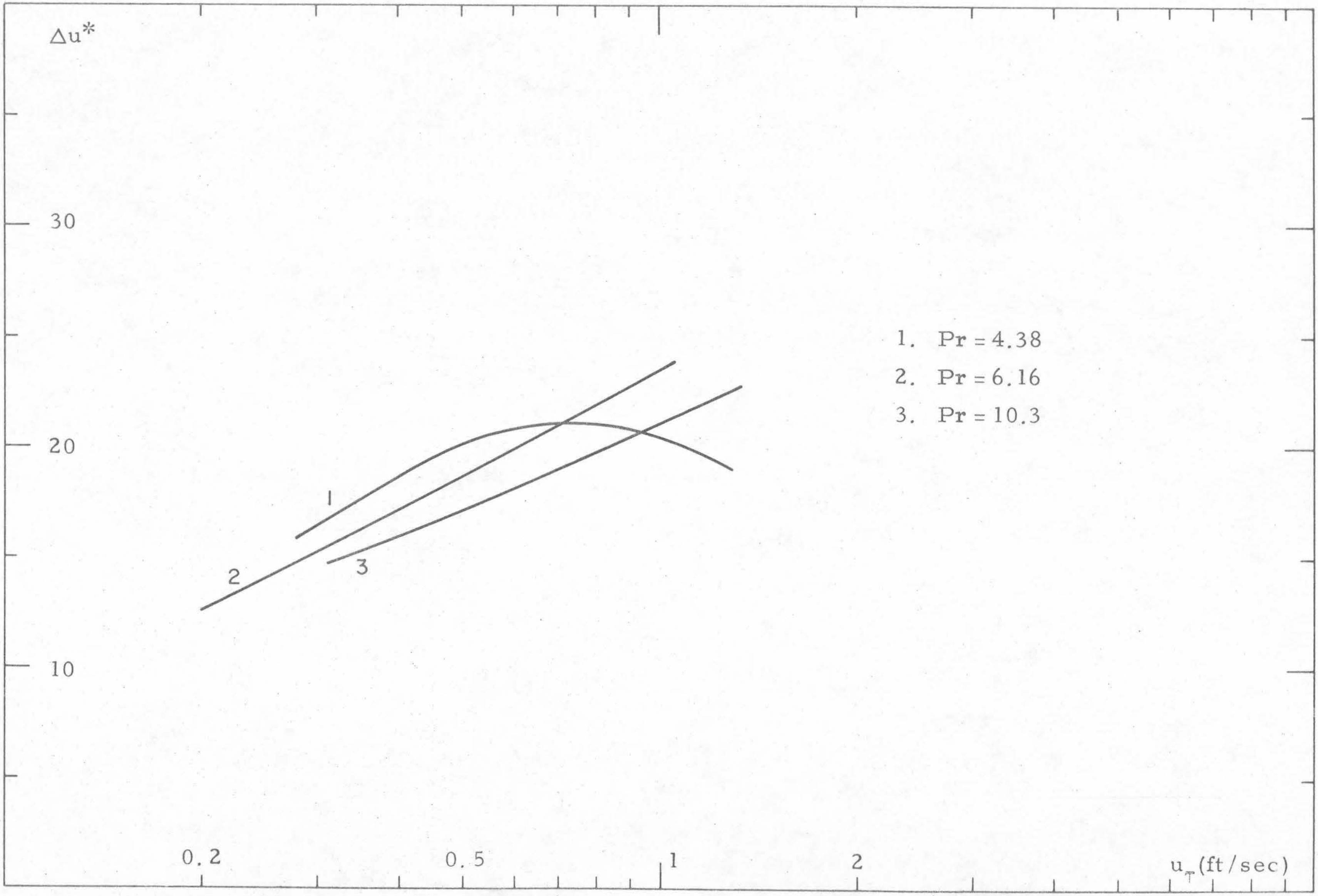

Fig. 35. Polyox 10 ppm, Δu^* vs. u_τ for tube E-3 at Pr = 4.38, 6.16 and 10.3.

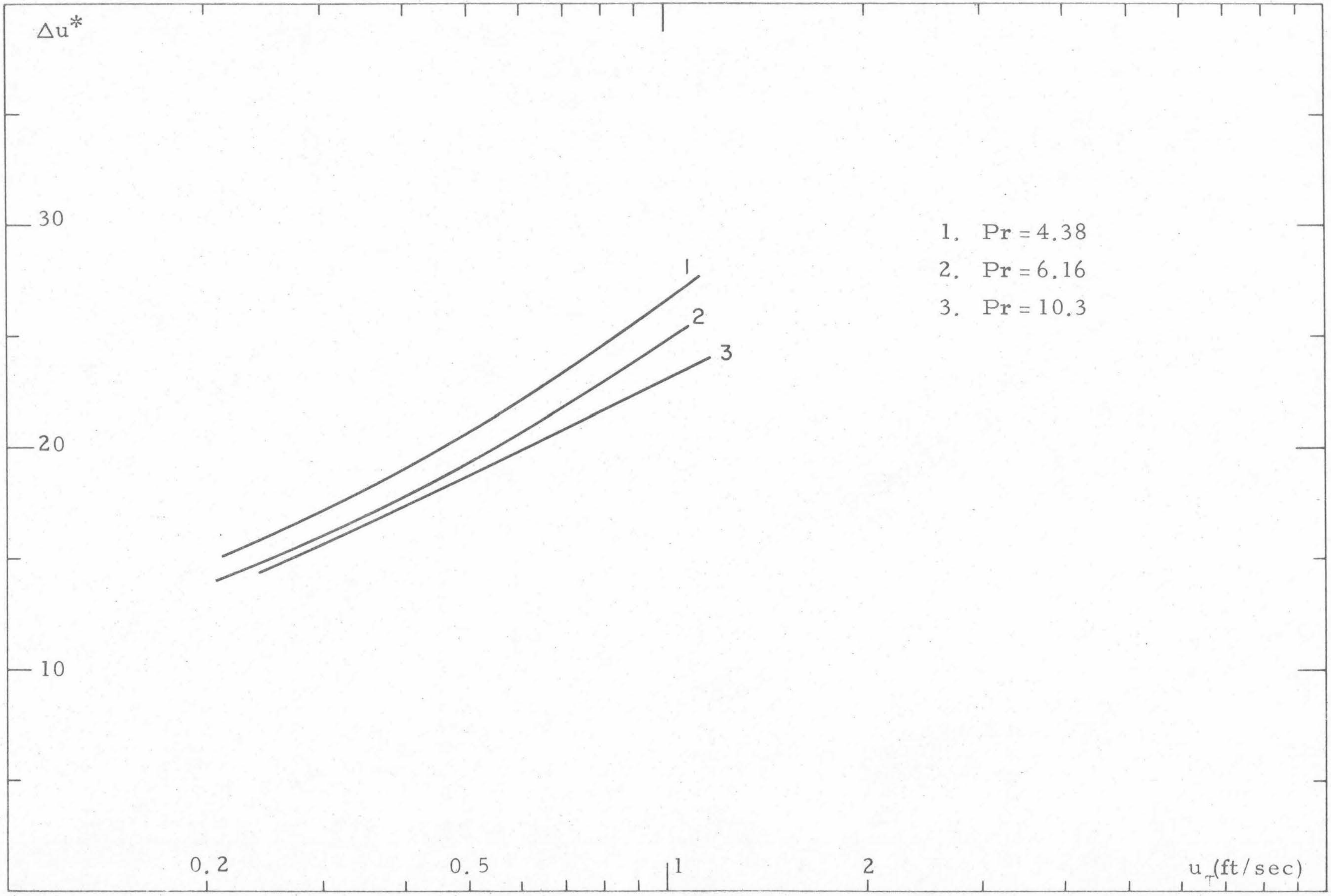

Fig. 36. Polyox 50 ppm, Δu^* vs. u_τ for tube E-3 at $Pr = 4.38$, 6.16 and 10.3.

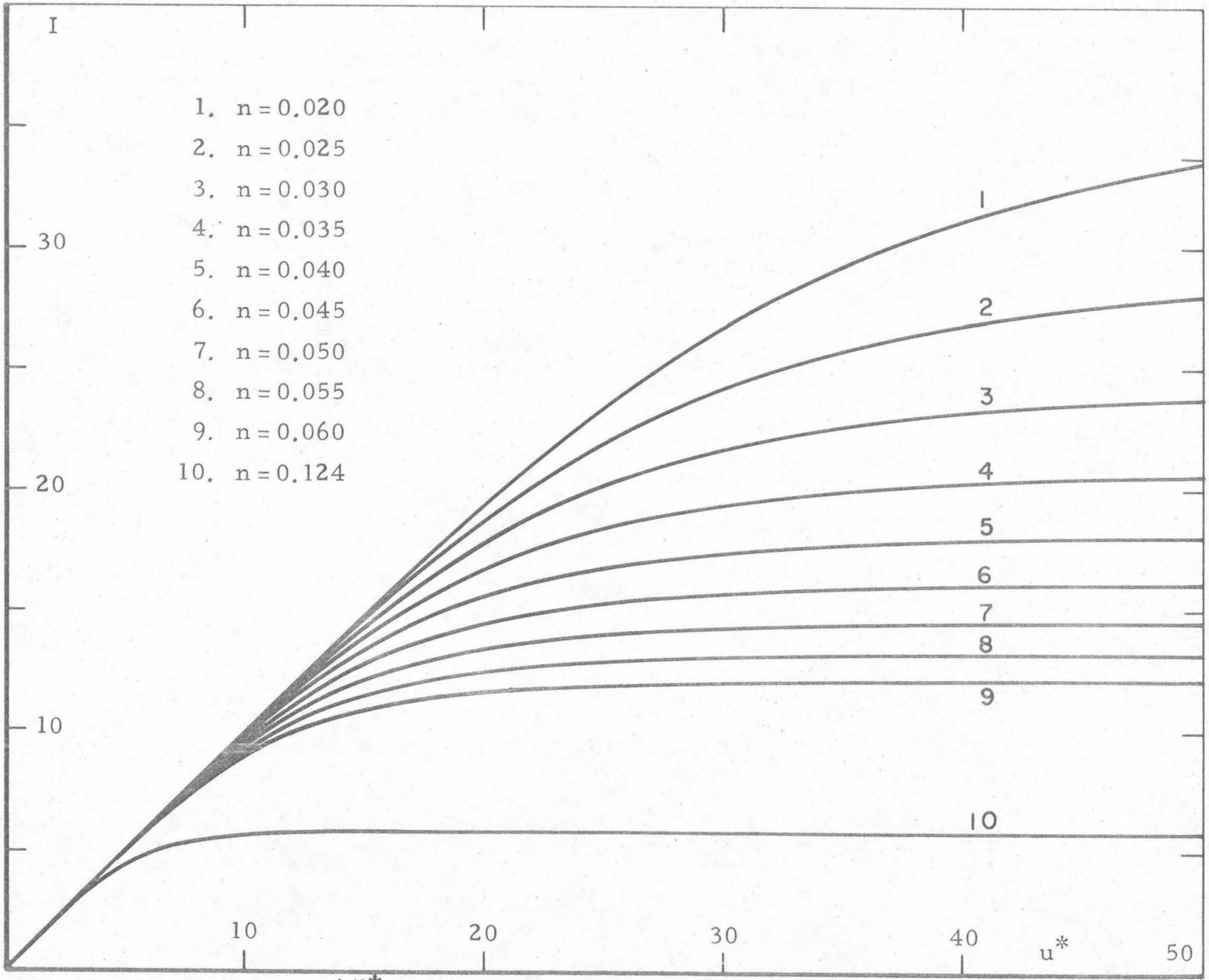

Fig. 37. $I = \int_0^{u^*} du^*/(1 + \mathrm{Pr}\, \epsilon_M/\nu)$ vs. u^* for different n (Eqn. 93).

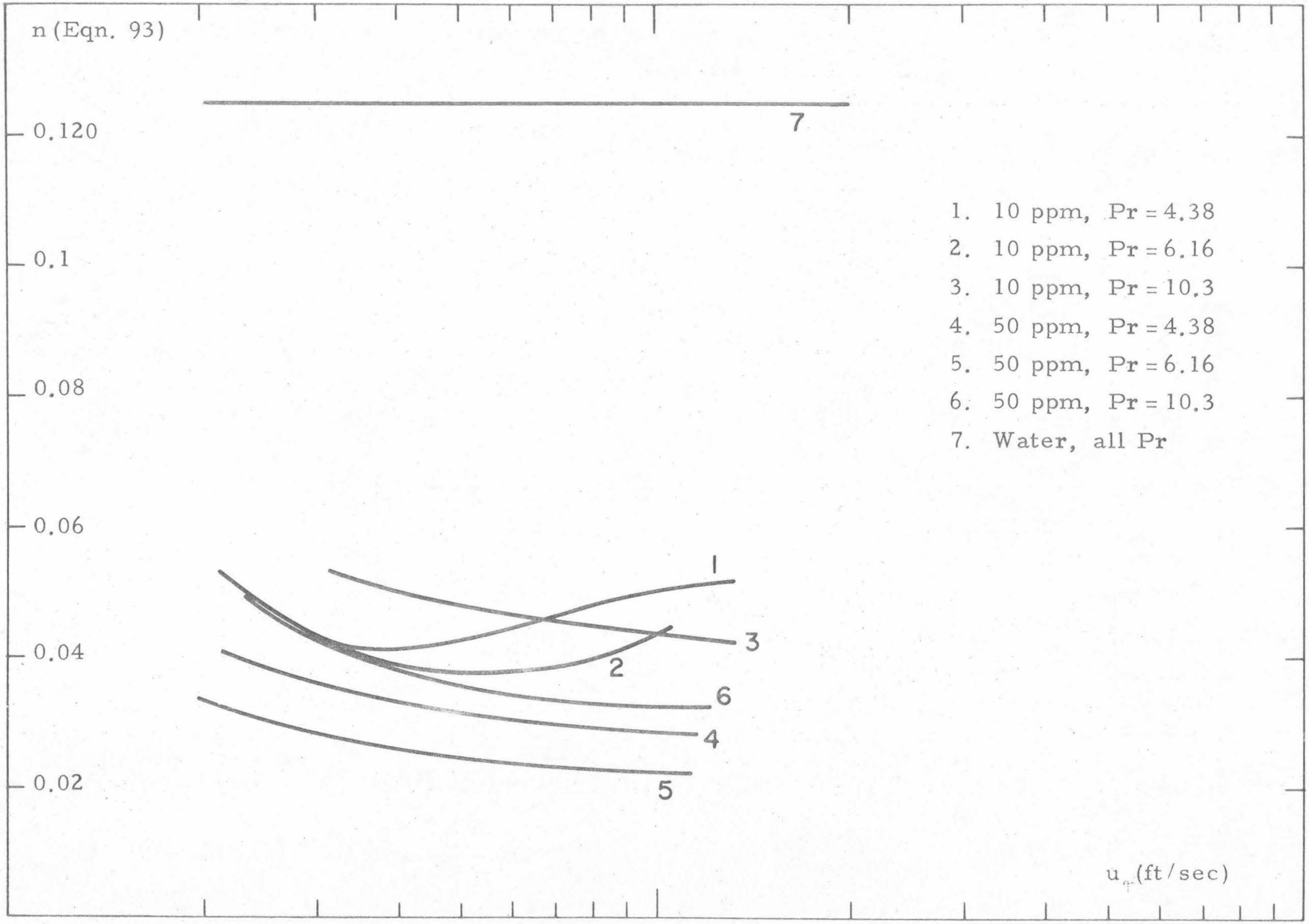

Fig. 38. Polyox 10 and 50 ppm, n (Eqn. 93) vs. u_τ for tube E-3 at Pr = 4.38, 6.16 and 10.3.

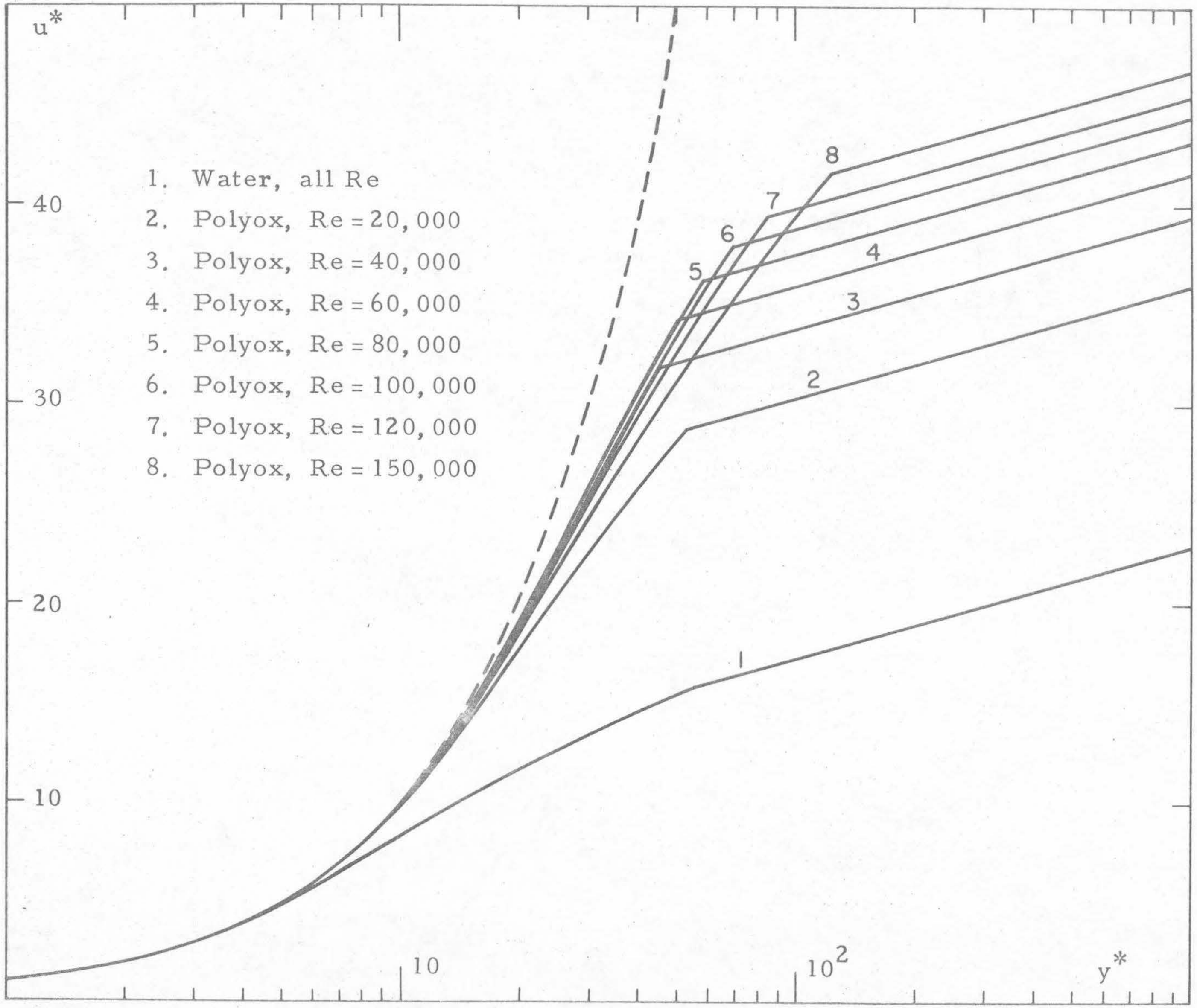

Fig. 39. Polyox 10 ppm, u* vs. y* from Eqn. (95) for different Re at Pr = 6.16 (E-3).

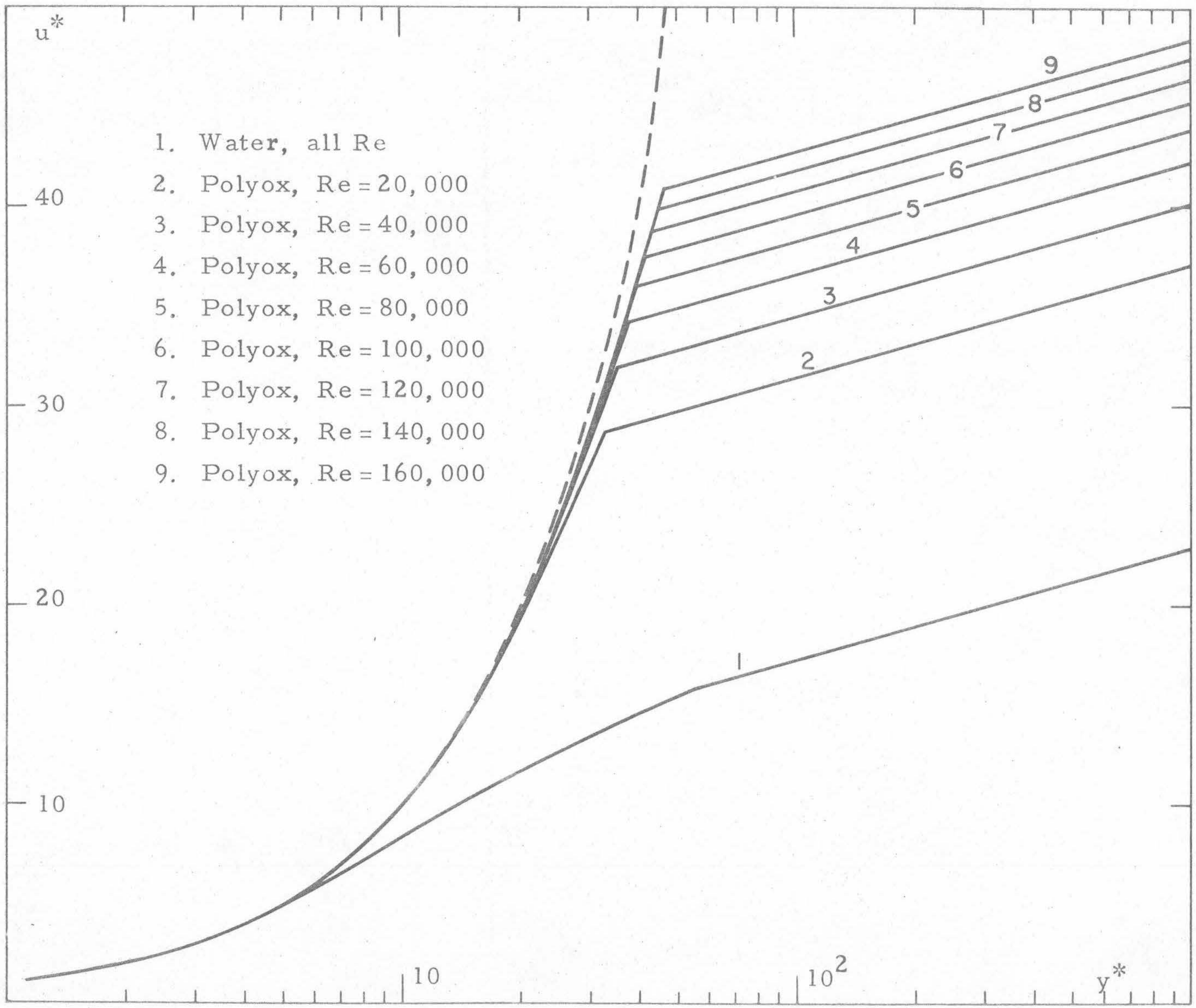

Fig. 40. Polyox 50 ppm, u^* vs. y^* from Eqn. (95) for different Re at Pr = 6.16 (E-3).

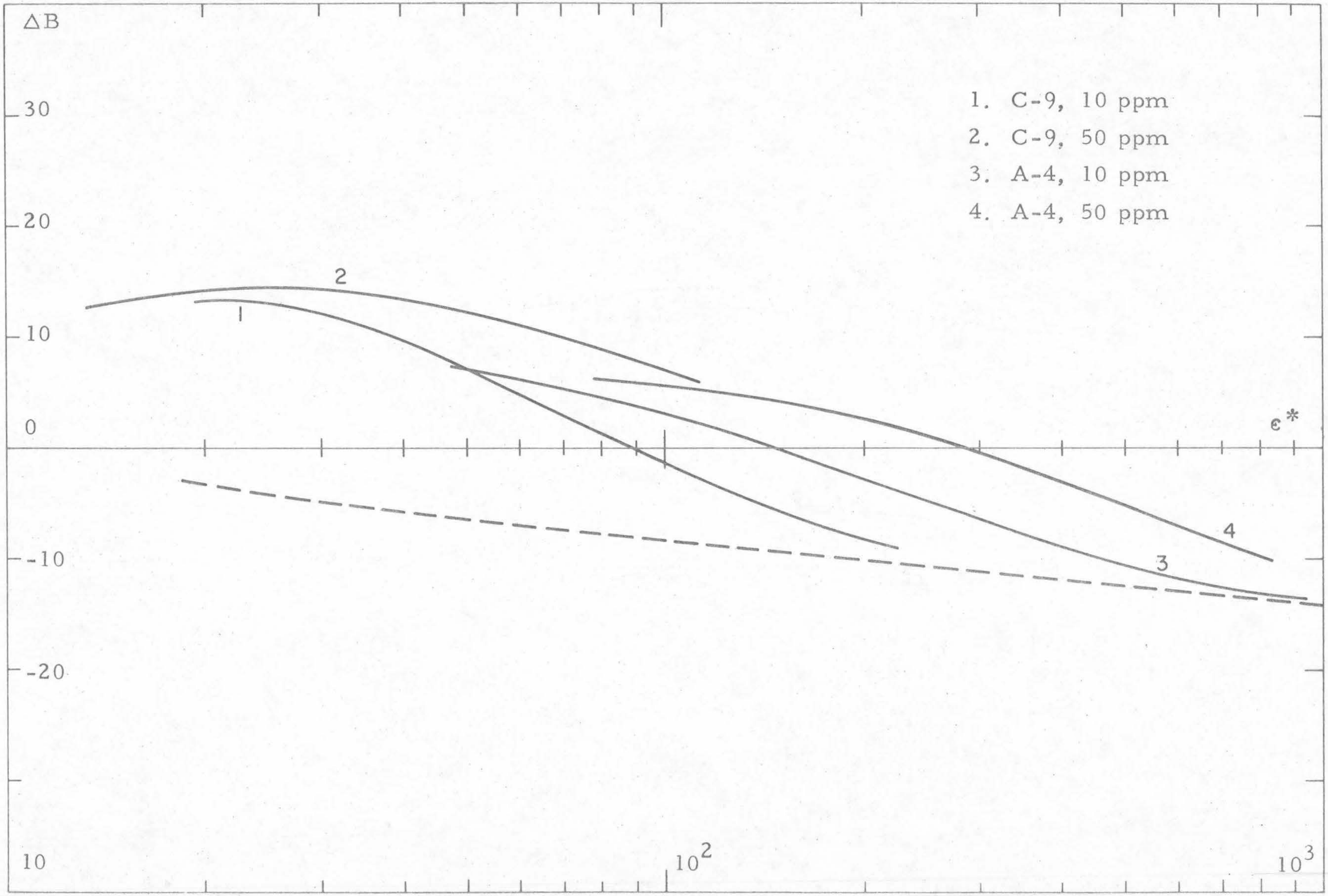

Fig. 41. Polyox, 10 and 50 ppm, ΔB vs. ε* for rough tubes at Pr = 4.38.

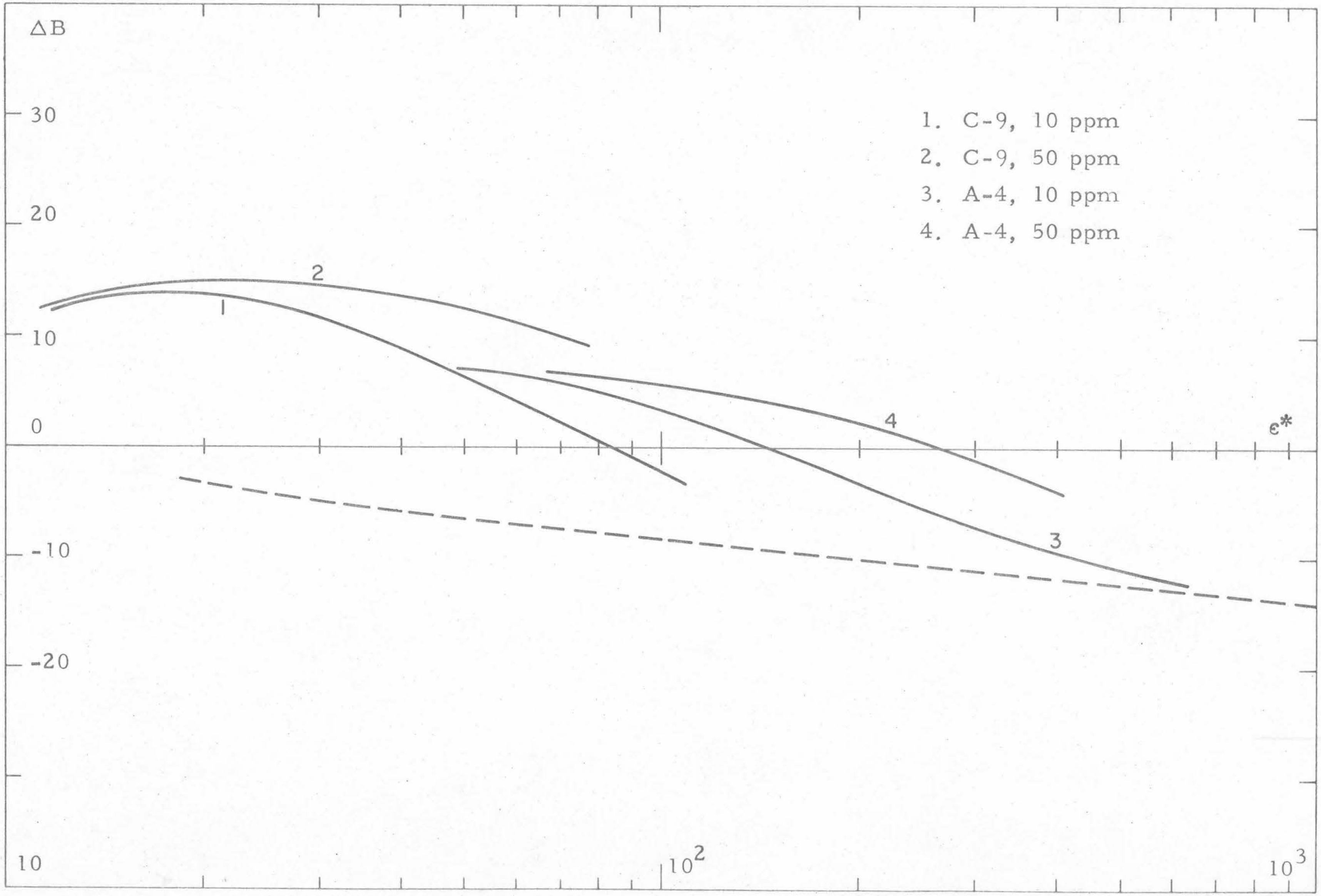

Fig. 42. Polyox 10 and 50 ppm, ΔB vs. ε* for rough tubes at Pr = 6.16.

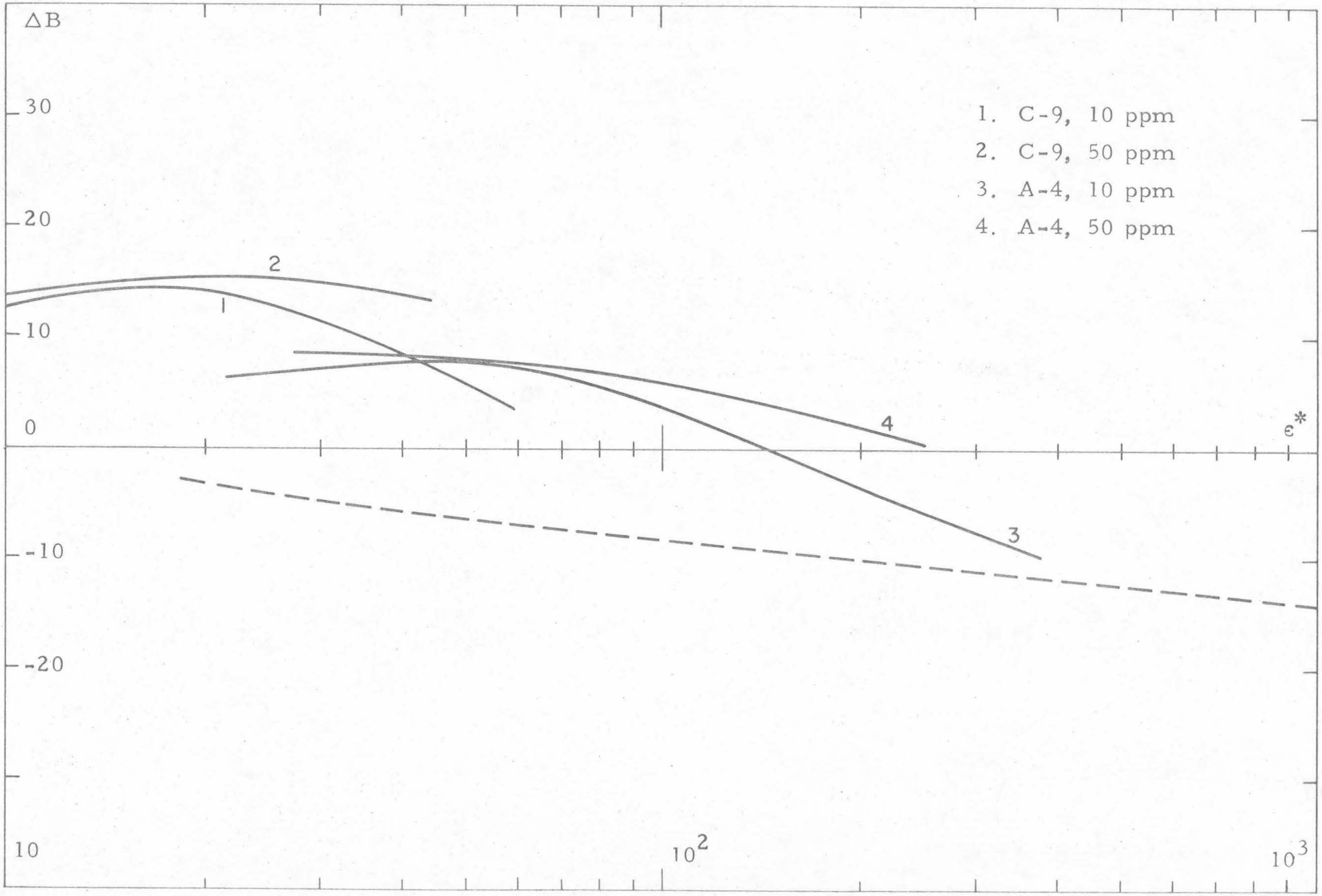

Fig. 43. Polyox 10 and 50 ppm, ΔB vs. ε* for rough tubes at Pr = 10.3.

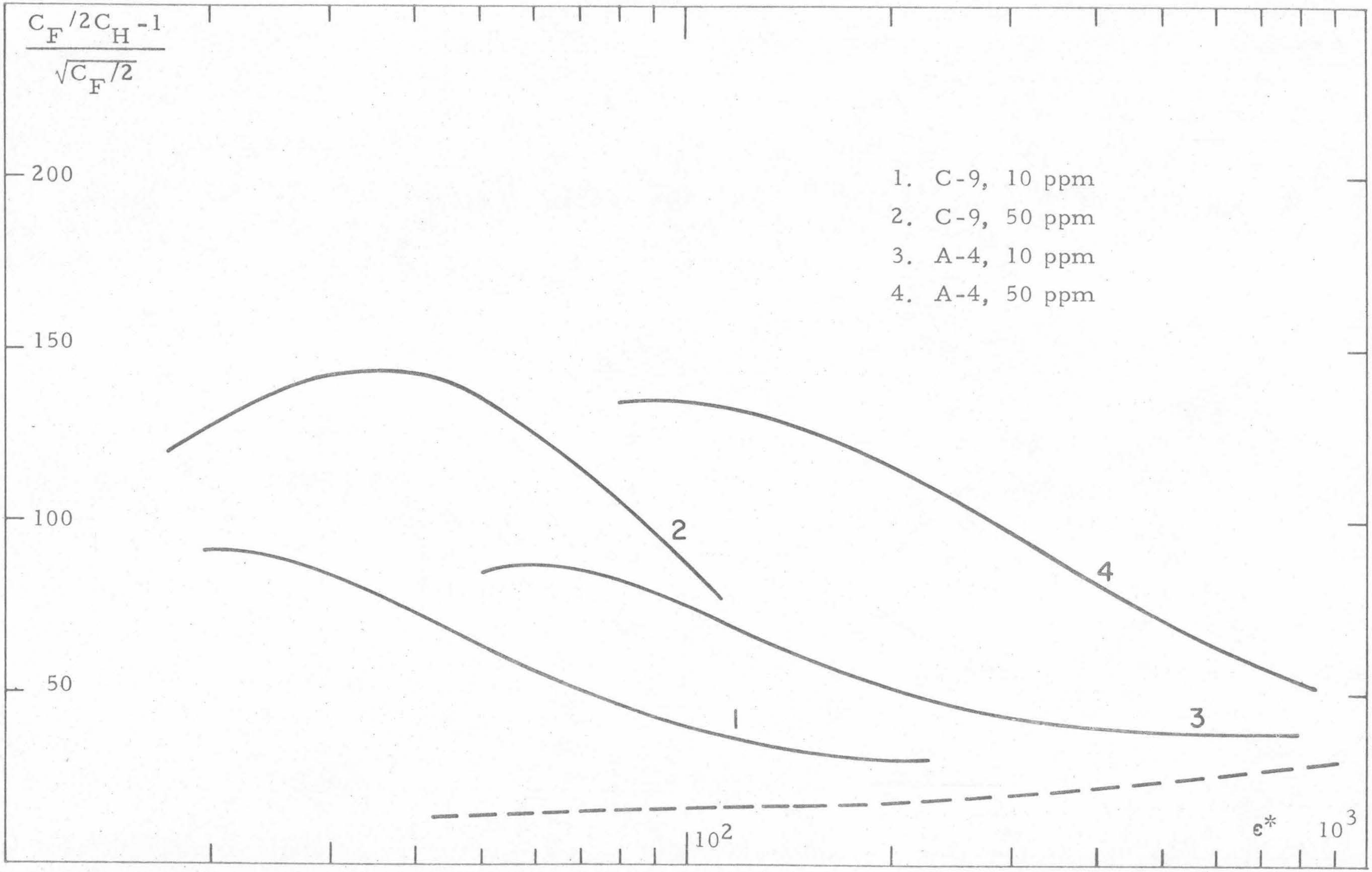

Fig. 44. Polyox 10 and 50 ppm, $(C_F/2C_H-1)/\sqrt{C_F/2}$ vs. ε* for rough tubes at Pr = 4.38.

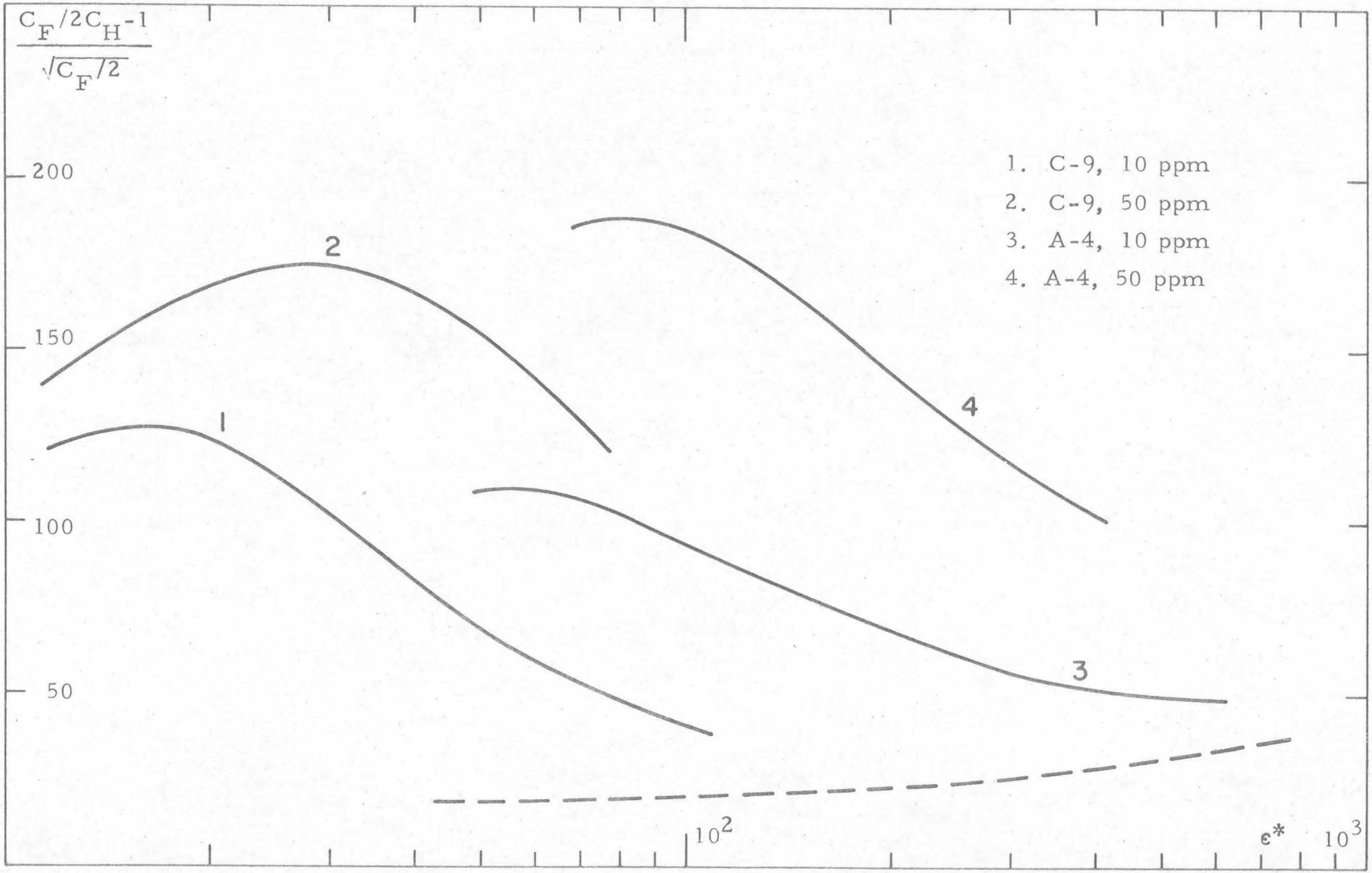

Fig. 45. Polyox 10 and 50 ppm, $(C_F/2C_H-1)/\sqrt{C_F/2}$ vs. ε^* for rough tubes at Pr = 6.16.

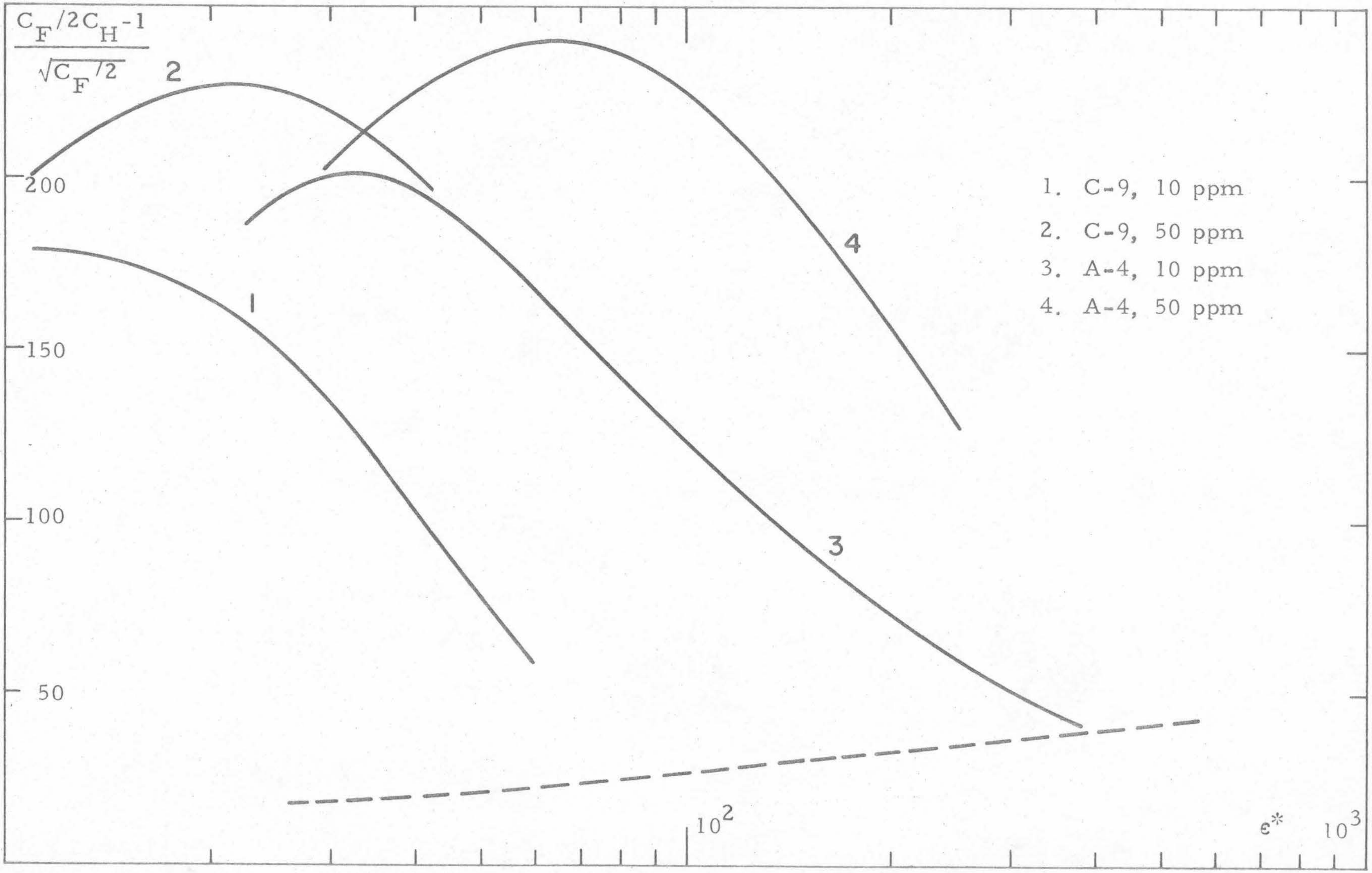

Fig. 46. Polyox 10 and 50 ppm, $(C_F/2C_H - 1)/\sqrt{C_F/2}$ vs. ε^* for rough tubes at $Pr = 10.3$.

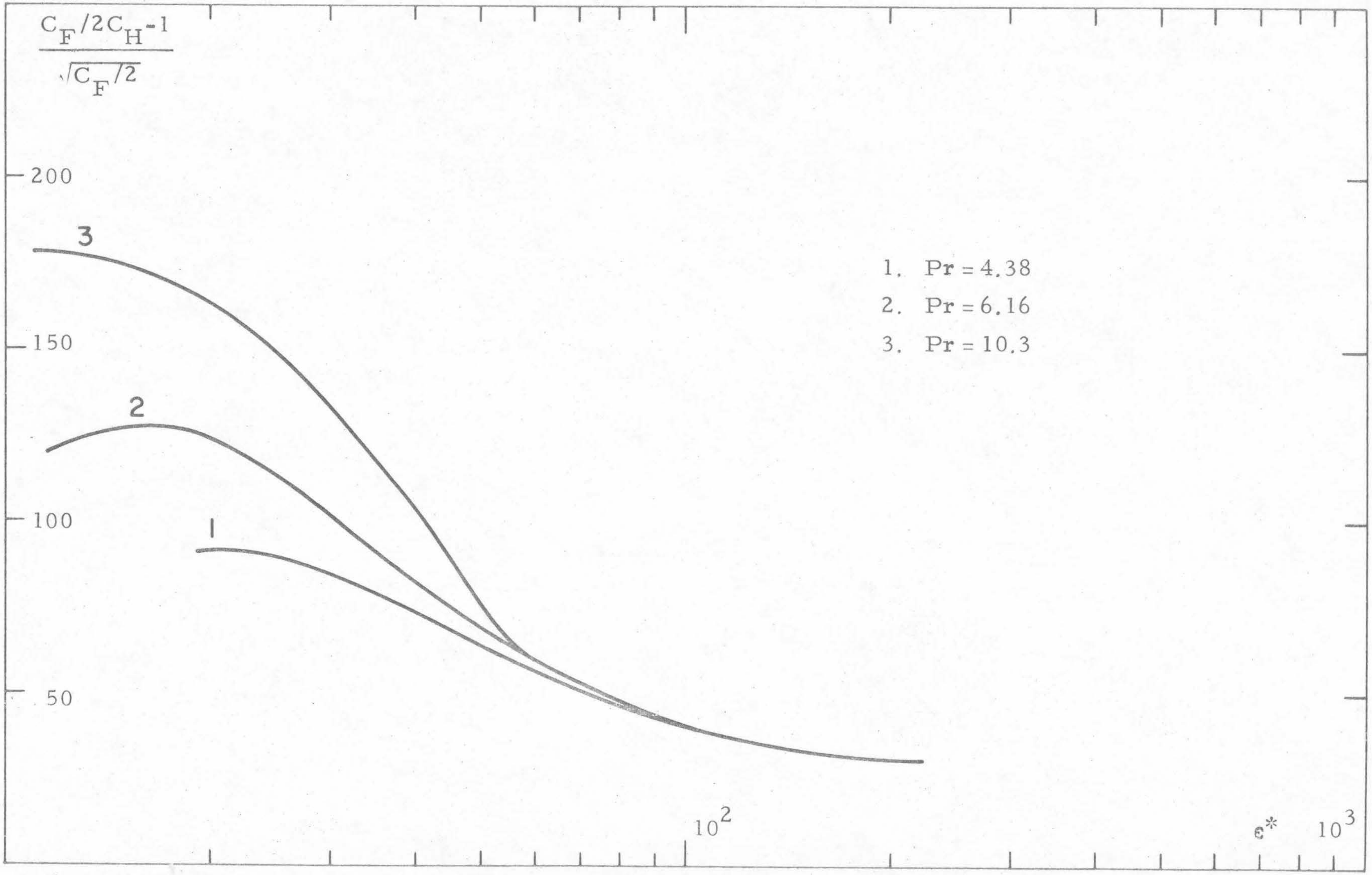

Fig. 47. Polyox 10 ppm, $(C_F/2C_H-1)/\sqrt{C_F/2}$ vs. ε^* for C-9 tube: Pr effect.

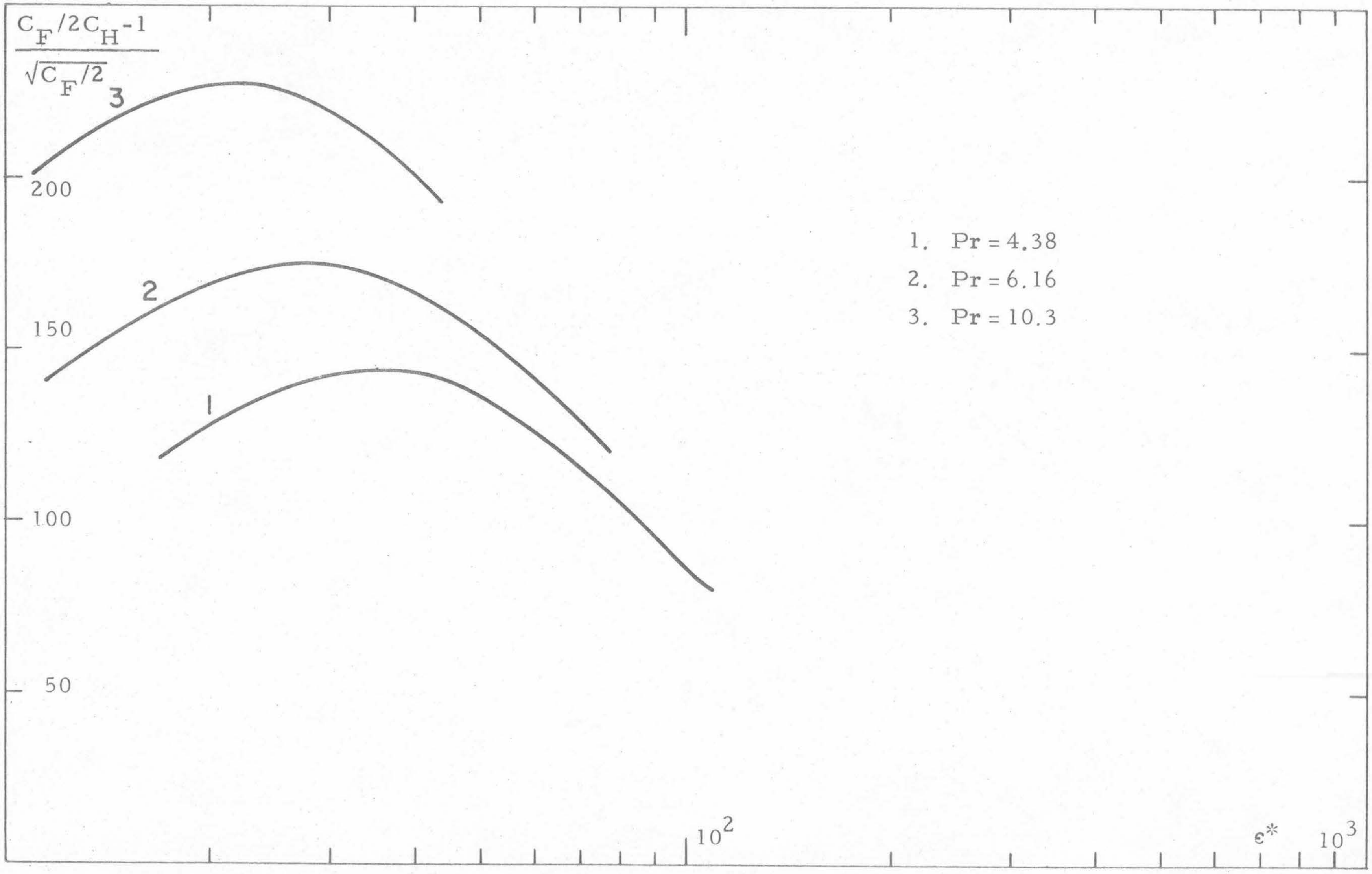

Fig. 48. Polyox 50 ppm, $(C_F/2C_H-1)/\sqrt{C_F/2}$ vs. ε* for C-9 tube: Pr effect.

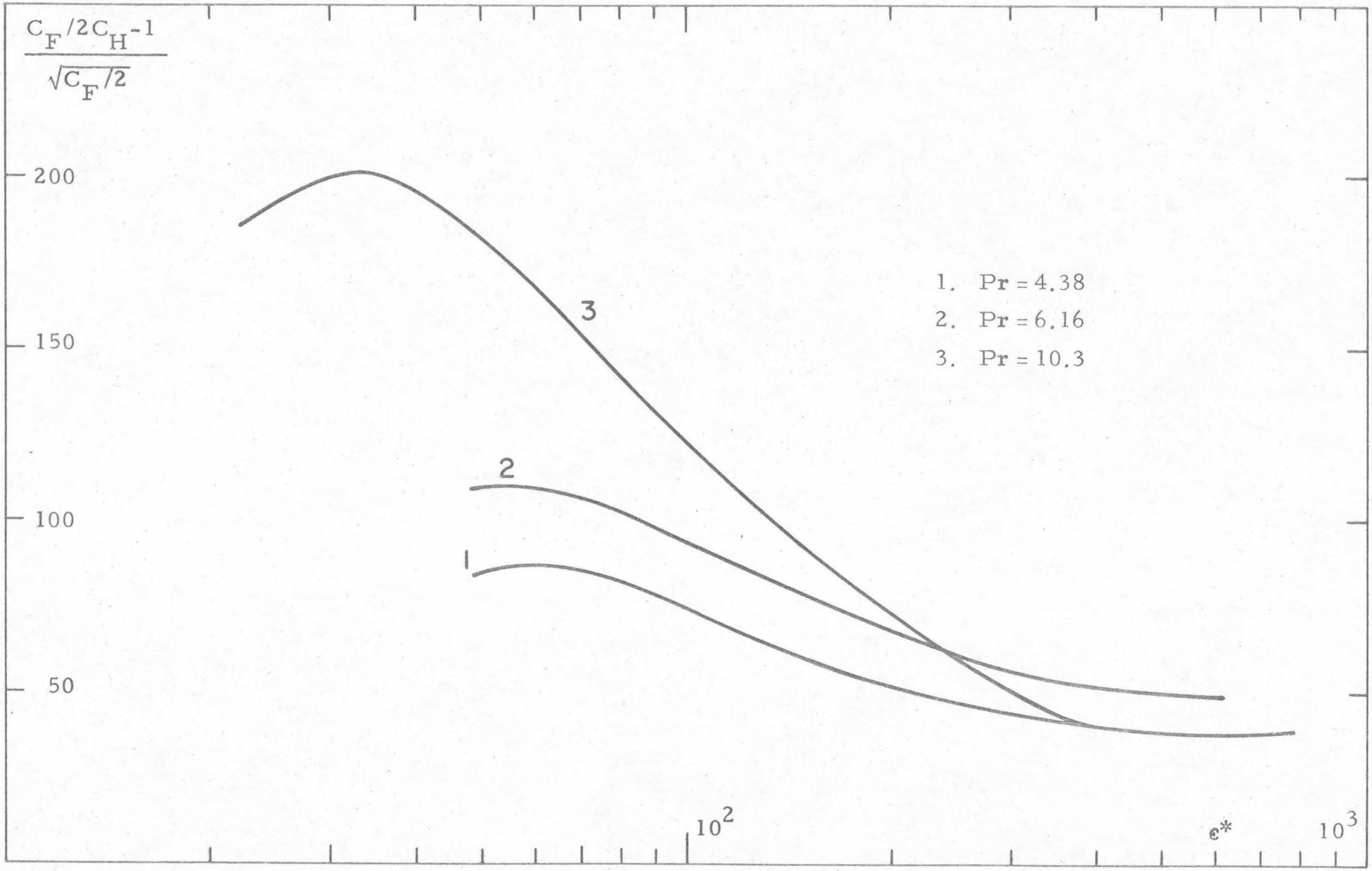

Fig. 49. Polyox 10 ppm, $(C_F/2C_H-1)/\sqrt{C_F/2}$ vs. ϵ^* for A-4 tube: Pr effect.

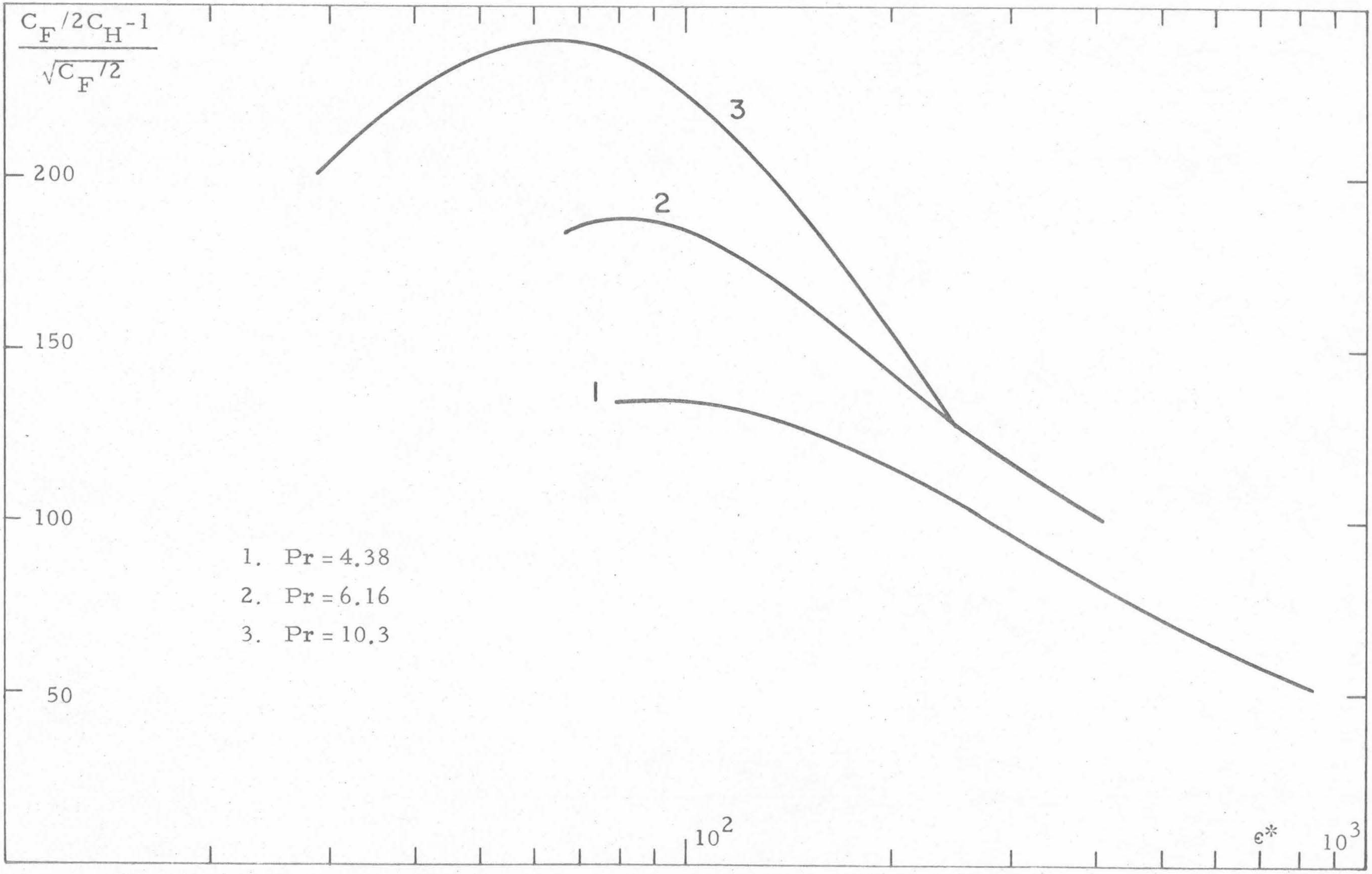

Fig. 50. Polyox 50 ppm, $(C_F/2C_H-1)/\sqrt{C_F/2}$ vs. ε^* for A-4 tube: Pr effect.

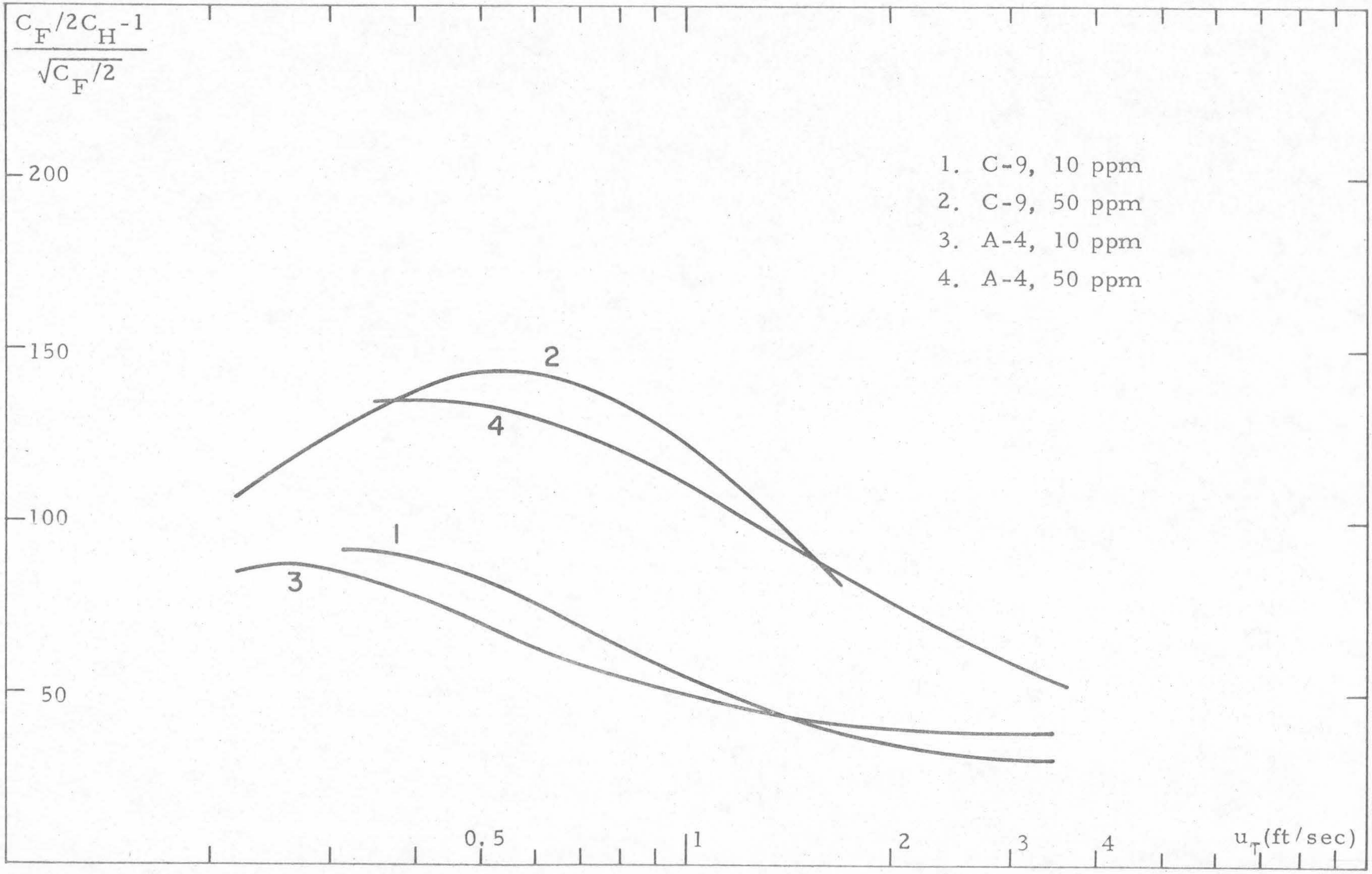

Fig. 51. Polyox 10 and 50 ppm, $(C_F/2C_H-1)/\sqrt{C_F/2}$ vs. u_τ for rough tubes at Pr = 4.38.

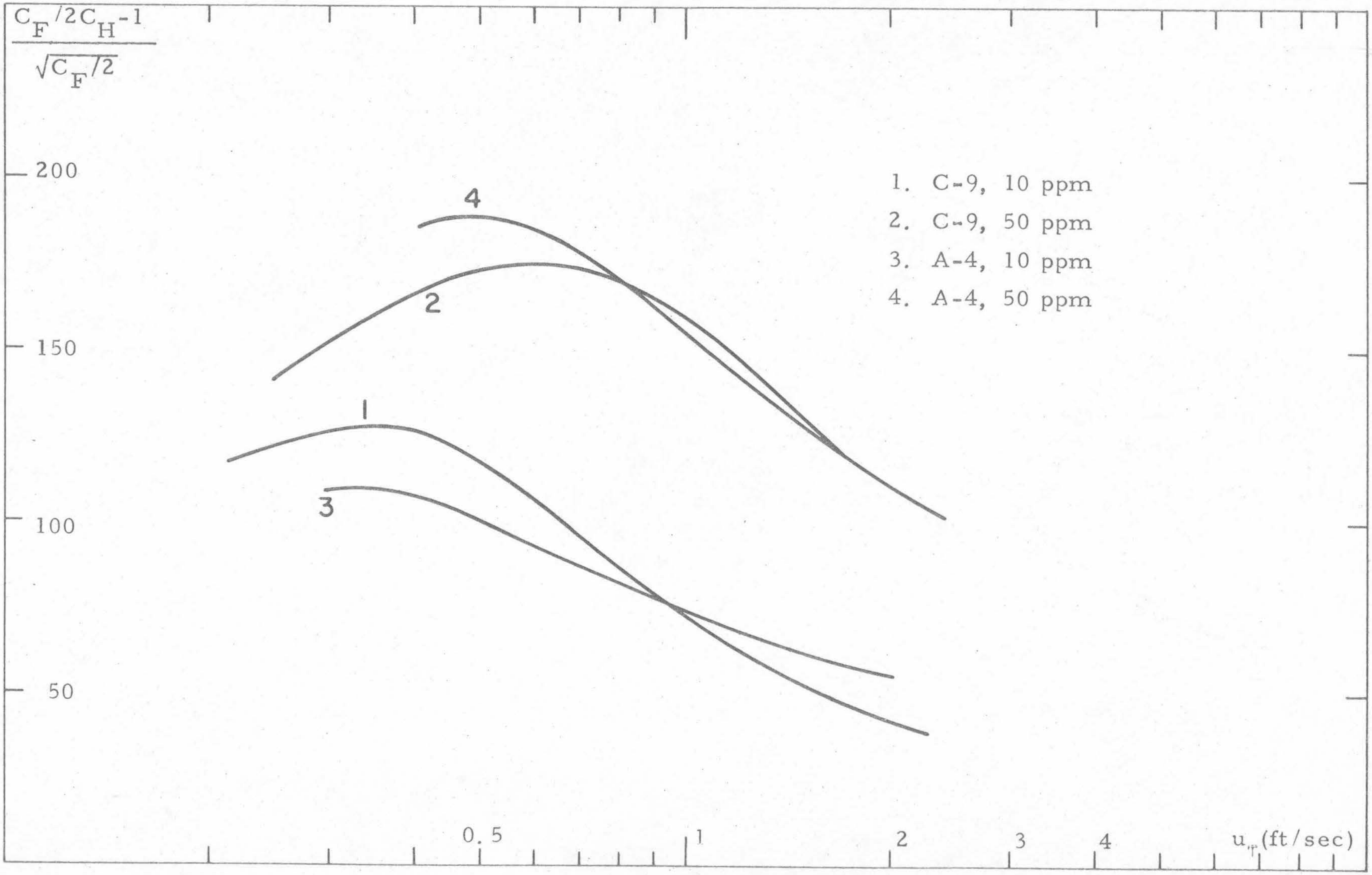

Fig. 52. Polyox 10 and 50 ppm, $(C_F/2C_H-1)/\sqrt{C_F/2}$ vs. u_τ for rough tubes at Pr = 6.16.

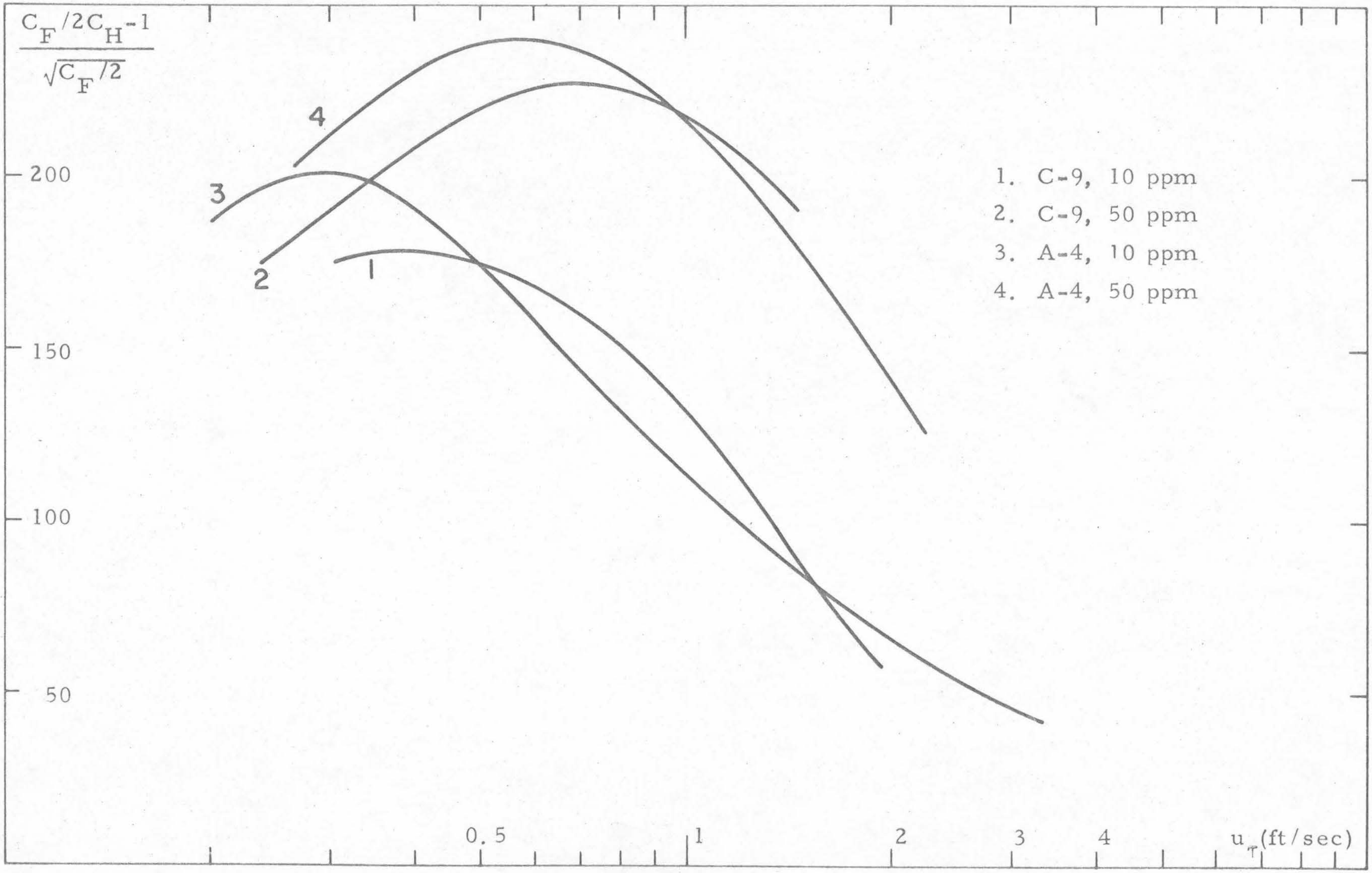

Fig. 53. Polyox 10 and 50 ppm, $(C_F/2C_H-1)/\sqrt{C_F/2}$ vs. u_τ for rough tubes at Pr = 10.3.

Appendix I

CALIBRATIONS

A. Pressure Drop Measurements

The differential pressure transducer (0 - 50 psig) was calibrated against a quartz tube standard at the Jet Propulsion Laboratory of the California Institute of Technology (JPL). The differential pressure was thus known as a function of the output voltage of the gage. A standard cell was used to calibrate the different scales of the amplifier and recorder (Visicorder) simultaneously. A selected microvoltage was supplied to the amplifier, itself connected to the recorder. The amplifier's output produced a deflection of a lightspot on a photosensitive chart and the measurements of these deflections gave a direct correlation between the position of the spot and the excitation of the amplifier. Thus these two calibrations connected the deviation of the lightspot on the visicorder chart with the actual pressure drop between the two test section pressure taps.

The calibration of the system amplifier - recorder was repeated at different times in the test program with no appreciable changes being observed. It should also be mentioned that the transducer's power source,designed to supply 10V exactly, was checked prior to each series of tests and was found to remain remarkably reliable.

B. Flow Rate Measurements

As stated in Chapter IV, Section C, the flow rate is derived from the speed of the gear driving the piston actuator, and the speed of the gear in turn is determined from the rate at which the gear teeth pass a magnetic sensor. The number of teeth per revolution of the gear –70–, as well as the corresponding displacement of the piston are known. The volume of water displaced during a revolution was calculated from the cylinder's inside diameter, and checked by weighing the water discharged during a displacement of the piston corresponding to a given number of revolutions of the gear. The calculated value was in agreement with the measured one within the limits of accuracy of the test. There was no measurable leakage past the piston. A relation between the number of teeth passing the magnetic pick-up in seconds and the flow rate was thus established. From the flow rate the average velocity of the flow in the test section could be calculated.

C. Power Measurements

The power required to heat the tube walls was derived from the voltage drop across the test section and the electric resistance of each tube as a function of temperature. The power factor was assumed to be unity. This assumption seemed justified because the tube represents a simple resistive load, and because of the similarity of the present circuit to that of Dipprey's [10] who checked the power factor.

The voltage drop was measured on a RMS thermal voltmeter. It was found that a standard AC voltmeter graduated for a perfect sine wave signal was giving erroneous values, due to the slight distortion of the sinusoidal shape of the transformer's output. This wave distortion was observed on an oscilloscope.

The RMS voltmeter was calibrated against a higher order of accuracy standard potentiometer. (John Fluke meter calibrator, model 760, giving an accuracy of 0.25%) The resistance of each tube was determined by passing a known current supplied by a constant current source through the test section and by measuring the voltage drop across the electrodes on a 0.1% accuracy digital voltmeter. The tube was kept at a given temperature by forcing water through it; that temperature in turn was calculated from the recordings of the inlet, outlet and wall thermocouples. The results of the measurements are given in Table 1 in the form

$$R = C_0 + C_1 T + C_2 T^2 .$$

D. Temperature Measurements

Four thermocouples emfs, corresponding to the inlet, outlet, and wall temperatures at two locations were recorded on a two-channel x-y plotter. The outlet immersion couple signal was continuously recorded on one channel. The inlet and wall stations were connected with the second channel of the recorder by means of a selector switch. The differences $(T_{wall} - T_{outl})$ and $(T_{outl} - T_{in})$ resulting from the electric heating of the tube wall were considered to be of primary interest. These differences could be obtained as follows.

First each of the two systems amplifier - RC circuit - recorder was calibrated simultaneously, as was done for the calibration of the pressure transducer circuit. As a result of these calibrations, the deflection of the two pens of the plotter was known as a function of the amplifier input. The inlet and outlet thermocouples were calibrated at JPL in a control furnace and this gave the functions

$$T_{outl} = f_1(E_{outl})$$

$$T_{in} = f_2(E_{in})$$

as well as

$$\Delta E\,(\text{in-outl}) = (E_{in} - E_{outl})$$

evaluated at constant T. Isothermal test at low flow rate were performed with each tube at the three temperatures of the tests and the difference in emf between the wall station thermocouples and inlet thermocouples was determined as a function of the wall emfs

$$d(\text{wall-in}) = d\,[E_{wall}].$$

The emf difference between the inlet and outlet thermocouples was measured during tests performed at higher flow rates (i. e., actual flow rates of our experiments) and in the absence of electric heating. This difference was compared with ΔE which had been obtained from the direct calibration of the inlet and outlet thermocouples. From this comparison the friction heat $\delta(\dot{w}) = \delta(\text{outl-in})$ was determined as a function of the flow rate. It was assumed that $\delta(\dot{w})$ varied linearly with the axial position and hence we were able to determine $\delta(\text{wall-in})$. Note that in all cases the friction heat was found to be awfully small (0.05 - 0.10° F) compared to the temperature difference between the fluid and the wall ($\simeq$ 10° F) which are of principal importance in this investigation.

The isothermal tests were also used for the determination of the isothermal friction coefficients.

From the result of these isothermal tests, together with the calibrations of the channel 1 and outlet temperature, it follows that

$$T_{outl} = T_{outl}\left[E_{outl}(\text{meas.}) - \delta(\text{in-outl})\right].$$

Now

E_{wall} (without heat friction and measured with wall thermocouple) $= E_{wall} - \delta(\text{wall-in})$.

But

E_{wall} (measured with wall thermocouple) $= E_{wall}$ (if measured on inlet thermocouple) $+ d(\text{wall-in})\left[E_{wall}\right]$.

Hence

E_{wall} (if measured on inlet thermocouple) $= E_{wall} - \delta(\text{wall-in})\left[\dot{w}\right] - d(\text{wall-in})\left[E_{wall}\right]$.

Therefore from the calibrations of channel 2 and inlet thermocouple, one may calculate

$$T_{wall} = f_2\left[E_{wall} - \delta(\text{wall-in}) - d(\text{wall-in})\right]$$

$$T_{in} = f_2\left[E_{in}\right].$$

The calibrations of the combination of amplifier - RC circuit - recorder were performed several times during the experimental program and possible slight changes taken into account in the data reduction.

Appendix II

DATA REDUCTION. CALCULATION OF C_F AND C_H

A. Calculation of Friction Coefficient

The friction coefficient C_F can be expressed as

$$C_F = K_2 \frac{\rho \Delta P}{\dot{w}^2} \tag{II.1}$$

where ΔP is the pressure drop in the rough region and K_2 contains various dimensional conversion factors as well as the length and diameter of the rough part of the test section.

The pressure drop ΔP_{meas} measured with the pressure transducer between the two pressure taps is actually the sum of the pressure drop in the rough region ΔP, the pressure drop due to smooth pipe friction in two 0.5 in. smooth regions ΔP_S (immediately following the upstream tap and preceding the downstream one), the difference in dynamic pressure due to a slight difference in diameter at the two measuring stations $(q_2 - q_1)$, and the contraction loss ΔP_{contr} and expansion loss ΔP_{ex} due to a change in diameter between the smooth sections near the taps and the rough part of the test section (see Figure 5). Thus

$$\Delta P = \Delta P_{meas} - \left[\Delta P_S + (q_2 - q_1) + \Delta P_{contr} + \Delta P_{ex}\right]. \tag{II.2}$$

Therefore

$$C_F = K_2 \left[\frac{\rho \Delta P_{meas}}{\dot{w}^2} - \gamma\right] \tag{II.3}$$

where

$$\gamma = \frac{\rho}{\dot{w}^2}\left[\Delta P_S + (q_2 - q_1) + \Delta P_{contr} + \Delta P_{ex}\right]. \qquad \text{(II.4)}$$

In this expression of γ, $(q_2 - q_1)$ and ΔP_{ex} are constants of the tube, while ΔP_S is directly proportional to C_F in smooth tube, and ΔP_{contr} must be experimentally determined in hydraulic tests.

The quantity γ was calculated following Dipprey [10]. In the present calculations, the value of $\Delta P_{contr}/\dot{w}^2$ was taken to be equal to that used by Dipprey for water. An average value of the friction coefficient for Polyox in smooth pipe was taken to determine ΔP_S. Table 1 contains the values calculated by Dipprey, of all constants appearing in the data reduction.

The user of these constants in a subsequent work must keep in mind that some of these values are only valid for tests performed with water under certain flow conditions and ought to be reevaluated if another fluid is used, or if the test conditions differ from those of [10].

B. Calculation of Heat Transfer Coefficient

The heat transfer coefficient may be written in the form

$$C_H = \frac{\dot{q}_{0_x}}{C_p \Delta T_{f_x}} \frac{\pi/4\ D^2}{\dot{w}} \qquad \text{(II.5)}$$

where

ΔT_{f_x} = wall to mixed-fluid temperature difference at station x

$= T_{ins.\ wall_x} - T_{L_x}$

$\dot{q}_{0_x}$ = local heat flux

D = inside diameter of tube

$\dot{w}$ = flow rate.

In order to express ΔT_{f_x} in terms of measured quantities, i. e., outer wall to outlet temperature differences ($T_{\text{out. wall}} - T_{\text{outl}}$) and outlet temperature (T_{outl}), we write ΔT_f, evaluated at station x, as follows:

$$\begin{aligned}\Delta T_f &= T_{\text{ins. wall}} - T_L \\ &= (T_{\text{outl}} - T_L) + (T_{\text{out. wall}} - T_{\text{outl}}) - (T_{\text{out. wall}} - T_{\text{ins. wall}})\end{aligned} \qquad \text{(II.6)}$$

($T_{\text{out. wall}} - T_{\text{outl}}$) can be calculated from thermocouple outputs. In order to calculate C_H from Eqns. (II.5) and (II.6), it is first necessary to calculate the wall temperature drop ($T_{\text{out. wall}} - T_{\text{ins. wall}}$), as well as the outlet temperature to local bulk temperature difference ($T_{\text{outl}} - T_{L_x}$) and local heat flux $\dot{q}_{0_x}$.

a) Wall Temperature Drop

The expression used to compute the local wall temperature drop is developed in Appendix IV-B of [10] and is written

$$\Delta T_w = \Delta T_{wp}\left[1 - \frac{1}{6}(t/R) + \left(\frac{\alpha}{2} + \frac{\beta}{6}\right)\Delta T_{wp}\right] \qquad \text{(II.7)}$$

where

$\dot{q}_0$ = local heat flux normal to the tube wall

t = local tube wall thickness

k = thermal conductivity evaluated at the outer wall temperature

R = tube radius

$$\alpha = \frac{dk/dT}{k\,[T_{out.wall}]}$$

$$\beta = \frac{d\rho_e/dT}{\rho_e\,[T_{out.wall}]}$$

ρ_e = electrical resistivity.

The quantity $\frac{t}{R}$, appearing in Eqn. (II.7) may be replaced by an average value evaluated for the whole test section. Likewise, the multiplying factor ΔT_{wp} becomes

$$\Delta T_{wp} = \dot{q}_0 \frac{\overline{t}}{2k\,[T_{out.wall}]}. \tag{II.8}$$

Moreover,

$$k = k_0\,[1+\alpha(T-T_0)]$$

where k_0 is the thermal conductivity evaluated at the reference temperature T_0, and

$$\frac{1}{k\,[T_{out.wall}]} = \frac{1}{k_0} + \frac{d(1/k)}{dT}(T_{out.wall} - T_0). \tag{II.9}$$

Using (II.8) and (II.9) and regrouping terms yields

$$\Delta T_{w_x} = K_6 \dot{q}_{0_x} t_x \left[1+K_7 T_x\right]\left[1-K_8 \dot{q}_{0_x}\right]. \tag{II.10}$$

The first bracketed term on the right accounts for the variation of thermal conductivity of the wall with temperature. The correction term [1-1/6 t/R] in Eqn. (II.7) is absorbed here in K_6 while the second bracketed term represents the other correction term in Eqn. (II.7).

b) Determination of $\dot{q}_{0_x}$ and $(T_{outl} - T_{L_x})$

Theoretically, the determination of local $\dot{q}_0$ and local T_L result in inseparable, integral equations. The value of $\dot{q}_0$ depends on the local resistivity of the tube wall ρ_e, which in turn depends on the effective local wall temperature, defined as the temperature in the center of the wall. This effective wall temperature is determined by

1) the local T_L
2) the heat transfer film conductance of the fluid (h)
3) the thermal conductivity of the wall, evaluated at the local wall temperature.

The pertinent Eqns. (II.11) are

(1) $$\dot{q}(x) = \frac{I^2}{2\pi r(x) A(x)} \rho_e \, [T_{eff}(x)]$$

(2) $$T_L(x) = T_L(x_0) + \int_{x_0}^{x} \frac{2\pi r(x)\, \dot{q}(x)}{\dot{w} C_p} dx$$

$$\text{using} \quad \dot{w} C_p \left[T_{L_x} - T_{L_{x_0}} \right] = 2\pi \int_{x_0}^{x} \dot{q}(x) r(x)\, dx$$

(3) $$T_{eff}(x) = T_{ins.wall}(x) + \frac{\Delta T_w(x)}{2} \qquad \text{(II.11)}$$

$$= T_L(x) + \frac{\dot{q}(x)}{h} + \frac{1}{4} \frac{t(x)\, \dot{q}(x)}{k[T_{out.wall}(x)]}$$

(retaining only first order terms in $\Delta T_w(x)$)

(4) $$T_{out.wall}(x) = T_L(x) + \dot{q}(x) \left[\frac{1}{h} + \frac{1}{2} \frac{t(x)}{k[T_{out.wall}(x)]} \right].$$

Moreover

$$\rho[T] = \rho[T_0] + \beta[T - T_0]$$

$$k[T] = k[T_0] + \alpha[T - T_0].$$

The symbols used in these equations have been defined previously in this appendix, except

I = electric current

r = local radius of tube

A = area of a surface passing across the tube in such a way that it is everywhere normal to the current flux lines

$T_L(x_0)$ = bulk temperature at reference station x_0.

Dipprey [10] treated this problem by putting first the above equations into dimensionless form. Then he evaluated the maximum excursions of the various dimensionless coefficients in terms of the parameters of his experiments and expanded the various functional forms in Taylor's series. He was thus able to produce linearized, separated expressions for $\dot{q}_0(x)$ and $T_L(x)$, retaining only first order corrections to account for the various interactions, and dropping out the terms that turn out to be negligible. A careful examination of the various approximations introduced in the linearization revealed that Dipprey's results remain valid under our flow conditions.

The resulting expressions have the form

$$\frac{W_{TS}}{\pi D L \dot{q}_{0_x}} = M_x\left[1 + B_x\left(\frac{Q_x}{M_x^2}\right) + \Gamma_x\left(\frac{N_x}{M_x}\right)\right] \qquad \text{(II.12.1)}$$

$$\frac{T_{out1}-T_{L_x}}{T_{out1}-T_{in}} = M_{xx}\left[1-\frac{B_x\left(\frac{x}{L}\right)}{2(1+\Gamma_x)}-\frac{\Gamma_x S_x}{(1+\Gamma_x)}\right] \tag{II.12.2}$$

where the subscript x refers to a particular local thermocouple station, W_{TS} is the power released in the test section, and L and D are the length and diameter of the heated test section. M_x, N_x, Q_x, M_{xx} and S_x represent various definite integrals depending only on the variation of wall thickness with longitudinal station and on the position of the thermocouple station. Defining $\left(\frac{R}{L}\right)_x$ as the electrical resistance per unit length of pipe at station x and r_{i_x} as the inside tube radius at station x,

$$M_x = \frac{1}{L\left(\frac{R}{L}\right)_x}\int_0^L \frac{R}{L}\,[\xi]\,d\xi$$

$$\begin{cases} \text{with } \frac{R}{L}=\left(\frac{R}{L}\right)_0 [1-bx] \\ b \simeq 4.75\ 10^{-3}\ \text{ohm/in} \end{cases}$$

$$N_x = \frac{r_{i_x}}{L\left(\frac{R}{L}\right)_x^2}\int_0^L \frac{\left(\frac{R}{L}\right)^2[\xi]}{r_i\,[\xi]}\,d\xi - M_x$$

$$Q_x = \frac{(R/L)^2_{ref}}{(R/L)^2_x}\left[Q_{ref}+\frac{M_{ref}}{L}\int_x^{x_{ref}} \frac{\left(\frac{R}{L}\right)[\xi]}{\left(\frac{R}{L}\right)_{ref}}\,d\xi\right]$$

with

$$Q_{ref} = \frac{1}{L^2\left(\frac{R}{L}\right)^2_{ref}}\int_0^L \frac{R}{L}\,[\xi]\int_{x_{ref}}^{x} \frac{R}{L}\,(\xi')\,d\xi'\,d\xi$$

$$M_{xx} = \frac{L}{L-x} \frac{\int_x^L \frac{R}{L}[\xi]\,d\xi}{\int_0^L \frac{R}{L}[\xi]\,d\xi}$$

$$S_x = \frac{({}_xN_L)_x}{({}_xM_L)_x} - \frac{N_x}{M_x}$$

where $({}_xN_L)_x$ and $({}_xM_L)_x$ are defined as N_x and M_x respectively, but this time the integrals are evaluated from x to L.

Finally, B_x and Γ_x appearing in Eqn. (II.12) are defined as

$$B_x = \frac{\frac{d\rho_e}{dT}[T_{out1} - T_{in}]}{\rho[T_{eff}(x)]}$$

$$= \frac{\beta}{\rho_0 + \beta[T_{eff} - T_0]} [T_{out1} - T_{in}] \qquad \text{(II.13)}$$

$$\Gamma_x \simeq B_x\left(\frac{D}{4L}\right)\left(\frac{1}{\overline{C_H}}\right).$$

Thus B_x is determined from the resistivity of the wall material, a rough estimate of the wall temperature and the measurement of the temperature rise of the fluid passing through the test section $(T_{out1} - T_{in})$.

The factor Γ_x contains the first order correction for the effect of the error caused by estimating the local effective wall temperature to be equal to the local mixed fluid temperature. A crude preliminary estimate of $\overline{C_H}$ in terms of the conditions of the test gives an adequate accuracy.

Using the definition of Γ_x, Eqn. (II.1) may be written

$$\frac{W_{TS}}{\dot{q}(x)} = a_x [1 + B_x b_x]$$

or

$$\dot{q}(x) = \frac{W_{TS}}{a_x(1 + b_x B_x)}$$

$$\simeq a'_x \, W_{TS} [1 - b_x B_x]. \tag{II.14}$$

Likewise, Eqn. (II.2) becomes

$$T_{out1} - T_{L_x} = (T_{out1} - T_{in}) M_{xx}\left[1 - \frac{B_x}{1+\Gamma_x}\left(\frac{x/L}{2} + \frac{\Gamma_x}{B_x} S_x\right)\right]$$

or, after expanding $(1 + \Gamma_x)^{-1}$ in Taylor's series

$$T_{out1} - T_{L_x} \simeq (T_{out1} - T_{in}) M_{xx} [1 - c_x B_x + d_x B_x^2]. \tag{II.15}$$

It is now possible to calculate C_H from the flow rate ($\dot{w}$), the power released in the test section (W_{TS}), the wall-to-outlet temperature differences and outlet to inlet temperature difference.

C. Computer Program

A standard program was written in AID (Time Sharing System) to reduce the data from all tubes. The values of the constants K_i, used in this paragraph, as well as γ, a'_x, b_x, c_x, d_x, t_x, M_{xx} are given in Table 1 for all tubes. The subscript x appearing in the sequence of operations presented hereafter means that the computation was repeated for the two wall stations. The input consisted in:

1) Q(0) = reading (in chart divisions) of the inlet electromotive force.

2) Q(1) = reading (in chart divisions) of the outlet electromotive force.

3) Q(2) = reading (in chart divisions) of the wall electromotive force ≠ 1.

4) Q(3) = reading (in chart divisions) of the wall electromotive force ≠ 2.

5) N = number of teeth passing the magnetic pick-up in 10 sec (determination of flow rate).

6) n = reading (in chart divisions) of the pressure transducer output.

7) V = voltage drop across electrodes of test section.

8) s, r = integers identifying the scales used on amplifiers and recorders.

The following calibration curves were stored in memory:

1) Calibration of channel 1 of plotter (on different scales) $E_1 = E_1$ (number of divisions).

2) Calibration of channel 2 of plotter (on different scales) $E_2 = E_2$ (number of divisions).

3) Calibration of outlet immersion thermocouple: $T_{outl} = T_{outl}(E_{outl})$.

4) Calibration of inlet immersion thermocouple: $T_{in} = T_{in}(E_{in})$.

5) Isothermal emf difference between the 2 wall and inlet thermocouples

$$d_2(\text{wall 1-in}) = d_2\,[E_{wall}]$$

$$d_3(\text{wall 2-in}) = d_3\,[E_{\text{wall}}].$$

6) Friction heat between inlet and outlet

$$\delta(\text{outl-in}) = \delta_0(\dot{w}).$$

7) Friction heat between wall station and inlet

$$\delta(\text{wall-in}) = \delta_1(\dot{w}).$$

8) Calibration of pressure transducer

$$\Delta p = \Delta p(\Delta P\ \text{emf}).$$

9) Calibration of amplifier-recorder circuit (on different scales)

$$\Delta P\ \text{emf} = f(\text{number of divisions}).$$

10) From calibration tests, rough calculation of $\Delta T_w = f(V, T_{in})$. This will be used in the computation of the average test section temperature.

11) $\rho, C_p, \mu, Pr = f(T)$. These expressions are least square fits of the values of density, specific heat, absolute viscosity, and Prandtl numbers tabulated in [13].

The sequence of operations performed by the machine (IBM 370) is:

1) Calculation of Temperatures

$E_0 = E_2(Q(0))$

$E_1 = E_1(Q(1))$

$E_2 = E_2(Q(2))$

$E_3 = E_2(Q(3))$

$d_2 = d_2\,[E_2]$

$$d_3 = d_3[E_3]$$

$$T_{in} = T_{in}[E_0]$$

$$\rho = \rho[T_{in}]$$

$$\dot{w} = K_1 N\rho \quad K_1 = \text{constant}$$

$$\delta(\text{outl-in}) = \delta_0(\dot{w})$$

$$\delta(\text{wall-in}) = \delta_1(\dot{w})$$

$$T_{outl} = T_{outl}[E_1 - \delta(\text{outl-in})]$$

$$T_{out.wall\ 1} = T_{in}[E_2 - \delta(\text{wall-in}) - d_2]$$

$$T_{out.wall\ 2} = T_{in}[E_3 - \delta(\text{wall-in}) - d_3].$$

2) Calculation of C_F

$$T_{av} = T_{in} + (T_{outl} - T_{in})/2$$

$$\rho = \rho[T_{av}]$$

$$\dot{w} = K_1 N\rho$$

$$\Delta p = \Delta p(\Delta P\ \text{emf})$$

$$C_F = K_2\left[\frac{\rho \Delta p}{\dot{w}^2} - \gamma\right] \qquad \gamma \text{ is a constant.}$$

The latter computation is also performed on data from the non-heating calibration tests to obtain isothermal C_F values.

3) Calculation of C_H

Calculation of average temperature in the center of wall:

$T_{av\ eff}$.

$$T_{av\ eff} = T_{out.wall} - (T_{out} - T_{in})K_3 - \overline{\Delta T_w}/2$$

K_3 is a constant depending on the position of the thermocouple station. $\overline{\Delta T_w}$ is the average wall temperature drop, estimated from calibration tests as a function of V and T_{in}.

$R_{TS} = R_{TS}[T_{av \cdot eff}]$ R_{TS} = test section electric resistance

$W = K_4 V^2/R_{TS}$ W = electric power released in TS

$C_p = C_p(T_{av})$

$C = wC_p(T_{outl} - T_{in})$ C = calorimetrically measured rate of heat addition to the fluid

$\% \delta W = 100(C-W)/W$ % discrepancy between C and W

$B_x = (T_{outl} - T_{in})/(K_5 + T_{out.wall\,x})$ approximation of Eqn. (II.13)

$\dot{q}_x = a'_x W[1 + b_x B_x]$ Eqn. (II.14)

$\Delta T_{w_x} = K_6 \dot{q}_x t_x \times [1 + K_7 T_{out.wall\,x}][1 - K_8 \dot{q}_x]$ Eqn. (II.10)

$T_x = T_{in} + K_9(T_{outl} - T_{in})$ T_x = first order approximation for the local bulk fluid temperature

$\mu_x = \mu(T_x)$

$C_{p_x} = C_p(T_x)$

$Re_x = K_{10} \dot{w}/\mu_x$ Re_x = local Reynolds number

$Pr_x = Pr(T_x)$

$T_{outl} - T_{L_x} = (T_{outl} - T_{in})M_{xx}[1 - c_x B_x + d_x B_x^2]$ Eqn. (II.15)

$\Delta T_{f_x} = (T_{outl} - T_{L_x}) + (T_{out.wall\,x} - T_{outl}) - \Delta T_{w_x}$ Eqn. (II.6)

$$C_{H_x} = K_{11} \frac{\dot{q}_x}{C_p \Delta T_{f_x} \dot{w}} \qquad \text{(Eqn. II.5)}$$

$$\overline{C_H} = (C_{H_{x_1}} + C_{H_{x_2}})/2 .$$

The output consisted of

T_{in}

T_{out1}

$T_{out1-in}$

$T_{out.wall\ 1}$

$T_{out.wall\ 2}$

$T_{out.wall\ 1,\ 2} - T_{out1}$

W

C

$\%\ \delta\ W$

$\dot{w}$

ΔP

C_F

$\dot{q}_x$

ΔT_{f_x}

Re

Pr

$C_{H_1}, C_{H_2}, \overline{C_H}$

C_F and $\overline{C_H}$, once calculated from the data, were used as described in Chapter V.

D. Table of Constants used in Computer Program (Table 1)

Are constant for all tubes:

$K_1 = 3.10^{-4}$

$K_4 = 0.9482.10^{-3}$

$K_5 = 211.$

	E-3 Tube	C-9 Tube	A-4 Tube
C_0 in	0.001695	0.001858	0.001660
C_1 $R_{TS} = C_0$	5.648 10^{-6}	6.98 10^{-6}	6.95 10^{-6}
C_2 $+C_1T+C_2T^2$	5.22 10^{-9}	0	0
K_2	2.77 10^{-5}	3.59 10^{-5}	3.87 10^{-5}
K_3	0.370	0.3765	0.368
K_6	408.0	389.3	380.5
K_7	7.54 10^{-4}	7.07 10^{-4}	7.07 10^{-4}
K_8	0.005	0.004	0.004
K_9	0.871	0.878	0.869
K_{10}	40.5	38.85	38.3
K_{11}	0.1117	0.1213	0.1250
γ	-1.34	19.6	9.2
a'_x	0.0485	0.0452	0.0444
b_x	0.344	0.300	0.337
c_x	0.41	0.38	0.399
d_x	1.65	0.94	0.55
t_x	0.02007	0.01763	0.01874
M_{xx}	0.130	0.126	0.128

Appendix III

CONFIDENCE LIMITS EVALUATION

The purpose of this section is to discuss the major sources of error or uncertainty in the C_F and C_H determinations of these experiments. The evaluation of error limits must be based to some extent on the experimenter's judgment, and therefore is somewhat subjective. Nevertheless, an attempt has been made to set limits which are compatible with the observed degree of agreement among redundant measurements and the degree of reproducibility among repeated measurements.

A. Friction Coefficients

The equation used for determination of the friction coefficients can be expressed

$$C_F = \frac{\pi^2 D^5}{32\, L_R}\left(\frac{\Delta P_{TS}}{K^2 N^2 \rho_{av}} - \gamma\right) \qquad \text{(III.1)}$$

where

K is a calibration constant, appearing in the calculation of the flow rate $\dot{w} = KN\rho_{av}$.

N is the number of teeth of the gear passing the magnetic pick-up per second (see Chapter IV).

L_R is the length of the rough tube between the pressure tap and the group $\gamma = \rho_{av}(\delta\Delta P_{TS})/\dot{w}^2$ is a constant correction to the pressure drop accounting for the effects discussed in Appendix II.

The uncertainties in the C_F determination can be ascertained from the error made in the measurements of D, L_R, ΔP_{TS}, K, N and γ (the error on ρ is negligible, as ρ varies very slowly with T).

a. Error on ΔP_{TS}

The differential gage used for the measurements of ΔP_{TS} was calibrated in the Jet Propulsion Laboratory and the balance of the transducer excitation circuit, as well as the output voltage of the transducer power supply were checked prior to each series of tests. No time-dependent changes were observed. Systematic errors in the differential pressure measurements due to air trapped or density variations in the gage lines were eliminated by the procedure used before each test and described in Chapter IV (Test Operations). Thus the primary errors remaining in the pressure-drop measurement are assumed to be limited to normally distributed reading errors. The calibration of the circuit amplifier-recorder was performed many times during the experimental program, and the results were repeatable within ±0.4%. This calibration error, combined with a slight vibration existing in the system and producing a periodic oscillation of the transducer's response limited the reading accuracy to approximately ±1.5% to 4%, depending on the flow rate.

b. Error on γ

The largest value of the pressure-drop correction constant (γ) applied to any of the tubes amounted to 7% of C_F. Assuming that this roughly estimated correction could be in error by ±10%, a possible systematic error of 0.7% could have been introduced to the C_F determination from this cause. This error source is negligible for the smooth tube. This error will be combined with the other systematic errors by adding it directly rather than by using the root mean square combination used for errors assumed to be normally distributed.

c. Error on K

The factor K is defined from the equation

$$\dot{w} = KN\rho_{av}.$$

Physically, K represents the volume discharged during a displacement ℓ of the piston corresponding to a rotation of the gear of 360/70 degrees (a full revolution corresponds to 70 teeth passing the magnetic probe)

$$K = \ell \pi R_c^2 \qquad (R_c = \text{cylinder radius})$$

ℓ was determined by measuring several times the displacement L of the piston during a large number of revolutions (about 40 to 50). Therefore

$$\ell = \frac{L}{70 \times (\text{no.of revol.})} = \frac{L}{N}.$$

It is estimated that L and N could be measured with an accuracy of ±0.15% and 0.025% respectively. The inside diameter of the cylinder is (10 ± 0.040) in (standard tolerance). Thus the maximum error on R_c is 0.4%. Combining all the errors on K, one obtains $\%\delta K = 0.85$ (systematic error, normally distributed). (The operator $(\%\delta)$ indicates that the variation of the operand is expressed as a percentage of its mean value.)

d. Error on D

According to Dipprey [10], who worked with the same tubes, the largest diameter uncertainty (A-4 tube) is ±1.3%. The error in the smooth tube internal diameter is taken as ±0.3%. Variations in tube diameter due to thermal expansion are negligible. The systematic error in diameter determination is assumed to be normally distributed.

e. Error on L_R

The percentage error in the length measurement is negligible in comparison with other errors in the C_F determination.

f. Error on N

N was measured over a period of 10 sec and varied from about 200 (low flow rates) to 1200. The uncertainty on N is ±1, so that

$$\%\delta N = 0.5 \text{ to } 0.1.$$

The combined systematic error in C_F becomes

$$\%\delta C_{F_{syst}} = \pm\left(\left[5(\%\delta D)^2 + (\%\delta K)^2\right]^{1/2} + 0.07\,[\%\delta \gamma]\right).$$

For E-3 tube,

$$\%\delta C_{F_{syst}} = \pm\left(\left[5(0.3)^2 + (0.85)^2\right]^{1/2}\right) \qquad (\%\delta \gamma \text{ negligible})$$

$$= \pm 1.1.$$

For C-9 tube,

$$\%\delta C_{F_{syst}} = \pm 3.2.$$

For A-4 tube,

$$\%\delta C_{F_{syst}} = \pm 3.8.$$

The combined random error is written

$$\%\delta C_{F_{rand}} = \pm [(\%\delta \Delta P_{TS})^2 + (\%\delta N)^2]^{1/2}$$

$$= \pm \begin{array}{ll} 4.1 & \text{(maximum)} \\ 1.6 & \text{(minimum)} \end{array} \quad \text{for every tube.}$$

The random error on each C_F is combined with the systematic error determined for each tube to yield the total estimated percentage error on each point.

For E-3 tube, $\%\delta C_F = \begin{cases} \pm 2.25 & \text{(min)} \\ \pm 4.3 & \text{(max)} \end{cases}$

For C-9 tube, $\%\delta C_F = \begin{cases} \pm 3.6 & \text{(min)} \\ \pm 5.2 & \text{(max)} \end{cases}$

For A-4 tube, $\%\delta C_F = \begin{cases} \pm 4.1 & \text{(min)} \\ \pm 5.6 & \text{(max).} \end{cases}$

The maximum error on each point occurs when tests are run at low Reynolds numbers ($\simeq$ 15,000 to 30,000). The scatter present in the data (see Figures 10, 11, 12, 18, 19, 23 and 24) rarely exceeds the calculated percentages. One ought to keep in mind that some of this scatter might be caused by a slightly different behavior of solutions coming from different batches (possible mechanical or thermal degradation during the preparation of the solutions).

B. Heat Transfer Coefficients

In these experiments, C_H is determined from

$$C_{H_x} = \frac{(\pi/4)D^2\dot{q}_{0_x}}{\dot{w}C_p[\Delta_x T_{11} + (T_{outl} - T_{L_x}) - \Delta T_{w_x}]} \tag{III.2}$$

where

$\Delta_x T_{11}$	denotes the measured temperature difference between the outside tube wall and the exit fluid
$(T_{outl} - T_{L_x})$	is the temperature rise in the fluid between the wall-thermocouple station and the exit
ΔT_{w_x}	is the local temperature drop through the wall.

The tube wall thermocouples are placed sufficiently far from the electrode blocks so that the effects of end conduction of heat along the tube wall introduce negligible error into the determination of C_H (see Appendix V of [10]). Moreover, the errors in $(T_{outl} - T_{L_x})$ are negligible with respect to errors in $\Delta_x T_{11}$; ΔT_{w_x} is adequately approximated by $\dot{q}_{0_x} t_x/2k$, and the error contributions from measurements of the fluid density and the tube length are negligible. Making the above mentioned allowances, Eqn. (II.12.1, App. II) can be written

$$\dot{q}_0 = \frac{K_2}{L}\left(\frac{W_p}{D}\right) \tag{III.3}$$

where K_2 is a dimensionless constant. Then using the latter equation in the preceding approximation for ΔT_w,

$$\Delta T_w = \frac{K_2}{2L}\left[\frac{W_p t}{kD}\right]. \tag{III.4}$$

Using the simplifying assumptions discussed above substituting Eqns. (III.3) and (III.4), as well as $\dot{w} = KN\rho_0$ into Eqn. (III.2), taking the reciprocal and rearranging, one obtains

$$\begin{aligned}\frac{1}{C_H} &= \left(\frac{L\rho_0 C_{p0}}{\pi/4\,K_2}\right)\frac{KN}{D}\left[\frac{\Delta_x T_{11}}{W_p} - \frac{K_2}{2L}\left(\frac{t}{kD}\right)\right] \\ &= K_3\,\frac{KN}{D}\left[\frac{\Delta_x T_{11}}{W_p} - \frac{K_2}{2L}\left(\frac{t}{kD}\right)\right].\end{aligned} \tag{III.5}$$

A differentiation of the logarithm of Eqn. (III.5) shows that percentage errors in the heat transfer coefficients ($\%\delta C_H$) can be deduced from the following percentage errors

$$\begin{gathered}\%\delta K \\ \%\delta N \\ (1-\eta)\%\delta D \\ (1+\eta)\%\delta \Delta_x T_{11} \\ (1+\eta)\%\delta W_p \\ \eta\%\delta t \\ \eta\%\delta k\end{gathered} \tag{III.6}$$

where

$$\eta = \left(\frac{K_2}{2L}\,\frac{t}{kD}\right)\Big/\left[\frac{\Delta_x T_{11}}{W_p} - \frac{K_2}{2L}\left(\frac{t}{kD}\right)\right]$$

$$= \frac{\Delta T_w}{\Delta T_f}$$

or, using Eqns. (III.3) and (III.4) and evaluating ΔT_f from the definition of C_H,

$$\eta = \frac{2C_p t}{\pi D^2} \frac{\dot{w} C_H}{k[T]}. \qquad \text{(III.7)}$$

Thus the ratio η of the temperature drop in the wall to temperature drop in the fluid serves to amplify the effect of most of the error sources involved in the experimental method used.

In addition to the seven error sources listed in Eqn. (III.6), an additional uncertainty stems from an observed circumferential variation in heat transfer coefficient at the two separate thermocouple points, possibly due to local variations in wall thickness and local variations in flow conditions.

a. Error on K, N and D ($\%\delta K$, $\%\delta N$, $\%\delta D$)

The error terms $\%\delta K$, $\%\delta N$ and $\%\delta D$ have been discussed in connection with the C_F error analysis.

b. Error on ΔT_f, or Error on $\Delta_x T_{11}$, W_p, t and k

It is first noted that errors due to effects such as heat conduction along the thermocouple wires and spurious heat losses from the fluid are essentially cancelled out by the technique used for calibrating the wall thermocouples against the inlet-water thermocouple in the non-heating tests.

Oscilloscope measurements revealed alternating current (AC) emf's to be superposed on the direct current (DC) emf's in the thermocouple network. It was assumed that no errors in the thermocouple measurements were produced by the presence of these AC voltages, following the conclusions of Allen [2] and Dipprey [10] on possible spurious AC effects on thermocouple measurements made under similar circumstances. Finally, it was assumed that all the "cold junctions" of the thermocouples were at the same ice-bath temperature.

c. Error on $\Delta_x T_{11}$

It was shown in Appendix II that $\Delta_x T_{11}$ can be written as

$$\Delta_x T_{11} = T_{wall}\left\{E_x(n) - d_x(n)\right\} - T_{outl}\left\{E_{outl}(n)\right\} \qquad (III.8)$$

where

n is the number of divisions read on the plotter

E is the emf corresponding to n divisions of the plotter

d is the difference of emf between the wall and outlet thermocouple outputs at a given inlet-water temperature, expressed as a function of n (inlet).

In Eqn. (III.8), we neglected the friction heats δ_x and δ(outl-in), as they do not contribute to the error on $\Delta_x T_{11}$.

The functions $E_x(n)$ and $E_{outl}(n)$ are known from the calibrations of the two channels of the plotter (see Appendix I). These calibrations were performed several times during our experimental program, and the maximum discrepancy observed between two different values of n for a given voltage was 0.6 divisions, which corresponds to $\simeq 4.5\mu V$ (as one division is roughly equivalent to $7.65\mu V$). An average emf $\overline{E}$ was chosen for each value of n, and

$$E(n) = (\overline{E} \pm 2.25\mu V)_n .$$

The value of $d_x(n)$ was determined from numerous isothermal tests and could be measured repeatedly with an accuracy of ±.15 divisions, which corresponds to ± 1μV. Here again, an average value $\overline{d}(n)$ was selected and

$$d_x(n) = (\overline{d} \pm 1\mu V)_n.$$

One can show that the percentage error on $[E_x(n) - d_x(n)]$ can be decomposed into the following two error elements

$$\frac{E_x}{E_x - d_x} \% \delta E_x$$

and

$$\frac{d_x}{E_x - d_x} \% \delta d_x .$$

$\% \delta E_x$ is itself composed of two errors: the calibration error described above (2.25μV) and an error on the reading of n. It was estimated that in the worst case (when fluctuations in the wall emf were present, due to small fluctuations of power), n could be read with an accuracy of ±0.5 div, which corresponds to ≃ ±4μV.

Combining the errors on $[E_x(n) - d_x(n)]$,

$$\% \delta [E_x(n) - d_x(n)] = \pm \frac{1}{E_x - d_x} [(470)^2 + (100)^2]^{1/2} .$$

In a similar fashion, $\% \delta E_{outl}$ is the combination of two errors: a calibration error and an error on the reading of n. It was estimated that

$$\% \delta [E_{outl}] = \frac{340}{E_{outl}} .$$

Finally, $\%\delta(\Delta_x T_{11})$ can be decomposed into the following error elements

$$\frac{dT}{dE}\,\frac{[E_x(n) - d_x(n)]}{T_{wall} - T_{outl}}\,\%\delta[E_x(n) - d_x(n)]$$

and

$$\frac{dT}{dE}\,\frac{E_{outl}}{T_{wall} - T_{outl}}\,\%\delta[E_{outl}]$$

where dT/dE is the slope of the calibration curve $T = f(E)$, well approximated by the average value of 0.0445. Combining these two errors yields

$$\%\delta(\Delta_x T_{11}) = \frac{26.25}{T_{wall} - T_{outl}} = \frac{26.25}{\Delta_x T_{11}}.$$

In our tests, $T_{wall} - T_{outl}$ varied from about 10°F to 20°F. Calculating $\%\delta(\Delta_x T_{11})$ for an average $\Delta_x T_{11}$ of 15°F, one obtains

$$\%\delta(\Delta_x T_{11}) = \frac{26.25}{15} = 1.75.$$

d. Error on W_p

The electric power released in the test section was calculated from the expression

$$W_p = \frac{V^2}{R(T)} K_w$$

where

V	is the measured voltage drop across the test section electrodes
K_w	is a dimensional constant
$R(T)$	is the electric resistance of the test section, measured as described in Appendix I.

It was estimated that R(T) was determined with an accuracy of 1%. A check of these values against that due to Dipprey supports this estimation. The error on V, including the normal reading error, increasing when slight fluctuations in the power were observed, and the possible error in the calibration of the voltmeter itself, is of the order of 1.5% in the worst cases.

Combining the errors on W_p yields

$$\% \delta W_p = 3.2.$$

e. Error on t

Dipprey [10] estimates that

for the smooth tube $(\% \delta t)_S = \pm 2.0$

for rough tubes $(\% \delta t)_R = \pm 4.0.$

f. Error on k

Dipprey determined experimentally the thermal conductivity of the tube wall with an estimated accuracy of ±3.5%

$$\% \delta k = \pm 3.5.$$

As was stated previously, another source of C_H uncertainty which is not evident from the data reduction formula (Eqn. III.2) stems from an observed circumferential variation in heat transfer coefficients at the two separate thermocouple points, possibly due to local variations in wall thickness and local variations in flow conditions. These uncertainties are designated $\% \delta R.E$ (uncertainties due to local roughness effects) and are evaluated as follows

$$\%\delta R.E \text{ (E-3 tube)} = \pm 1.5$$

$$\%\delta R.E \text{ (C-9 tube)} = \pm 2.0$$

$$\%\delta R.E \text{ (A-4 tube)} = \pm 6.0.$$

Finally, the composite confidence limits on the reported C_H values can be written as

$$\begin{aligned}\%\,\delta C_H = \Big\{ & (\%\delta K)^2 + (\%\delta N)^2 + [(1-\eta)\%\delta D]^2 \\ & + \frac{1}{2}\Big[(1+\eta)\%\delta \Delta_x T_{11}\Big]^2 + \Big[(1+\eta)\%\delta W_p\Big]^2 \\ & + [\eta\%\delta t]^2 + [\eta\%\delta k]^2 + [\%\delta R.E]\Big\}^{1/2}\end{aligned} \qquad \text{(III.9)}$$

where η is given by Eqn. (III.7). The 1/2 factor in front of the fourth bracket of the right-hand side of Eqn. (III.9) accounts for the averaging of the results from the two circumferential locations on the tube. The minimum and maximum values of η reached at the lowest and highest flow rates respectively were calculated for each tube and the results are given hereafter

E-3 Tube	Flow rate = 0.3 lbm/sec	$\eta_{min} = 0.0045$
	= 2.4 lbm/sec	$\eta_{max} = 0.0504$
C-9 Tube	Flow rate = 0.3 lbm/sec	$\eta_{min} = 0.0033$
	= 2.4 lbm/sec	$\eta_{max} = 0.21$
A-4 Tube	Flow rate = 0.3 lbm/sec	$\eta_{min} = 0.0039$
	= 2.4 lbm/sec	$\eta_{max} = 0.28.$

The corresponding confidence limits for experimental heat transfer coefficients were computed using Eqn. (III.9) and have the following values

E-3 Tube Min $\%\delta C_H = \pm 3.9$
Max $\%\delta C_H = \pm 4.05$

C-9 Tube Min $\%\delta C_H = \pm 4.2$
Max $\%\delta C_H = \pm 4.9$

A-4 Tube Min $\%\delta C_H = \pm 7.1$
Max $\%\delta C_H = \pm 7.55$.

A slightly better accuracy in the measurement of C_H is achieved at low flow rate. Note that the high value of $\%\delta C_H$ for the A-4 tube is essentially due to the discrepancy between the values measured at the two circumferential locations on the tube (±6%).

Appendix IV

ANALOGY BETWEEN MOMENTUM AND HEAT TRANSFER IN ROUGH TUBES: GENERAL APPROACH

Let us divide the flow into two regions by an imaginary cylinder passing through the tips of the roughness elements at $y = \varepsilon$. At the interface, the axial velocity is u_g, the temperature T_g, the heat flux $\dot{q}_0$ and the shear stress τ_0. From the definition of C_H (the symbols used here are the same as those defined in Chapter III)

$$C_H = \frac{\dot{q}_0}{\rho \bar{u} C_p (T_w - T_L)}$$

or

$$\frac{1}{C_H} = \frac{\rho C_p \bar{u}}{\dot{q}_0}(T_w - T_g) + \frac{\rho C_p \bar{u}}{\dot{q}_0}(T_g - T_L). \qquad \text{(IV.1)}$$

We have seen in Chapter III that

$$\frac{\rho C_p \bar{u}(T_w - T_g)}{\dot{q}_0} = \frac{1}{\sqrt{\frac{C_F}{2}}\frac{u_g}{u_\tau} C_{H_c}} \qquad \text{(IV.2)}$$

where C_{H_c} is the Stanton number for the mean time cavity heat exchange.

The second term of the right-hand side of Eqn. (IV.1), will now be calculated without the simplifying assumptions used in Chapter III. In central flow

$$\frac{\tau}{\rho} = (\varepsilon_M + \nu)\frac{du}{dy} \qquad \text{(IV.3)}$$

$$-\frac{\dot{q}}{\rho C_p} = (\varepsilon_H + \frac{\nu}{Pr})\frac{dT}{dy}. \qquad \text{(IV.4)}$$

The boundary conditions at the interface ($y = \epsilon$) are written

$$\frac{\tau_0}{\rho} = \left[(\epsilon_M + \nu)\frac{du}{dy}\right]_{y=\epsilon} \qquad \text{(IV.5)}$$

$$-\frac{\dot{q}_0}{\rho C_p} = \left[(\epsilon_H + \frac{\nu}{Pr})\frac{dT}{dy}\right]_{y=\epsilon}. \qquad \text{(IV.6)}$$

We define θ, Φ, ξ, η as

$$\theta = \frac{T - T_w}{T_{CL} - T_w} \qquad \text{(IV.7)}$$

$$\Phi = \frac{u}{u_{CL}} \qquad \text{(IV.8)}$$

$$\xi = \frac{T - T_g}{T_{CL} - T_g} \qquad \text{(IV.9)}$$

$$\eta = \frac{u - u_g}{u_{CL} - u_g} \qquad \text{(IV.10)}$$

θ and Φ vary from 0 to 1 as y goes from zero (wall) to R (centerline), while ξ and η vary from 0 to 1 as y goes from ϵ (interface) to R (centerline).

θ and ξ are related by

$$\xi = \frac{1}{1 + \frac{T_w - T_g}{T_{CL} - T_w}}\left(\theta - \frac{T_g - T_w}{T_{CL} - T_w}\right). \qquad \text{(IV.9')}$$

Likewise

$$\eta = \frac{1}{1 - \frac{u_g}{u_{CL}}}\left(\Phi - \frac{u_g}{u_{CL}}\right). \qquad \text{(IV.10')}$$

Dividing (IV.6) by (IV.4) and using (IV.9′) yields

$$\frac{\dot{q}_0}{\dot{q}} = \frac{\left[\epsilon_H + \frac{\nu}{Pr}\right]_{y=\epsilon}}{\epsilon_H + \frac{\nu}{Pr}} \; \frac{\left. d\xi/dy \right|_{y=\epsilon}}{d\xi/dy}$$

or

$$\frac{d\xi}{d(y/R)} = \frac{\dot{q}}{\dot{q}_0} \; \frac{\left[1+\epsilon_H Pr/\nu\right]_{y=\epsilon}}{1+\epsilon_H Pr/\nu} \; \left.\frac{d\xi}{d(y/R)}\right|_{y=\epsilon} . \tag{IV.11}$$

Similarly, using Eqns. (IV.3), (IV.5) and (IV.10′),

$$\frac{d\eta}{d(y/R)} = \frac{\tau}{\tau_0} \; \frac{\left[1+\frac{\epsilon_M}{\nu}\right]_{y=\epsilon}}{1+\frac{\epsilon_M}{\nu}} \; \left.\frac{d\eta}{d(y/R)}\right|_{y=\epsilon} . \tag{IV.12}$$

Dividing (IV.11) by (IV.12) and assuming the same variation of $\dot{q}$ and τ with respect to y yields

$$\frac{d\xi}{d\eta} = \left.\frac{1+\frac{\epsilon_H Pr}{\nu}}{1+\frac{\epsilon_M}{\nu}}\right|_{y=\epsilon} \; \frac{1+\frac{\epsilon_M}{\nu}}{1+\frac{Pr\,\epsilon_H}{\nu}} \; \left.\frac{d\xi}{d\eta}\right|_{y=\epsilon}$$

or

$$\frac{d\xi}{d\eta} = C \times \left.\frac{d\xi}{d\eta}\right|_{y=\epsilon} \; \frac{1+\epsilon_M/\nu}{1+Pr\,\epsilon_H/\nu} \tag{IV.13}$$

where

$$C = \left.\frac{1+\epsilon_H Pr/\nu}{1+\epsilon_M/\nu}\right|_{y=\epsilon} .$$

Now, making use of Eqn. (IV.6), the second term of the right-hand side of Eqn. (IV.2) may be written as

$$\frac{\rho C_p \bar{u}}{\dot{q}_0}(T_g - T_L) = -\frac{\bar{u}(T_g - T_L)}{\left[(\epsilon_H + \frac{\nu}{Pr})\frac{dT}{dy}\right]_{y=\epsilon}} \quad .$$

From Eqn. (IV.5),

$$\nu = \frac{\tau_0}{\rho} \left.\frac{1}{\frac{du}{dy}}\right|_{y=\epsilon} - \epsilon_M\Big|_{y=\epsilon}$$

and

$$\frac{\rho C_p \bar{u}}{\dot{q}_0}(T_g - T_L) = -\frac{\bar{u}(T_g - T_L)}{\left\{\left[\epsilon_H + \frac{1}{Pr}\left(\frac{\tau_0}{\rho}\frac{1}{\frac{du}{dy}} - \epsilon_M\right)\right]\frac{dT}{dy}\right\}_{y=\epsilon}} . \qquad \text{(IV.14)}$$

Assuming now a relation between ϵ_H and ϵ_M

$$\epsilon_H = \lambda\epsilon_M = \lambda Pr \frac{\epsilon_M}{Pr} = \frac{Pr^* \epsilon_M}{Pr} . \qquad \text{(IV.15)}$$

Introducing (IV.15) into (IV.14) and rearranging terms

$$\frac{\rho C_p \bar{u}}{\dot{q}_0}(T_g - T_L) = -\frac{\bar{u}(T_g - T_L)}{\left\{\frac{\epsilon_M}{Pr}(Pr^* - 1)\frac{dT}{dy} + \frac{1}{Pr}\frac{\tau_0}{\rho}\frac{dT/dy}{du/dy}\right\}_{y=\epsilon}}$$

or

$$\frac{\rho C_p \bar{u}}{\dot{q}_0}(T_g - T_L) = \frac{\dfrac{T_L - T_g}{T_{CL} - T_g}}{\left\{\dfrac{\epsilon_M}{Pr}(Pr^* - 1)\dfrac{d\dfrac{T}{T_{CL}-T_g}}{dy}\dfrac{1}{\bar{u}} + \dfrac{1}{2Pr}\,\dfrac{2\tau_0}{\rho\bar{u}^2}\,\dfrac{\bar{u}}{u_{CL}-u_g}\,\dfrac{d\dfrac{T}{T_{CL}-T_g}/dy}{d\dfrac{u}{u_{CL}-u_g}/dy}\right\}_{y=\epsilon}} . \tag{IV.16}$$

But from the previous definitions

$$\frac{2\tau_0}{\rho\bar{u}^2} = C_F$$

$$\frac{d\dfrac{T}{T_{CL}-T_g}}{dy} = \frac{d\xi}{dy}$$

$$\frac{d\dfrac{u}{u_{CL}-u_g}}{dy} = \frac{d\eta}{dy}$$

$$\begin{aligned}
\frac{\bar{u}}{u_{CL}-u_g} &= \frac{1}{1-\dfrac{u_g}{u_{CL}}}\Phi_m \qquad \text{with} \quad \Phi_m = \frac{\bar{u}}{u_{CL}} \\
&= \frac{\Phi_m}{1-\Phi_g} \qquad\qquad \text{with} \quad \Phi_g = \frac{u_g}{u_{CL}} \\
&= \frac{\Phi_g}{1-\Phi_g} + \eta_m \qquad \text{with} \quad \eta_m = \frac{\bar{u}-u_g}{u_{CL}-u_g}
\end{aligned} \tag{IV.17}$$

$$\frac{T_L - T_g}{T_{CL}-T_g} = \frac{1}{1-\dfrac{T_g - T_w}{T_{CL}-T_w}}\left(\theta_m - \frac{T_g - T_w}{T_{CL}-T_w}\right) \tag{IV.18}$$

$$\text{with} \quad \theta_m = \frac{T_L - T_w}{T_{CL} - T_w}$$

$$\frac{T_L - T_g}{T_{CL} - T_g} = \frac{\theta_m - \theta_g}{1 - \theta_g} \qquad \text{with} \quad \theta_g = \frac{T_g - T_w}{T_{CL} - T_w} \tag{IV.18 cont.}$$

$$= \xi_m .$$

$$\frac{1}{\bar{u}} \epsilon_M \, d\left(\frac{T}{T_{CL} - T_g}\right) / dy = \frac{1}{\bar{u}} \epsilon_M \frac{d\xi}{dy}$$

$$= - \frac{\overline{u'v'}}{u_\tau^2} \frac{d\xi}{d\eta} \frac{C_F}{2} \frac{\bar{u}}{u_{CL} - u_g}$$

using the definitions of ϵ_M and C_F.

Substituting in (IV.16)

$$\frac{\rho C_p \bar{u}}{\dot{q}_0} (T_g - T_L) = \frac{\dfrac{\theta_m - \theta_g}{1 - \theta_g}}{\left\{\dfrac{\Phi_m}{1 - \Phi_g} \dfrac{C_F}{2} \dfrac{d\xi}{d\eta} \dfrac{1}{Pr} \left[1 - \dfrac{\overline{u'v'}}{u_\tau^2} (Pr^* - 1)\right]\right\}_{y=\epsilon}} . \tag{IV.19}$$

It is now necessary to determine $\left.\frac{d\xi}{d\eta}\right|_{y=\epsilon}$ appearing in the denominator of Eqn. (IV.19). Integrating (IV.11) between the interface and centerline

$$\int_0^1 d\xi = 1 = \left.\frac{d\xi}{d\eta}\right|_{y=\epsilon} C \int_0^1 \frac{1 + \frac{\epsilon_M}{\nu}}{1 + Pr \frac{\epsilon_H}{\nu}} \, d\eta$$

or

$$\left.\frac{d\xi}{d\eta}\right|_{y=\epsilon} = \frac{1}{C\int_0^1 \frac{1+\frac{\epsilon_M}{\nu}}{1+Pr^*\frac{\epsilon_M}{\nu}}\,d\eta} = \frac{1}{C\left[\int_0^1 \frac{(Pr^*-1)}{(1+Pr^*\epsilon_M/\nu)Pr^*}\,d\eta + \int_0^1 \frac{d\eta}{Pr^*}\right]}. \qquad \text{(IV.20)}$$

Substituting (IV.20) into (IV.19), one finally obtains

$$\frac{\rho C_p \overline{u}}{\dot{q}_0}(T_g - T_L) = \frac{(\theta_m - \theta_g)C\left[\int_0^1 \frac{Pr^* - 1}{(1+Pr^*\epsilon_M/\nu)Pr^*}\,d\eta + \int_0^1 \frac{d\eta}{Pr^*}\right](1-\Phi_g)}{(1-\theta_g)\Phi_m \frac{C_F}{2}\frac{1}{Pr}\left[1 - \left.\frac{\overline{u'v'}}{u_\tau^2}\right|_{y=\epsilon}(Pr^*|_\epsilon - 1)\right]} \qquad \text{(IV.21)}$$

Next, let

$$\int_0^1 \frac{Pr^* - 1}{(1+Pr^*\frac{\epsilon_M}{\nu})Pr^*}\,d\eta + \int_0^1 \frac{d\eta}{Pr^*} = F$$

$$1 - \left.\frac{\overline{u'v'}}{u_\tau^2}\right|_{y=\epsilon}(Pr^*_\epsilon - 1) = G.$$

Then

$$\frac{\rho C_p \overline{u}}{\dot{q}_0}(T_g - T_L) = \frac{(\theta_m - \theta_g)CF(1-\Phi_g)Pr}{(1-\theta_g)\frac{C_F}{2}\Phi_m G.}. \qquad \text{(IV.21')}$$

Introducing (IV.21′) and (IV.2) into (IV.1) yields

$$\frac{1}{C_H} = \frac{1}{\sqrt{C_F/2}\,\frac{u_g}{u_\tau}\,C_{H_c}} + \frac{(\theta_m - \theta_g)CF(1-\Phi_g)Pr}{(1-\theta_g)\frac{C_F}{2}\,\Phi_m G}. \tag{IV.22}$$

Smooth Case

The discussion will be limited to the case when λ defined by Eqn. (IV.15) is constant. The appropriate relations will then be

a) $\frac{\rho C_p \overline{u}}{\dot{q}_0}(T_w - T_g) = 0$ or $\frac{1}{\sqrt{\frac{C_F}{2}}\,\frac{u_g}{u_\tau}C_{H_c}} = 0$

b) $\theta_g = \frac{T_g - T_w}{T_{CL} - T_w} = 0$

c) $C = 1$

d) $G = 1$ (IV.23)

e) $\Phi_g = 0$

f) $\xi = \theta$

g) $\eta = \Phi$

h) $F = \frac{1}{Pr^*}\left[\int_0^1 \frac{Pr^* - 1}{1 + Pr^* \frac{\epsilon_M}{\nu}}\,d\Phi + 1\right].$

Thus

$$\frac{1}{C_H} = \frac{\theta_m \left[\int_0^1 \frac{Pr^* - 1}{1 + Pr^* \frac{\epsilon_M}{\nu}} d\Phi + 1 \right]}{\Phi_m \frac{C_F}{2} \lambda}$$

or

$$C_H = \frac{\frac{C_F}{2} \frac{\Phi_m}{\theta_m} \frac{\epsilon_H}{\epsilon_M}}{1 + (Pr^* - 1) \int_0^1 \frac{d\Phi}{1 + Pr^* \frac{\epsilon_M}{\nu}}} . \qquad \text{(IV.24)}$$

Substituting Φ in terms of the variable $u^* = \frac{u}{u_\tau}$, it follows that

$$d\Phi = \frac{u_\tau}{u_{CL}} du^* = \frac{u_\tau}{\overline{u}} \frac{\overline{u}}{u_{CL}} du^*$$

$$= \sqrt{\frac{C_F}{2}} \, \Phi_m \, du^*$$

and the lower and upper limits of integration of the integral appearing in (IV.24) become 0 and u_{CL}/u_τ respectively. The expression for the heat transfer coefficient is finally written

$$C_H = \frac{\frac{C_F}{2} \frac{\Phi_m}{\theta_m} \frac{\epsilon_H}{\epsilon_M}}{1 + (Pr^* - 1) \Phi_m \sqrt{\frac{C_F}{2}} \int_0^{\frac{u_{CL}}{u_\tau}} \frac{du^*}{1 + Pr^* \frac{\epsilon_M}{\nu}}} . \qquad \text{(IV.25)}$$

Appendix V

TURBULENT FLOW RHEOMETER

It is well known that Polyox solutions are very easily subject to degradation (mechanical under high shear stress, or thermal, or biological), and that when aged they lose part of the elastic effects [20]. Gadd and Brennen reported that "ageing" can be greatly speeded up by very gentle mixing, and thus it seems that the performance of some dilute Polyox solutions depends very much on the mixing procedure. Differences in mixing procedure might account for some of the anomalous results which exist in the literature.

For practical reasons, we could not run all the tests relative to one curve with Polyox solution coming from a unique batch. Instead, 6 to 8 drums of solution were necessary for the evaluation of C_F and C_H at a given Prandtl number, concentration and roughness ratio $\frac{\varepsilon}{D}$. In order to detect possible differences in mixing procedure we had to imagine a standard test allowing us to verify that each of these Polyox batches performed identically under similar flow conditions. This is the reason why a small turbulent flow rheometer was devised. Its sketch is presented in Figure V-1. The standard test consisted of forcing a known volume of Polyox solution into a 0.055 I.D. and 100 diameter long stainless steel tube (1) by pressurizing the rheometer reservoir (2) with nitrogen under a constant pressure of 70 psi. The time required to discharge that known volume of fluid was measured on a stop watch and two different solutions were judged similar in performance when the time of discharge was found identical during their respective tests. The 70 psi pressure was set with help of two pressure regulators (3) in the pressure lines and read on a pressure gage (4). A safety device (5) prevented any excursion of pressure. A fluid level sight glass (6) allowed a visual check of the level of the fluid in the reservoir. The stop watch was started when the fluid level passed a mark on the gage glass tubing, and stopped when the level was down to another mark. The total volume discharged was 1295.05 cm^3 and the test was performed in about 57 sec with Polyox. The rheometer was first tested with water, and the friction coefficient was calculated as follows (using the CGS unit system):

1. Volume discharged/sec = 1295.05/t cm^3/sec where t is the time of discharge, around 88 sec for water at room temperature.

2. Average velocity in test section $= \dfrac{1295.05 \times 4}{\rho \pi d^2 t}$ cm/sec

$$= K_1/\rho t \text{ cm/sec} \qquad \text{(V.1)}$$

where

ρ is the fluid density expressed in gr/cm^3

d is the tube diameter in cm

K_1 is a constant.

3. $$\text{Re} = \frac{\bar{u} d}{\nu} = \frac{K_1}{\rho t}\,\frac{d}{\nu} = K_1 \frac{d}{\mu t} \qquad \text{(V.2)}$$

For water at room temperature, Re $\simeq$ 15150.

4. Total pressure,

$$p_{tot} = 70\text{ psi} = \Delta p_{T.S} + \Delta p_{elbow} + \Delta p_{45^\circ bend} + \Delta p_{\substack{sud.\\contr}} + \text{atm.press}$$

$$= \frac{\rho \bar{u}^2}{2}\left[4\,C_F\left(\frac{L}{D}\Big|_{TS} + k_2\right) + k_3\right] + 14.7 \qquad (V.3)$$

where k_2 and k_3 are constants.

5. From (V.3) we calculate C_F, knowing $\bar{u}$ from Eqn. (V.2).

The values of the friction coefficient thus calculated were in excellent agreement with the well-established values for water.

The time discharges obtained with all the fresh Polyox solutions tested were remarkably close, indicating that no drastic change took place in the mixing procedure of the different batches. This was confirmed by the very little scatter present in our data. A calculation of C_F and Re similar to that performed for water gave systematically too high values of the friction coefficient at a given Re (when compared to C_F obtained in the main apparatus). It is believed that the presence of bends and sudden contractions in the system is responsible for the disagreement observed. In estimating the pressure losses in fittings, (expressed in Eqn. (V.3)), each fitting was replaced by an equivalent length of a straight pipe of the same diameter and the same equivalent lengths as for pure water were taken. However, it appears that a polymeric additive that reduces drag in straight pipes will cause much less reduction in pressure loss across fittings. This conclusion is in agreement with [38].

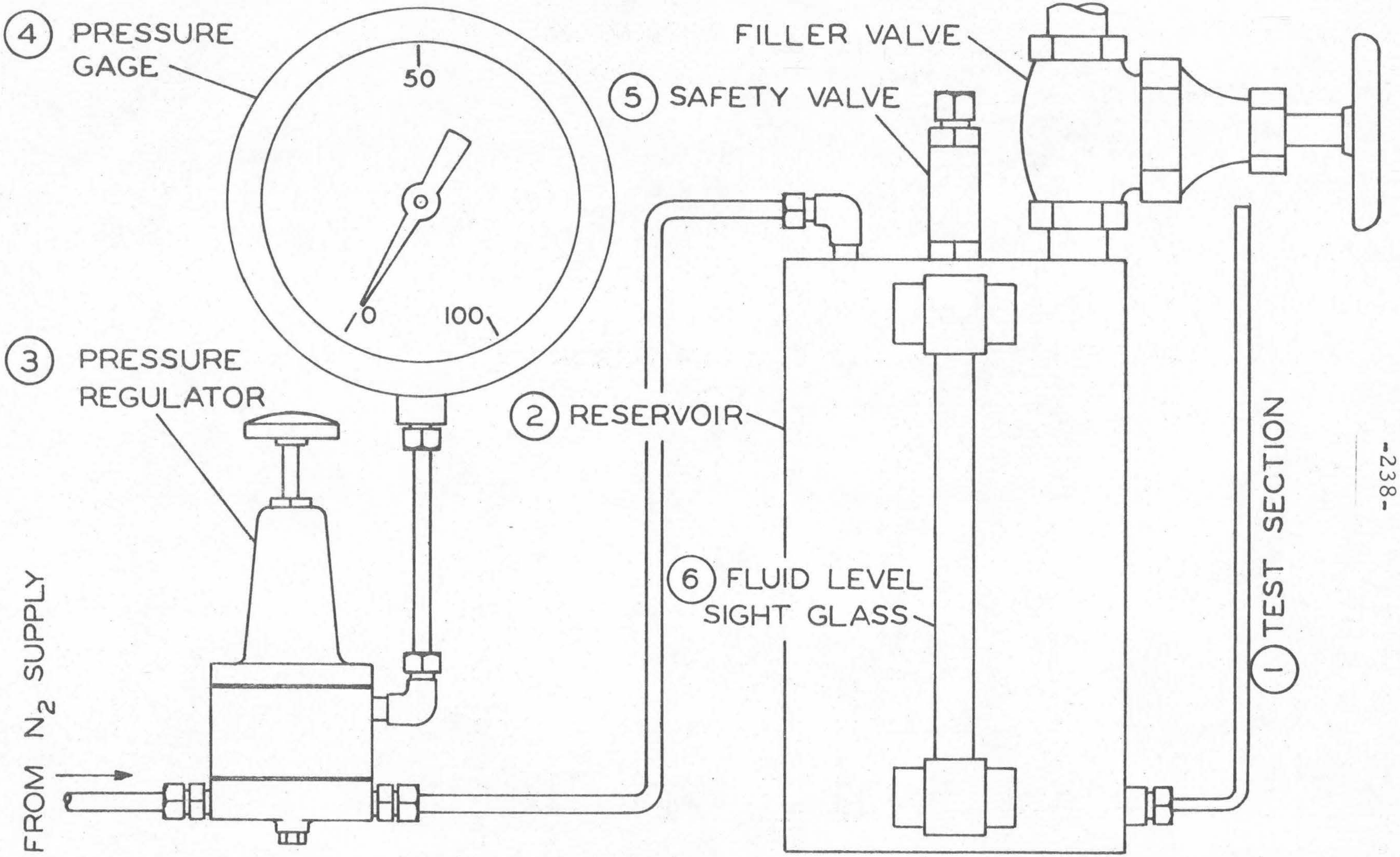

Fig. V-1. Schematic of Turbulent Flow Rheometer